R-05-81

SFR 1 – Post closure radionuclide release and dose calculations

Gavin Thomson, Bill Miller, Enviros Consulting Ltd

December 2005

Svensk Kärnbränslehantering AB
Swedish Nuclear Fuel
and Waste Management Co
Box 5864
SE-102 40 Stockholm Sweden
Tel 08-459 84 00
+46 8 459 84 00
Fax 08-661 57 19
+46 8 661 57 19

ISSN 1402-3091
SKB Rapport R-05-81

SFR 1 – Post closure radionuclide release and dose calculations

Gavin Thomson, Bill Miller, Enviros Consulting Ltd

December 2005

Executive summary

This report summarises the following sensitivity and supporting calculations undertaken as part of SKB's response to the Authorities' review of Project SAFE.

- Presentation of the central or 'Most likely scenario'.
- Alternative inventory assumptions.
- Alternative repository flow-fields from different calibration techniques.
- Sensitivity to uncertainties in radionuclide sorption in the near-field.
- Consideration of forest land use.

The results from the Most likely scenario are summarised below. Biosphere results are only summarised for the Reasonable Biosphere Development (RBD) model as these are the highest overall doses.

The table below summarises the maximum conditional risks for the Most likely scenario RBD model. The risks are reported as conditional as it has been cautiously assumed that the probability of the Most likely scenario occurring is unity. The risk per dose factor used is 0.06 Sv^{-1}, the ICRP recommended value.

Summary of Most likely scenario results.

	Near-field (Maximum flux, time and key contributor)	Geosphere (Maximum flux, time and key contributor)	RBD (Maximum dose, time and key contributor)
Silo	1.3E+07 Bq/y at c. 3,900 AD	1.2E+07 Bq/y at c. 3,900 AD	6.5E–07 Sv/y at c. 5,100 AD
	Organic C-14	Organic C-14	Organic C-14
BMA	9.1E+07 Bq/y at c. 3,100 AD	7.8E+07 Bq/y at c. 3,200 AD	4.2E–07 Sv/y at c. 8,000 AD
	Organic C-14	Organic C-14	I-129
1BTF	2.9E+08 Bq/y at c. 3,000 AD	1.3E+08 Bq/y at c. 3,100 AD	5.9E–07 Sv/y at c. 5,100 AD
	Organic C-14	Organic C-14	Organic C-14
2BTF	3.3E+06 Bq/y at c. 3,000 AD	2.7E+06 Bq/y at c. 3,100 AD	6.9E–08 Sv/y at c. 8,000 AD
	Organic C-14	Organic C-14	I-129
BLA	2.5E+08 Bq/y at 2,030 AD	2.3E+06 Bq/y at c. 2,200 AD	5.5E–09 Sv/y at c. 5,000 AD
	Co-60, Ni-63 and Cs-137	Ni-63	Inorganic C-14
SFR-1 total	3.5E+08 Bq/y at c. 3,000 AD	1.8E+08 Bq/y at c. 3,100 AD	1.6E–06 Sv/y at c. 5,100 AD
	1BTF	1BTF	Silo, BMA and 1BTF

Maximum conditional risks for Most likely scenario RBD model.

	Maximum conditional risk (y^{-1})
Silo	3.9E–08
BMA	2.5E–08
1BTF	3.5E–08
2BTF	4.2E–09
BLA	3.3E–10
SFR-1 total	9.4E–08

Contents

1 Introduction

Enviros has been supporting SKB in relation to its operation of the L/ILW repository, SFR-1, located near Forsmark.

- Enviros has developed a representation of the performance assessment calculations undertaken in Project SAFE in the compartmental code AMBER /Thomson 2005/.
- Enviros has developed an initial appraisal of the potential closure options for SFR-1 /Enviros 2004/.

This report summarises sensitivity and supporting calculations undertaken as part of SKB's response to the Authorities' review of Project SAFE. At this stage SKB wishes to prioritise resources on the following areas

- Presentation of the central or 'Most likely scenario'.
- Alternative inventory assumptions.
- Sensitivity of repository groundwater flow-fields to different calibration techniques used in the supporting hydrogeological model.
- Sensitivity to uncertainties in radionuclide sorption in the near-field.
- Consideration of forest land use.

Enviros' role is to provide SKB with additional calculations for the SFR-1 repository that can be used by SKB to further demonstrate the robustness and safety of the continued operation of the facility.

Chapter 2 of this report details the development of AMBER models of Project SAFE and also modifications in relation to the Reasonable Biosphere Development (RBD) model made in response to the authorities review comments on Project SAFE. Chapter 3 describes the data used in the calculations. Results for the Most likely scenario are contained in Chapter 4. Chapter 5 details the results of the sensitivity calculations. Chapter 6 discusses and compares the results for each facility and Chapter 7 provides a summary. References are provided in Chapter 8. Several appendices with supporting information are also included.

2 AMBER models of Project SAFE

SKB commissioned Enviros to replicate the existing Project SAFE assessment model using the AMBER code /Thomson 2005/. AMBER models were configured to represent each disposal feature within the near-field (Silo, BMA, 1BTF, 2BTF and BLA), the geosphere and the biosphere variants. The near-field and biosphere AMBER models used similar compartments and mathematical relationships to those within Project SAFE. The geosphere AMBER model was designed to approximate to the model used in Project SAFE by using a compartmentalised approach.

This section provides a description of the development of the AMBER models which updates /Thomson 2005/ but only discusses the Reasonable Biosphere Development biosphere variant.

2.1 AMBER

AMBER is a flexible, graphical-user-interface based tool that allows users to build their own dynamic compartmental models to represent the migration, degradation and fate of contaminants in an environmental system. AMBER allows the user to assess routine, accidental and long-term contaminant release. AMBER overcomes key limitations associated with most existing compartmental computer tools by giving the user flexibility. It allows the user the flexibility to define:

- Any number of compartments.
- Any number of contaminants and associated rates of degradation (both compartment dependent and independent).
- Any number of transfers between compartments.
- Sub-models within larger models.
- Algebraic expressions to represent transfer processes operating between compartments.
- Algebraic expressions to represent the uptake of contaminants by humans and other output quantities of interest.
- Non-linear transfer processes (e.g. solubility-limited leaching).
- Deterministic, probabilistic and time varying parameter values.

AMBER is used by 59 organisations in 24 different countries. Most of these users have focussed their application on performance assessments of nuclear waste facilities (including surface and deep facilities). A description of AMBER can be found in /QuantiSci and Quintessa 2002/; and /Enviros 2003/.

The approach followed in this study was to replicate using the AMBER code as closely as possible the conceptual model for SFR-1 employed in Project SAFE. For the near-field and biosphere, this was relatively straightforward because Project SAFE had adopted compartmental modelling approaches for these sub-systems. In so far as was possible, the AMBER model use the same number of compartments, with the same geometry and the same transfers between compartments as Project SAFE. In contrast, this was less easy for the geosphere where Project SAFE had employed an analytical approach and, thus, no direct correlation was possible with the compartments in the AMBER sub-model.

In so far as was possible, the input data used to constrain the AMBER model were the same as those used in Project SAFE (e.g. inventory data, sorption data, groundwater flow rates, etc). Data was obtained from the following sources.

- Radionuclide inventories were provided in spreadsheets by Kemakta.
- Compartment volumes and diffusive resistances were provided by Kemakta.
- Groundwater flow rates were provided in spreadsheets by Kemakta.
- Material properties of sorption, density and porosity were taken from /Lindgren et al. 2001/.

In some cases, where AMBER required numerical data that were not used in Project SAFE, especially when simulating the geosphere, the most appropriate information from other sources was used. In instances such as this (i.e. for the BLA, 1BTF and geosphere models) the data is highlighted.

Further information specific to the configuration of each disposal feature is provided below with reference to the data used to parameterise the model.

2.2 Near-field models

2.2.1 Mathematical representations

Advection

To represent the advective transport of radionuclides between adjacent compartments λ_{adv} (y^{-1}) is used

$$\lambda_{adv} = \frac{Q}{capacity} \qquad \text{(Equation 2-1)}$$

where

Q is the total flow through the compartment ($m^3\ y^{-1}$)

Capacity is the compartmental capacity (m^3)

Capacity is given by

$$capacity = \varepsilon.R.V \qquad \text{(Equation 2-2)}$$

V is the compartment volume (m^3)

ε is the effective porosity (–)

R is the retardation factor (–)

R is given by

$$R = 1 + \frac{(1-\varepsilon).\rho.K_d}{\varepsilon} \qquad \text{(Equation 2-3)}$$

ρ is the particle density ($kg\ m^{-3}$)

K_d is the sorption coefficient ($m^3\ kg^{-1}$)

Diffusion

To represent the diffusive transport of radionuclides between adjacent compartments λ_{dif} (y^{-1}) is used

$$\lambda_{dif} = \frac{1}{0.5 * (\mathrm{Re}s_i + \mathrm{Re}s_j) * capacity_i} \qquad \text{(Equation 2-4)}$$

where

Res_i is the diffusive resistance in compartment i (ym^{-3})

Res_j is the diffusive resistance in compartment j (ym^{-3})

Res is given by

$$\mathrm{Re}s = \frac{L}{A.D_e} \qquad \text{(Equation 2-5)}$$

L is the diffusion length (m)

A is the area for diffusion (m^2)

D_e is the effective diffusion coefficient (m^2y^{-1})

In order to correctly simulate diffusive transfers within AMBER it is necessary to include backwards and forwards transfers for compartments between which diffusion is occurring.

2.2.2 Silo

A schematic figure of the Silo model as used in Project SAFE is shown in Figure 2-1 /Lindgren et al. 2001/. The AMBER model was developed using this configuration of compartments with the following exception.

- Compartments numbers 37, 38, 39, 40, 41, 42, 48, 50, 51 and 52 were each sub-divided into 5 further compartments (as indicated in the key to Figure 2-1).

The configuration of the AMBER sub-model for the Silo was undertaken as follows.

- From the example NUCFLOW input files appended to /Lindgren et al. 2001/ the following information and data was obtained
  - Compartmental volumes and values of L/A (in x-, y- and z-directions) and material type.
  - Values of material density, porosity and effective diffusion.
  - Description of diffusive resistances (e.g. x-, y- or z-directions) used in transfers between compartments.
- Values of K_d were taken from /Lindgren et al. 2001/.
- Information on the distribution of the radionuclide inventory and the groundwater flowfields was taken from the original data used within the Project SAFE calculations.

/Lindgren et al. 2001/ described bitumen as being leached of the matrix at a constant rate over 100 years and this was implemented within AMBER as a non-depleting transfer of 0.01 1/y for 100 years and zero thereafter. Once the radionuclides have been leached from the bitumen matrix they are assumed to be available for transport.

Figure 2-2 shows a comparison of the estimated flux from the Silo for AMBER and NUCFLOW. The open symbols are NUCFLOW and the lines are AMBER. For the majority of radionuclide the output times for NUCFLOW and AMBER are identical, however, as NUCFLOW simulations are undertaken individually for each radionuclide some radionuclides have different output times.

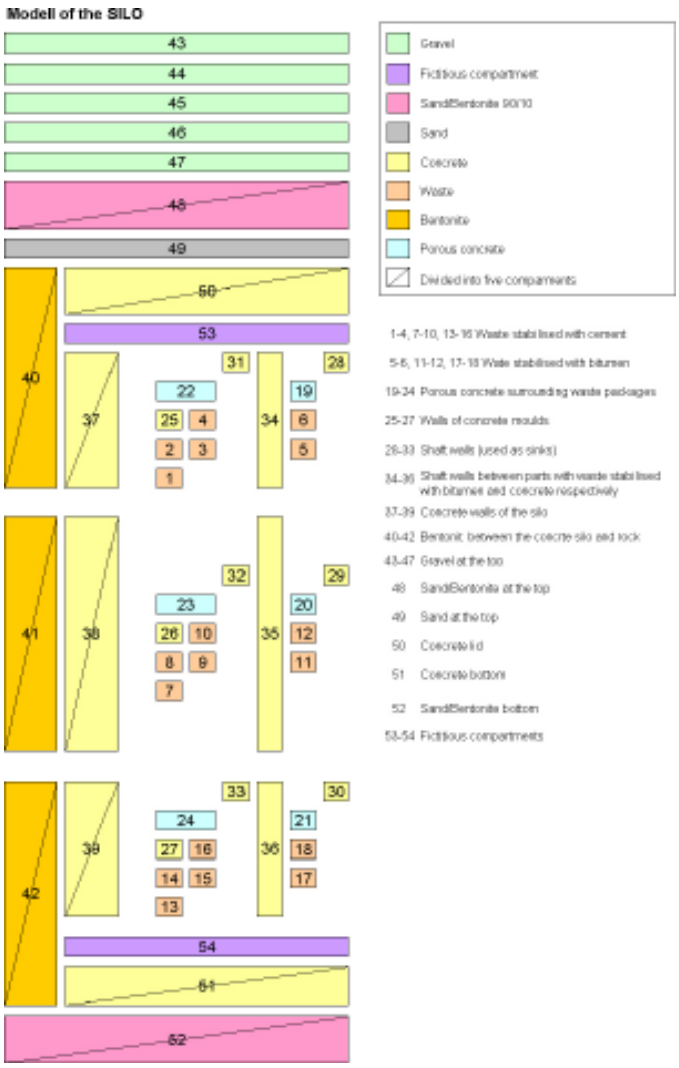

Figure 2-1. *Project SAFE Silo model /Lindgren et al. 2001/.*

The agreement for organic C-14, which is by far the dominant radionuclide in terms of near-field flux, is good, as it is for I-129. For other selected radionuclides such as Se-79, Ag-108m and Cs-135 there are some differences in the fluxes estimated by the two models with AMBER tending to slightly underestimate radionuclide fluxes.

2.2.3 BMA

A schematic figure of the BMA model as used in Project SAFE is shown in Figure 2-3 /Lindgren et al. 2001/. The AMBER model was developed using this configuration of compartments with the following exceptions.

- The “fictitious compartments” in Figure 2-3, compartment numbers 5, 6, 15, 16, 27, 28, 29, 30, 39, 40, 47, 48, 49, 50 and 121 were not considered within the AMBER model.

Configuration and parameterisation of the transfers followed the approach described previously for the Silo.

In the NUCFLOW input file for the BMA model the diffusive transport to and from the compartments representing the water inside the disposal structure is treated differently in that the diffusion resistance of the water is neglected. The transfers were also represented this way in the AMBER model, with the resistance for this transfer being taken as half the resistance of the non-water compartment.

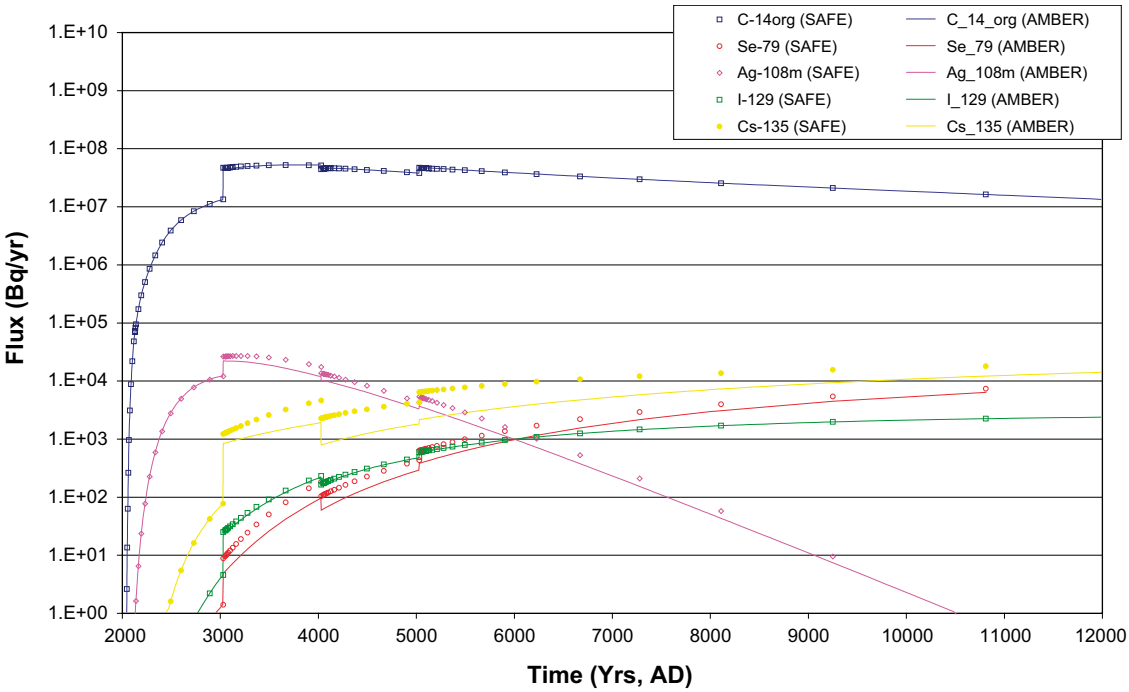

Figure 2-2. *Comparison of Silo near-field flux for selected radionuclides.*

Figure 2-3. *Project SAFE BMA model /Lindgren et al. 2001/.*

Figure 2-4 shows a comparison of the estimated flux from the BMA for AMBER and NUCFLOW. The open symbols are NUCFLOW and the lines are AMBER. For the majority of radionuclide the output times for NUCFLOW and AMBER are identical, however, as NUCFLOW simulations are undertaken individually for each radionuclide some radionuclides have different output times.

The agreement for the selected radionuclides is generally good although there are some differences in the fluxes estimated by the two models with AMBER tending to slightly underestimate radionuclide fluxes.

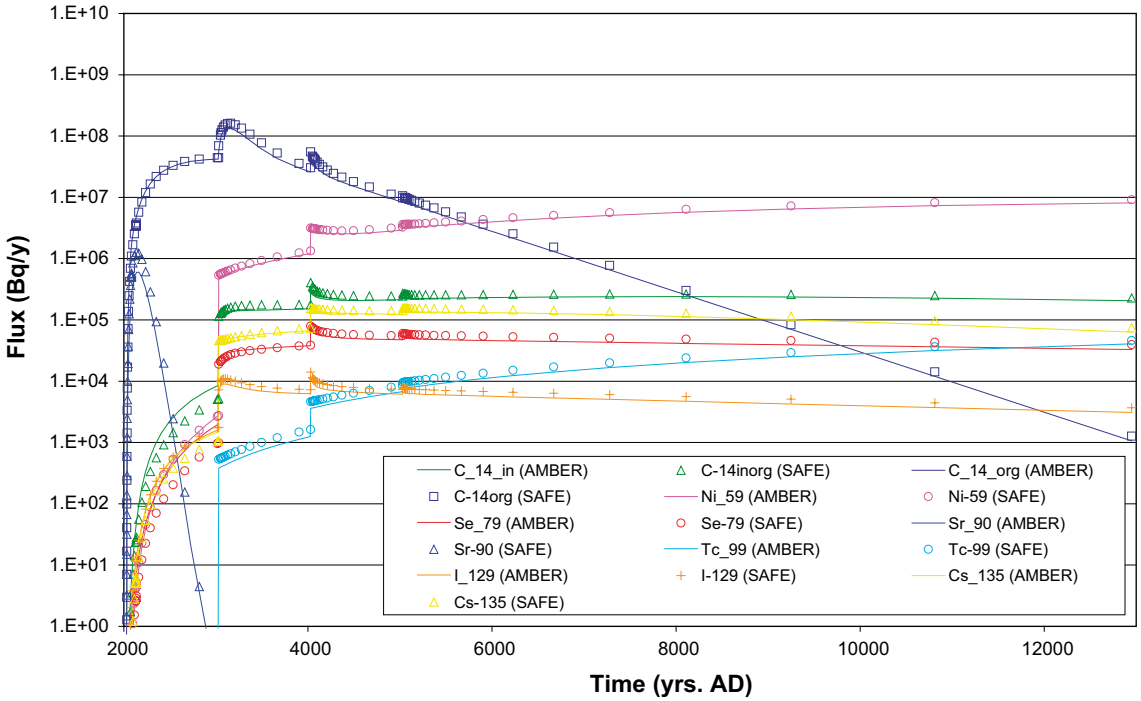

Figure 2-4. *Comparison of BMA near-field flux for selected radionuclides.*

2.2.4 1BTF

A schematic figure of the 1BTF model as used in Project SAFE is shown in Figure 2-5 /Lindgren et al. 2001/. The AMBER model was developed using this configuration of compartments with the following exceptions.

- The “fictitious compartments” in Figure 2-5, compartment numbers 1, 3, 4, 5, 7, 8, 9, 10, 11, 13, 14, 15, 16, 19, 20, 21, 23, 24, 25, 26, 29, 30, 31, 33, 34, 35, 36, 39, 40, 41, 43, 44, 45, 46, 49, 50, 63, 84, 85, 86, 87, 88, 89, 90, 91, 92, 93, 94, 95, 96, 97, 98, 99, 100, 101, 102, 103, 104, 105, 106, 107, 108, 109, 110, 111, 112, 113, 114, 115, 116, 117 and 125 were not considered within the AMBER model.

Configuration and parameterisation of the transfers followed the approach described previously for the Silo.

Figure 2-6 shows a comparison of the estimated flux from the 1BTF for AMBER and NUCFLOW. The open symbols are NUCFLOW and the lines are AMBER. For the majority of radionuclide the output times for NUCFLOW and AMBER are identical, however, as NUCFLOW simulations are undertaken individually for each radionuclide some radionuclides have different output times.

The agreement for the selected radionuclides is generally good although there are some differences in the fluxes estimated by the two models with AMBER tending to slightly underestimate radionuclide fluxes for all selected radionuclides except organic C-14 which are slightly overestimated.

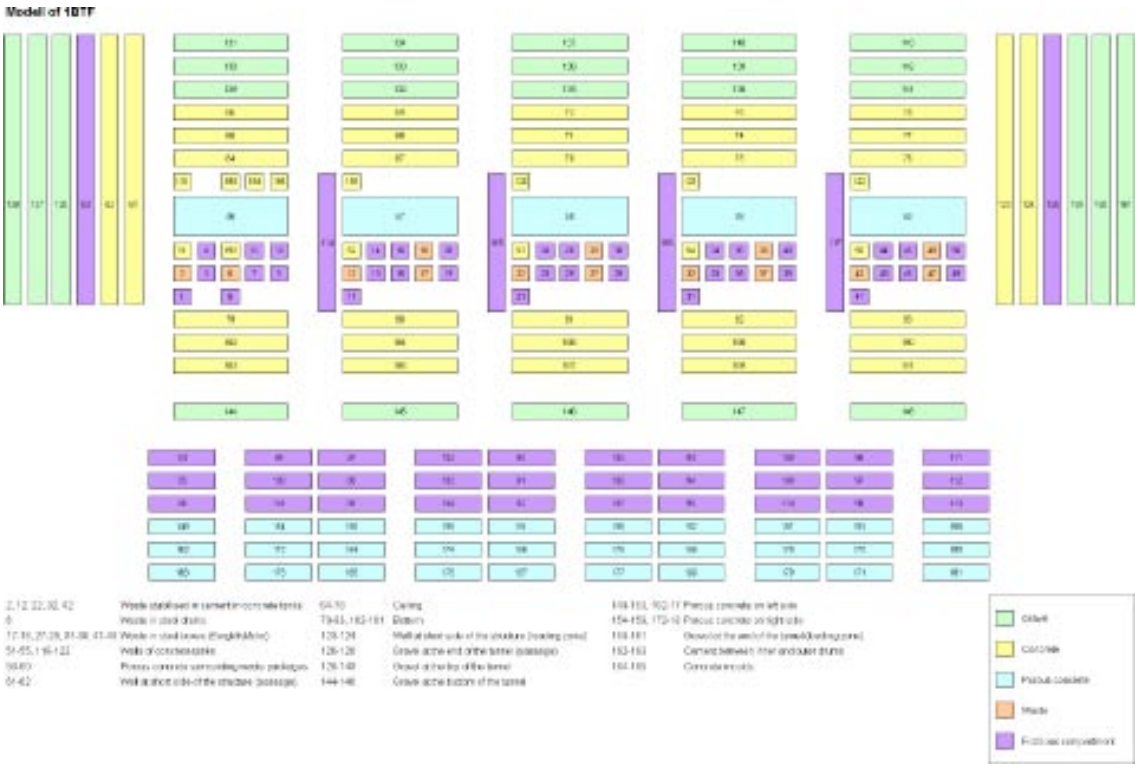

Figure 2-5. *Project SAFE 1BTF model /Lindgren et al. 2001/.*

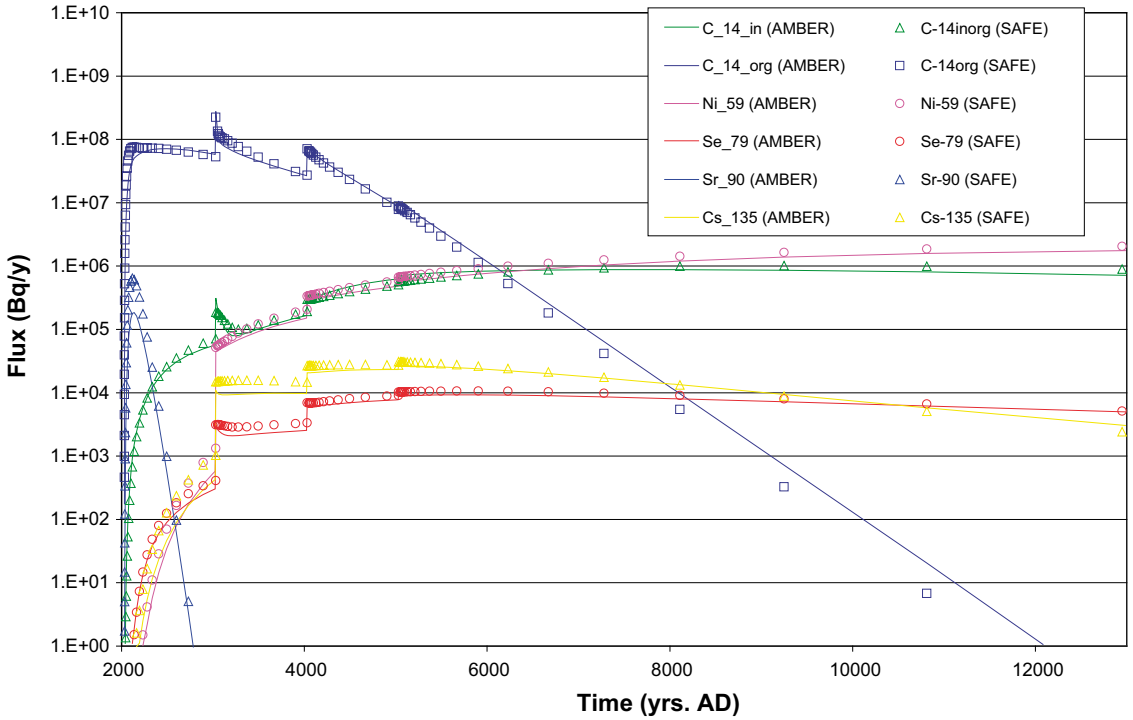

Figure 2-6. *Comparison of 1BTF near-field flux for selected radionuclides.*

2.2.5 2BTF

A schematic figure of the 2BTF model as used in Project SAFE is shown in Figure 2-7 /Lindgren et al. 2001/. The AMBER model was developed using this configuration of compartments with the following exceptions.

- The “fictitious compartments” in Figure 2-7, compartment numbers 1, 3, 4, 5, 6, 7, 8, 9, 10, 11, 13, 14, 15, 16, 17, 18, 19, 20, 21, 23, 24, 25, 26, 27, 28, 29, 30, 31, 33, 34, 35, 36, 37, 38, 39, 40, 41, 43, 44, 45, 46, 47, 48, 49, 50, 63, 84, 85, 86, 87, 88, 89, 90, 91, 92, 93, 94, 95, 96, 97, 98, 99, 100, 101, 102, 103, 104, 105, 106, 107, 108, 109, 110, 111, 112, 113, 114, 115, 116, 117 and 125 were not considered within the AMBER model.

Configuration and parameterisation of the transfers followed the approach described previously for the Silo.

Figure 2-8 shows a comparison of the estimated flux from the 2BTF for AMBER and NUCFLOW. The open symbols are NUCFLOW and the lines are AMBER. For the majority of radionuclide the output times for NUCFLOW and AMBER are identical, however, as NUCFLOW simulations are undertaken individually for each radionuclide some radionuclides have different output times.

The agreement for the selected radionuclides is generally good although there are some differences in the fluxes estimated by the two models with AMBER tending to underestimate organic C-14 fluxes in the very-long term.

2.2.6 BLA

The schematic figure of the BLA model used in Project SAFE is shown in Figure 2-9 /Lindgren et al. 2001/ and was used to develop the AMBER model.

Figure 2-7. *Project SAFE 2BTF model /Lindgren et al. 2001/.*

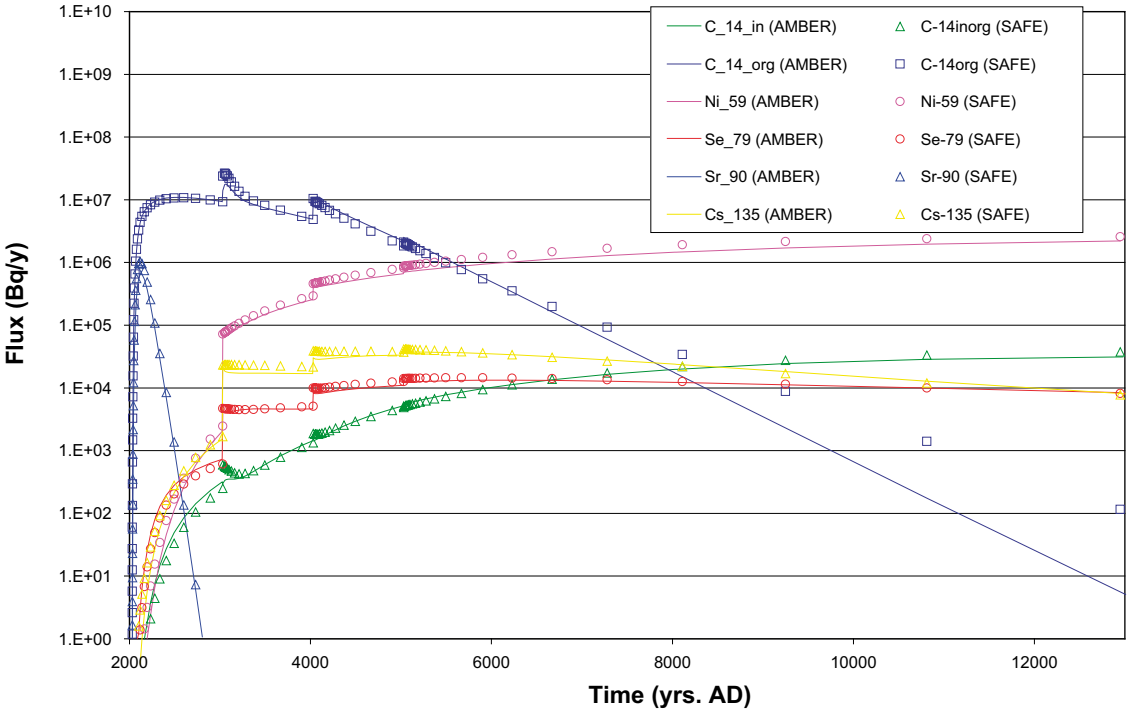

Figure 2-8. *Comparison of 2BTF near-field flux for selected radionuclides.*

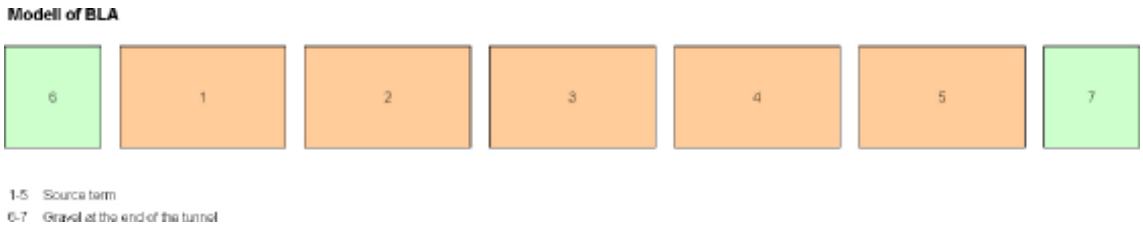

Figure 2-9. *Project SAFE BLA model /Lindgren et al. 2001/.*

Configuration and parameterisation of the transfers followed the approach described previously for the Silo. However, it should be noted that the diffusion resistances between the waste compartments were not included in the NUCFLOW input files but it is stated in /Lindgren et al. 2001/ that the BLA was considered to be a "stirred tank" (i.e. a mixing model). Values of L/A were therefore set to 1E+12 m^{-1}.

Figure 2-10 shows a comparison of the estimated flux from the BLA for AMBER and NUCFLOW. The open symbols are NUCFLOW and the lines are AMBER. For the majority of radionuclide the output times for NUCFLOW and AMBER are identical, however, as NUCFLOW simulations are undertaken individually for each radionuclide some radionuclides have different output times.

The agreement for the selected radionuclides is generally very good.

2.2.7 Summary of near-field comparisons

A summary is given below in Table 2-1 of the comparisons of the AMBER and NUCFLOW models. In each cell the upper set of numbers is from the AMBER model and bottom set are from NUCFLOW. For each set the first number is the maximum flux (Bq/y) and the second number in parentheses is the time of maximum flux (years).

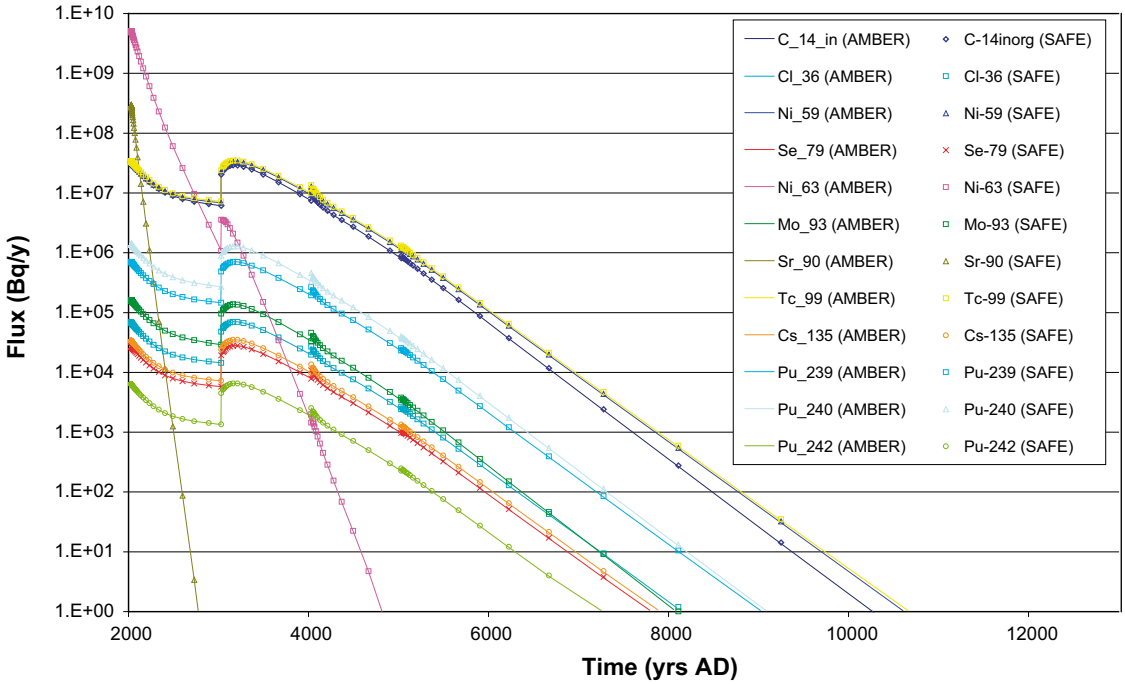

Figure 2-10. *Comparison of the BLA near-field flux for selected radionuclides.*

2.3 Geosphere model

The geosphere is represented in AMBER as a two dimensional array of compartments. In one dimension, compartments are linked together to represent the advective flow path along a fracture. The number of compartments in this dimension was chosen as 40 to reduce the effects of numerical dispersion on the simulation. In the perpendicular dimension, compartments were included to represent parts of the adjacent rock matrix that undergo diffusive exchange (matrix diffusion).

The approach is based on guidance contained in an AMBER paper on the use of AMBER to represent transport through fractured media. /Enviros and Quintessa 2005/.

Advection and dispersion

The advective transfer from compartment i (donor) to j (receptor) is given by:

$$\lambda_{A\_ij} = \frac{v}{R_f L_i} \qquad \text{(Equation 2-6)}$$

where:

$\lambda_{A,ij}$ is the contaminant transfer rate by advection from compartment *i* to *j* (y^{-1});

v is the average linear groundwater velocity (my^{-1});

R_f is the effective retardation within the fracture (–)

L_i is the length of compartment *i* (m);

Table 2-1. Summary of comparisons for AMBER near-field models and NUCFLOW models.

	C-14in	C-14org	Ni-59	Se-79	Tc-99	Ag-108m	I-129	Cs-135	Cs-137
Silo	3.189E+00 (1.3E+04)	5.269E+07 (1.9E+03)	3.895E+03 (1.3E+04)	1.075E+04 (1.3E+04)	2.266E–03 (1.3E+04)	2.206E+04 (1.1E+03)	2.628E+03 (1.3E+04)	1.888E+04 (1.3E+04)	9.068E+00 (3.1E+02)
	3.616E+00 (1.3E+04)	5.228E+07 (1.6E+03)	1.122E+04 (1.3E+04)	1.163E+04 (1.3E+04)	3.400E–03 (1.3E+04)	2.706E+04 (1.2E+03)	2.625E+03 (1.3E+04)	2.318E+04 (1.3E+04)	8.786E+00 (3.1E+02)
BMA	3.430E+05 (2.0E+03)	1.344E+08 (1.1E+03)	8.631E+06 (1.3E+04)	7.718E+04 (2.0E+03)	4.937E+04 (1.3E+04)	6.511E+05 (1.0E+03)	1.216E+04 (2.0E+03)	1.421E+05 (2.0E+03)	8.958E+04 (1.3E+02)
	4.045E+05 (2.0E+03)	1.612E+08 (1.1E+03)	9.740E+06 (1.3E+04)	7.954E+04 (2.0E+03)	5.543E+04 (1.3E+04)	6.400E+05 (1.0E+03)	1.410E+04 (2.0E+03)	1.559E+05 (2.0E+03)	7.292E+04 (1.3E+02)
1BTF	8.793E+05 (6.0E+03)	2.766E+08 (1.0E+03)	1.838E+06 (1.3E+04)	9.288E+03 (3.6E+03)	7.223E+03 (1.3E+04)	1.416E+05 (1.0E+03)	1.322E+03 (3.0E+03)	2.676E+04 (3.0E+03)	2.242E+03 (1.6E+02)
	1.021E+06 (7.2E+03)	2.229E+08 (1.0E+03)	2.137E+06 (1.3E+04)	1.067E+04 (3.9E+03)	8.450E+03 (1.3E+04)	1.914E+05 (1.0E+03)	1.506E+03 (3.0E+03)	3.098E+04 (3.0E+03)	7.331E+03 (1.6E+02)
2BTF	3.123E+04 (1.1E+04)	1.775E+07 (1.0E+03)	2.335E+06 (1.3E+04)	1.330E+04 (4.2E+03)	9.763E+03 (1.3E+04)	2.502E+05 (1.0E+03)	1.908E+03 (3.0E+03)	3.748E+04 (3.0E+03)	1.151E+04 (1.6E+02)
	3.810E+04 (1.1E+04)	2.640E+07 (1.0E+03)	2.646E+06 (1.3E+04)	1.450E+04 (3.9E+03)	1.182E+04 (1.3E+04)	2.748E+05 (1.0E+03)	2.090E+03 (3.0E+03)	4.168E+04 (3.0E+03)	3.749E+04 (1.1E+02)
BLA	3.233E+07 (0)	2.710E+04 (0)	3.332E+07 (1.1E+03)	2.808E+04 (1.1E+03)	3.496E+07 (1.1E+03)	1.840E+06 (0)	2.108E+03 (1.1E+03)	3.508E+04 (1.1E+03)	3.098E+09 (0)
	3.230E+07 (0)	2.712E+04 (0)	3.316E+07 (1.1E+03)	2.793E+04 (1.1E+03)	3.482E+07 (1.1E+03)	1.838E+06 (0)	2.097E+03 (1.1E+03)	3.494E+04 (1.1E+03)	3.097E+09 (0)

The inclusion of effective retardation in the fracture results from considering a thin layer of matrix and so

$$R_f = 1 + a_w d_0 \theta R_m \qquad \text{(Equation 2-7)}$$

Where

a_w is the flow wetted surface area ($m^2\ m^{-3}$)

d_0 is the thickness of the thin layer (m)

θ is the matrix porosity (–)

R_m is the retardation within the rock matrix (–)

$$R_m = 1 + \rho.K_d/\theta \qquad \text{(Equation 2-8)}$$

ρ is the rock matrix density ($kg\ m^{-3}$)

K_d is the distribution coefficient for the rock matrix ($m^3\ kg^{-1}$)

The following relationship was used to determine an approximate value of d_0.

$$d_0 = \sqrt{\frac{2D_e t_f}{\theta R_m}} \qquad \text{(Equation 2-9)}$$

Where

D_e is the effective matrix diffusion coefficient ($m^2\ y^{-1}$)

t_f is the travel time (y)

A value of 0.0001 m for d_0 was estimated using data for plutonium as this is the most strongly sorbed radionuclide and so requires the finest resolution. This value for used for all radionuclides.

The forward and backward dispersive transfers are given by:

$$\lambda_{D\_ij} = \lambda_{D\_ji} = \frac{\frac{\nu * L_{tot}}{R_f P_e} - \frac{\nu * L_i}{2 * R_f}}{L_i^2} \qquad \text{(Equation 2-10)}$$

where:

$\lambda_{D,ij}$ is the contaminant transfer rate by dispersion from compartment i to j (y^{-1})

$\lambda_{D,ji}$ is the contaminant transfer rate by dispersion from compartment j to i (y^{-1})

L_{tot} is the total flow path length (m)

Pe is the Peclet number (–).

Matrix diffusion

The rate of diffusion from the fracture into the initial matrix compartment, λ_{RMD_in1}, is given by:

$$\lambda_{RMD\_in1} = \frac{2a_w D_e}{R_f d_1} \qquad \text{(Equation 2-11)}$$

Where

d_1 is the depth of the initial matrix compartment (m)

The rate of diffusion from matrix compartment *j* to *j+1* is given by:

$$\lambda_{RMD\_inj,j+1} = \frac{2D_e}{\vartheta R_m d_j (d_j + d_{j+1})} \qquad \text{(Equation 2-12)}$$

Where

d_j is the depth of the matrix compartment *j* (m)

d_{j+1} is the depth of the matrix compartment *j+1* (m)

The rate of diffusion from the initial matrix compartment into fracture, λ_{RMD_out1}, is given by:

$$\lambda_{RMD\_out1} = \frac{2D_e}{\vartheta R_m d_1^{\,2}} \qquad \text{(Equation 2-13)}$$

The rate of diffusion from matrix compartment *j+1* to *j* is given by:

$$\lambda_{RMD\_inj+1,j} = \frac{2D_e}{\vartheta R_m d_{j+1} (d_j + d_{j+1})} \qquad \text{(Equation 2-14)}$$

The data used in the revised model is shown in Table 2-2. Data for K_d and D_e were taken from /Lindgren et al. 2001/.

Figure 2-11 shows a comparison of the estimated geosphere flux from the BLA for AMBER and FARF. The open symbols are FARF and the lines are AMBER. For the majority of radionuclide the output times for FARF and AMBER are identical, however, as FARF simulations are undertaken individually for each radionuclide some radionuclides have different output times.

Generally AMBER estimates the maximum fluxes of conservative (e.g. Cl-36 and Mo-93) and slightly sorbing radionuclides (e.g. Ni-59, Ni-63, Sr-90) well although AMBER tends to slightly underestimate the tails of the breakthrough curves for slightly sorbing radionuclides. The plots for strongly sorbing radionuclides Tc-99 and Pu-239 show some differences which are particularly apparent for the breakthrough when the contributions from dispersion are important.

A summary is given below in Table 2-3 of the comparison of the AMBER and FARF model results. The results for release from the BLA are chosen to correspond to the figure above. In each cell the upper set of numbers are from the AMBER model and bottom set are from FARF. For each set the first number is the maximum flux (Bq/y) and the second number in parentheses is the time of maximum flux (years).

Table 2-2. Compilation of geosphere data.

Parameter	Value	Reference
Travel time, t_f, (y)	50	/Lindgren et al. 2001/
Peclet number, P_e (–)	10	/Lindgren et al. 2001/
Flow wetted surface area, a_w, ($m^2\ m^{-3}$)	120	/Lindgren et al. 2001/
Matrix porosity, θ, (–)	0.005	/Lindgren et al. 2001/
Pathlength, L_{tot}, (m)	60	Assumed
Groundwater velocity, υ, ($m\ y^{-1}$)	1.2	Calculated as L_{tot}/t_f
Depth of thin matrix layer, d0, (m)	0.0001	Calculated for Pu
Depth of 1st matrix compartment, d1 (m)	0.0005	Fitted so that the total depth of the matrix compartments matches the maximum diffusion depth in the FARF31 calculations of 2.0 m
Depth of 2nd matrix compartment, d2, (m)	0.0025	
Depth of 3rd matrix compartment, d3, (m)	0.0125	
Depth of 4th matrix compartment, d4, (m)	0.0625	
Depth of 5th matrix compartment, d5, (m)	0.3125	
Depth of 6th matrix compartment, d6, (m)	1.6095	

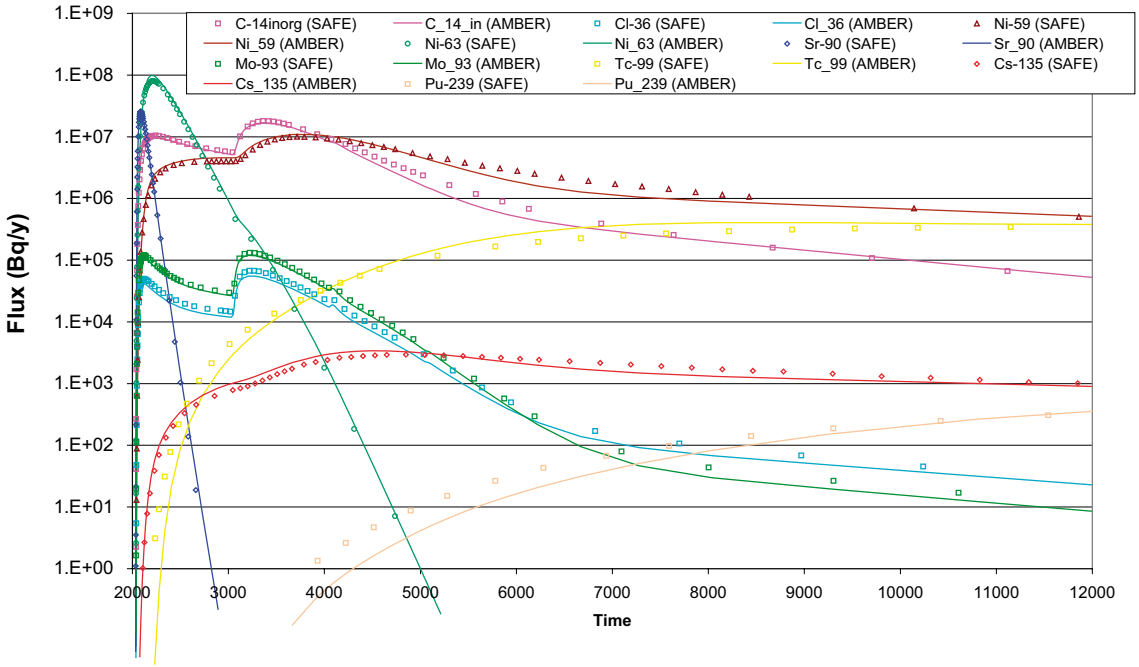

Figure 2-11. *Results from AMBER geosphere model (release from AMBER BLA model).*

Table 2-3. Summary of comparisons for AMBER geosphere models and FARF.

	C-14 inorganic	Cl-36	Ni-59	Ni-63	Sr-90	Tc-99	Cs-135
BLA	1.690E+7 (1.3E+03)	5.524E+4 (1.2E+03)	1.089E+7 (1.6E+03)	9.893E+7 (1.6E+02)	2.579E+7 (5.8E+01)	4.066E+5 (6.0E+03)	3.400E+3 (2.5E+03)
	1.797E+7 (1.3E+03)	6.727E+4 (1.2E+03)	1.006E+7 (1.7E+03)	8.010E+7 (1.8E+02)	2.547E+7 (5.8E+01)	3.486E+5 (1.1E+04)	2.940E+3 (2.8E+03)

It is considered that AMBER is capable for producing an acceptable agreement to FARF for the purposes of a post-closure safety assessment.

2.4 Biosphere model

The biosphere models considered within Project SAFE are described by /Karlsson et al. 2001/, and provide the basis for the AMBER biosphere calculations considered. The scenario assessing release during reasonable biosphere development is considered here.

The endpoint is the biological uptake from multiple exposure pathways and the resulting maximum annual radiation dose (Sv y^{-1}) to an average individual of the inhabiting population.

As in Project SAFE, AMBER also applies a first-order differential equation to numerically solve each transfer expression between compartments and uses transfer coefficients, or rate constants, to model the annual migration and accumulation of radionuclides.

For the reasonable biosphere development case, the various defined stages of biosphere development comprise: release into today's biosphere conditions (prevailing until 5,000 AD), release to a lake (prevailing until 8,000 AD) and release to agricultural land (prevailing until 12,000 AD). Figure 2-12 below illustrates the progressive biosphere development.

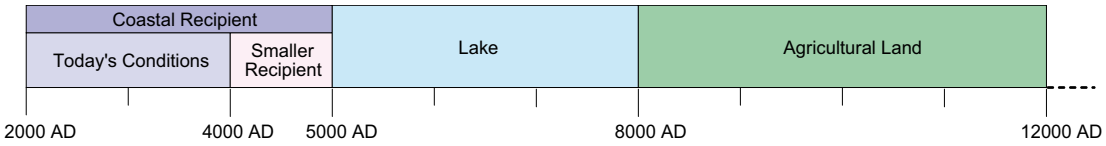

Figure 2-12. *Timeline of stages in Reasonable Biosphere Development*

2.4.1 Configuration of RBD model in AMBER

These changes in the biosphere conditions affect the exposure pathways through which radionuclides are taken-up by human and non-human biota. Information on the biosphere configuration within Project SAFE was taken from /Karlsson et al. 2001/. A fuller description of the mathematical relationships and data used is given in Appendix A.

Of particular note within the reasonable biosphere development was the need to represent the evolution from coastal recipient, to a lake and then to agricultural land. As part of the representation of evolution contamination resulting from activity that was discharged earlier is conserved in later biosphere models. This is done conveniently in AMBER by having continuity of the relevant compartments, as indicated below.

- Model area upper sediment.
- Agricultural land deep soil.
- Lake sediment.
- Agricultural land top soil.
- Model Area sediment.
- Agricultural land saturated solid.

In order to ensure that the biosphere models are configured correctly within AMBER it is necessary to encode all the transfers within the models and then ensure that the correct sub-set of transfers only operate within the appropriate time period. This was achieved by using time-dependent parameters as "on-off" switches (which multiplied transfer rates by 0 to turn them off and by 1 to turn them on).

Two parameters required further consideration before they could be represented in AMBER. They are the calculation of radionuclide concentrations in:

- irrigated root crops, and
- irrigated root vegetables.

The concentration of radionuclides in irrigated root crops, U_i (Bq kg^{-1}), in /Karlsson et al. 2001/ is given as:

$$U_i = C_s.RUF_R + \sum_{0}^{Nr_{IRR}} I.TL.C_w \qquad \text{(Equation 2-15)}$$

where

C_s = Concentration of radionuclides in soil (Bq kg^{-1}dw) from the dispersion model

RUF_R = Root uptake factors for root crops (soil to plant transfer factors) ((Bq kg^{-1} ww)/ Bq kg^{-1} dw))

Nr_{IRR} = Number of irrigation occasions (y^{-1})

I = Remaining water on the vegetation after each irrigation occasion (m)

TL = Translocation from plant surface to edible parts of plant, ((Bq kg^{-1}ww)/(Bq m^{-2}))

C_w = Concentration of radionuclides in irrigation water (Bq m^{-3}), from the dispersion model

This was implemented in AMBER as follows:

$$U_i = C_s.RUF_R + Nr_{IRR2}.I.TL.C_w \qquad \text{(Equation 2-16)}$$

where

Nr_{IRR2} = Annual number of irrigation events (–)

The concentration of radionuclides in irrigated root vegetables, U_v (Bq kg^{-1}), in /Karlsson et al. 2001/ is given as:

$$U_v = C_s.RUF_v + \frac{C_w}{Y_v}.\frac{I}{t_{tot}}.\sum_{Nr_{IRR}}\int_0^{t_n} e^{-\tau.t_n}\,dt \qquad \text{(Equation 2-17)}$$

where

C_s = Concentration of radionuclides in soil (Bq kg^{-1}dw), from the dispersion model

RUF_v = Root uptake factor for vegetables (soil to plant transfer factor) ((Bq kg^{-1} ww)/ Bq kg^{-1} dw))

C_w = Concentration of radionuclides in irrigation water (Bq m^{-3}), from dispersion model

Y_v = Yield of vegetables (kg m^{-2}·y^{-1})

I = Remaining water on the vegetation after each irrigation occasion (m)

t_{tot} = Irrigation period, fraction of year (y^{-1})

Nr_{IRR} = Number of irrigation occasions per year (y^{-1})

t_n = Time between last irrigation occasion and harvest (days)

τ = ln2/$T_{½w}$ where $T_{½w}$ = weathering half-life (day)

This was implemented in AMBER as follows:

$$U_v = C_s.RUF_v + Nr_{IRR}\frac{C_w}{Y_v}.\frac{I}{t_{tot}}.\frac{1}{\tau}\left(1-e^{-\tau t_n}\right) \qquad \text{(Equation 2-18)}$$

The Project SAFE biosphere calculations were undertaken probabilistically using sampled parameters, some of which were correlated. Correlated datasets were produced external to AMBER using the @risk software. Simulations of 1000 Monte Carlo samples were performed, a similar number to the runs in Project SAFE and the results are shown below for release from the BMA. The open symbols are Project SAFE results and the solid lines are sampled AMBER calculations. Overall it can be seen that the AMBER runs with sampled and correlated datasets show a good agreement with the Project SAFE results.

It should be noted that the BMA source term used in Figure 2-13 is from AMBER not NUCFLOW and therefore also shows the result of propagating differences from the near-field models through the biosphere.

2.4.2 Modifications to RBD model

The Authorities' review /SKI and SSI 2004/ noted the concerns with the RBD model which have been addressed through simple modifications.

1. "The coastal model comprises three sub-models of different geographical scales – the model area (a few km^2), Grepen (hundreds of km^2) and the Baltic Sea (thousands of km^2). The radionuclides from the repository are directly taken to the water phase in the calculation model for the model area and can then be transported to Grepen and out into the Baltic Sea. A certain sedimentation of radionuclides in the water phase is assumed to occur. The review committee considers that the modeling should also include the possibility that radionuclides can enter the biosphere through sediment in order to, thereby, take into consideration the

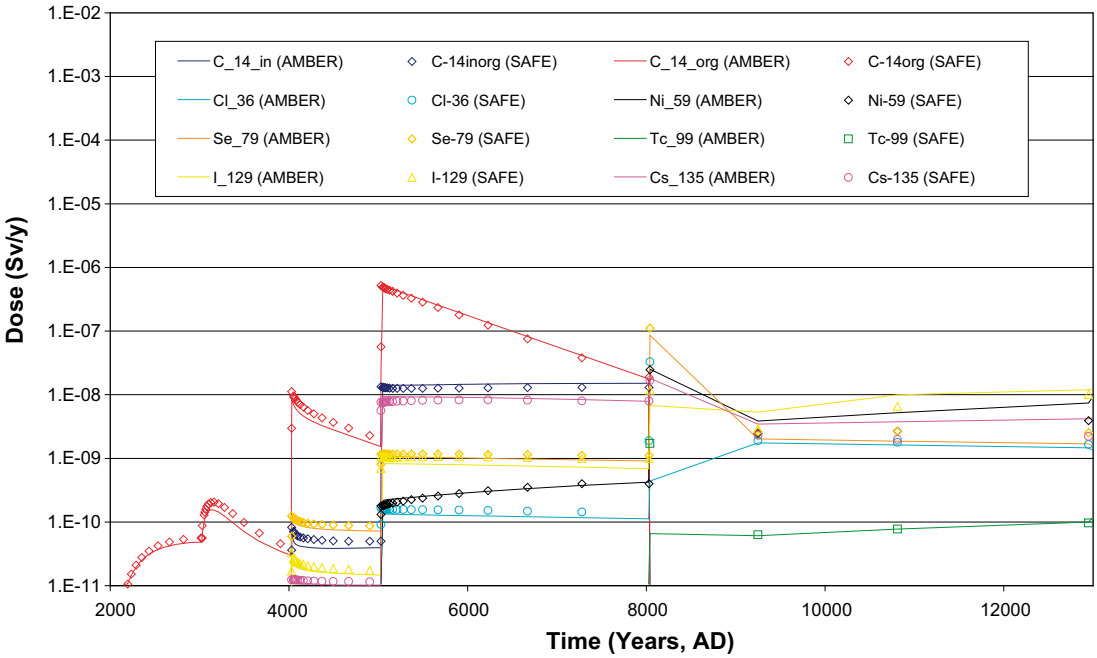

Figure 2-13. *Comparison of probabilistic simulations for RBD (release from AMBER BMA model).*

accumulation of radionuclides in the sediment that this can lead to. Such an accumulation could mean that additional radioactive substances could become available at a later stage in the arable soil in the agricultural model. In turn, this could result in greater consequences than the present calculations show. "

2. "SKB states that the most significant consequences can be expected in the discharge area from the repository, and therefore this has been defined as a model area. In the view of the review committee, while this in itself may be a reasonable assumption, it would like to emphasize that this should be better justified with respect to the fact that a very substantial portion of radionuclides leave the model area in the surface or groundwater, depending on the ecosystem and it is not clear what effects these radionuclides can have on man and the environment in the near field (or further away)."

The first issue concerning the representation of the geosphere-biosphere interface zone (GBIZ) was addressed using the approach developed in the interim report for SR-Can /SKB 2004/ and shown below in Figure 2-14.

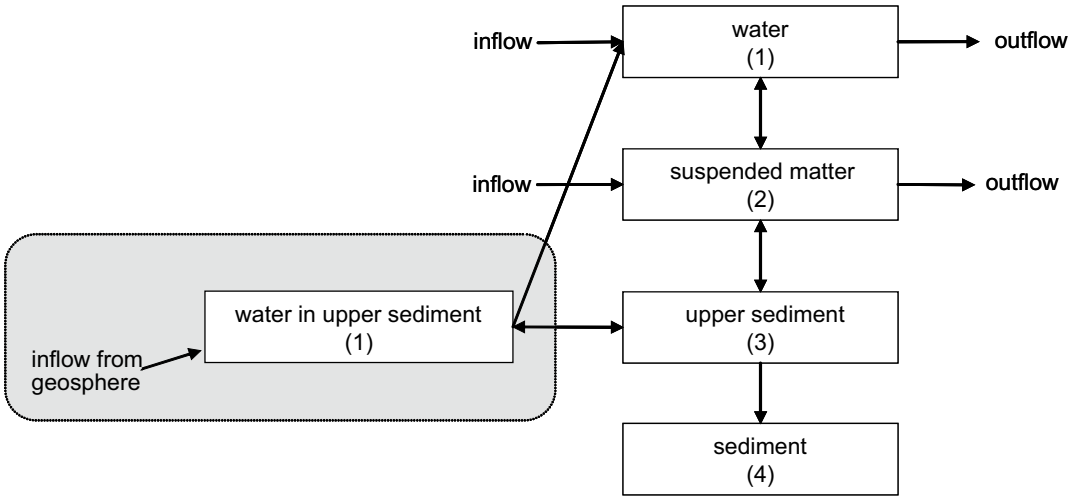

Figure 2-14. *Modified GBIZ for release to marine and lake waters (redrawn from /SKB 2004/).*

Transport from (5) to (1) (TC_{51}) is expressed as

$$TC_{51} = \frac{\ln 2}{\frac{DS}{V_{adv}}} \qquad \text{(Equation 2-19)}$$

The exchanges between (5) and (3) are expressed as

$$TC_{53} = \frac{K_d \rho}{\varepsilon} \frac{\ln 2}{T_k} \qquad \text{(Equation 2-20)}$$

$$TC_{35} = \frac{\ln 2}{T_k} \qquad \text{(Equation 2-21)}$$

Where

K_d is the distribution coefficient (m^3/kg)

ε is the sediment porosity (–)

ρ is the sediment bulk density (kg/m^3)

T_k is the half-time to reach sorption equilibrium (y)

DS is the depth of upper sediment (m)

V_{adv} is the velocity of water flow from the upper sediment to the water body (m/y)

The revised approach considers the release of radionuclides into a compartment which represents the porewater in the upper sediment layer in the module of interest (coastal or lake). Radionuclides exchange between the upper sediment and its porewater in response to sorption and desorption and release from the upper sediment porewater to coastal or lake water is also considered.

The data required to parameterise these exchanges are all available in the original biosphere model /Karlsson et al. 2001/ with the exception of the groundwater velocity within the upper sediment porewater which was taken to be the same as the groundwater flow rate used in the geosphere (Table 2-2).

The running waters biosphere as described in /Bergström et al. 1999/ was used as a basis for an additional exposure scenario inserted into the existing RBD model in order to address the second issue. The addition implemented was used to assess the outflow from the lake which was assumed to be confined to a river from which water was taken to irrigate a domestic garden on which produce was grown and consumed, the river was also a source of drinking water and fish were caught from it. The concentrations of radionuclides within the river water were assumed to be diluted by the addition of surface run-off from uncontaminated areas of the river's catchment.

The river bed sediments were not assumed to be available for use as agricultural land later due to their limited extent.

The modified AMBER model layout is shown below in Figure 2-15 with the additional compartments for the river model highlighted on the left of the screenshot.

The river receives radionuclides from turnover of water and suspended sediment from the lake.

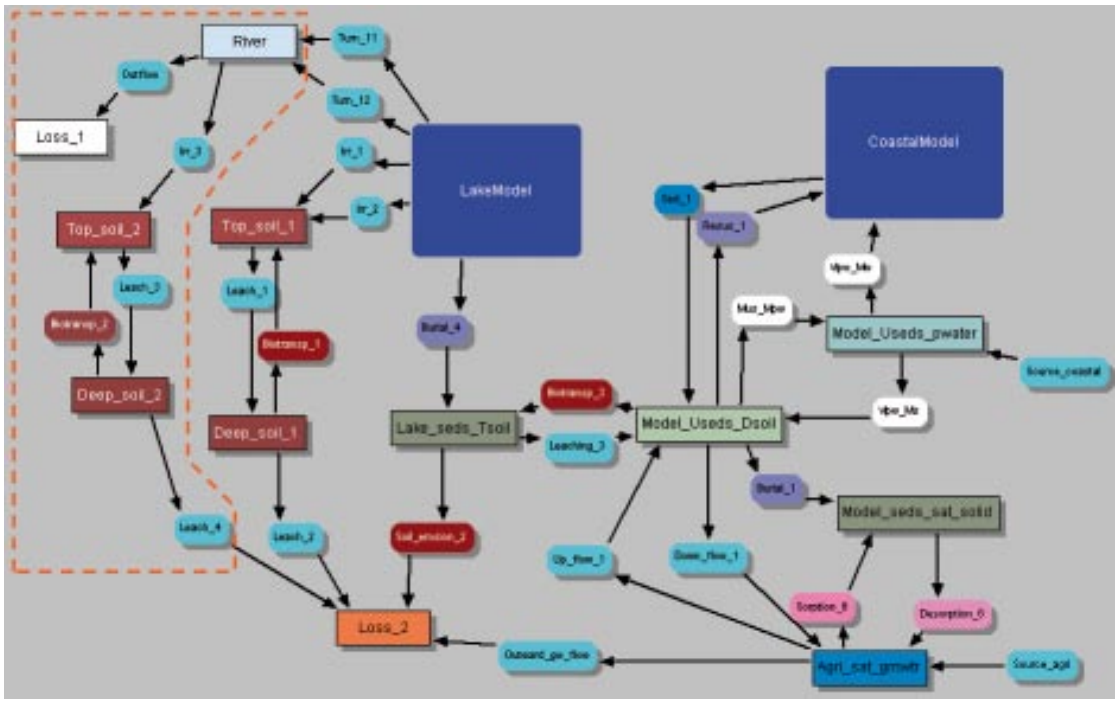

Figure 2-15. *AMBER screenshot highlighting additional river model added to RBD.*

Each transfer is identical and is represented as:

$$\lambda_{turnover} = \frac{1}{RT\_lake} \qquad \text{(Equation 2-22)}$$

where

RT_lake is the retention time within the lake (y) (an existing RBD parameter)

These transfers existed previously and in effect all that has been done is routing of them from a loss compartment to a compartment that is used to represent a river.

Water is removed from the river to irrigate a plot of land and this is represented as:

$$\lambda_{irrigation} = \frac{V_{irr} * N_{irr} * A_{irr}}{Volume_{river}} \qquad \text{(Equation 2-23)}$$

where

V_{irr} is the volume of water used in each irrigation event ($m^3/m^2/y$) (an existing RBD parameter)

N_{irr} is the number of irrigation events per year (–) (an existing RBD parameter)

A_{irr} is the area irrigated (in this case a garden) (m^2) (an existing RBD parameter)

$Volume_{river}$ is the mixing volume of the river compartment (m^3)

$Volume_{river}$ was calculated as A_c * Runoff * 1 (y) after /Jones et al. 2004/

where

A_c is the catchment area (m^2) (2E+07 m^2, taken from /Jones et al. 2004/)

Runoff is the runoff ($m^3/m^2/y$) (an existing RBD parameter)

Outflow from the river is taken to be same as the inflow. The exposure pathways considered are:

- Consumption of water.
- Consumption of fish.
- Consumption of milk and meat.
- Consumption of cereals, root crops and green vegetables.
- Consumption of soil.
- Inhalation of resuspended particles from soil.
- External exposure from contaminated ground.

No additional data is required to represent these exposure pathways as they are the same as those considered within the lake model. The same correlation factors are also assumed to apply here.

3 Data for calculations

The following calculations have been undertaken and reported in order to support the Project SAFE update.

- The most likely Base Scenario ('Most likely scenario').
- An alternative inventories based on more conservative assumptions.
- Alternative near-field flow fields based on different calibration techniques used in the supporting hydrogeological model.
- Uncertainties in radionuclide sorption in the near-field.
- A case which considers the combination of the alternative inventories and near-field flow fields.

3.1 Most likely scenario

Following the Authorities' review comments on the base scenario presented in Project SAFE /SKI and SSI 2004/, SKB has chosen to clarify the most likely Base scenario ('Most likely scenario').

A description of the Most likely scenario is given by /Wiborgh 2005/ and is summarised below.

- Repository – Intact engineered barriers
  - All engineered barriers initially assumed to be as designed
  - Barrier properties remain unchanged over time
  - Groundwater flow through the repository changes due to land uplift.
- Geosphere – Retardation
  - Radionuclide retardation is accounted for
  - Constant conditions assumed throughout the assessment period.
- Biosphere – Reasonable biosphere development
  - Release of radionuclides to Öregrundsgrepen during the time period 2,000 AD to 5,000 AD
  - Release to a lake during the period 5,000 AD to 8,000 AD
  - Release to agricultural land during the period 8,000 AD to 12,000 AD.

The following near-field parameters were identical to those described for the Base scenario main case (intact barriers) in /Lindgren et al. 2001/.

- Facility designs
- Compartment dimensions
- Material properties
  - Sorption coefficients
  - Effective diffusivities
  - Density
  - Porosity
  - Ratio of diffusion length to cross sectional area.
- Near-field flow fields

A major change to the near-field data was the inclusion of a revised inventory, which included the following differences to that originally considered within Project SAFE.

- Overall waste arisings have been estimated on the basis of 40 years of reactor operations /Johansson 2004, Torstenfeldt 2005a/.
- Additional measurements have been undertaken for C-14, Ni-59, Ni-63 and I-129 to improve the estimates for these radionuclides /Torstenfeldt 2005b/.
- The amount of organic C-14 is assumed to be 19% of total C-14 for the Silo, BMA and BLA and 10% of total C-14 for the BTF /Magnusson and Stenström 2005, Torstenfeldt 2005c/.

The inventory for the Most likely scenario is summarised below in Table 3-1. All those radionuclides (and decay chains) included within Project SAFE were considered in these calculations.

Table 3-1. Inventory for Most likely scenario.

Radionuclide	Inventory (Bq) Silo	BMA	1BTF	2BTF	BLA
H-3	5.50E+10	4.35E+09	6.82E+08	4.84E+08	3.51E+07
C-14 inorganic	1.88E+12	4.84E+11	1.65E+12	4.93E+10	1.91E+09
C-14 organic	4.40E+11	1.13E+11	1.83E+11	5.47E+09	4.47E+08
Cl-36	2.21E+09	5.03E+08	3.32E+08	4.53E+07	1.42E+06
Co-60	8.26E+13	7.01E+12	3.24E+12	4.53E+07	1.11E+11
Ni-59	6.54E+11	1.68E+11	8.30E+09	1.87E+10	6.59E+08
Ni-63	9.32E+13	2.20E+13	1.26E+12	2.35E+12	9.45E+10
Se-79	8.84E+08	2.01E+08	1.13E+07	1.81E+07	5.68E+05
Sr-90	1.02E+13	1.87E+12	1.66E+11	1.86E+11	7.61E+09
Zr-93	1.29E+10	3.32E+09	1.43E+08	6.68E+07	1.30E+07
Nb-93m	4.37E+11	6.68E+10	8.11E+09	7.68E+09	4.59E+08
Nb-94	1.29E+09	3.31E+09	1.64E+08	3.69E+08	1.30E+07
Mo-93	6.41E+09	1.65E+09	7.14E+08	3.32E+08	6.47E+06
Tc-99	1.11E+12	2.51E+11	1.41E+10	2.27E+10	7.10E+08
Pd-107	2.21E+08	5.03E+07	2.82E+06	4.53E+06	1.42E+05
Ag-108m	7.39E+10	1.86E+10	9.55E+08	2.08E+09	4.60E+08
Cd-113m	3.00E+10	4.50E+09	6.19E+08	2.72E+08	2.65E+07
Sn-126	1.11E+08	2.51E+07	1.41E+06	2.26E+06	7.10E+04
I-129	7.53E+08	1.71E+08	9.61E+06	1.54E+07	4.84E+05
Cs-135	1.11E+09	2.51E+08	1.41E+07	2.27E+07	7.10E+05
Cs-137	1.06E+14	2.13E+13	1.70E+12	1.52E+12	7.79E+10
Sm-151	5.11E+11	1.09E+11	7.08E+09	9.40E+09	3.45E+08
Eu-152	3.59E+09	4.91E+08	1.12E+09	2.89E+07	2.21E+09
Eu-154	2.51E+12	2.94E+11	6.29E+10	1.11E+10	2.98E+09
Ho-166m	5.07E+09	1.30E+09	5.67E+08	2.62E+08	5.12E+06
Pu-238	3.45E+10	5.12E+10	6.44E+08	4.10E+08	7.11E+07
Pu-239	7.98E+09	2.37E+09	4.76E+08	3.59E+08	1.74E+07
Pu-240	1.59E+10	4.73E+09	4.08E+08	6.03E+02	3.48E+07
Pu-242	7.17E+07	3.97E+07	1.95E+06	1.08E+06	1.11E+05
Am-241	4.94E+11	1.20E+10	1.05E+09	2.10E+08	5.83E+07
Total	3.00E+14	5.38E+13	8.30E+12	4.18E+12	3.01E+11

In order to input this inventory into the AMBER models it was assumed that it was distributed between compartments in the same manner as for Project SAFE[1].

The approach to modelling the geosphere has been described previously in Section 2.2 and this approach was for the Most likely scenario. All geosphere parameters were taken from /Lindgren et al. 2001/ with the additional data for the AMBER representation as summarised in Table 2-2.

The biosphere was the modified RBD model with the changed GBIZ and additional river exposure model as described in Section 2.4.2. However, it should be noted that the model conditions at 1,200 AD were assumed to remain until up to 1,000,000 years post-closure in order that extended estimates of dose could be calculated in the very long-term. It is not considered likely that the model conditions will remain constant for such a period of time given the likelihood that the area may undergo several cycles of extreme environmental change resulting in periodic glaciations and therefore these estimates have a degree of uncertainty associated with them. However, the agricultural biosphere conditions were used as a means of measuring the potential very long-term exposures that could result from the release of long-lived and/or relatively immobile radionuclides.

3.2 Alternative inventory

The Alternative inventory considered is the conservative inventory reported in /Riggare and Johansson 2001/ and previously used in Project SAFE /Lindgren et al. 2001/. The only change made to the inventory was that the amounts of organic C-14 were estimated using the same approach as for the Most likely scenario inventory (i.e. 19% of total C-14 for the Silo, BMA and BLA and 10% for the BTF). The total amount of C-14 remained unchanged for Project SAFE. This inventory is summarised in Table 3-2 and was in input to AMBER using the same approach as described for the Most likely scenario inventory.

Table 3-3 summarises the ratio of the Alternative inventory (Table 3-2) to the inventory from 40 years reactor operations used in the Most likely scenario (Table 3-1). Cells shaded red highlight values in which the Alternative inventory is greater than that of the Most likely scenario by a factor of 50 or more. Cells shaded orange highlight values in which the Alternative inventory is greater than that of the Most likely scenario by a factor of between 1 and 50. Cells shaded grey highlight values in which the Alternative inventory is lower than that of the Most likely scenario.

It can be seen that overall the inventories for each of the disposal facilities are increased for the Alternative inventory. Relatively few radionuclides show increased inventories for the Most likely scenario BMA: Zr-93, I-129; 1BTF: Cl-36, I-129; BLA: Eu-152.

The geosphere and biosphere remain unchanged from the Most likely scenario.

[1] There is an exception in the case of the BMA as in the original Project SAFE calculations there were 6 compartments in BMA that were previously assumed to have 0% organic carbon but in the Most likely scenario the C-14 was distributed within these compartments as 19% organic and 81% inorganic as in the remainder of the BMA waste.

Table 3-2. Alternative inventory.

Radionuclide	Inventory (Bq)				
	Silo	BMA	1BTF	2BTF	BLA
H-3	5.79E+11	3.32E+10	3.25E+09	5.28E+09	6.62E+08
C-14 inorganic	1.73E+13	1.68E+12	2.23E+12	2.66E+11	3.16E+10
C-14 organic	4.05E+12	3.95E+11	2.48E+11	2.95E+10	7.41E+09
Cl-36	4.71E+10	3.39E+09	3.04E+08	5.40E+08	8.17E+07
Co-60	1.80E+15	7.07E+13	5.43E+12	9.06E+12	1.03E+12
Ni-59	2.14E+13	2.09E+12	1.83E+11	2.96E+11	3.91E+10
Ni-63	3.56E+15	3.24E+14	2.89E+13	4.69E+13	6.16E+12
Se-79	1.88E+10	1.36E+09	1.21E+08	2.16E+08	3.27E+07
Sr-90	2.42E+14	1.36E+13	1.30E+12	2.31E+12	3.61E+11
Zr-93	2.14E+10	2.09E+09	1.83E+08	2.97E+08	3.92E+07
Nb-93m	7.58E+12	4.86E+11	4.72E+10	7.64E+10	9.72E+09
Nb-94	2.14E+11	2.09E+10	1.82E+09	2.96E+09	3.91E+08
Mo-93	1.06E+11	1.04E+10	9.08E+08	1.47E+09	1.95E+08
Tc-99	2.36E+13	1.70E+12	1.52E+11	2.70E+11	4.08E+10
Pd-107	4.71E+09	3.39E+08	3.04E+07	5.40E+07	8.17E+06
Ag-108m	1.23E+12	1.18E+11	1.04E+10	1.68E+10	2.22E+09
Cd-113m	8.25E+11	3.62E+10	3.64E+09	6.45E+09	1.03E+09
Sn-126	2.36E+09	1.70E+08	1.52E+07	2.70E+07	4.08E+06
I-129	1.41E+09	1.02E+08	9.11E+06	1.62E+07	2.45E+06
Cs-135	2.36E+10	1.70E+09	1.52E+08	2.70E+08	4.08E+07
Cs-137	2.48E+15	1.42E+14	1.35E+13	2.39E+13	3.74E+12
Sm-151	1.13E+13	7.52E+11	6.86E+10	1.22E+11	1.86E+10
Eu-152	9.24E+10	3.98E+09	4.38E+11	7.11E+08	1.13E+08
Eu-154	7.86E+13	2.67E+12	2.79E+11	4.79E+11	7.63E+10
Ho-166m	8.43E+10	8.19E+09	7.16E+08	1.16E+09	1.53E+08
Pu-238	2.81E+12	1.50E+11	1.15E+10	8.89E+09	8.52E+09
Pu-239	2.78E+11	1.49E+10	1.18E+09	9.07E+08	8.48E+08
Pu-240	5.55E+11	2.97E+10	2.35E+09	1.81E+09	1.69E+09
Pu-242	2.51E+09	1.34E+08	1.06E+07	8.16E+06	7.63E+06
Am-241	6.09E+12	4.31E+10	3.39E+09	2.61E+09	2.45E+09
Total	8.26E+15	5.61E+14	5.28E+13	8.38E+13	1.15E+13

Table 3-3. Ratio of Alternative inventory to inventory for most like scenario.

Radionuclide	Silo	BMA	1BTF	2BTF	BLA
H-3	11	8	5	11	19
Inorganic C-14	9	3	1	5	17
Organic C-14	9	3	1	5	17
Cl-36	21	7	1	12	58
Co-60	22	10	2	200,087	9
Ni-59	33	12	22	16	59
Ni-63	38	15	23	20	65
Se-79	21	7	11	12	57
Sr-90	24	7	8	12	47
Zr-93	2	1	1	4	3
Nb-93m	17	7	6	10	21
Nb-94	166	6	11	8	30
Mo-93	17	6	1	4	30
Tc-99	21	7	11	12	58
Pd-107	21	7	11	12	58
Ag-108m	17	6	11	8	5
Cd-113m	27	8	6	24	39
Sn-126	21	7	11	12	58
I-129	2	1	1	1	5
Cs-135	21	7	11	12	58
Cs-137	23	7	8	16	48
Sm-151	22	7	10	13	54
Eu-152	26	8	391	25	0
Eu-154	31	9	4	43	26
Ho-166m	17	6	1	4	30
Pu-238	82	3	18	22	120
Pu-239	35	6	2	3	49
Pu-240	35	6	6	3,002,166	49
Pu-242	35	3	5	8	69
Am-241	12	4	3	12	42
Total	28	10	6	20	38

3.3 Alternative near-field flow fields

The Project SAFE assessment calculations were underpinned by a study in which hydrogeological models at different levels of discretisation were undertaken (from a regional model to local models to detailed models of individual disposal tunnels or caverns) /Holmén and Stigsson 2001ab/. These models provided information on groundwater flows into and out of the repository, geosphere flowpaths and discharge areas.

The Authorities' review /SKI and SSI 2004/ noted the following concerns in relation to the hydrogeological modelling of SFR-1.

"Taking into account the considerable importance of the groundwater flow for engineered barrier degradation and radionuclide transport from SFR 1, it is vital that the flow data that are used should be adequately supported. However, the review committee has identified several weaknesses in SKB's hydrogeological modeling work, including the representation of heterogeneity, calibration and justification of material data for different repository parts. It is also a deficiency that a thorough uncertainty analysis is lacking. In the light of this, the review committee does not consider that SKB has convincingly justified the groundwater flows that have been used in the consequence analysis for SSR 2001."

In order to address this SKB has commissioned further hydrogeological modelling studies /Holmén 2005/. The general purpose of this additional study was to estimate the uncertainty in the calibration of the hydrogeological model of SFR-1 (reported in /Holmén and Stigsson 2001a/) and to explore the effect of these uncertainties on the values of tunnel flow previously estimated.

It is important here to note the different models used in the hydrogeological studies and their relationship to the flow fields developed for the original Project SAFE calculations undertaken using NUCFLOW. This information is shown schematically in Figure 3-1.

It should be noted that whilst the uncertainty analysis in /Holmén 2005/ is confined to the Local Model, the repository flow fields used in the consequence calculations undertaken in NUCFLOW were derived from the Detailed Model, which was reported in /Holmén and Stigsson 2001b/. Therefore a means is required of considering the effects of the uncertainty studies of /Holmén 2005/ on the repository flow fields.

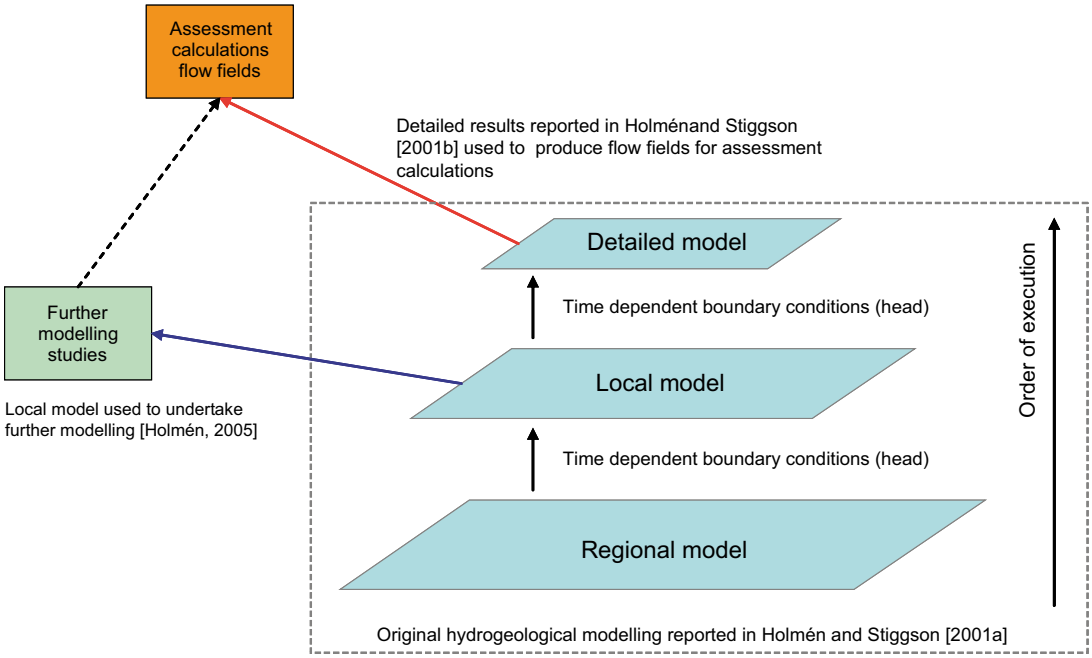

Figure 3-1. *Relationship between hydrogeological studies and assessment calculations.*

'Uncertainty factors' were calculated and presented in /Holmén 2005/ which relate the results of that study to the corresponding flow values given in /Holmén and Stigsson 2001a/.

It is stated in /Holmén 2005/ that the uncertainty factors maybe used in combination with the detailed results given in /Holmén and Stigsson 2001a/; because by multiplying the detailed results given in /Holmén and Stigsson 2001a/ with an uncertainty factor, it is possible to derive a value of flow from /Holmén and Stigsson 2001a/ that corresponds to a certain uncertainty.

As a means of exploring the sensitivities it was assumed that a simple linear relationship can be used such that a repository flow field is multiplied by the appropriate uncertainty factor in order to explore the effects of calibration uncertainty on groundwater flow through the repository. This obviously assumes that there is a direct and linear relationship between the Local Model and Detailed Model flow components.

Values of uncertainty factors are presented for two cases in /Holmén 2005/[2].

- The base case, in which the rock mass between identified fracture zones was defined as homogeneous, consistent with the structural geological interpretation applied in /Holmén and Stigsson 2001a/.
- An alternative case, in which the rock mass between identified fracture zones was defined as heterogeneous. The alternative case is also consistent with the structural geological interpretation applied in /Holmén and Stigsson 2001a/, as all identified fracture zones are included in the sensitivity case. However, this case also includes an additional heterogeneity within the rock mass. The heterogeneity of the permeability field between identified fractures zones is unknown and so this case seeks to explore the sensitivity of tunnel flows to this uncertainty.

Only those values for the homogeneous rock mass summarised in Table 3-3 (the base case in /Holmén 2005/) were used in the sensitivity analysis.

The uncertainty factors were parameterised as cumulative distribution functions (CDF) within @risk and the arithmetic average of 1,000 samples of each CDFs was taken[3]. These values are tabulated in Table 3-4 and then used within AMBER as a multiplier of the original flow values. For example, for the Silo the original flow fields at 2,000 AD and 3,000 AD were multiplied by 0.71 and the original flow fields at 4,000 AD and 5,000 AD were multiplied by 1.02.

The geosphere and biosphere remain unchanged from the Most likely scenario.

---

[2] It should be noted that there appears to be a slight confusion in /Holmén 2005/ at this point. It is stated in Chapter 9 of /Holmén 2005/ that the uncertainty factor (F) is calculated as

$F = Q_{NEW\_Percentile} / Q_{OLD\_Calibrated}$

$Q_{NEW\_Percentile}$ = Flow of /Holmén 2005/) for a certain percentile.

$Q_{OLD\_Calibrated}$ = Calibrated flow of /Holmén and Stigsson 2001a/.

This would suggest that *F* is dimensionless as shown in Figures 9-1 to 9-10 and Figures 10-21 to 10-30 of /Holmén 2005/, whereas in Tables 9-1, 9-2, 10-3 and 10-4 of /Holmén 2005/ it is given units of (m^3/year). For the purposes of this study it has been assumed that *F* is dimensionless.

[3] In order to specify a CDF within @risk the maximum and minimum values are required. These were not given within /Holmén 2005/ so it was therefore assumed for the BMA, BTF and BLA that the minimum value was 0.1 below the 1st percentile and the maximum value was 0.1 above the 95th percentile and for the Silo the minimum value was 0.01 below the 1st percentile and the maximum value was 0.01 above the 95th percentile.

Table 3-3. Uncertainty factors from /Holmén 2005/.

Percentiles	Uncertainty factors at 2,000 AD				
	BMA	BLA	1BTF	2BTF	Silo
1	2.3	0.6	0.5	0.4	0.47
5	2.6	0.6	0.5	0.5	0.49
10	2.7	0.7	0.6	0.6	0.50
20	2.9	0.8	0.7	0.6	0.56
30	3.1	0.8	0.7	0.7	0.61
40	3.2	0.9	0.8	0.7	0.67
50	3.4	1.0	0.9	0.8	0.69
60	3.5	1.2	1.1	1.0	0.72
70	3.7	1.4	1.3	1.3	0.76
80	4.2	1.6	1.5	1.4	0.83
90	5.0	2.1	2.0	1.9	0.95
95	5.8	2.6	2.4	2.3	1.04
Percentiles	**Uncertainty factors at 4,000 AD**				
	BMA	**BLA**	**1BTF**	**2BTF**	**Silo**
1	2.4	2.2	2.7	2.3	0.69
5	2.5	2.3	2.8	2.4	0.70
10	2.7	2.7	3.2	2.7	0.75
20	2.9	2.9	3.6	2.9	0.79
30	3.0	3.1	3.7	3.1	0.87
40	3.2	3.3	4.3	3.5	0.92
50	3.3	3.6	4.8	3.9	0.96
60	3.6	4.2	5.7	4.7	0.99
70	3.9	4.9	7.0	5.8	1.09
80	4.5	5.4	7.5	6.2	1.25
Percentiles	**Uncertainty factors at 4,000 AD**				
	BMA	**BLA**	**1BTF**	**2BTF**	**Silo**
90	5.2	7.1	9.8	8.1	1.44
95	6.5	8.6	11.7	9.9	1.59

Table 3-4. Flow multiplication factors used in AMBER sensitivity calculations.

	2,000 AD	4,000 AD
Silo	0.71	1.02
BMA	3.62	3.67
1BTF	1.15	5.65
2BTF	1.07	4.75
BLA	1.25	4.29

3.4 Uncertainties in radionuclide sorption in the near-field

The Authorities' review /SKI and SSI 2004/ noted the following concerns in relation to the derivation of the K_d values used in the Project SAFE calculations.

"There are weaknesses in the data for the selection of K_d values with respect to sorption in the near field (cement, gravel and bentonite). The review committee would like to see a more detailed discussion of uncertainties and realism of chosen data, which for example includes how sorption of important nuclides are affected by factors such as pH, redox, speciation, ion strength, measurement uncertainty, conversion of sorbants. In the opinion of the review committee, a sensitivity analysis should also have been conducted for the K_d values of the near field, especially to illustrate the effects during the initial Baltic Sea period. For the K_d values in the biosphere models, a sensitivity analysis has been presented /Karlsson et al. 2001/, however, not for other parts of the system."

Cement/concrete, sand/gravel, bentonite and sand/bentonite are the near-field materials recommended for study by the Authorities.

/Cronstrand 2005/ has compiled and tabulated the relevant sorption values for use in the sensitivity study which are reproduced here as Tables 3-5 to 3-8. The recommended values are those used in the Most likely scenario and the minimum and maximum values are those to be used within the sensitivity calculations.

Two simulations were undertaken

- Minimum near-field sorption using minimum sorption coefficient values.
- Maximum near-field sorption using maximum sorption coefficient values.

Table 3-5. Sorption coefficients for concrete and cement /Cronstrand 2005/.

Element	Sorption coefficients (m^3 kg^{-1})		
	Min	Max	Recommended
H	0	0	0
C (inorganic)	0.01	4	0.2
C (organic)	0	0	0
Cl	0.0006	0.06	0.006
Ni	0.008	0.2	0.04
Co	0.004	0.4	0.04
Se	0.0001	0.4	0.006
Sr	0.0005	0.05	0.001
Zr	0.05	5	0.5
Mo	0.0001	0.4	0.006
Nb	0.1	2.5	0.5
Tc	0.05	5	0.5
Pd	0.004	0.4	0.04
Ag	0.00002	0.05	0.001
Cd	0.002	0.8	0.04
Sn	0.025	10	0.5
I	0.0003	0.03	0.003
Cs	0.0001	0.01	0.001
Sm	1	25	5
Eu	1	25	5
Ho	1	25	5
Pu	1	25	5
Am	0.2	5	1

Table 3-6. Sorption coefficients for Bentonite /Cronstrand 2005/.

Element	Sorption coefficients (m^3 kg^{-1})		
	Min	Max	Recommended
H	0	0	0
C (inorganic)	0	0	0
C (organic)	0	0	0
Cl	0	0	0
Ni	0.004	0.1	0.02
Co	0.002	0.2	0.02
Se	0	0.003	0
Sr	0.0002	0.005	0.001
Zr	0.002	1	0.05
Mo	0	0.003	0
Nb	0	0.2	0
Tc	0.001	0.1	0.01
Pd	0	0.1	0
Ag	0	0.005	0
Cd	0.001	0.4	0.02
Sn	0.0005	0.2	0.01
Cs	0.0005	0.05	0.005
Sm	0.04	1	0.2
Eu	0.04	1	0.2
Ho	0.04	1	0.2
Pu	0.2	5	1
Am	0.2	5	1

Table 3-7. Sorption coefficients for sand and gravel /Cronstrand 2005/.

Element	Sorption coefficients (m^3 kg^{-1})		
	Min	Max	Recommended
H	0	0	0
C (inorganic)	0.00002	0.01	0.0005
C (organic)	0	0	0
Cl	0	0	0
Ni	0.002	0.05	0.01
Co	0.001	0.1	0.01
Se	0.00001	0.03	0.0005
Sr	0.00002	0.0005	0.0001
Zr	0.05	5	0.5
Nb	0.1	2.5	0.5
Tc	0.03	3	0.3
Pd	0.0001	0.01	0.001
Ag	0.0002	0.5	0.01
Cd	0.0005	0.2	0.01
Sn	0	0.01	0
Cs	0.001	0.12	0.01
Sm	0.2	5	1
Eu	0.2	5	1
Ho	0.2	5	1
Pu	0.2	5	1
Am	0.2	5	1

Table 3-8. Sorption coefficients for sand-bentonite mixture /Cronstrand 2005/.

Element	Sorption coefficients (m^3 kg^{-1})		
	Min	Max	Recommended
H	0	0	0
C (inorganic)	0.00002	0.009	0.0005
C (organic)	0	0	0
Cl	0	0	0
Ni	0.002	0.05	0.01
Co	0.001	0.1	0.01
Se	0.000009	0.03	0.0005
Sr	0.00004	0.001	0.0002
Zr	0.02	9	0.5
Mo	0	0.0004	0
Nb	0.1	2	0.5
Tc	0.01	5	0.3
Pd	0.0001	0.02	0.0009
Ag	0.0002	0.45	0.009
Cd	0.0005	0.2	0.01
Sn	0.00005	0.03	0.001
I	0	0.0001	0
Cs	0.0008	0.1	0.01
Sm	0.2	5	0.9
Eu	0.2	5	0.9
Ho	0.2	5	0.9
Pu	0.2	5	1
Am	0.2	5	1

The geosphere and biosphere remain unchanged from the Most likely scenario.

3.5 Combination of Alternative inventory and near-field flow fields

This sensitivity calculation used the Alternative inventory described in Section 3.2 and the Alternative near-field flow fields described in Section 3.3.

The geosphere and biosphere remain unchanged from the Most likely scenario.

4 Most likely scenario results

This section presents the results for the Most likely scenario (results for the sensitivity calculations, are presented in Chapter 6). This section is sub-divided into six sections, one for each disposal facility and one for SFR-1 as a whole. All the sub-sections have the same structure: firstly, the release from the near-field is presented; secondly, the geosphere flux is presented; thirdly the doses to the RBD and River models are presented. The final sub-section contains an additional tabulated summary of the peak radionuclide fluxes from the near-field and geosphere and the peak biosphere doses, along with estimates of the times of peaks and the key radionuclides (or disposal facilities) whose contributions dominate the flux or dose at the time of the peak.

Due to the extended period of the simulation time and the relatively few output times used for the biosphere calculations[4], the lines on the graphs are interpolated between points. For this reason it is considered appropriate that the timings given for maximum doses (and fluxes) are reported as approximate values only.

The reasonable development of the biosphere in the area of SFR-1 assumes that the release of radionuclides from the time of closure of the repository to around 5,000 AD occurs to a coastal recipient corresponding to a part of Öregrundsgrepen. It is assumed that the conditions of today prevail until around 4,000 AD. After this the size of Öregrundsgrepen is assumed to decrease as a consequence of the land rise and therefore a smaller water volume and therefore increased retention times have been assumed for the time period 4,000 AD to 5,000 AD. After around 5,000 AD the release of radionuclides occurs to a lake which has developed in the area. This lake is used as a recipient until around 8,000 AD when it is assumed that this area is drained and used for agricultural purposes.

As was noted in Section 3.1 the simulation time has been extended up to 1,000,000 years post-closure in order that extended estimates of dose could be calculated in the very long-term. These estimates are based on assuming that the model conditions that exist at 12,000 AD remain consistent for this extended time period. There is therefore a degree of uncertainty associated with such estimates, however, the consideration of such timescales provides a means of measuring the potential very long-term exposures that could result from the release of long-lived and/or relatively immobile radionuclides. In order to emphasis such uncertainties the times 10,000 years post-2030 AD and 100,000 years post-2030 are highlighted when presenting the results.

The results are presented in graphs where the radionuclide flux (Bq/y) or the arithmetic mean of the individual annual dose or "dose" (Sv/y) is plotted as a function of time. Most commonly log-scales are used on both axes in order to readily present a range of data. As seen in Figure 4-1, for example, there is often a sudden increase, or sometimes a decrease, in near-field radionuclide flux, especially evident at 1,000 years post-closure. This is an artefact which results from the method used to represent time-dependent flowfields within the near-field model (the continuously changing flowfields are represented by a series of discrete stepwise changes). The effects in the near-field are propagated into the geosphere and biosphere as well. The doses estimated for the reasonable biosphere development also show sudden increases at around 4,000 AD and 5,000 AD, as well as an increase or decrease at 8,000 AD. These stepwise changes in dose are due to changes in the characteristics of the biosphere (e.g. shallowing of the Öregrundsgrepen, change to the Lake period etc).

In general the doses increase as the Reasonable Biosphere Development model changes from Öregrundsgrepen to a coast with smaller water volume as well as when the coast changes to a lake. This is mainly due to decreased dilution as water volumes decrease and retention times

[4] It was considered necessary to use a reduced number of output times for the probabilistic biosphere simulations in order to keep the AMBER output files of manageable size.

increase. Another important factor is that additional exposure pathways are considered in the lake model compared to the coastal models as freshwater is also used for consumption and irrigation. The agricultural land model is very different from the other used as the radionuclide release occurs to the soil instead of to sediment. In the agricultural land model the accumulation of radionuclides in soil is an important process whereas dilution is the most important process in the coastal and lake models.

In the agricultural land model it is also assumed that radionuclides which have accumulated in sediments earlier during the coastal and lake stages are present within the soil and available for exposure to humans. This can be seen as a peak in the dose curves at around 8,000 AD. Processes like erosion of the uppermost soil layer and mixing between soil layers results in a decrease of the accumulated radionuclides with time leading to decreasing doses. For some radionuclides it can be seen that the dose curves increase again after an initial decrease. This is because additional quantities of radionuclides are supplied from the groundwater which discharges into the soil.

One radionuclide which deserves special attention here is C-14 for which the dose curves decrease drastically when the use of the agricultural land model starts. This is due to the fact that no root uptake of carbon is considered in the model (carbon is fixed by the green parts above the ground). For the purposes of this model humans are assumed only to intake C-14 via inadvertent consumption of soil (e.g. via insufficiently washed vegetables) and through the consumption of milk and meat from cattle which have consumed contaminated soil when grazing. This leads to a much lower exposure for C-14 in the agricultural land model compared to other radionuclides, which are also taken up by crops. C-14 is also one of the radionuclides which give the highest doses in the lake model (the uptake in fish is very large) which exacerbates the impression that the doses decrease at around 8,000 AD.

4.1 Silo

Figure 4-1 shows the near-field radionuclide flux from the Silo for the Most likely scenario. The peak radionuclide flux occurs at around 3,900 AD and is of the order of 1.3E+07 Bq/y. It can be seen that up to around 50,000 years post-2030 AD the radionuclide flux is dominated by the breakthrough of organic C-14, during this period a small release of H-3 is estimated at about 2,100 AD (six orders of magnitude below the overall maximum) and a larger release of Ag-108m peaks at around 3,100 AD (four orders of magnitude below the overall maximum). Fluxes of Cl-36, Se-79, Mo-93, I-129 and Cs-135 are also important between 10,000 and 100,000 years post-2030 AD (although they are least four orders of magnitude below the overall maximum) and in the very long-term the key radionuclides are Ni-59 and Tc-99 but these are at least three orders of magnitude below the overall maximum.

Figure 4-2 shows the geosphere radionuclide flux from the Silo for the Most likely scenario. Overall the trends shown by the geosphere radionuclide flux are similar to those of the near-field radionuclide flux: the timing and magnitude of the maximum flux are the same order as for the near-field radionuclide flux. 1.2E+07 Bq/y at around 3,800 AD; up to around 50,000 years post-2030 AD the radionuclide flux is dominated by the breakthrough of organic C-14; fluxes of Cl-36, Se-79, Mo-93, I-129 and Cs-135 are also important between 10,000 and 100,000 years post-2030 AD (again at least four orders of magnitude below the overall maximum); the key radionuclides for the very long-term are Ni-59 and Tc-99 but these are also again at least three orders of magnitude below the overall maximum. The main differences are the lack of an observable H-3 breakthrough and the delay in the breakthrough of Se-79, Ag-108m and Cs-135 and reduction in the magnitude of the peak fluxes.

Figure 4-3 shows the doses estimated to the RBD model from the Silo Most likely scenario. The maximum dose, 6.5E–07 Sv/y, is estimated to occur at around 5,100 AD during the lake period. The dominant radionuclide during the initial 6,000 years (i.e. during the coastal and lake periods) is organic C-14 (there is also a minor contribution from I-129 during the lake period). During the agricultural period the key radionuclide is I-129.

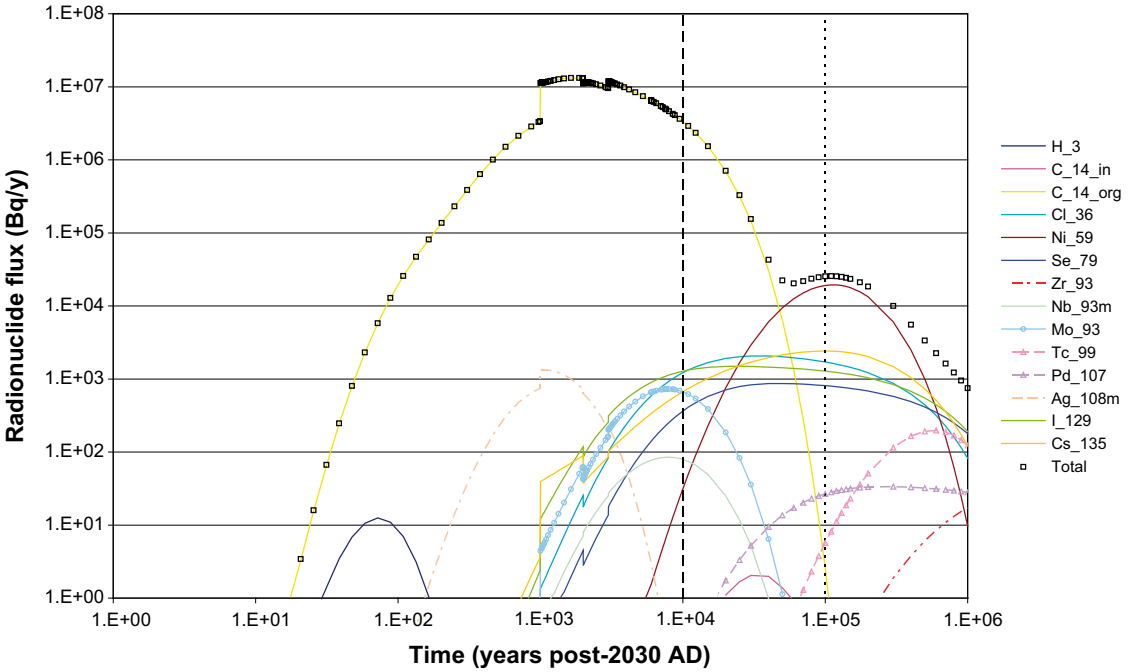

Figure 4-1. *Silo near-field radionuclide fluxes for Most likely scenario.*

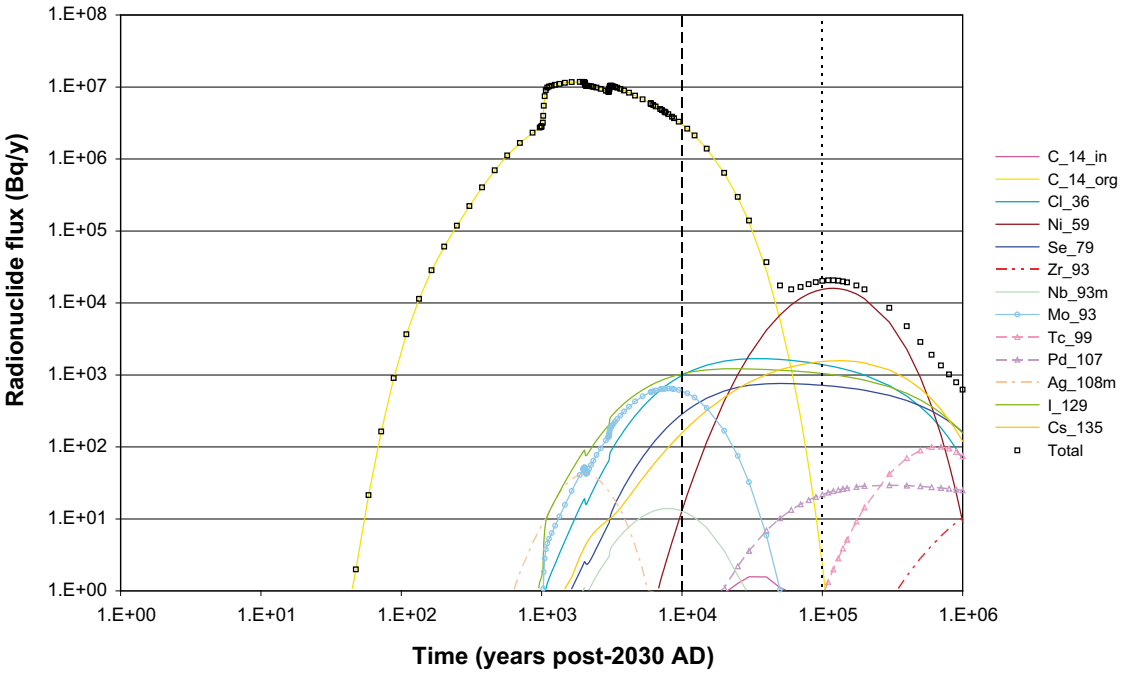

Figure 4-2. *Silo geosphere radionuclide fluxes for Most likely scenario.*

Figure 4-4 shows the doses estimated to the River model from the Silo Most likely scenario (please note that the x-axis is not a logarithmic scale). The maximum dose, 1.2E–07 Sv/y, is solely due to contributions from organic C-14. The maximum dose is estimated to occur at the same time as the maximum dose from the RBD model but the maximum dose in the RBD model is larger than that for the River model by a factor of approximately 5. The lower doses from the River model compared to those from the Lake are due to the dilution that occurs downstream which arises from the input of clean water from the river catchment area.

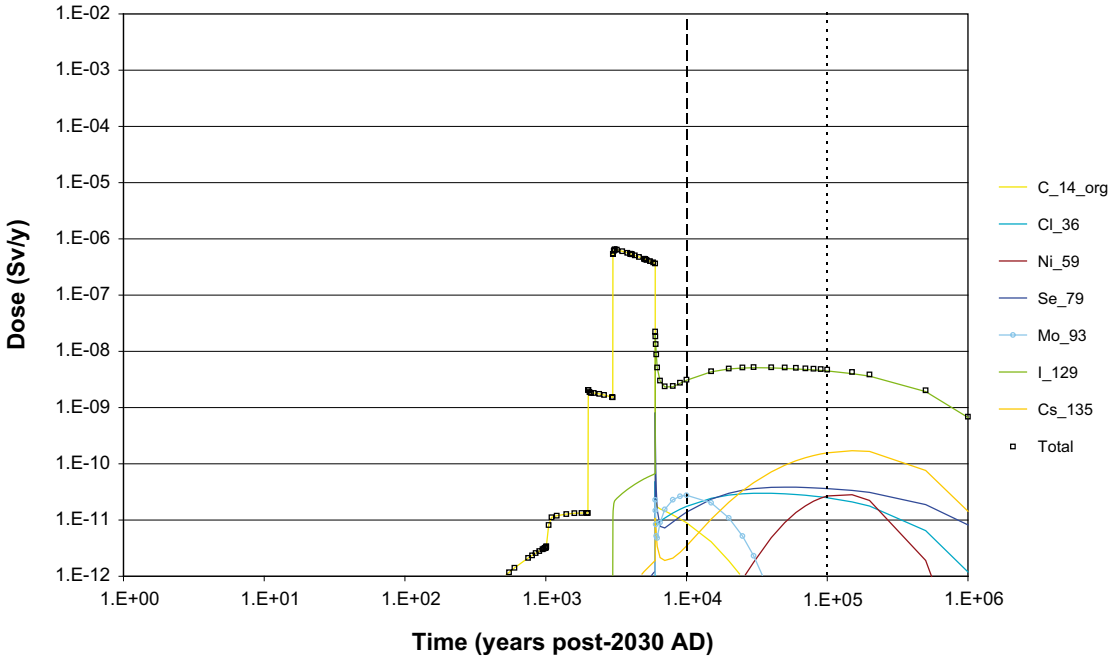

Figure 4-3. *Doses to RBD for Silo Most likely scenario.*

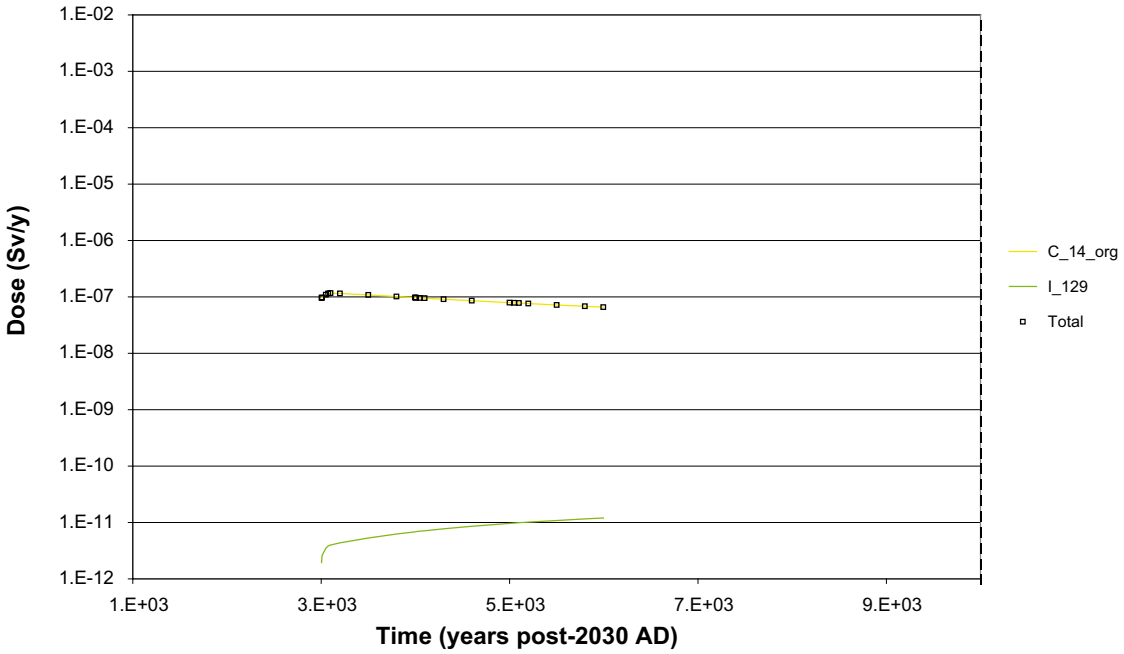

Figure 4-4. *Doses to river biosphere for Silo Most likely scenario.*

4.2 BMA

Figure 4-5 shows the near-field radionuclide flux from the BMA for the Most likely scenario. The peak radionuclide flux occurs at around 3,100 AD and is of the order of 9.1E+07 Bq/y. It can be seen that up to around 8,000 AD the radionuclide flux is dominated by the breakthrough of organic C-14, during this period a smaller releases of H-3, Sr-90 and Cs-137 are estimated at about 2,100 AD (more than two orders of magnitude below the overall maximum) and a larger release of Ag-108m peaks at 3,100 AD but these are at least three orders of magnitude below the overall maximum but these are at least three orders of magnitude below the overall maximum.

In the very long-term the key radionuclides are Ni-59, Zr-93 and Tc-99.

Figure 4-6 shows the geosphere radionuclide flux from the BMA for the Most likely scenario. Overall the trends shown by the geosphere radionuclide flux are similar to those of the near-field radionuclide flux: the timing of peak is delayed slightly to 3,200 AD and magnitude is reduced to 7.8E+07 Bq/y; up to 5,500 years post-2030 AD the radionuclide flux is dominated by the breakthrough of organic C-14; fluxes of Cl-36, Se-79, Mo-93, I-129 and Cs-135 are also important between 1,000 and 100,000 years post-2030 AD; the key radionuclides for the very long-term are Ni-59 and Tc-99. The main differences from the near-field breakthrough curves are the lack of an observable Cs-137 breakthrough, the reduction and delay in the releases of Ag-108m and Cs-135 and the delay in the breakthrough of Tc-99.

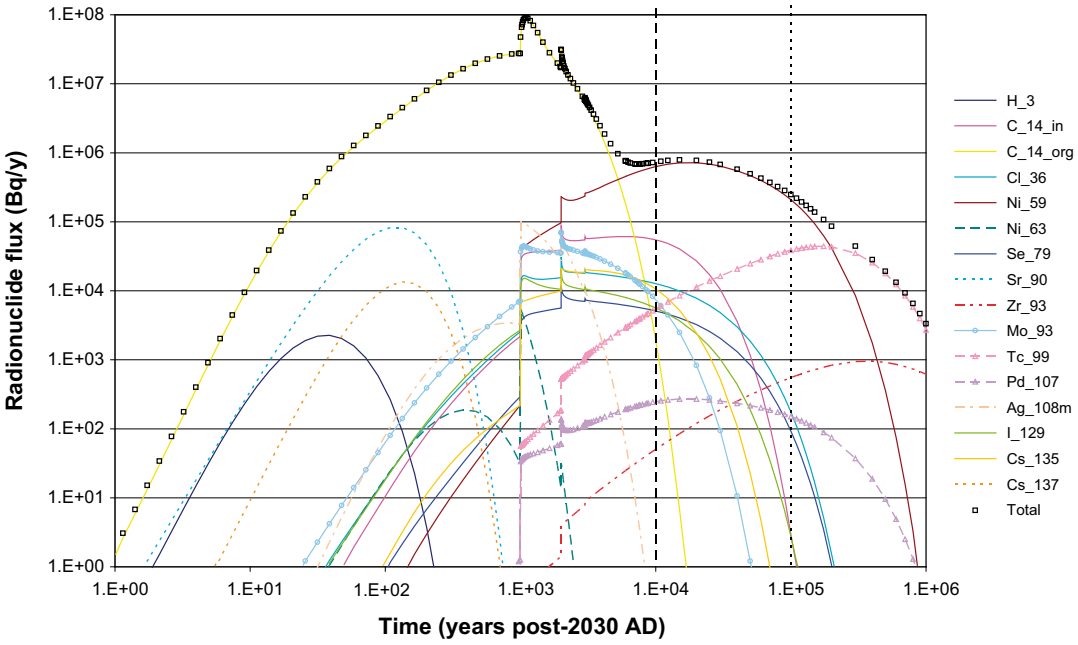

Figure 4-5. *BMA near-field radionuclide fluxes for Most likely scenario.*

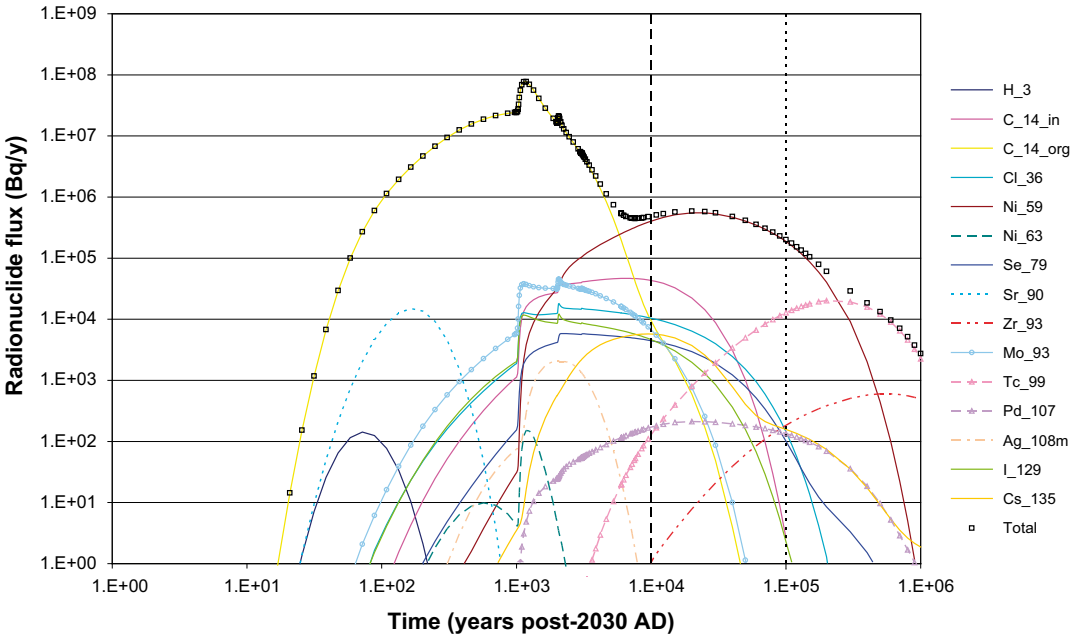

Figure 4-6. *BMA geosphere radionuclide fluxes for Most likely scenario.*

Figure 4-7 shows the doses estimated to the RBD model from the BMA Most likely scenario. The dominant radionuclide during the initial 6,000 years (i.e. the coastal and lake models) is organic C-14 (there is also a minor contribution from inorganic C-14during the lake period). The maximum dose is estimated to occur at the onset of the agricultural model and is 4.2E–7 Sv/y. This peak is considered to be associated with the initial exposure to radionuclides that were released into the coastal and lake sediments which are used in the agricultural soil model. It can be seen from the detail in Figure 4-8 that the initial doses reduce rapidly over a period of 50 years or so. This feature can be considered to be an artefact of the modelling approach to

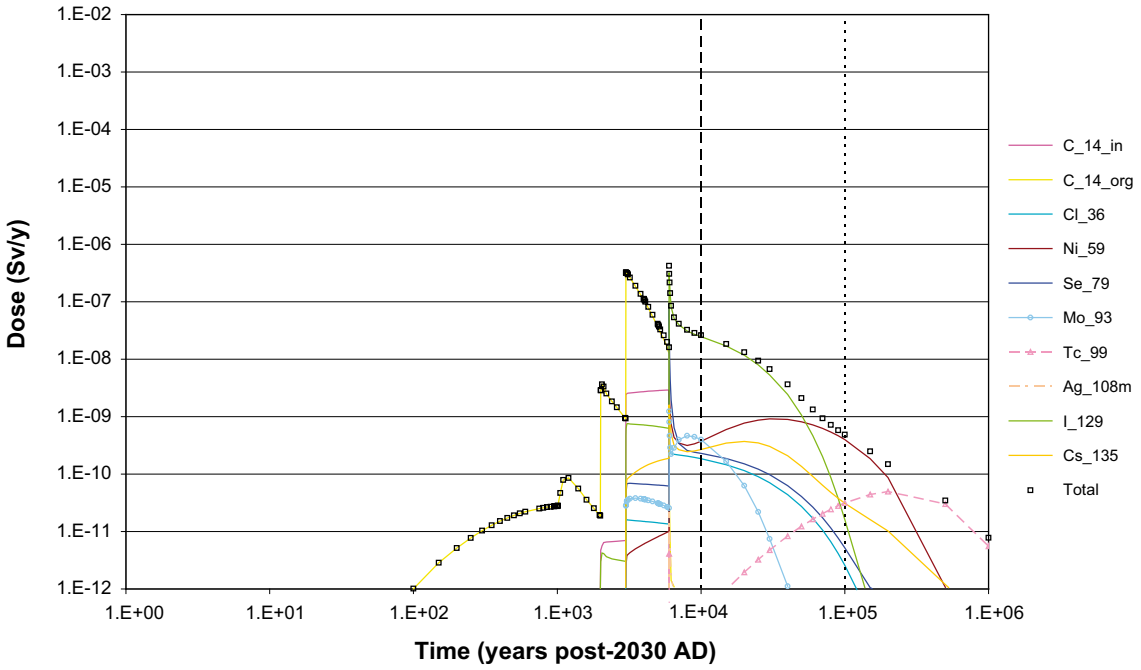

Figure 4-7. *Doses to RBD for BMA Most likely scenario.*

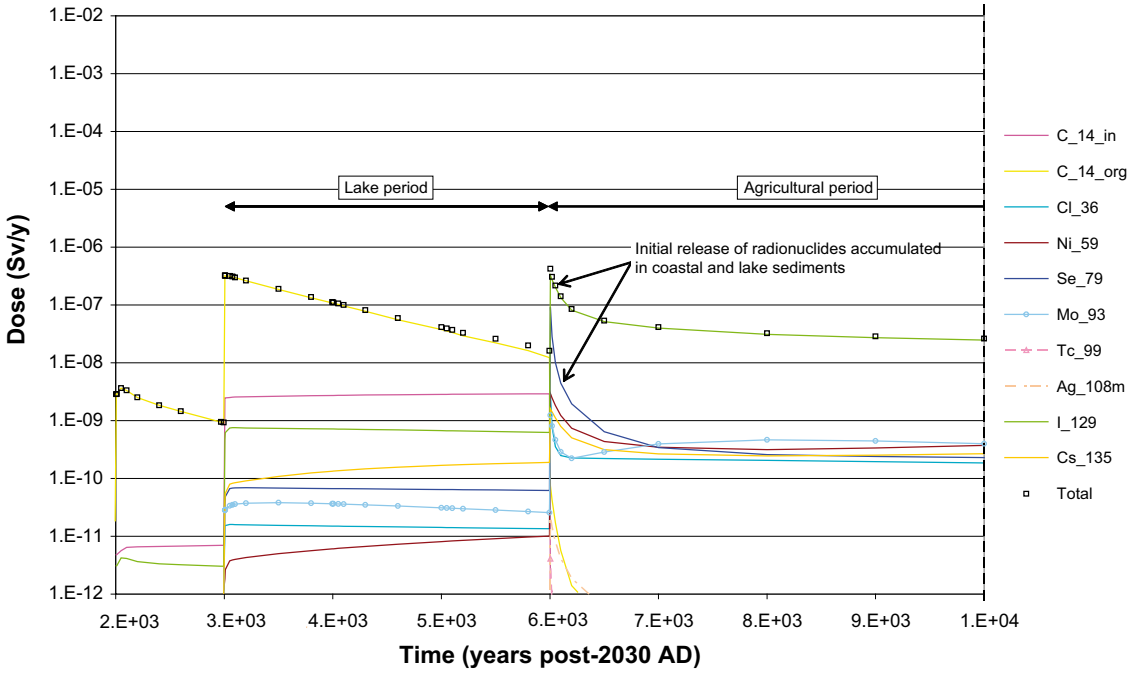

Figure 4-8. *Detail of doses in agricultural land period for BMA Most likely scenario.*

some degree as only radioactive decay was assumed to reduce radionuclide concentrations in the coastal sediments during the lake period. From the onset of the agricultural period the key radionuclide is I-129 until around 50,000 years post-2030 AD at which point Ni-59 and then Tc-99 are the most important radionuclides. Other significant radionuclides during the agricultural period are Cl-36, Se-79, Mo-93 and Cs-135.

Figure 4-9 shows the doses estimated to the River model from the BMA Most likely scenario (please note that the x-axis is not a logarithmic scale). The maximum dose, 5.8E–8 Sv/y, is estimated to occur at the onset of the River model and is due to organic C-14. The maximum dose in the RBD model is larger than that for the River model for reasons explained previously.

4.3 1BTF

Figure 4-10 shows the near-field radionuclide flux from 1BTF for the Most likely scenario. The peak radionuclide flux occurs at around 3,000 AD and is of the order of 2.9E+08 Bq/y. It can be seen that up to around 6,000 AD the radionuclide flux is dominated by the breakthrough of organic C-14, during this period smaller releases of H-3 and Sr-90 are estimated at about 45 and 100 years post-2030 AD, respectively (but at least four orders of magnitude below the overall maximum). Beyond 6,000 AD the key radionuclide is inorganic C-14 until around 30,000 years post-2030 AD when Ni-59 and Tc-99 reach their maximums (around three orders of magnitude or more below the overall maximum).

Figure 4-11 shows the geosphere radionuclide flux from the 1BTF for the Most likely scenario. Overall the trends shown by the geosphere radionuclide flux are similar to those of the near-field radionuclide flux: the timing of peak is delayed slightly to around 3,100 AD and the magnitude is reduced to 1.3E+08 Bq/y; up to around 4,500 years post-2030 AD the radionuclide flux is dominated by the breakthrough of organic C-14; thereafter fluxes of inorganic C-14 dominate until around 30,000 years post-2030 AD; the key radionuclides in the very long-term are Ni-59 and Tc-99. The main differences are the reduction and delay in the releases of Ag-108m and Cs-135 and the delay in the breakthrough of Zr-93 and Tc-99.

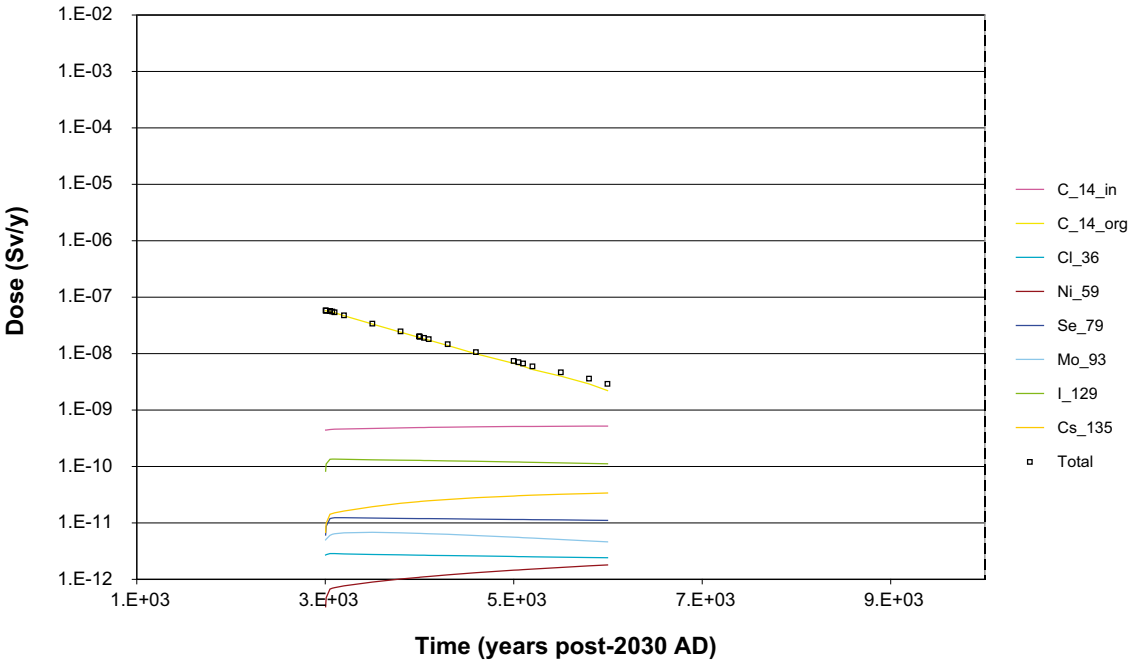

Figure 4-9. *Doses to river biosphere for BMA Most likely scenario.*

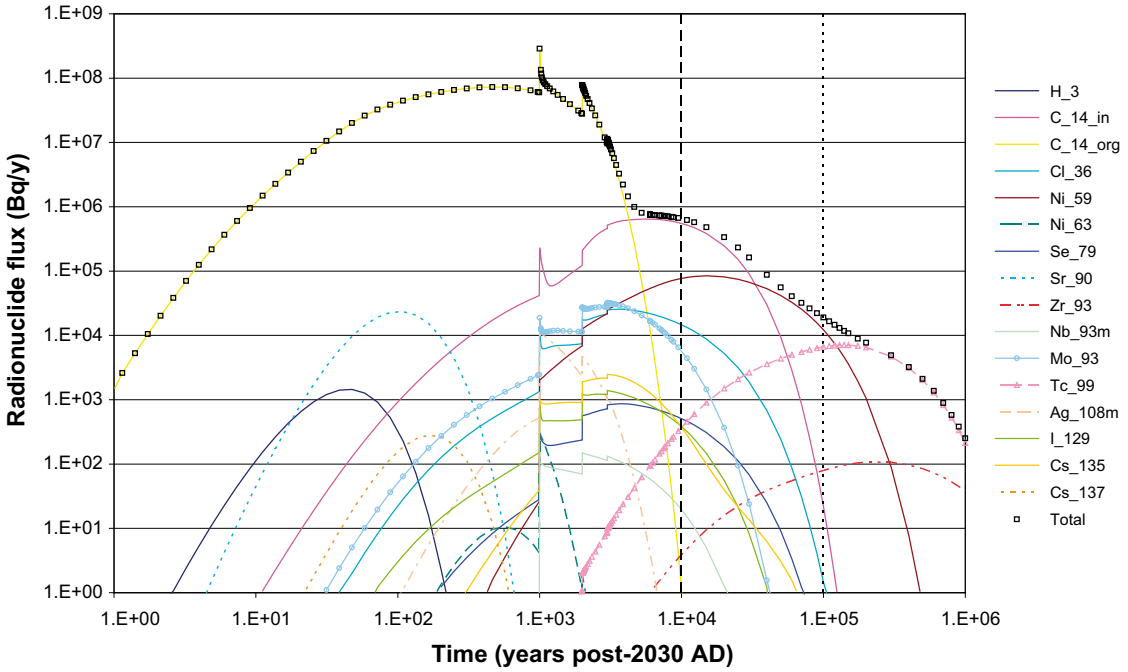

Figure 4-10. *1BTF near-field radionuclide fluxes for Most likely scenario.*

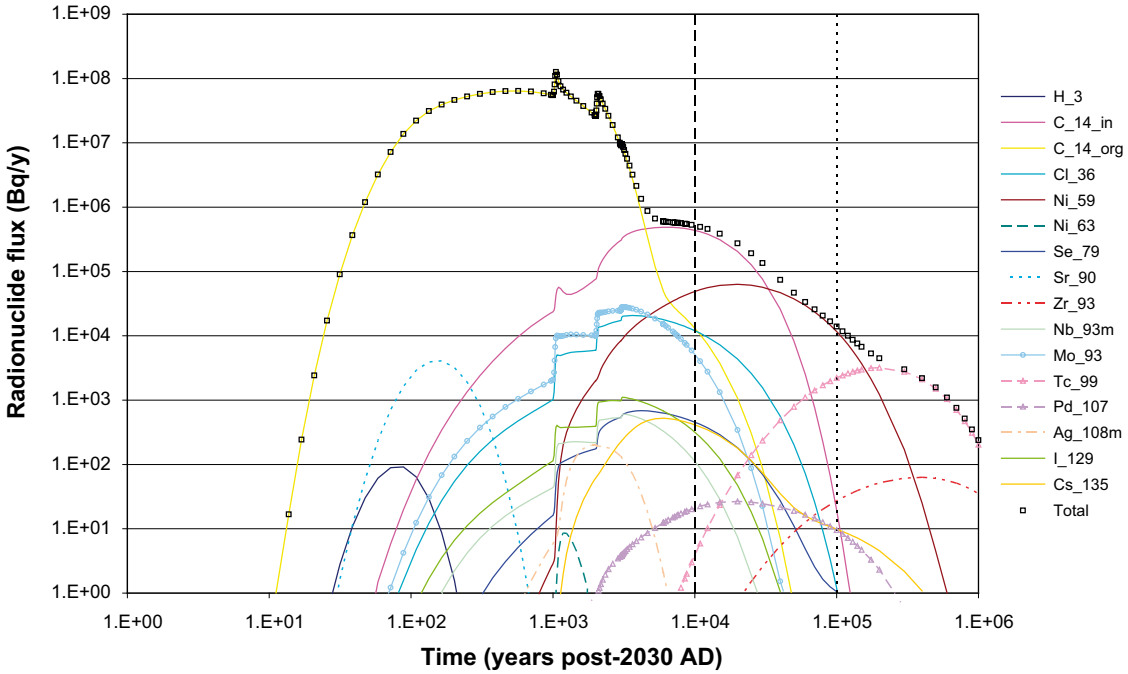

Figure 4-11. *1BTF geosphere radionuclide fluxes for Most likely scenario.*

Figure 4-12 shows the doses estimated to the RBD model from the 1BTF Most likely scenario. The dominant radionuclide during the coastal period and initial phase of the lake period is organic C-14, in the latter half of the lake period inorganic C-14 is the dominant radionuclide. The maximum dose is estimated to occur at 5,100 AD, around the onset of the lake model, and is 5.9E–7 Sv/y. From the onset of the agricultural period the key radionuclide is I-129 until 30,000 years post-2030 AD at which point Ni-59 and Tc-99 become the dominant radionuclides. Other significant radionuclides during the agricultural period are Cl-36, Se-79, Mo-93 and Cs-135.

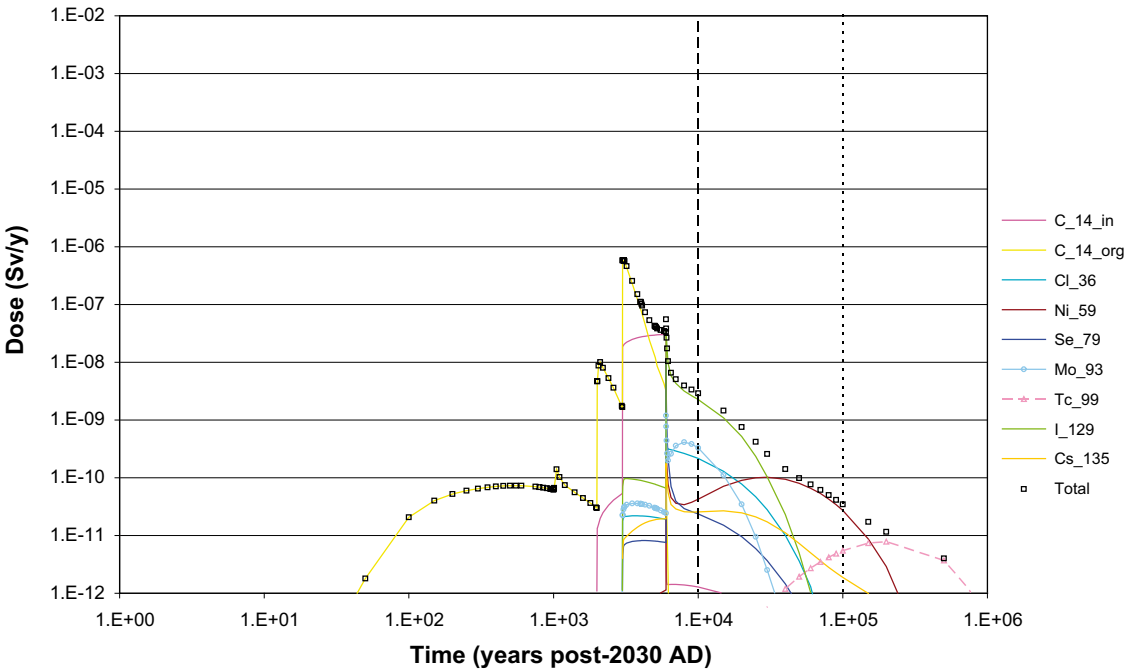

Figure 4-12. *Doses to RBD for 1BTF Most likely scenario.*

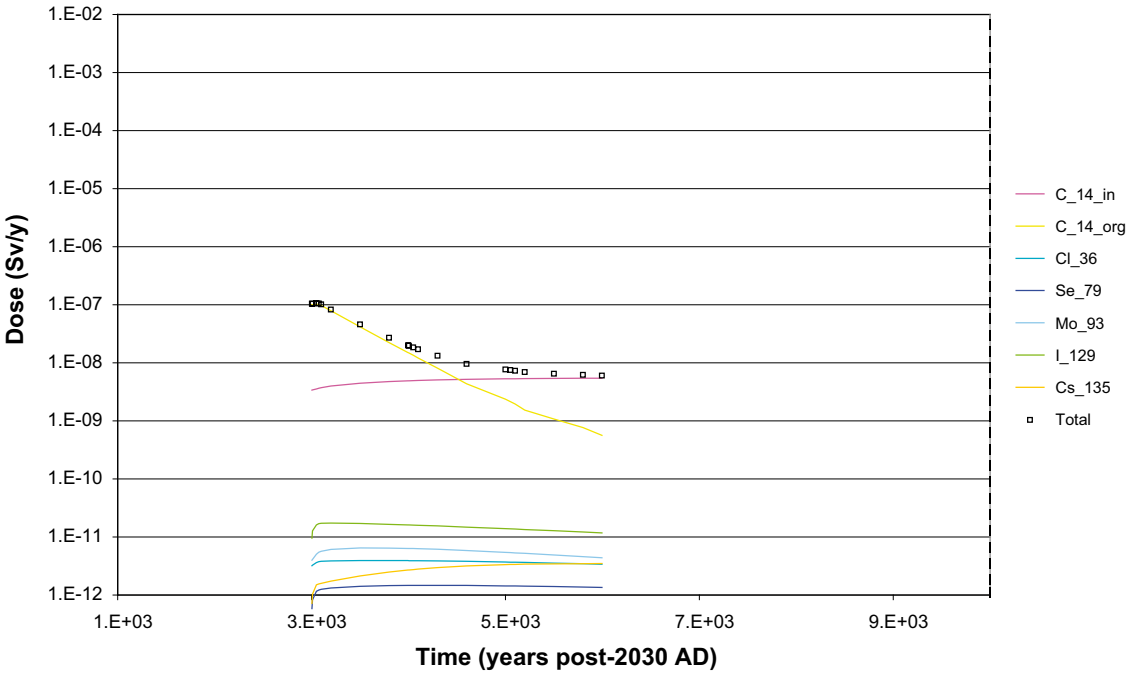

Figure 4-13. *Doses to River model for 1BTF Most likely scenario.*

Figure 4-13 shows the doses estimated to the River model from 1BTF Most likely scenario (please note that the x-axis is not a logarithmic scale). The maximum dose, 1.1E–7 Sv/y, is estimated to occur at the onset of the River model and is due to organic C-14, although towards the end of the River model inorganic C-14 is the dominant contributor to dose. The maximum dose in the RBD model is larger than that for the River model for reasons explained previously.

4.4 2BTF

Figure 4-14 shows the near-field radionuclide flux from 2BTF for the Most likely scenario. The peak radionuclide flux occurs at around 3,000 AD and is of the order of 3.3E+06 Bq/y. It can be seen that up to around 6,500 AD the radionuclide flux is dominated by the breakthrough of organic C-14, initially smaller releases of H-3, Sr-90 and Cs-137 are estimated and a larger release of Ag-108m peaks at around 3,100 AD but they are all two or more orders of magnitude below the overall maximum. In the very long-term the key radionuclides are Ni-59 and Tc-99 but these are around two and three orders of magnitude below the overall maximum, respectively.

Figure 4-15 shows the geosphere radionuclide flux from 2BTF for the Most likely scenario. Overall the trends shown by the geosphere radionuclide flux are similar to those of the near-field radionuclide flux: the timing of peak is delayed slightly to 3,100 AD and the magnitude is reduced to 2.7E+06 Bq/y; up to 5,000 years post-2030 AD the radionuclide flux is dominated by the breakthrough of organic C-14; the breakthrough of Cl-36, Se-79, Mo-93, I-129 and Cs-135 are also important between 1,000 and 100,000 years post-2030 AD; the key radionuclides for the very long-term are Ni-59 and Tc-99. The main differences are the lack of a Cs-137 breakthrough, the reduction and delay in the breakthrough of Ag-108m and Cs-135 and the delay in the breakthrough of Tc-99.

Figure 4-16 shows the doses estimated to the RBD model from the 1BTF Most likely scenario. The dominant radionuclide during the initial 6,000 years (i.e. the coastal and lake models) is organic C-14 (there is also minor contributions from Ni-59, Se-79, I-129 and Cs-135 during the lake period). The maximum dose is estimated to occur at the onset of the agricultural model and is 6.9E–8 Sv/y. This exposure is associated with the initial inventory in the soils and not the groundwater flux (as for the BMA). From the onset of the agricultural period the key radionuclide is I-129 and in the very long-term Ni-59 becomes the dominant radionuclide. Other significant radionuclides during the agricultural period are Cl-36, Se-79, Mo-93 and Cs-135.

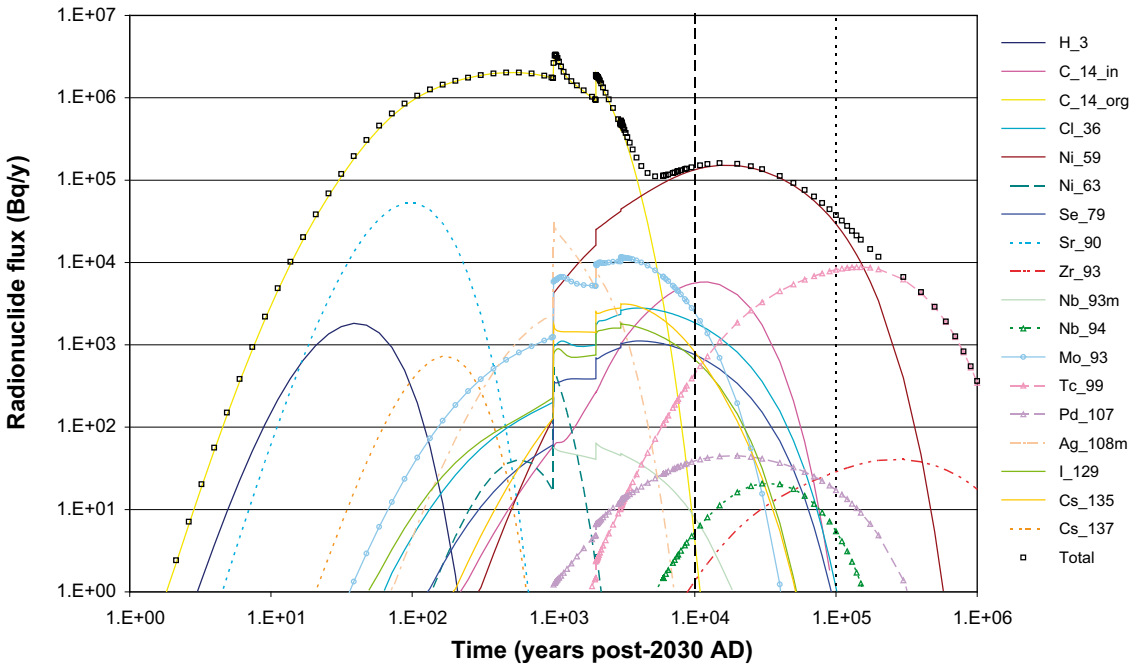

Figure 4-14. *2BTF near-field radionuclide fluxes for Most likely scenario.*

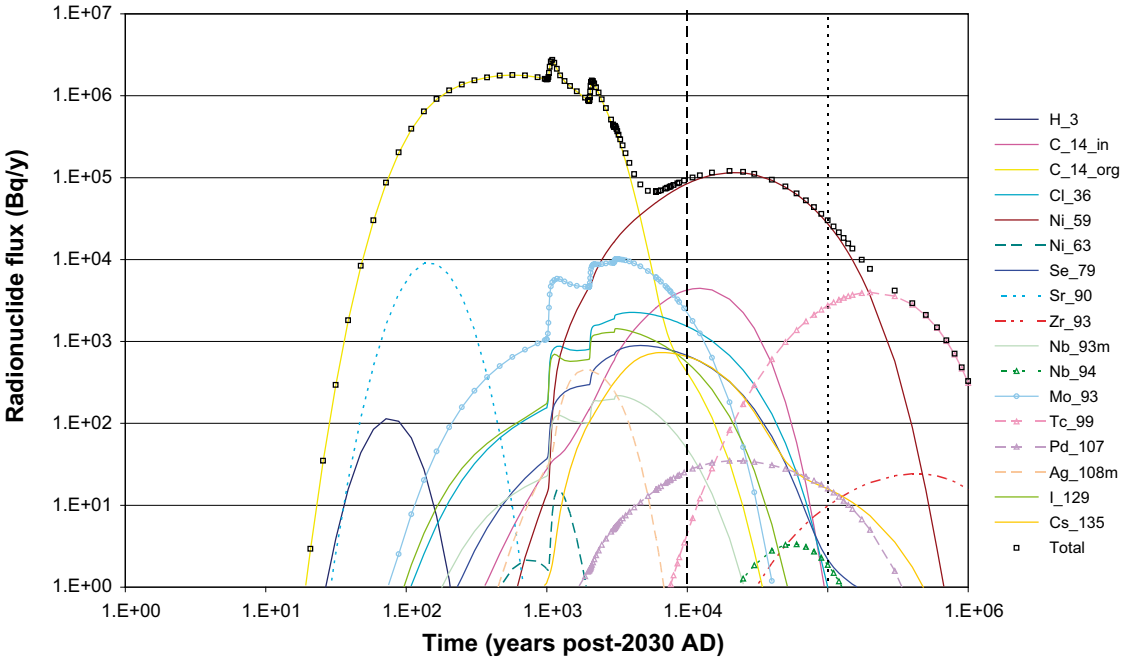

Figure 4-15. *2BTF geosphere radionuclide fluxes for Most likely scenario.*

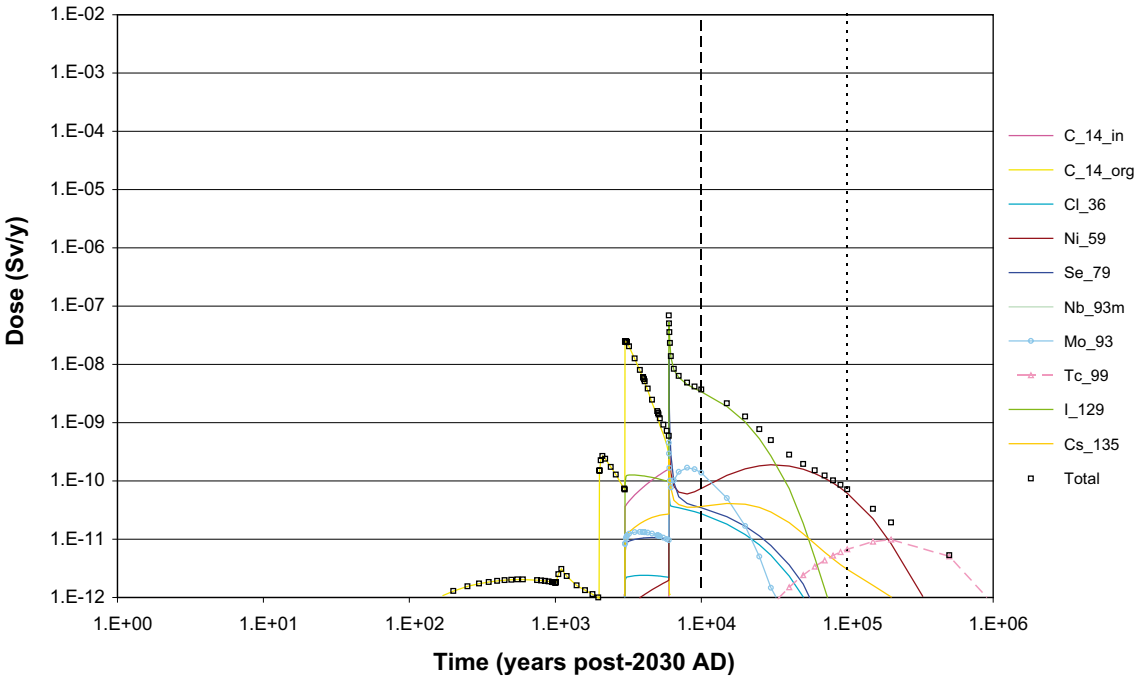

Figure 4-16. *Doses to RBD for 2BTF Most likely scenario.*

Figure 4-17 shows the doses estimated to the River model from 2BTF Most likely scenario (please note that the x-axis is not a logarithmic scale). The maximum dose, 4.5E–9 Sv/y, is estimated to occur at around 5,000 AD, the onset of the River model and is due to organic C-14. The maximum dose in the RBD model is larger than that for the River model for reasons explained previously.

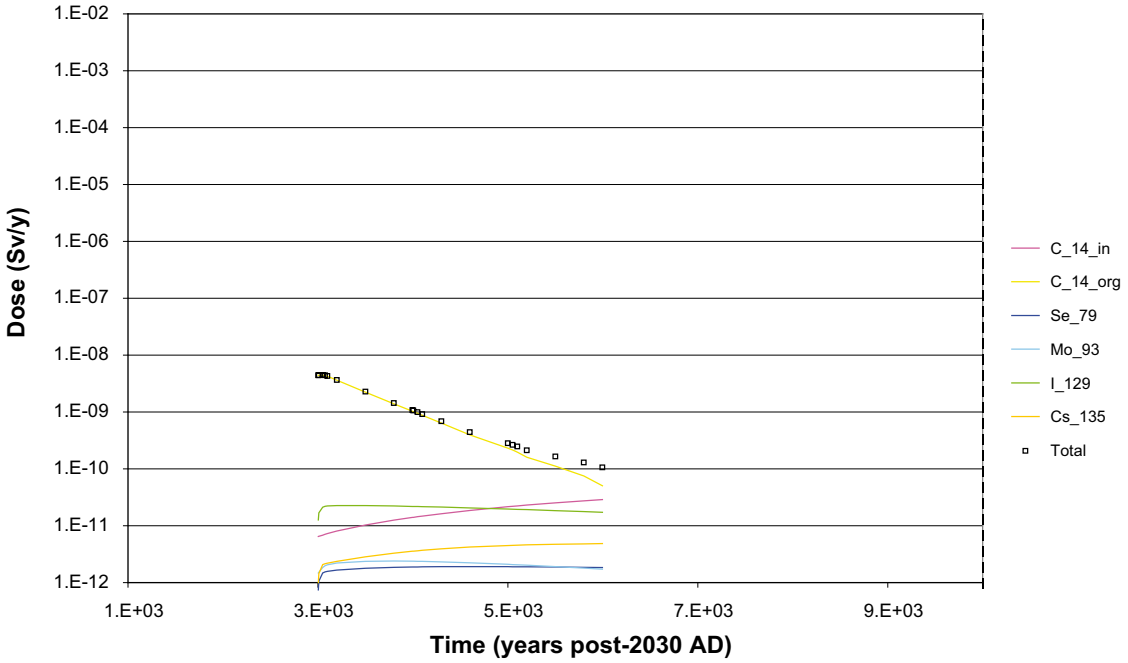

Figure 4-17. *Doses to River biosphere for 2BTF Most likely scenario.*

4.5 BLA

Figure 4-18 shows the near-field radionuclide flux from the BLA for the Most likely scenario. The peak radionuclide flux occurs initially, is of the order of 2.5E+08 Bq/y and is due to releases of Co-60, Ni-63 and Cs-137 which dominate up to 2,600 AD. Inorganic C-14 is the key radionuclide from 2,600 AD. The BLA generally shows maximum releases for all radionuclides due to absence of barriers and sorption from the model. Negligible release rates from the BLA are estimated beyond 10,000 AD.

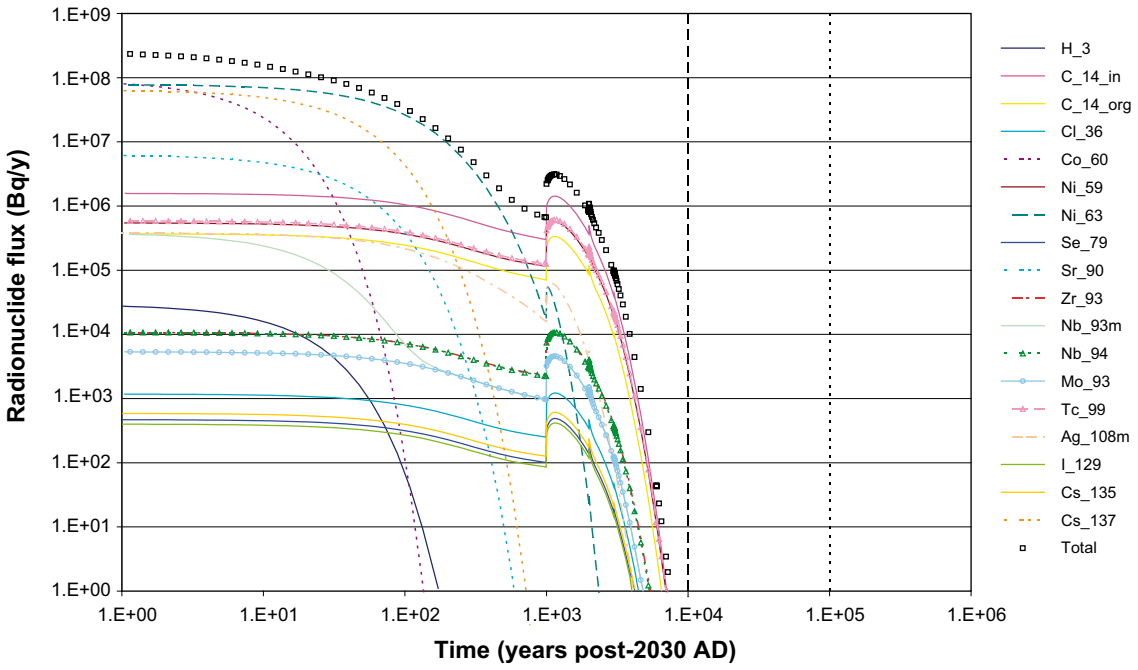

Figure 4-18. *BLA near-field radionuclide fluxes for Most likely scenario.*

Figure 4-19 shows the geosphere radionuclide flux from the BLA for the Most likely scenario. The peak radionuclide flux is estimated to occur at 2,200 AD and is of the order of 2.3E+06 Bq/y. This peak coincides with the maximum release rate of Ni-63, although there are also contributions from the breakthrough of inorganic and organic C-14, Ni-59 and Sr-90. Inorganic C-14 dominates releases from 450 to 3,000 years post-closure, then the breakthrough of Ni-59 until 15,000 years post-2030 AD when the breakthrough of Tc-99 becomes most significant.

Figure 4-20 shows the doses estimated to the RBD model from the BLA Most likely scenario. Doses around 1E–10 Sv/y or less are estimated for the coastal period. The maximum dose is estimated to occur at around 5,000 AD which is the onset of the lake model and is 5.5E–9 Sv/y.

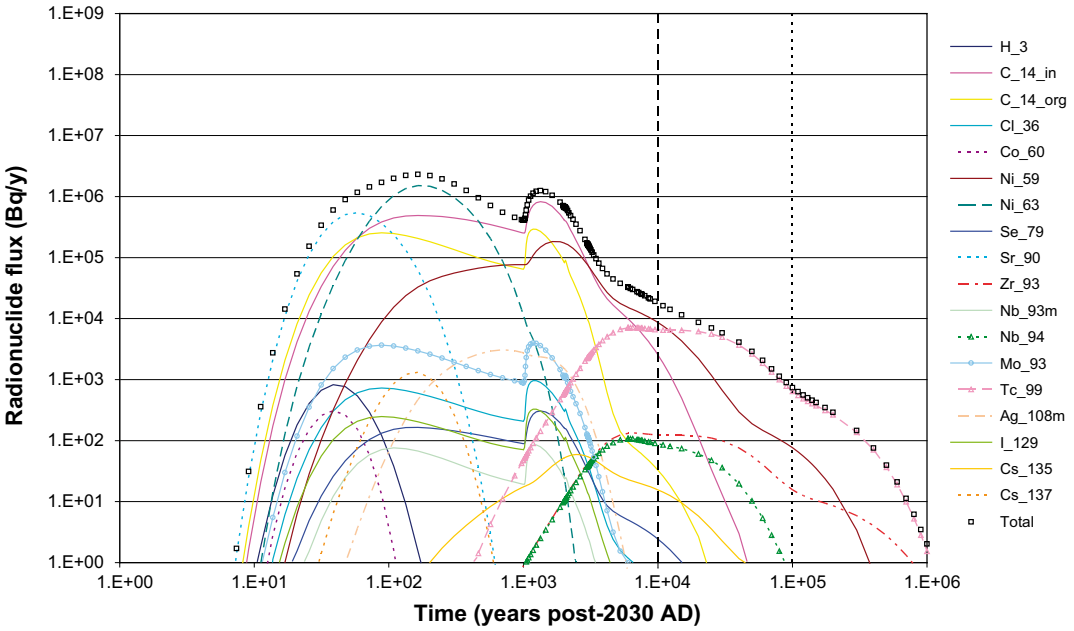

Figure 4-19. *BLA geosphere radionuclide fluxes for Most likely scenario.*

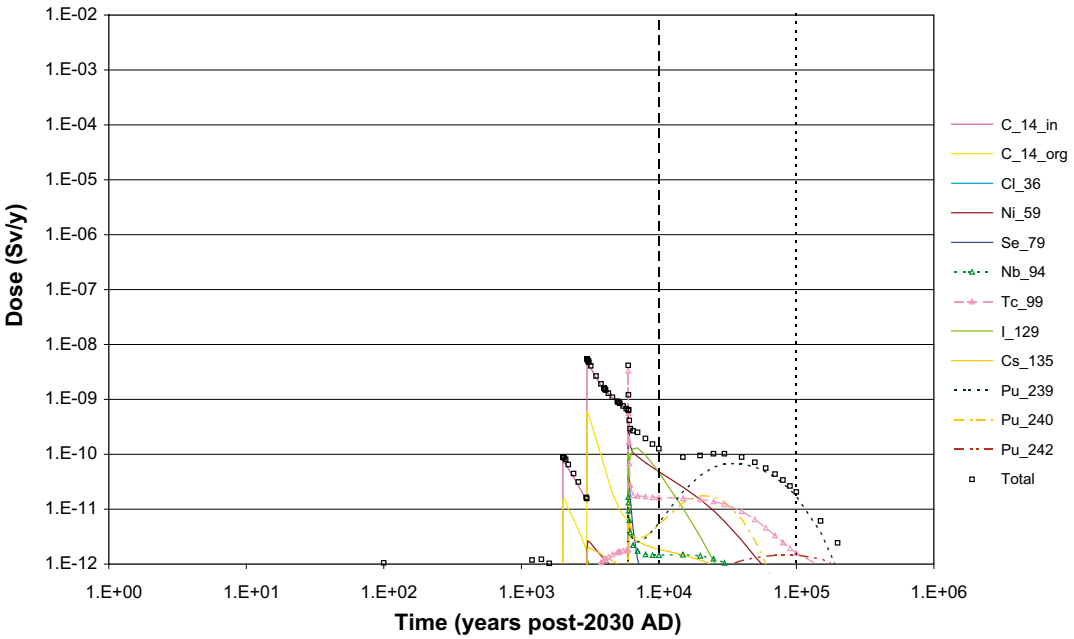

Figure 4-20. *Doses to RBD for BLA Most likely scenario.*

The key radionuclides within the coastal and lake period are inorganic and organic C-14. At the onset of the agricultural period the key radionuclide is Tc-99 (due accumulation previously in coastal and lake sediments as for the BMA and 2BTF), exposures are then dominated by Ni-59, I-129 and Pu-239 in the very long term.

Figure 4-21 shows the doses estimated to the River model from the BLA Most likely scenario (please note that the x-axis is not a logarithmic scale). The maximum dose, 9.8E–8 Sv/y, is estimated to occur at around 5,000 AD, the onset of the River model and is due to inorganic C-14. The maximum dose in the RBD model is larger than that for the River model by a factor of approximately 5.

4.6 SFR-1 summary for Most likely scenario

Figure 4-22 summarises the near-field radionuclide flux from each part of the repository and the total for the whole of SFR-1 for the Most likely scenario. The initial few decades are dominated by the release of radionuclides from the BLA. Thereafter the dominant contributors to the overall radionuclide flux are the BMA and 1BTF in the short-term and additionally the Silo in the long-term. The very long term releases are dominated by the release of radionuclides from the BMA. The peak near-field radionuclide flux from SFR-1 is 3.5E+08 Bq/y at 3,000 AD and is dominated by the release of radionuclides from 1BTF.

Figure 4-23 summarises the geosphere radionuclide flux from each part of the repository and the total for the whole of SFR-1 for the Most likely scenario. The initial few years are dominated by the release of radionuclides from the BLA. Thereafter the dominant contributors to the overall radionuclide flux are the BMA and 1BTF in the short-term and additionally the Silo in the long-term. The very long term releases are dominated by the release of radionuclides from the BMA. The peak geosphere radionuclide flux from SFR-1 is 1.8E+08 Bq/y at 3,100 AD.

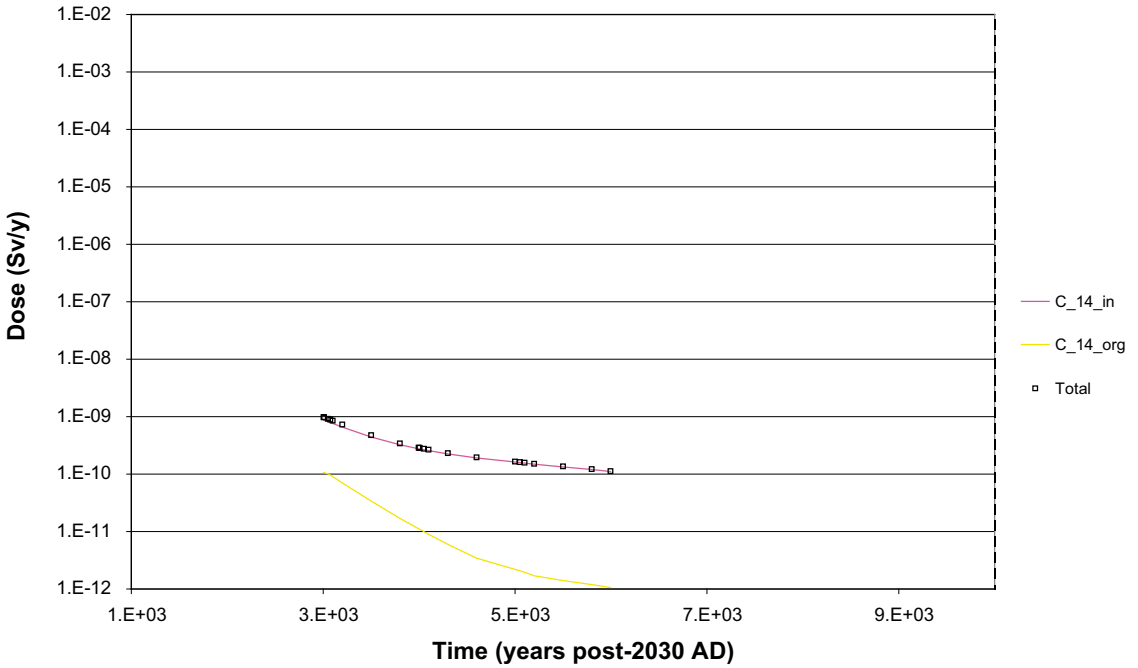

Figure 4-21. *Doses to river biosphere for BLA Most likely scenario.*

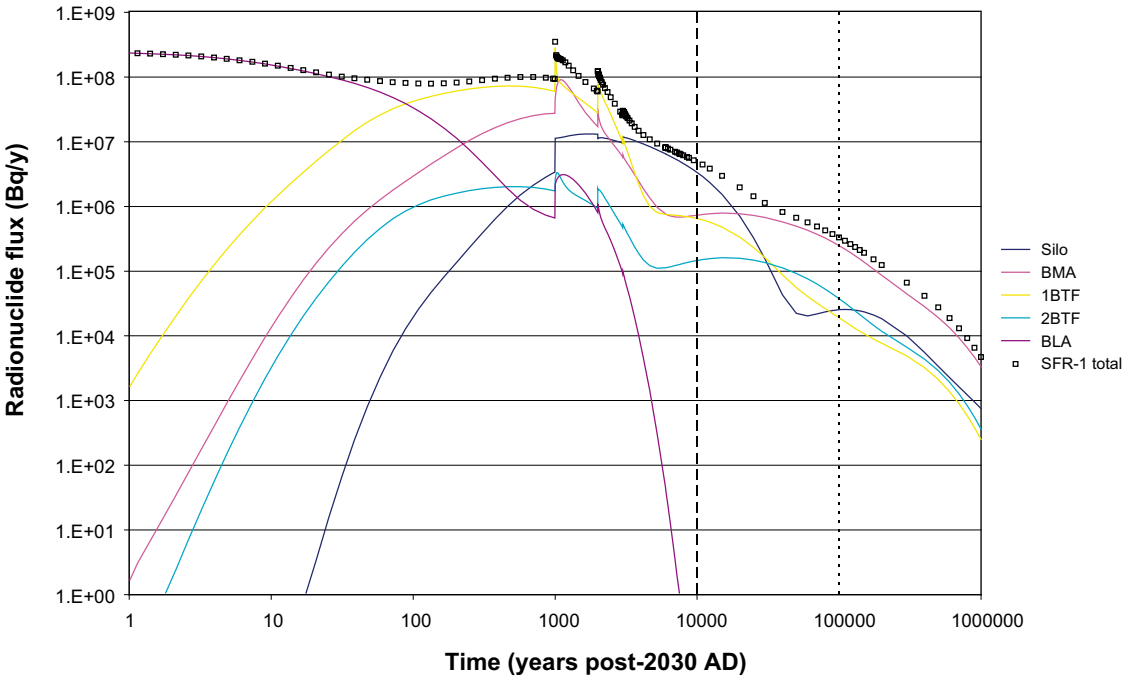

Figure 4-22. *Near-field radionuclide fluxes for Most likely scenario.*

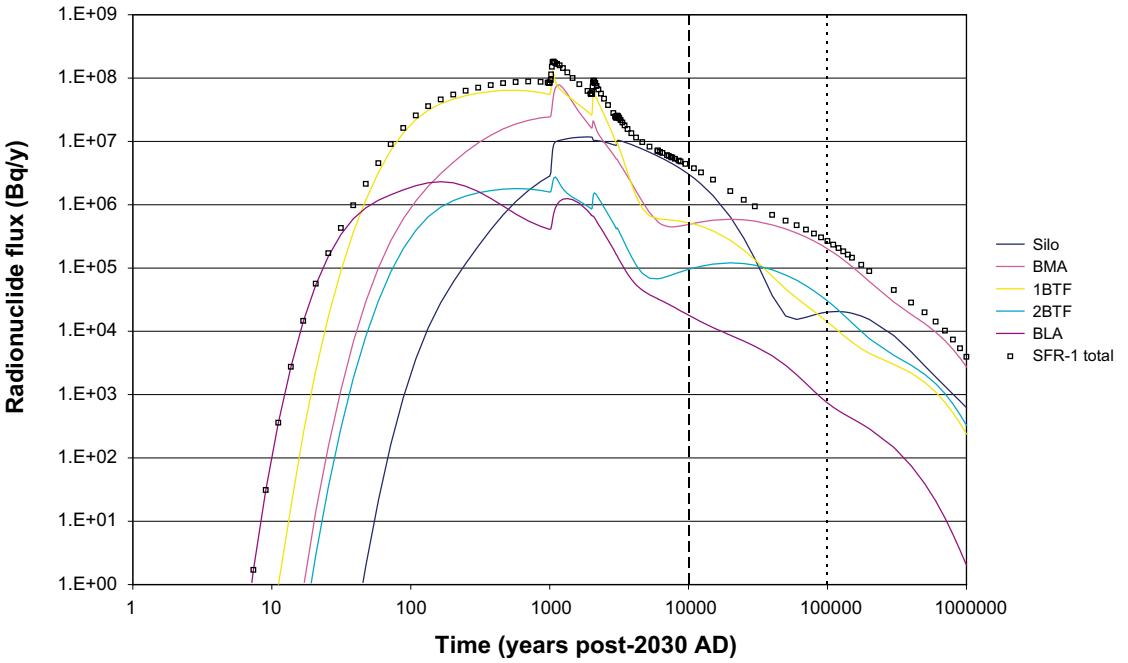

Figure 4-23. *Geosphere radionuclide fluxes for Most likely scenario.*

Figure 4-24 summarises the estimated dose for RBD from each part of the repository and the total for the whole of SFR-1 for the Most likely scenario. Doses during the Coastal period are dominated by releases from 1BTF and the BMA. Doses during the Lake period are dominated by release from the Silo, 1BTF and the BMA. The maximum dose is estimated to be 1.6E–06 Sv/y at 5,100 AD which is in the early stages of the Lake period and is driven by releases from the Silo. Very long term doses during the agricultural period are dominated by contributions from the BMA and Silo.

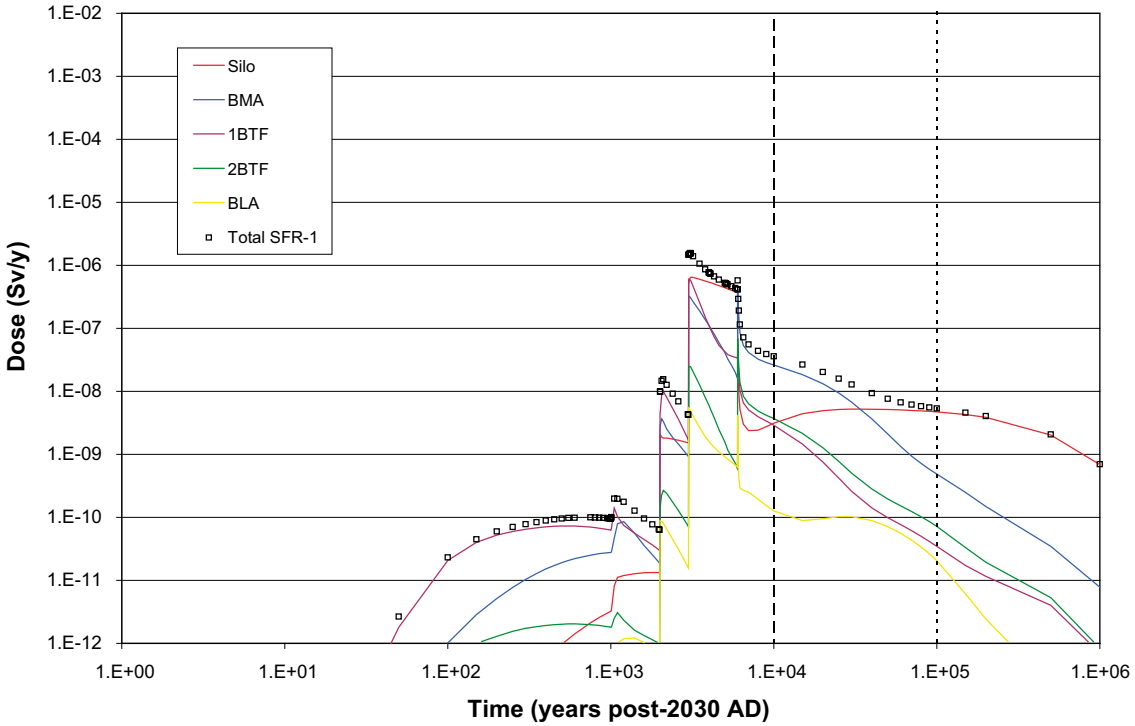

Figure 4-24. *Dose for RBD from the Most likely scenario.*

The results from the Most likely scenario are summarised in Table 4-1. For each disposal facility and the SFR-1 as a whole the time and magnitude of the maximum near-field and geosphere fluxes and RBD dose are given. Also given is the radionuclide (or facility) that dominates at the time of the maximum. For example, considering the Silo near-field flux, the maximum value for the Silo as a whole is 1.3E+07 Bq/y at around 3,900 AD which is dominated by organic C-14. However this does not necessarily mean that the radionuclide flux of organic C-14 is 1.3E+07 Bq/y at around 3,900 AD as there may be contributions to the total from other radionuclides at this time. Similarly, the totals for SFR-1 at the bottom of the table are not simply the sum of the values above them. Biosphere results are only summarised for the RBD model as these are the highest overall doses.

Table 4-2 summarises the maximum conditional risks for the Most likely scenario RBD model. These are also shown in Figure 4-25. The risks are reported as conditional as it has been cautiously assumed that the probability of the Most likely scenario occurring is unity. The risk per dose factor used is 0.06 Sv^{-1} based on recommended values from the ICRP /ICRP 1991/. The dose was multiplied by this value in order to derive a value of conditional risk.

The maximum conditional risk for an individual facility is 3.9E–08 y^{-1} for the Silo (although the conditional risks from the BMA and 1BTF are 2.5E–08 y^{-1} and 3.5E–08 y^{-1}, respectively) and the overall maximum conditional risk for SFR-1 is 9.4E–08 y^{-1}. Both these values are significantly below the risk target of 1E–06 y^{-1}.

Table 4-1. Summary of Most likely scenario results.

	Near-field	Geosphere	RBD
Silo	1.3E+07 Bq/y at c. 3,900 AD Organic C-14	1.2E+07 Bq/y at c. 3,900 AD Organic C-14	6.5E–07 Sv/y at c. 5,100 AD Organic C-14
BMA	9.1E+07 Bq/y at c. 3,100 AD Organic C-14	7.8E+07 Bq/y at c. 3,200 AD Organic C-14	4.2E–07 Sv/y at c. 8,000 AD I-129
1BTF	2.9E+08 Bq/y at c. 3,000 AD Organic C-14	1.3E+08 Bq/y at c. 3,100 AD Organic C-14	5.9E–07 Sv/y at c. 5,100 AD Organic C-14
2BTF	3.3E+06 Bq/y at c. 3,000 AD Organic C-14	2.7E+06 Bq/y at c. 3,100 AD Organic C-14	6.9E–08 Sv/y at c. 8,000 AD I-129
BLA	2.5E+08 Bq/y at closure Co-60, Ni-63 and Cs-137	2.3E+06 Bq/y at c. 2,200 AD Ni-63	5.5E–09 Sv/y at c. 5,000 AD Inorganic C-14
SFR-1	3.5E+08 Bq/y at c. 3,000 AD 1BTF	1.8E+08 Bq/y at c. 3,100 AD 1BTF	1.6E–06 Sv/y at c. 5,100 AD Silo, BMA, 1BTF

Table 4-2. Maximum conditional risks for Most likely scenario RBD model.

	Maximum conditional risk (y^{-1})
Silo	3.9E–08
BMA	2.5E–08
1BTF	3.5E–08
2BTF	4.2E–09
BLA	3.3E–10
SFR-1	9.4E–08

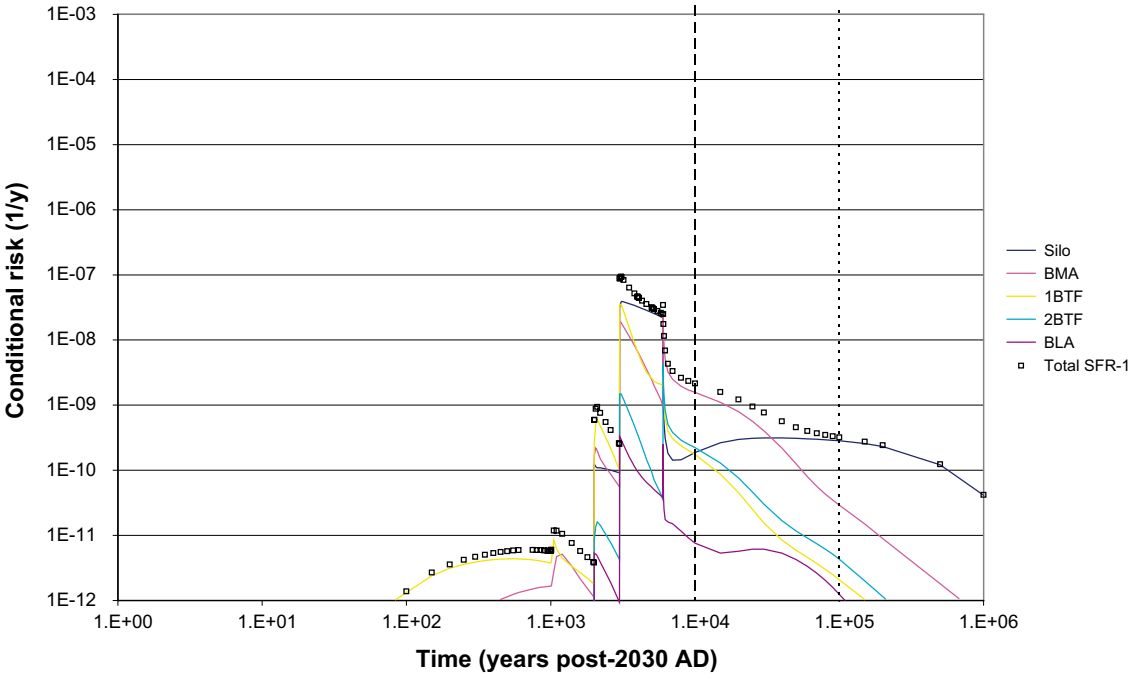

Figure 4-25. *Conditional risks for RBD from the Most likely scenario.*

4.7 Comparison of Most likely scenario results with project SAFE

Table 4-3 shows a comparison of the RBD doses of the Most likely scenario with the Project SAFE Intact barriers calculations /Lindgren et al. 2001/[5]. The following differences in the codes, models and data used in the calculations should be first noted.

- In Project SAFE the near-field calculations were undertaken in NUCFLOW, the geosphere using FAR31 and the biosphere using ACTIVI, BIOPATH and PRISM /Lindgren et al. 2001/.
- The effect of the geosphere was not considered within the doses calculated within Project SAFE but it is included in the Most likely scenario.
- The Most likely scenario was undertaken using AMBER models developed to represent the Project SAFE models as closely as possible using available information. However, the AMBER models show some differences to those from Project SAFE (see Chapter 2).
- Modifications have also been made to the version of the Reasonable Biosphere Development model used in the Most likely scenario, in particular to the geosphere-biosphere interface zone.
- The Most likely scenario has an updated and revised inventory with important changes in values for inorganic and organic C-14, Ni-59 and Ni-63 and I-129 amongst other radionuclides. The inventory used in the Most likely scenario is not necessary lower than that used on a radionuclide by radionuclide basis although it is in terms of the overall totals.

The differences in the results of the Most likely scenario and Project SAFE Intact barriers calculations can be summarised as follows:

- The RBD doses from the Most likely scenario calculations are lower than those from the Project SAFE Intact barriers calculations for all repository features except 1BTF which is a factor of around 1.5 higher.
- Regarding 1BTF the following are considered to be plausible explanations.
  - It is noted that the organic C-14 inventory in the Most likely scenario is higher than that in Project SAFE whereas those for the other facilities are lower.
  - The AMBER 1BTF model also tends to slightly over predict the organic C-14 flux.
- The time of the peak dose for 2BTF is delayed to the onset of the agricultural period for the Most likely scenario. It is considered that the most plausible reason for this is the changes to the geosphere-biosphere interface zone discussed in Section 2.4.2 which leads to the accumulation of radionuclides such as I-129 as noted elsewhere for the Most likely scenario.
- The time of the peak dose for the BLA is brought forward to the onset of the lake period for the Most likely scenario. The Most likely scenario includes the geosphere which provides an important barrier for the BLA (for which no near-field barriers are assumed) and this reduces the contributions from radionuclides such as Pu-239 which are retarded within the geosphere (see /Lindgren et al. 2001/ for a discussion on this).

[5] Some additional information was taken from biosphere output files (Studsvik) to enable the times of peak to be derived for Project SAFE.

Table 4-3. Comparison of results from Most likely scenario and Project SAFE.

	RBD dose (Sv/y) Most likely scenario	Project SAFE (Base Scenario: Intact Barriers)
Silo	6.5E–07 Sv/y at c. 5,100 AD	3E–06 at c. 5,000 AD
	Organic C-14	Organic C-14
BMA	4.2E–07 Sv/y at c. 8,000 AD	5E–07 at c. 5,000 AD
	I-129	Organic C-14
1BTF	5.9E–07 Sv/y at c. 5,000 AD	4E–07 at c. 5,000 AD
	Organic C-14	Organic C-14
2BTF	6.9E–08 Sv/y at c. 8,000 AD	9E–08 at c. 5,000 AD
	I-129	Organic C-14
BLA	5.5E–09 Sv/y at c. 5,000 AD	2E–07 at c. 8,000 AD
	Inorganic C-14	Pu-239
SFR-1	1.6E–06 Sv/y at c. 5,100 AD	4E–06 at c. 5,000 AD
	Silo	Silo

5 Sensitivity and supplementary calculations

The data and interpretation in this section focuses on the near-field and biosphere, summary information only is provided on radionuclide fluxes from the geosphere.

5.1 Alternative inventory

5.1.1 Silo

Figure 5-1 shows the radionuclide flux from the Silo for the Alternative inventory sensitivity case. The maximum total radionuclide flux occurs at around 3,900 AD and is 1.2E+08 Bq/y. Breakthrough of organic C-14 dominates the near-field release until 25,000 years post-2030 AD. Early releases of H-3, Sr-90 and Cs-137 are observed in the first few hundred years and the breakthrough of Ag-108m reaches a maximum at 3,100 AD; these are at least five orders of magnitude below the overall maximum. The releases are dominated in the very long-term by Ni-59 and Tc-99; these are at least two orders of magnitude below the overall maximum.

Figure 5-2 shows the doses estimated to the RBD model from the Silo for the Alternative inventory. The doses during the coastal period are dominated by contributions from organic C-14 and are below 2E–08 Sv/y. The peak dose is estimated as 6.0E–06 Sv/y, occurring during the lake period at around 5,100 AD and is dominated by organic C-14. Doses during the agricultural period are dominated initially by contributions from I-129 and then by Ni-59 and Cs-135.

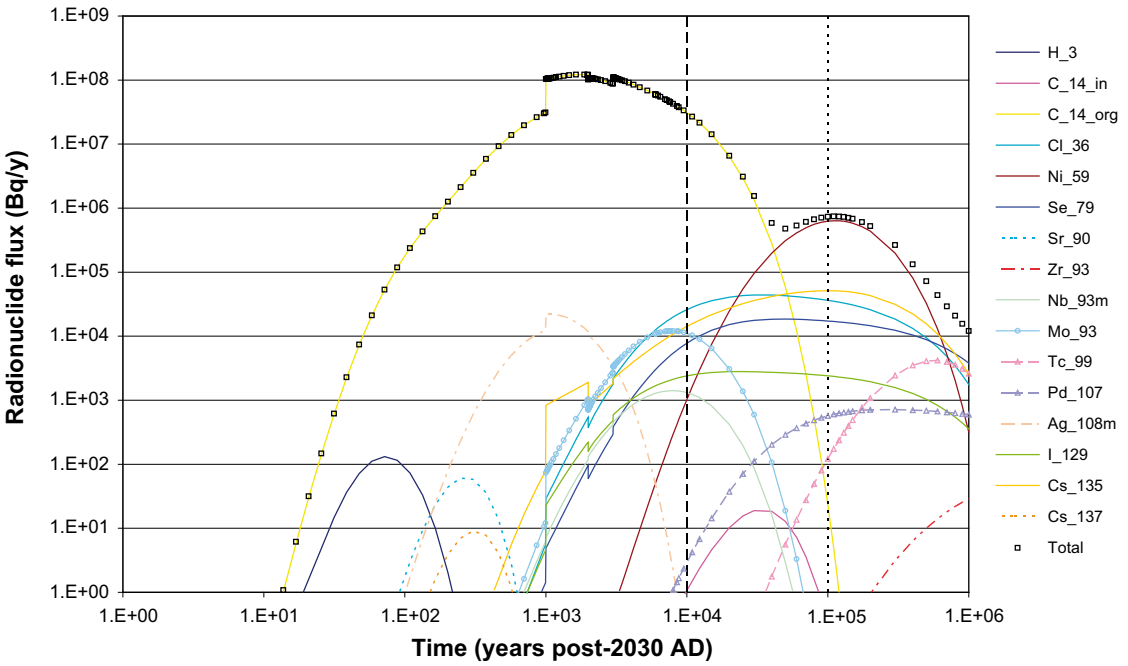

Figure 5-1. *Silo near-field radionuclide fluxes for Alternative inventory.*

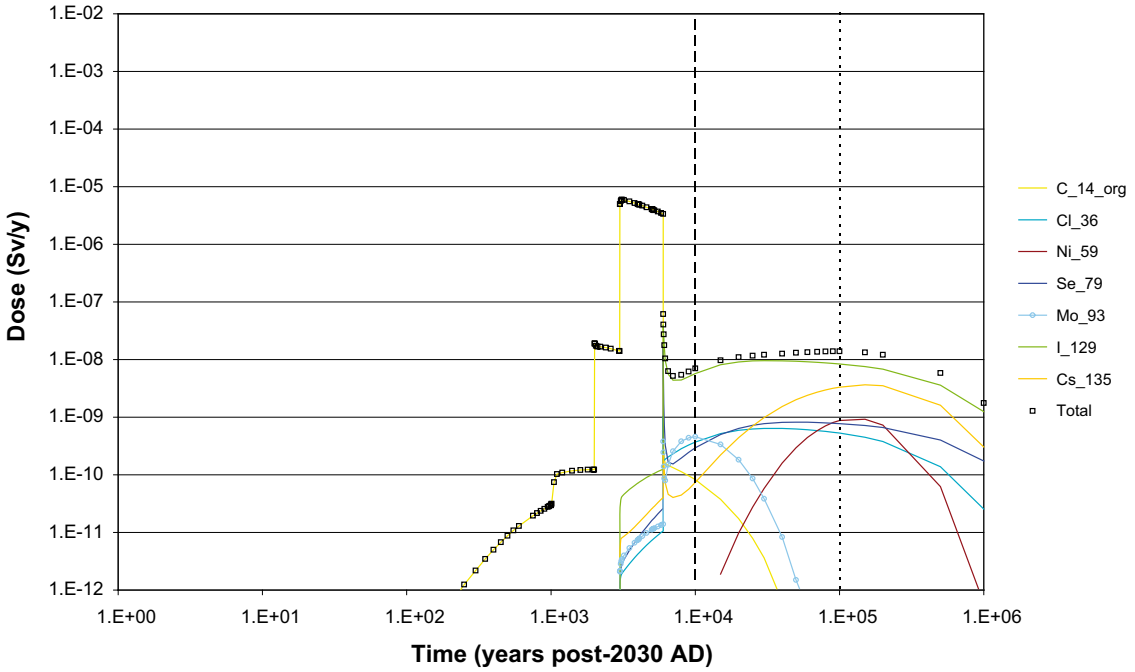

Figure 5-2. *Silo dose for RBD from Alternative inventory.*

5.1.2 BMA

Figure 5-3 shows the radionuclide flux from the BMA for the Alternative inventory. The maximum radionuclide flux of 3.2E+08 Bq/y occurs at around 3,100 AD and is dominated by organic C-14. Early releases of H-3, Sr-90 and Cs137 are estimated within the first 150 years (two or more orders of magnitude below the overall maximum). Between 1,000 and 20,000 years post-2030 AD several radionuclide contribute to the total flux including inorganic C-14, Cl-36, Se-79, Mo-93, Ag-108m and Cs-135 (around three or more orders of magnitude below the overall maximum). Ni-59 is the dominant radionuclide from 6,000 AD eventually being replaced as Tc-99 breaks through but these are orders of magnitude below the overall maximum.

The doses estimated from the BMA to the RBD model are shown in Figure 5-4. Doses during the coastal period are 2E–08 Sv/y or less and are dominated by organic C-14. The maximum dose is estimated to be 1.1E–06 Sv/y which occurs at the onset of the lake period (5,000 AD), and is due to organic C-14. Doses also estimated to arise during the lake period from other radionuclides, in particular inorganic C-14, Se-79, I-129 and Cs-135. The agricultural period is initially dominated by doses from Se-79 and I-129 at the onset which have accumulated in the coastal and lake sediments and then from groundwater discharges of I-129, Ni-59 and Tc-99.

5.1.3 1BTF

Figure 5-5 shows the radionuclide flux from 1BTF for the Alternative inventory. The release is dominated by organic C-14 up to 4,000 years post-2030 AD and the maximum flux is estimated to be 3.9E+08 Bq/y at around 3,000 AD. Fluxes of H-3, Sr-90 and Cs-137 are estimated reach a maximum within 200 years of closure but these are all three or more orders of magnitude below the overall maximum. During the period from 1,000 to 10,000 years post-2030 AD the release rates of organic C-14 and Ni-59 increase. Several other radionuclides contribute to the total flux between 1,000 and 20,000 years post-2030 AD including Cl-36, Se-79, Mo-93, Ag-108m and Cs-135 (these are all two or more orders of magnitude below the overall maximum). Ni-59 becomes the dominant radionuclide from 6,000 AD (two or more orders of magnitude below the overall maximum), and in the very long term Tc-99 is the most important radionuclide (more than three orders of magnitude below the overall maximum).

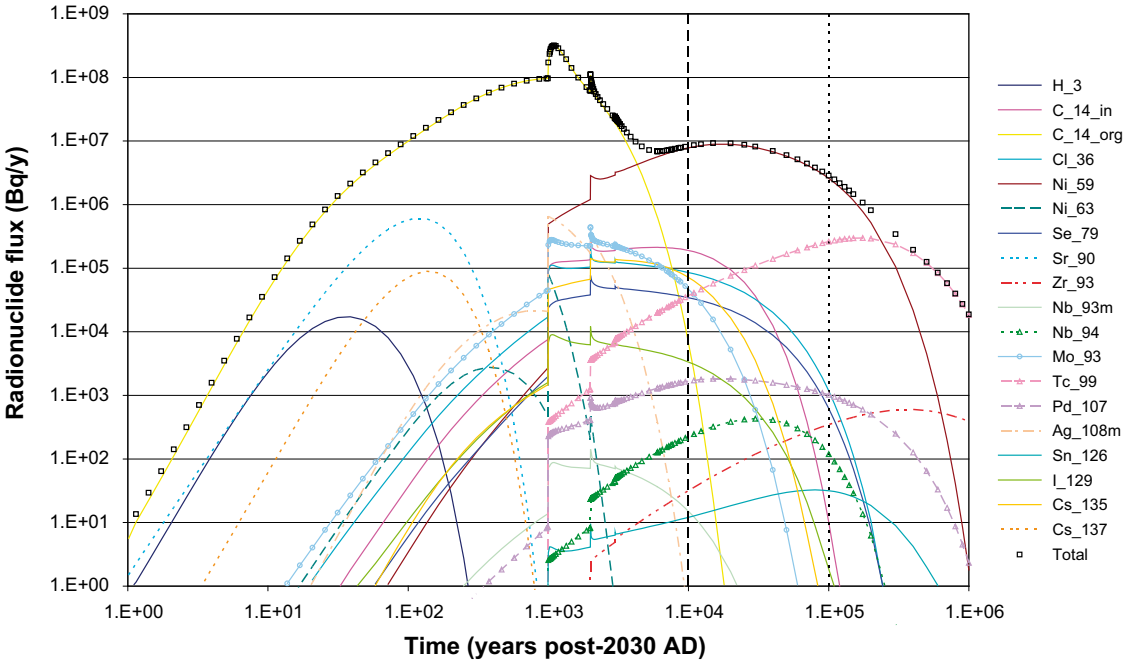

Figure 5-3. *BMA near-field radionuclide fluxes for Alternative inventory.*

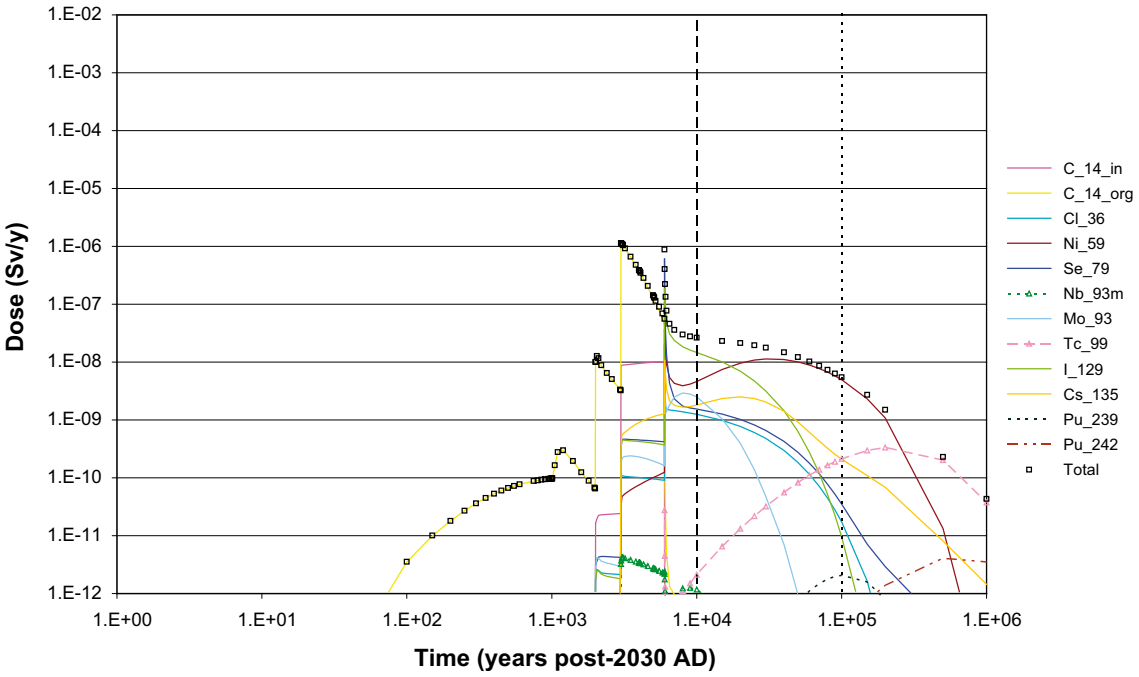

Figure 5-4. *BMA dose for RBD from Alternative inventory.*

Figure 5-6 summarises doses estimated from 1BTF to the RBD model for the Alternative inventory. Doses during the coastal period are less than 1E–08 Sv/y and are dominated by organic C-14. The maximum dose is estimated to be 8.0E–07 Sv/y which occurs at 5,100 AD, the onset of the lake period, and is due to organic C-14. Doses are also estimated to arise during the lake period from other radionuclides, in particular inorganic C-14 which dominates in the latter part of the lake period, as well as Se-79, I-129 and Cs-135. The agricultural period is initially dominated by doses from Se-79 at the onset and then I-129, Ni-59 and Tc-99.

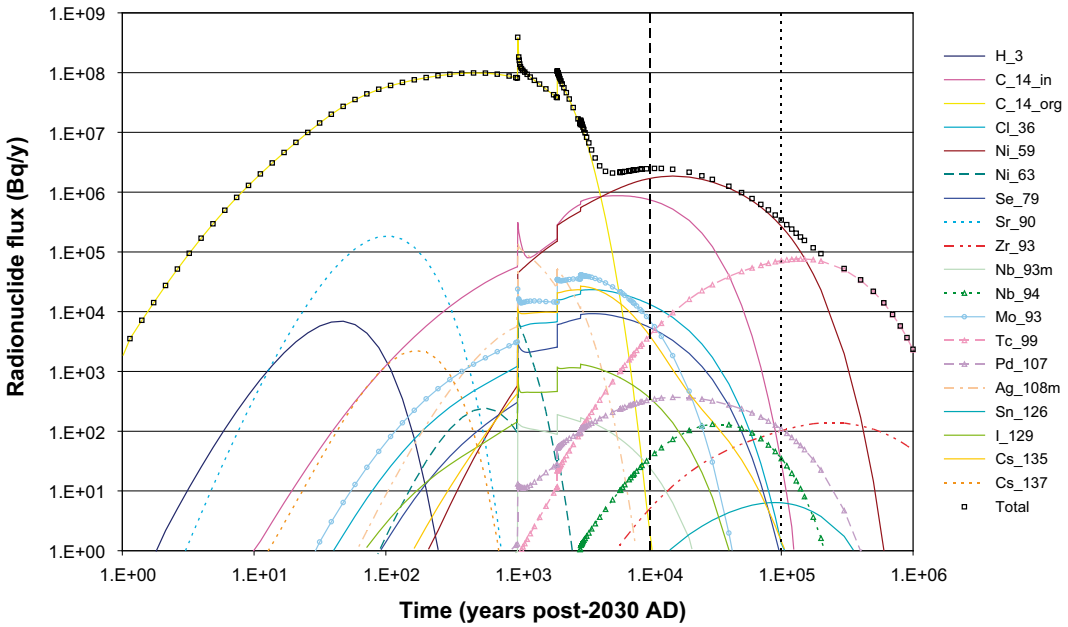

Figure 5-5. *1BTF near-field radionuclide fluxes for Alternative inventory.*

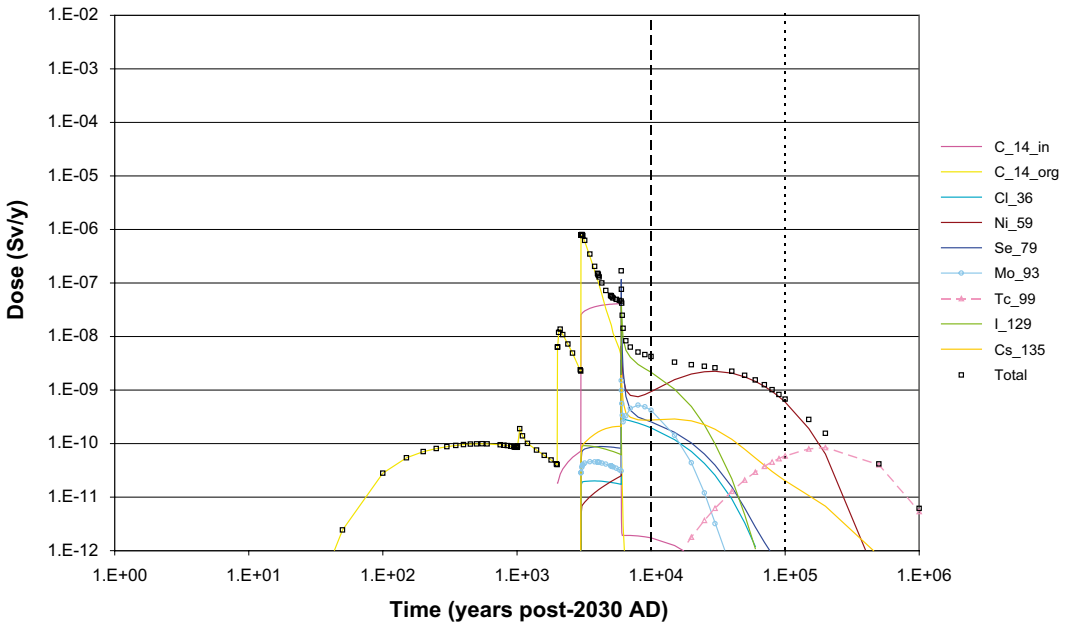

Figure 5-6. *1BTF dose for RBD from Alternative inventory.*

5.1.4 2BTF

Figure 5-7 shows the radionuclide flux from 2BTF for the Alternative inventory. The release is dominated by organic C-14 up to 6,000 AD and the maximum flux is estimated to be 1.8E+07 Bq/y at 3,100 AD. Fluxes of H-3, Sr-90 and Cs-137 are estimated reach a maximum within 200 years of closure (these are all more than an order of magnitude below the overall maximum). During the period from 1,000 to 10,000 years post-2030 AD the release rate of Ni-59 increases. Several other radionuclides contribute to the total flux between 1,000 and 20,000 years post-2,030 AD including inorganic C-14, Cl-36, Se-79, Mo-93, Ag-108m and Cs-135 (these are all two or more orders of magnitude below the overall maximum). Ni-59 becomes the dominant component of radionuclide flux from 4,000 to 200,000 years

post-2030 AD (more than an order of magnitude below the overall maximum), at which point the release of Tc-99 make this the most important radionuclide (around three or more orders of magnitude below the overall maximum).

Figure 5-8 summarises doses estimated from 2BTF to the RBD model for the Alternative inventory sensitivity calculation. Doses during the coastal period are less than 2E–09 Sv/y and during the lake period doses are estimated to be 1E–07 Sv/y or below dominated by organic C-14 in both cases. Exposures are also estimated to arise during the latter part of the lake period from other radionuclides, in particular inorganic C-14, Se-79, I-129 and Cs-135. The maximum dose is estimated to be 2.5E–07 Sv/y which occurs at the onset of the agricultural period, and is due to Se-79 (and I-129) which have previously accumulated in coastal and lake sediments. Doses during the agricultural period is initially dominated by contributions from Se-79 (and I-129) at the onset, and then by I-129, Ni-59 and finally Tc-99.

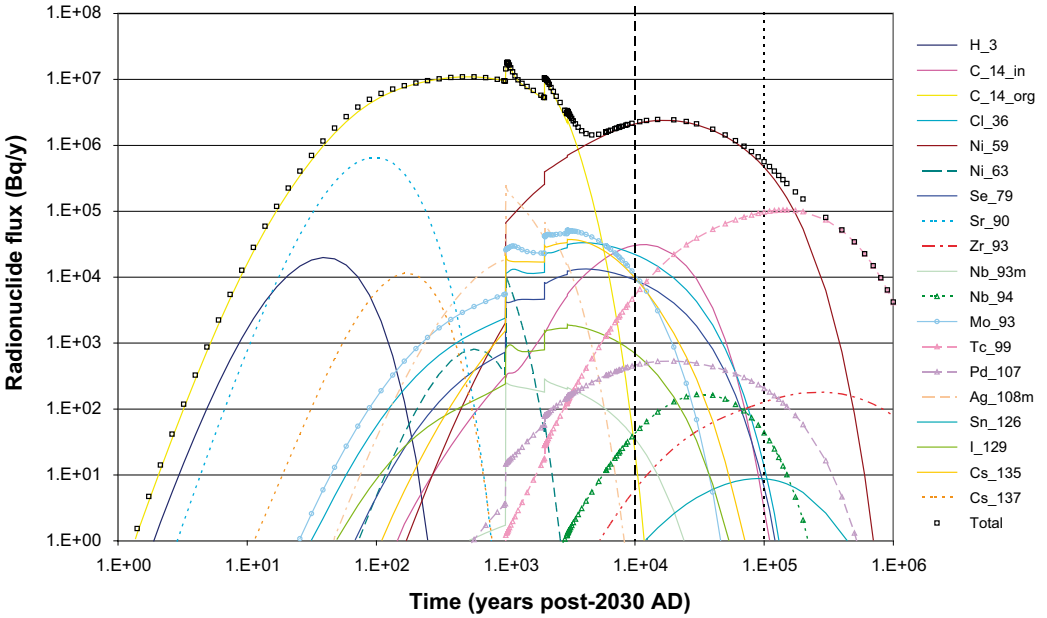

Figure 5-7. *2BTF near-field radionuclide fluxes for Alternative inventory.*

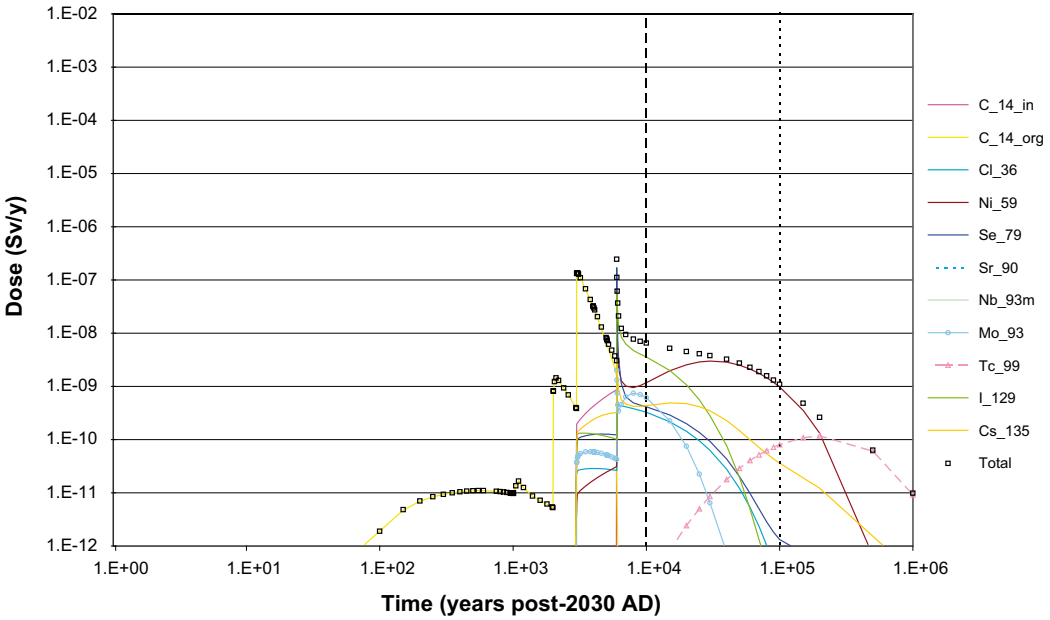

Figure 5-8. *2BTF dose for RBD from Alternative inventory.*

5.1.5 BLA

Figure 5-9 shows the radionuclide flux from the BLA for the Alternative inventory. The maximum radionuclide release of 9.6E+09 Bq/y occurs shortly after the repository is closed and is dominated by Ni-63 and Cs-137 with significant contributions from Co-60 and Sr-90. The total release rate from the BLA beyond 11,000 AD is estimated as being below 1 Bq/y.

The doses estimated to the RBD model from the BLA are shown in Figure 5-10. During the coastal period doses are below 2E–09 Sv/y and are dominated by contributions initially from Sr-90 and then by inorganic and organic C-14. Doses during the lake period are dominated by

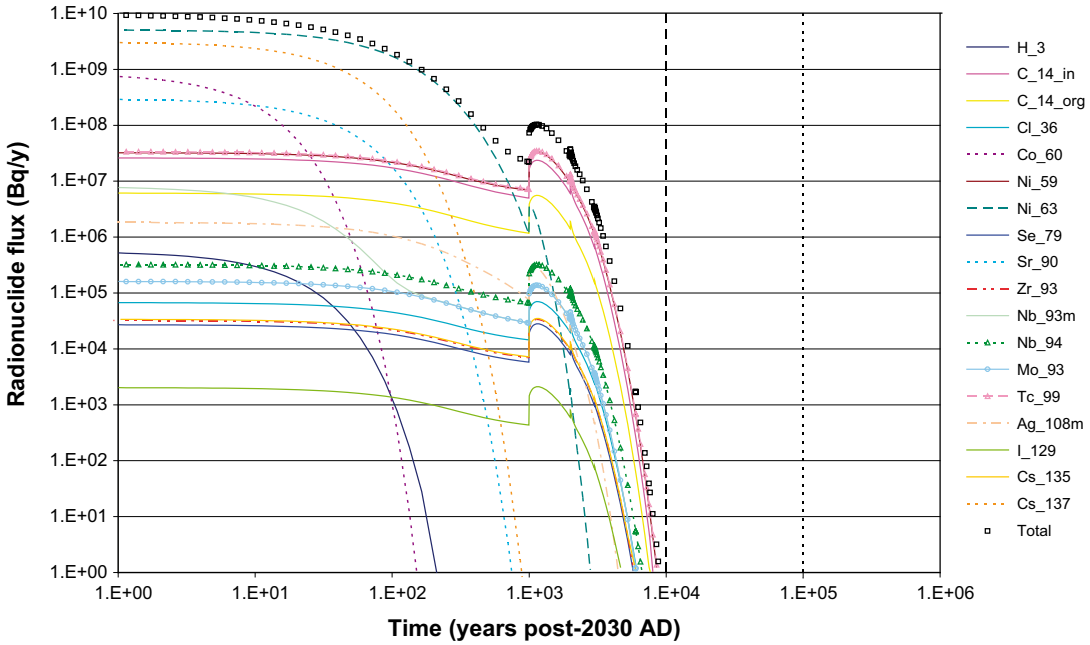

Figure 5-9. *BLA near-field radionuclide fluxes for Alternative inventory.*

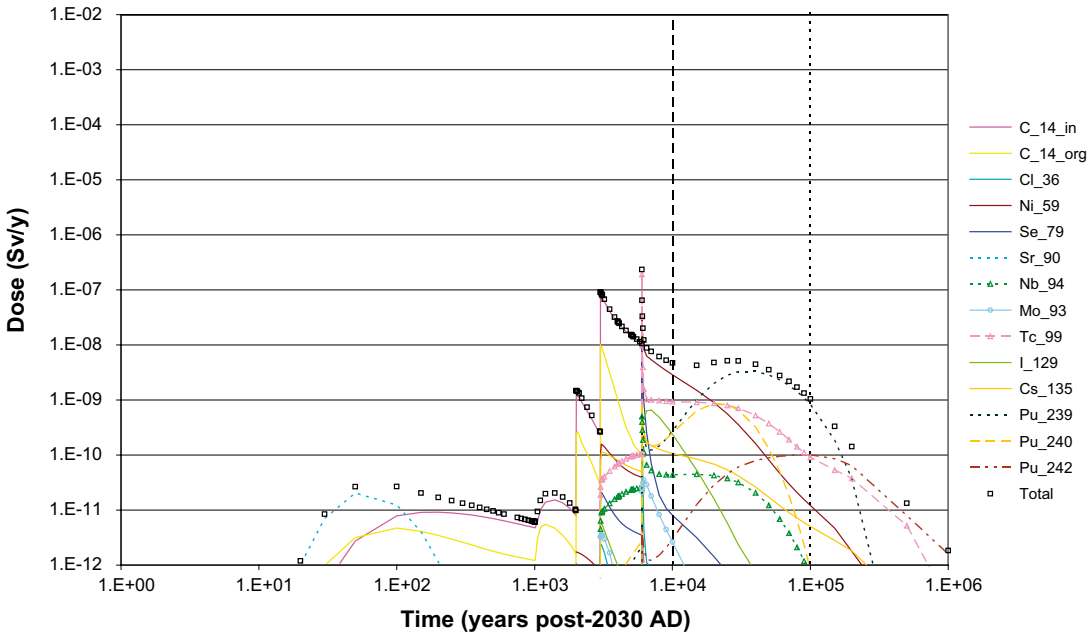

Figure 5-10. *BLA dose for RBD from Alternative inventory.*

inorganic and organic C-14 and are 1E–07 Sv/y or less. The maximum dose, 2.3E–07 Sv/y, is estimated to occur at the onset of the agricultural period (8,000 AD) and is due to Tc-99 which has previously accumulated in sediments. Thereafter the dose is dominated by contributions from Ni-59, Pu-239 and Pu-242.

5.1.6 SFR-1 summary for Alternative inventory

Figure 5-11 summarises the near-field radionuclide fluxes from each part of the repository and the total for the whole of SFR-1 for the Alternative inventory. The peak radionuclide flux, 9.6E+09 Bq/y, is estimated to occur initially and is due to releases of radionuclides from the BLA. Approximately 500 years following closure the largest radionuclide fluxes are from the Silo and 1BTF and this continues until 3,000 AD when releases from the Silo, BMA, 1BTF and BLA all contribute to the overall SFR-1 radionuclide flux. Subsequently, the long-term and very long-term radionuclide flux is due to contributions from the Silo and the BMA in the main, although these are an order of magnitude below the overall peak in the long-term and at least three orders of magnitude in the very long-term.

Figure 5-12 summarises the geosphere radionuclide fluxes from each part of the repository and the total for the whole of SFR-1 for the Alternative inventory. The peak radionuclide flux, 5.0E+09 Bq/y, is estimated to occur at around 3,200 AD and is due to releases from the BMA. The short-term release is due to contributions from the BLA and 1BTF. The long-term and very long-term radionuclide flux is due to contributions from the Silo and the BMA in the main.

Figure 5-13 summarises the estimated dose for the RBD model from each part of the repository and the total for the whole of SFR-1 for the Alternative inventory. Doses during the coastal period are initially dominated by releases from 1BTF and the BMA and latterly by the Silo. Doses during the lake period are dominated by release from the Silo and 1BTF and the BMA. The maximum dose is estimated to be 8.0E–06 Sv/y at 5,100 AD and is driven by releases from the Silo. Very long term doses during the agricultural period are dominated by contributions from the BMA and Silo.

The results for the Alternative inventory sensitivity case are summarised in Table 5-1.

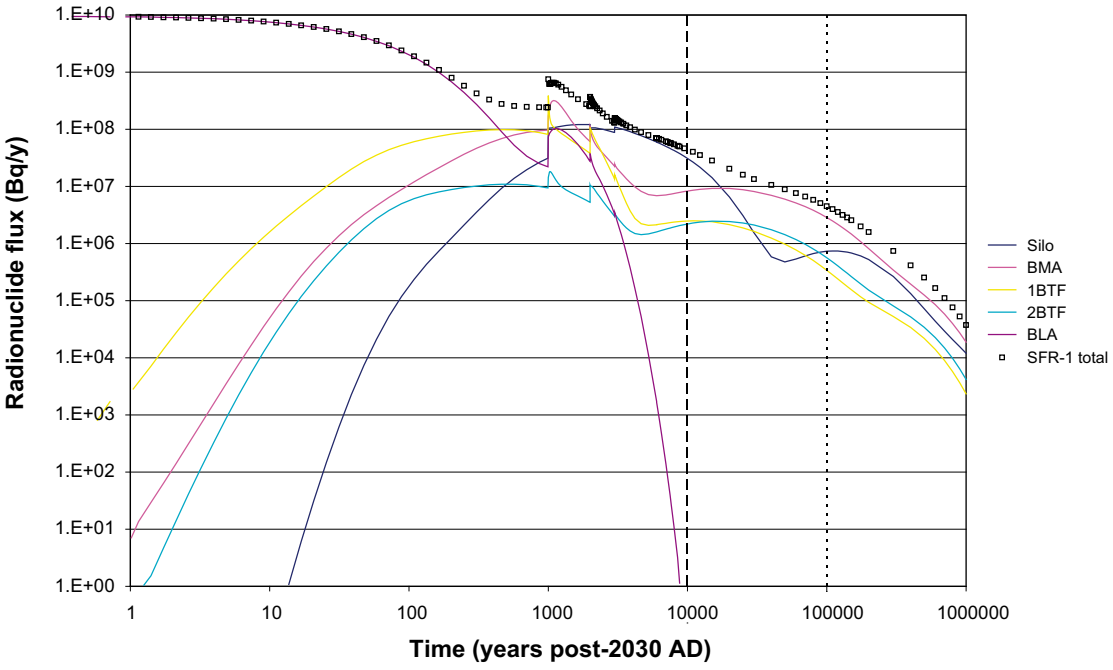

Figure 5-11. *Near-field radionuclide fluxes for the Alternative inventory.*

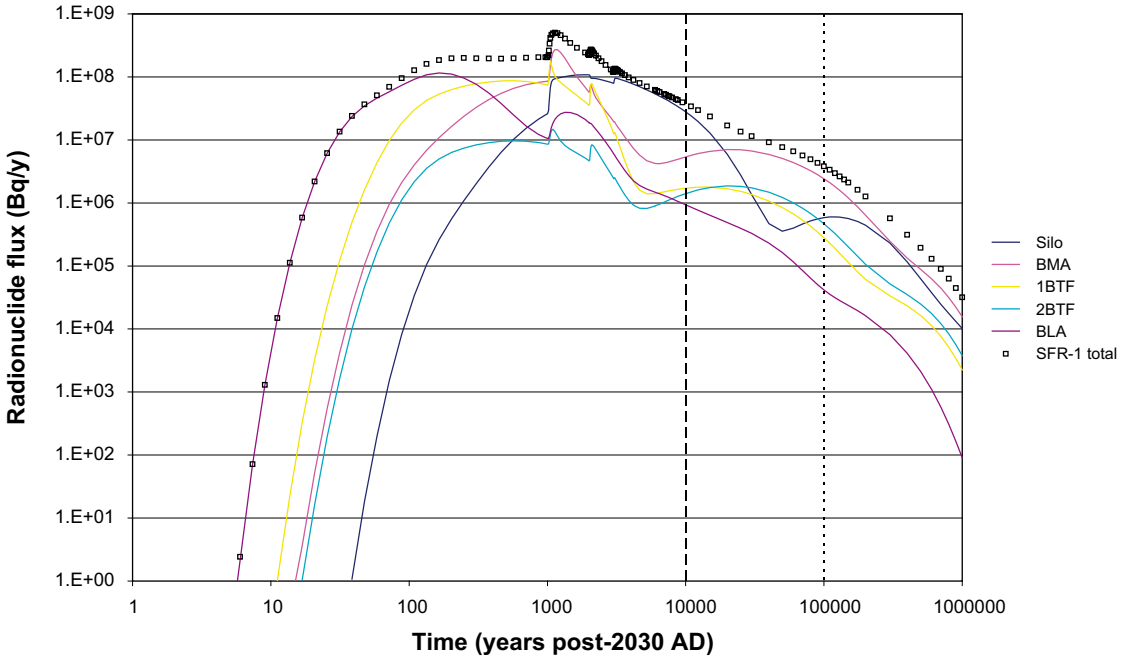

Figure 5-12. *Geosphere radionuclide fluxes for the Alternative inventory.*

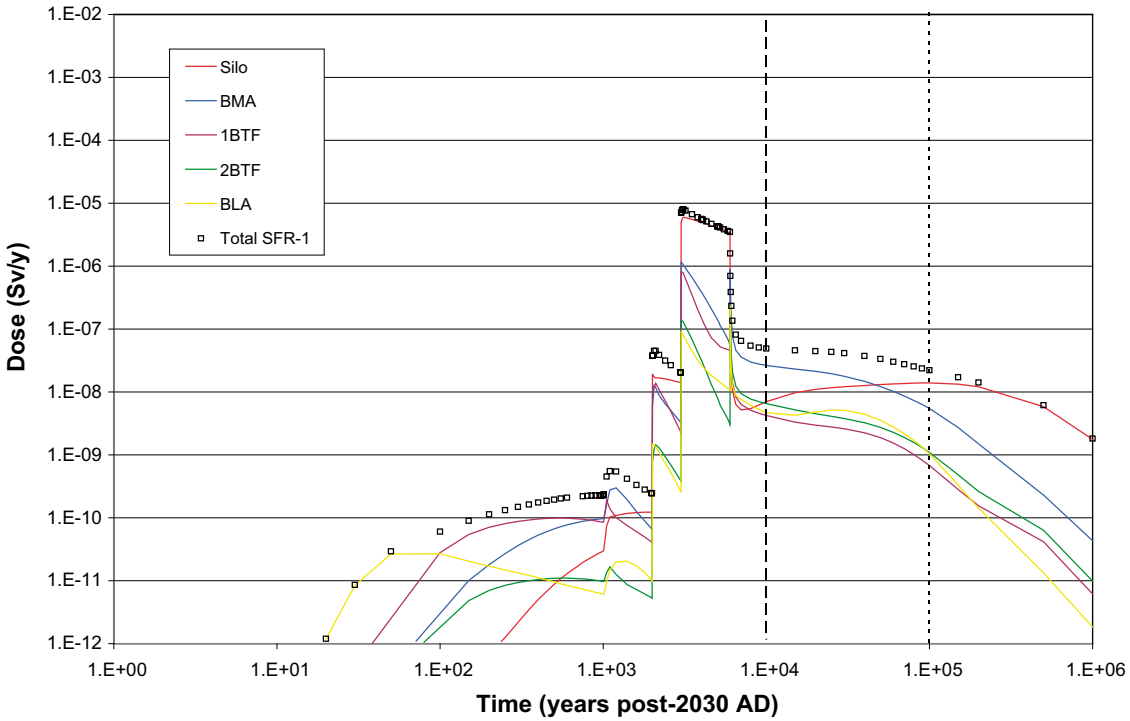

Figure 5-13. *Dose for RBD from the Alternative inventory.*

Table 5-1. Summary of Alternative inventory results.

	Near-field	Geosphere	RBD
Silo	1.2E+08 Bq/y at c. 3,900 AD	1.1E+08 Bq/y at c. 3,900 AD	6.0E–06 Sv/y at c. 5,100 AD
	Organic C-14	Organic C-14	Organic C-14
BMA	3.2E+08 Bq/y at c. 3,100 AD	2.7E+08 Bq/y at c. 3,200 AD	1.1E–06 Sv/y at c. 5,000 AD
	Organic C-14	Organic C-14	Organic C-14
1BTF	3.9E+08 Bq/y at c. 3,000 AD	1.7E+08 Bq/y at c. 3,100 AD	8.0E–07 Sv/y at c. 5,100 AD
	Organic C-14	Organic C-14	Organic C-14
2BTF	1.8E+07 Bq/y at c. 3,100 AD	1.5E+07 Bq/y at c. 3,100 AD	2.5E–07 Sv/y at c. 8,000 AD
	Organic C-14	Organic C-14	Se-79 and I-129
BLA	9.6E+09 Bq/y at 2,030 AD	1.2E+08 Bq/y at c. 2,200 AD	2.3E–07 Sv/y at c. 8,000 AD
	Ni-63 and Cs-137	Ni-63	Tc-99
SFR-1	9.6E+09 Bq/y at 2,030 AD	5.0E+08 Bq/y at c. 3,200 AD	8.0E–06 Sv/y at c. 5,100 AD
	BLA	BMA	Silo

5.2 Alternative near-field flow fields

5.2.1 Silo

Figure 5-14 shows the radionuclide flux from the Silo for the Alternative near-field flow fields. Breakthrough of organic C-14 dominates up to 50,000 years post-2030 AD. The maximum release rate is estimated to occur of 1.2E+07 Bq/y at around 4,100 AD. Ni-59 dominates the release profile from 25,000 years post-2030 AD until around 600,000 years post-2030 AD although the Ni-59 peak flux is more than three orders of magnitude below the overall maximum. At 600,000 years post-2030 AD the breakthrough of Tc-99 is dominant (but more than four orders of magnitude below the overall maximum).

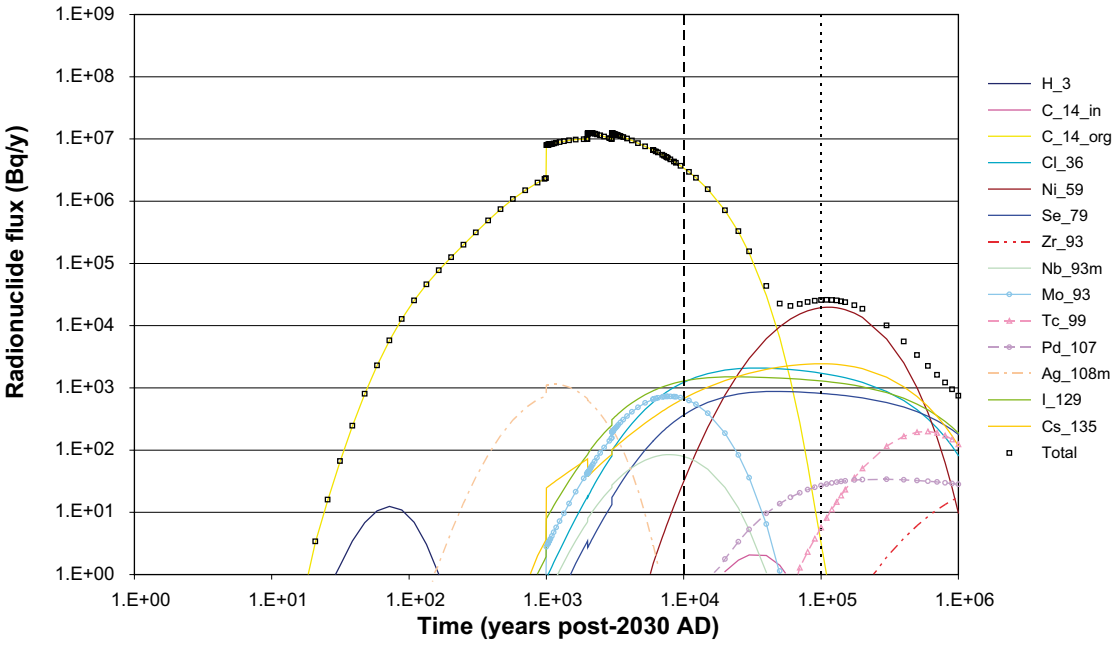

Figure 5-14. *Silo near-field radionuclide fluxes for Alternative near-field flow fields.*

Figure 5-15 shows the doses estimated to the RBD model from the Silo for the Alternative near-field flow fields. The doses during the coastal period are dominated by contributions from organic C-14 and are below 2E–09 Sv/y. The peak dose is estimated as 6.7E–07 Sv/y, it occurs during the lake period at around 5,100 AD and is dominated by organic C-14. Doses during the agricultural; period are dominated by contributions from I-129.

5.2.2 BMA

Figure 5-16 shows the radionuclide flux from the BMA for the Alternative near-field flow fields. Releases of organic C-14 dominate up to 6,500 AD. The maximum release rate is estimated to occur of 1.3E+08 Bq/y at 3,100 AD. Early releases of H-3, Sr-90 and Cs137 are estimated within the first 100 years (but these are two orders of magnitude or more below the overall

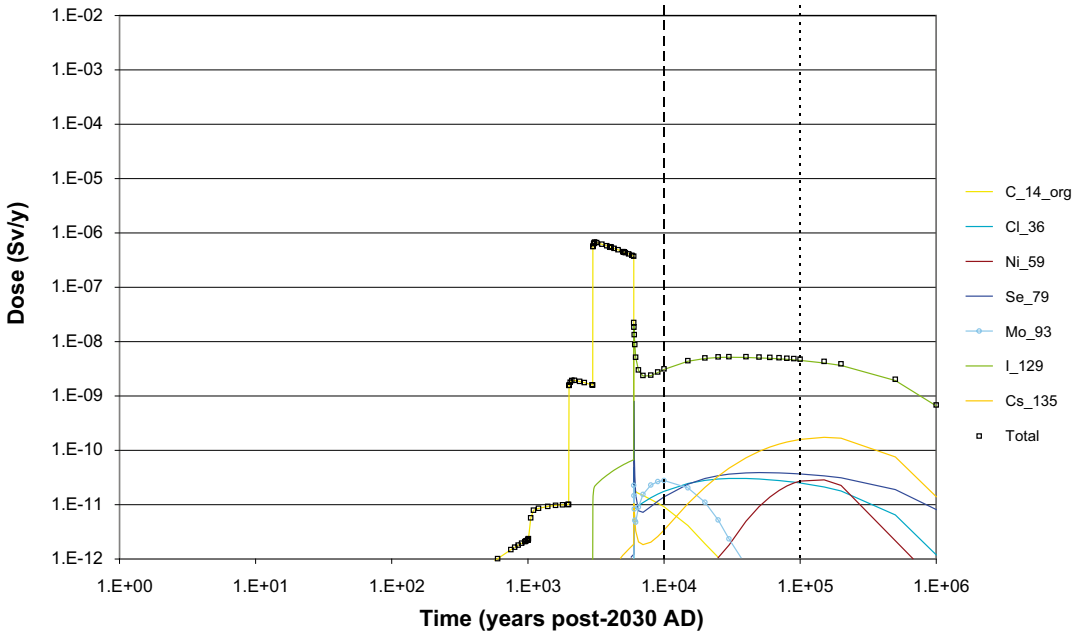

Figure 5-15. *Silo dose for RBD from Alternative near-field flow fields.*

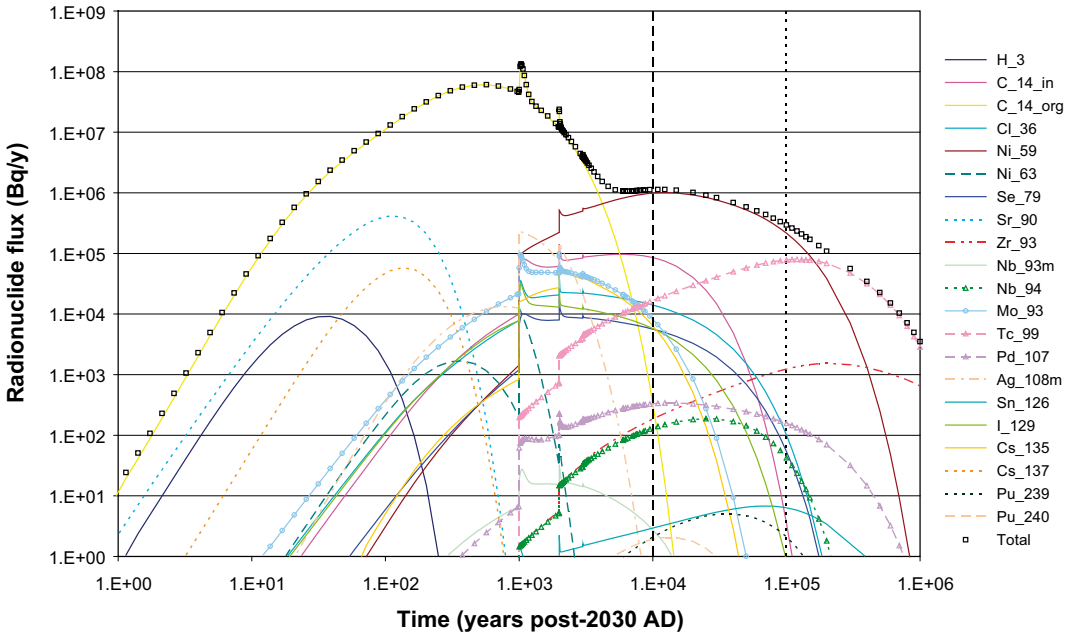

Figure 5-16. *BMA near-field radionuclide fluxes for Alternative near-field flow fields.*

maximum). Between 1,000 and 20,000 years post-2030 AD several radionuclides contribute to the total flux including inorganic C-14, Cl-36, Se-79, Mo-93, Tc-99, Ag108m and Cs-135 (these are all two orders of magnitude or more below the overall maximum). Ni-59 breakthrough dominates the release profile from 6,500 AD in the very long term the breakthrough of Tc-99 dominates (these are both also two orders of magnitude or more below the overall maximum).

Figure 5-17 shows the doses estimated to the RBD model from the BMA for the Alternative near-field flow fields. The doses during the coastal and lake periods are dominated by contributions from organic C-14 and are below 3E–09 Sv/y and 2E–07 Sv/y, respectively. The peak dose is estimated as 4.9E–07 Sv/y, it occurs at the onset of the agricultural period, 8,000 AD, and is dominated by I-129. This exposure is likely to be associated with the accumulation of activity within the coastal and lake sediments, as discussed previously. Doses during the agricultural period are then dominated by contributions from initially Ni-59 and then Tc-99.

5.2.3 1BTF

Figure 5-18 shows the radionuclide flux from the 1BTF for the Alternative near-field flow fields. Releases of organic C-14 dominate up to 6,500 AD. The maximum release rate is estimated to occur of 3.7E+08 Bq/y at around 4,000 AD. The breakthrough of inorganic C-14 increases at 4,000 AD and it dominates the release profile from 5,000 AD. Between 1,000 and 20,000 years post-2030 AD several other radionuclides contribute to the total flux including Cl-36, Ni-59 and Mo-93 (but these are all around three orders of magnitude or more below the overall maximum). At around 50,000 years post-2030 AD the release of Tc-99 makes this the dominant radionuclide.

Figure 5-19 summarises doses estimated from 1BTF to the RBD model for the Alternative near-field flow fields. Doses during the coastal period are less than 3E–08 Sv/y and are dominated by organic C-14, although inorganic C-14 contributes towards the end of the period. The maximum dose is estimated to be 2.4E–07 Sv/y which occurs at the end of the lake period, and is due to inorganic C-14. Dose contributions also occur during the lake period from organic C-14 and Cl-36, Mo-93 and I-129. The agricultural period is dominated by doses from I-129 at the onset and then by Ni-59 and Tc-99.

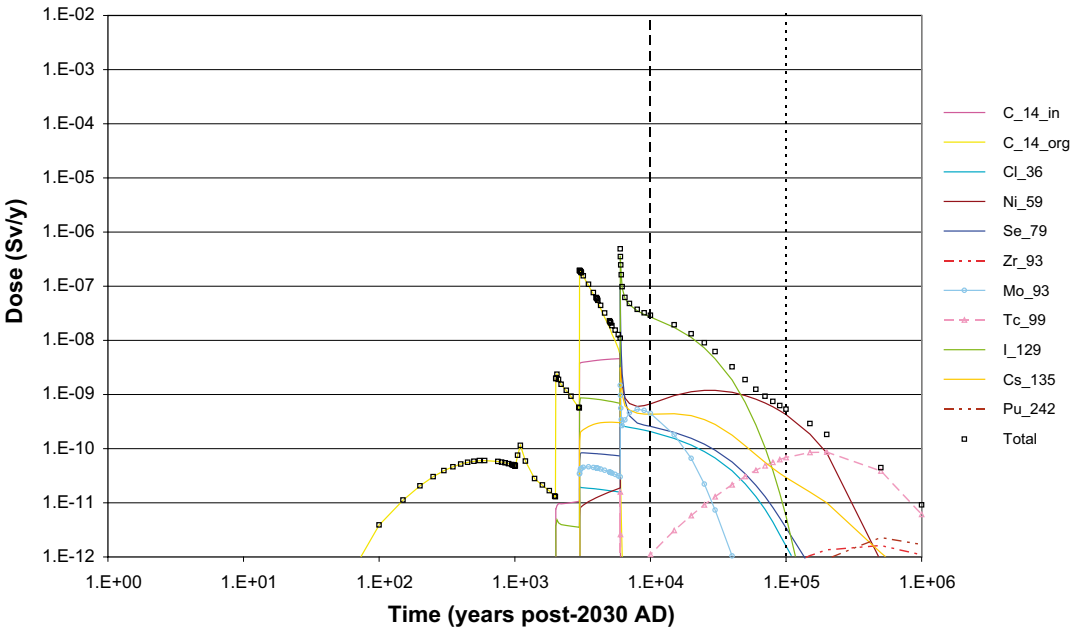

Figure 5-17. *BMA dose for RBD from Alternative near-field flow fields.*

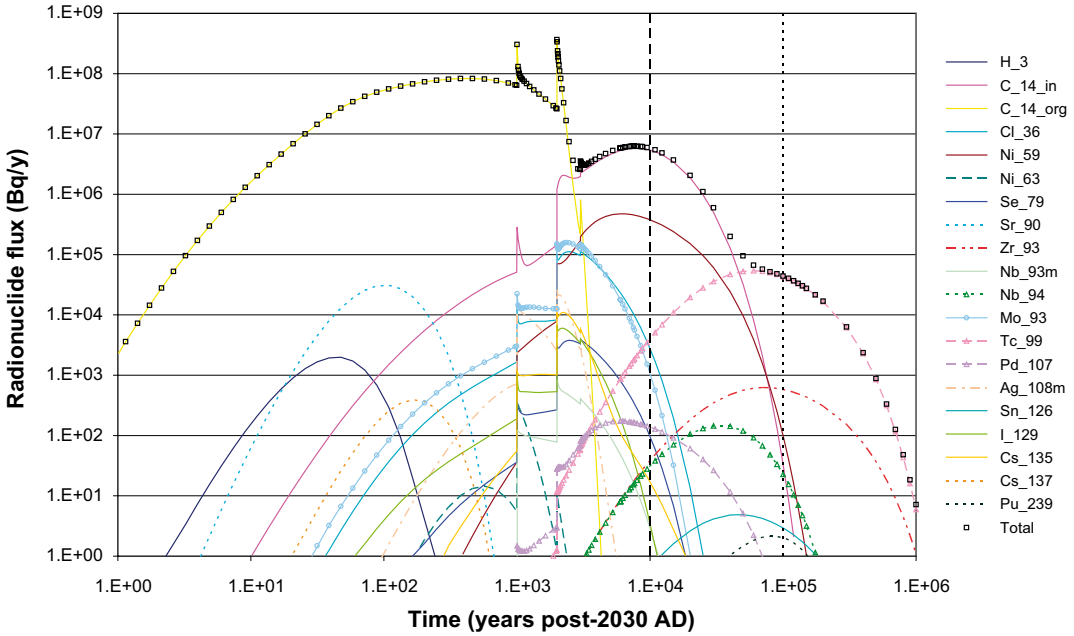

Figure 5-18. *1BTF near-field radionuclide fluxes for Alternative near-field flow fields.*

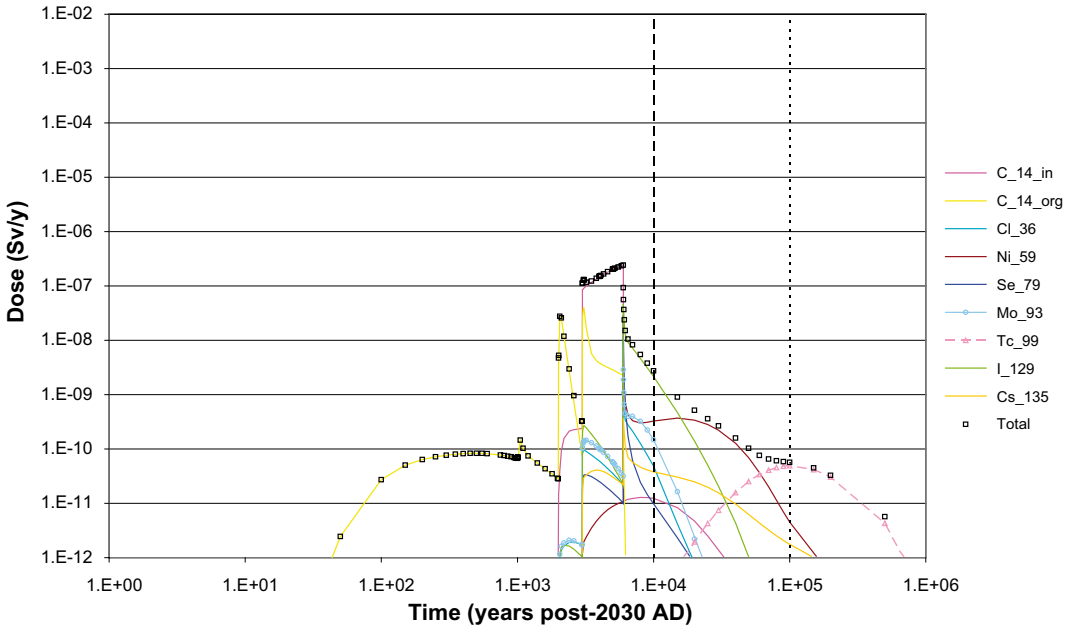

Figure 5-19. *1BTF dose for RBD from Alternative near-field flow fields.*

5.2.4 2BTF

Figure 5-20 shows the radionuclide flux from 2BTF for the Alternative near-field flow fields. The release is dominated by organic C-14 up to 3,000 years post-2030 AD and the maximum flux is estimated to be 8.36 Bq/y at 400 AD. Fluxes of H-3, Sr-90 and Cs-137 are estimated to reach a maximum within 200 years of closure but these peaks are more than two orders of magnitude below the overall maximum. During the period from 1,000 to 10,000 years post-2030 AD the release rate of Ni-59 increases becoming the dominant radionuclide from 3,000 to 100,000 years post-2030 AD, at which point the breakthrough of Tc-99 makes this the most important radionuclide but these peaks are one and two orders of magnitude below the overall maximum, respectively.

Figure 5-21 summarises doses estimated from 2BTF to the RBD model for the Alternative near-field flow fields. Doses during the coastal period are less than 1E–09Sv/y and are dominated by organic C-14. During the lake period doses are estimated to be 4E–09 Sv/y or below and initially are dominated by organic C-14 and later by inorganic C-14. Doses are also estimated to arise during the lake period from other radionuclides, in particular I-129 and Cs-135. The maximum dose is estimated to be 1.4E–07 Sv/y which occurs at the onset of the agricultural period, and is due to I-129 which has previously accumulated in the coastal (and lake) sediments. The agricultural period is dominated by doses from I-129 until 25,000 years post-2030 AD, and then by exposures from Ni-59 and Tc-99.

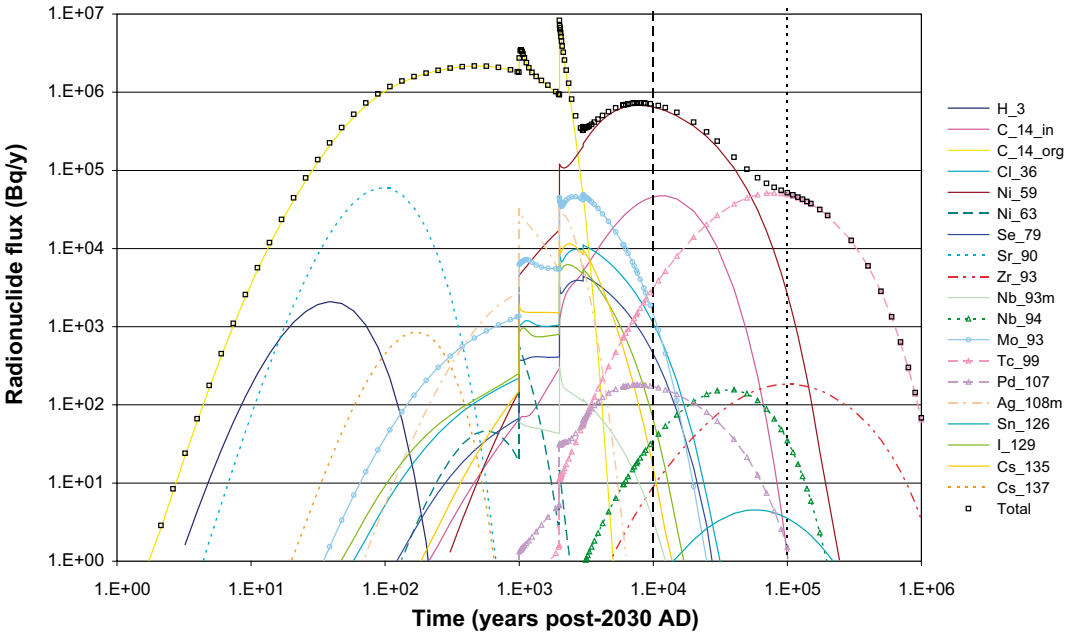

Figure 5-20. *2BTF near-field radionuclide fluxes for Alternative near-field flow fields.*

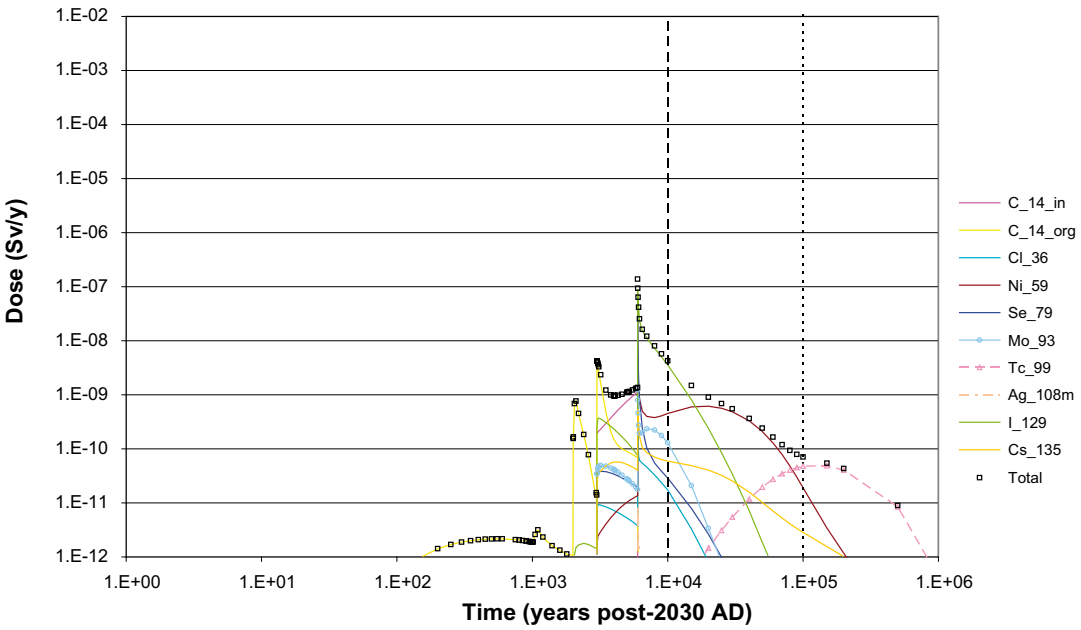

Figure 5-21. *2BTF dose for RBD from Alternative near-field flow fields.*

5.2.5 BLA

Figure 5-22 shows the radionuclide flux from the BLA for the Alternative near-field flow fields. The maximum radionuclide release of 3.1E+08 Bq/y occurs initially and is dominated by Co-60, Ni-63 and Cs-137. The release rate from the BLA beyond 5,500 AD is estimated as being below 1 Bq/y.

The doses estimated to the RBD model for the Alternative near-field flow fields are shown in Figure 5-23. During the coastal period doses are below 1E–10 Sv/y and are dominated by contributions from C-14. Doses during the lake period are dominated by inorganic and organic C-14 and are 2E–09 Sv/y or less. The maximum dose, 4.1E–09 Sv/y, is estimated to occur at the onset of the agricultural period (8,000 AD) and is due to Tc-99 which has previously accumulated in the coastal (and lake) sediments. Thereafter the dose is dominated by contributions from Ni-59, I-129 and Pu-239 (and to a lesser extent Tc-99, Pu-240 and Pu-242).

5.2.6 SFR-1 summary for Alternative near-field flow fields

Figure 5-24 summarises the near-field radionuclide fluxes from each part of the repository and the total for the whole of SFR-1 for the Alternative near-field flow fields. The peak radionuclide flux, 4.1E+08 Bq/y, is estimated to occur at 4,000 AD and is due to releases from the 1BTF and BMA. Releases from 1BTF dominate the radionuclide flux from 70 to 30,000 years post-2030 AD. Prior to this releases are dominated by the BLA and after by the BMA.

Figure 5-25 summarises the geosphere radionuclide fluxes from each part of the repository and the total for the whole of SFR-1 for the Alternative near-field flow fields. The peak radionuclide flux, 2.2E+08 Bq/y, is estimated to occur at 3,100 AD and is due to releases from the 1BTF and BMA. Releases from 1BTF dominate the radionuclide flux from 45 to 30,000 years post-2030 AD. Prior to this the breakthrough is dominated by the BLA and after by the BMA.

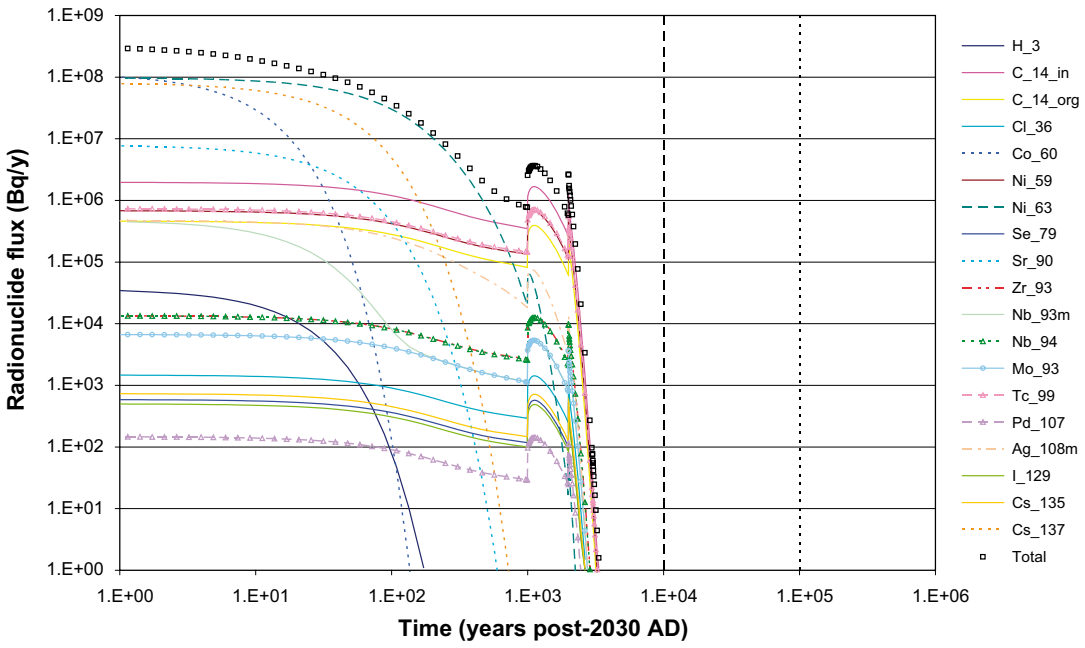

Figure 5-22. *BLA near-field radionuclide fluxes for Alternative near-field flow fields.*

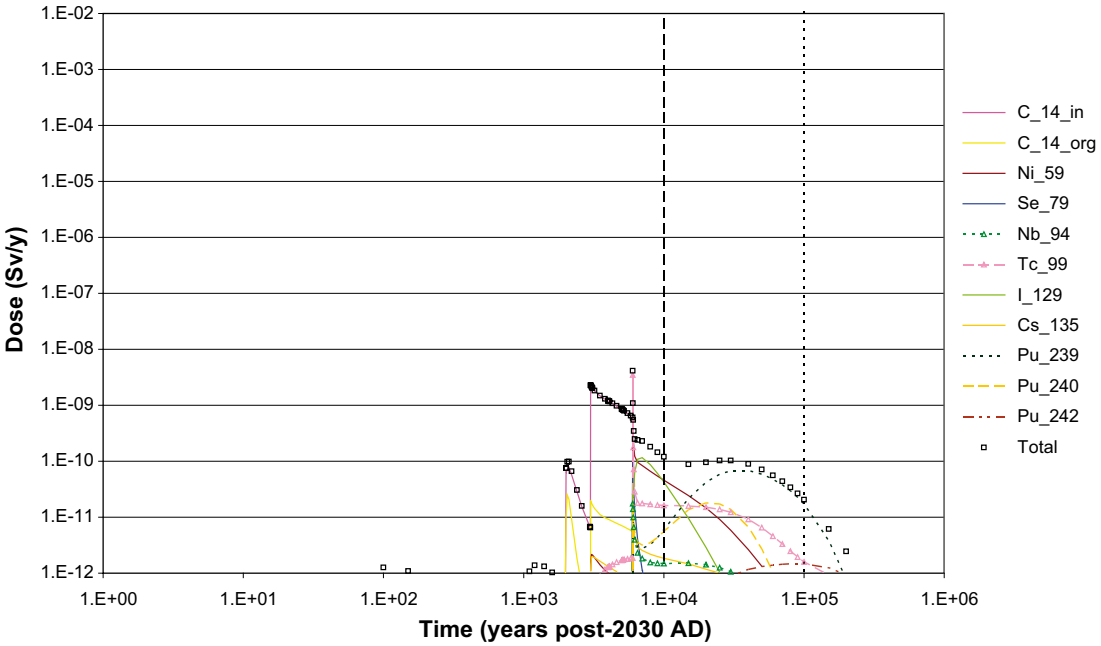

Figure 5-23. *BLA dose for RBD from Alternative near-field flow fields.*

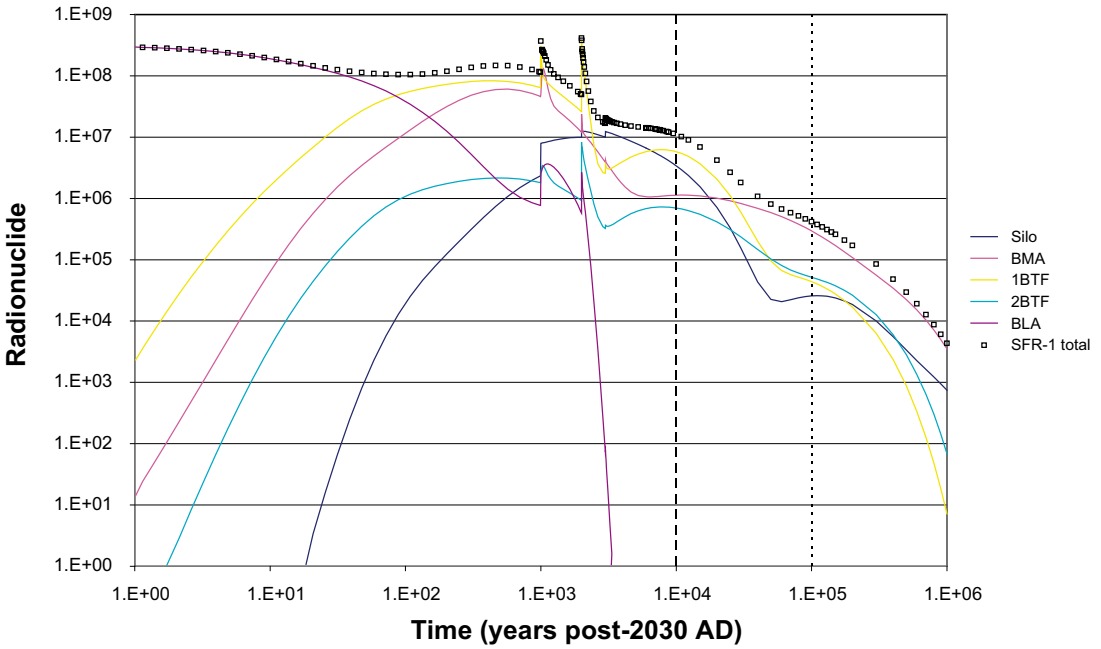

Figure 5-24. *Near-field radionuclide fluxes for Alternative near-field flow fields.*

Figure 5-26 summarises the estimated dose for RBD from each part of the repository and the total for the whole of SFR-1 for the Alternative near-field flow fields. Doses during the coastal period are initially dominated by exposures from radionuclides released from 1BTF and the BMA and latterly by the Silo. Doses during the lake period are dominated by radionuclide released from the Silo and also the BMA and 1BTF. The maximum dose is estimated to be 9.8E–07 Sv/y at the onset of the Lake period and is driven by releases from the Silo. Very long term doses during the agricultural period are dominated by contributions from the BMA and Silo.

Table 5-2 summarises the results from the Alternative near-field flow fields sensitivity case.

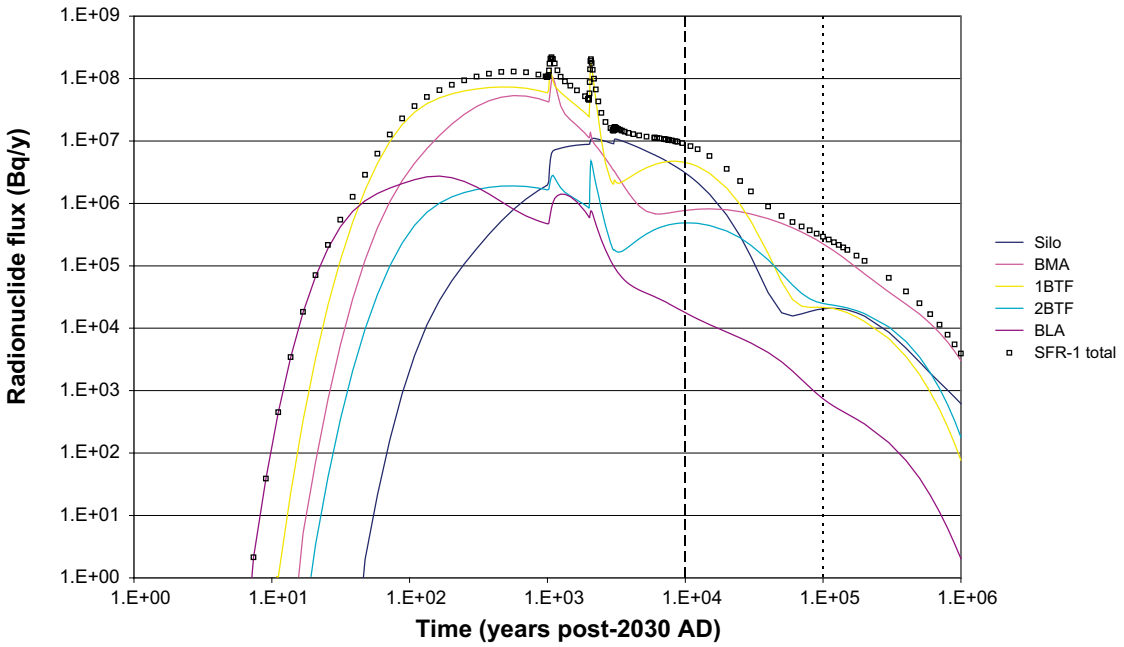

Figure 5-25. *Geosphere radionuclide fluxes for Alternative near-field flow fields.*

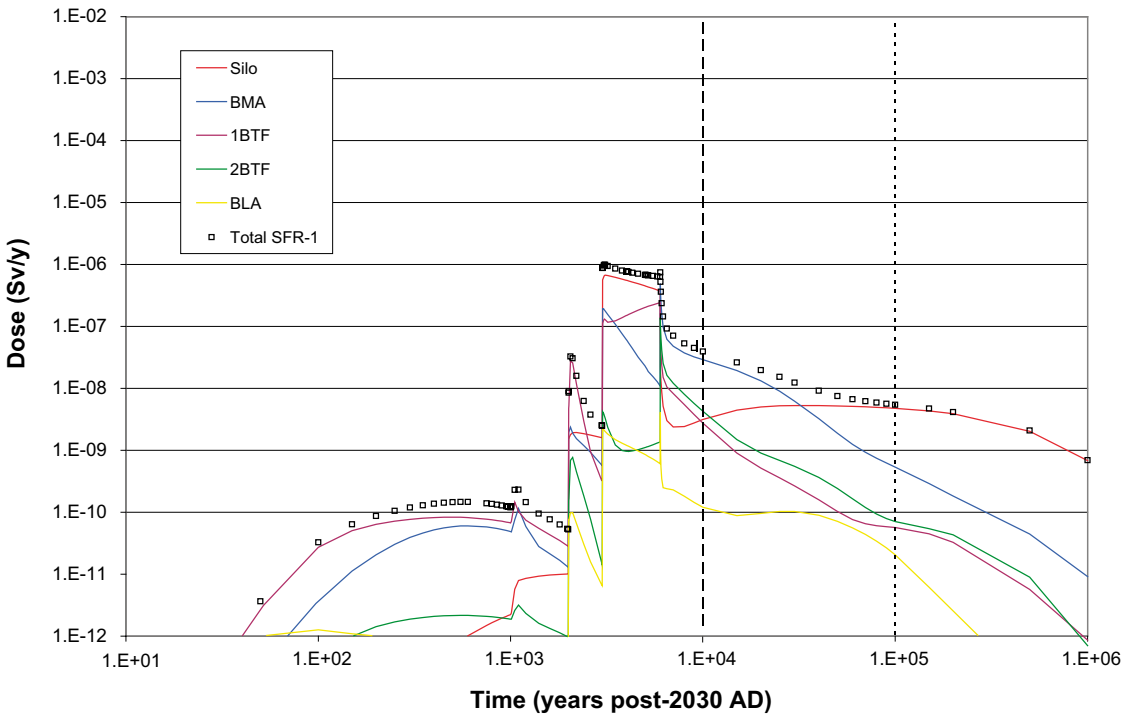

Figure 5-26. *Dose for RBD Alternative near-field flow fields.*

Table 5-2. Summary of Alternative near-field flow fields results.

	Near-field	Geosphere	RBD
Silo	1.2E+07 Bq/y at c. 4,100 AD	1.1E+07 Bq/y at c. 4,200 AD	6.7E–07 Sv/y at c. 5,100 AD
	Organic C-14	Organic C-14	Organic C-14
BMA	1.3E+08 Bq/y at c. 3,100 AD	1.0E+08 Bq/y at c. 3,100 AD	4.9E–07 Sv/y at c. 8,000 AD
	Organic C-14	Organic C-14	I-129
1BTF	3.7E+08 Bq/y at c. 4,000 AD	1.7E+08 Bq/y at c. 4,100 AD	2.4E–07 Sv/y at c. 8,000 AD
	Organic C-14	Organic C-14	Inorganic C-14
2BTF	8.3E+06 Bq/y at c. 4,000 AD	4.8E+06 Bq/y at c. 4,100 AD	1.4E–07 Sv/y at c. 8,000 AD
	Organic C-14	Organic C-14	I-129
BLA	3.1E+08 Bq/y at closure	2.7E+06 Bq/y at c. 2,200 AD	4.1E–09 Sv/y at c. 8,000 AD
	Co-60, Ni-63 and Cs-137	Ni-63	Tc-99
SFR-1	4.1E+08 Bq/y at c. 4,000 AD	2.2E+08 Bq/y at c. 3,100 AD	9.8E–07 Sv/y at c. 5,000 AD
	1BTF	BMA and 1BTF	Silo

5.3 Minimum near-field sorption

5.3.1 Silo

Figure 5-27 shows the radionuclide flux from the Silo for Minimum near-field sorption. Releases of organic C-14 dominate up to 15,000 years post-2030 AD. The maximum release rate estimated to occur is 1.3E+07 Bq/y at 3,900 AD. Releases of Ag-108m and Cs-137 at early times are significant and contribute to the total flux. Between 1,000 and 10,000 years post-2030 AD fluxes from Cl-36, Se-79, Nb-93, Mo-93, Ag-108m, I-129 and Cs-135 peak. Ni-59 dominates the release profile in the long-term with Tc-99.

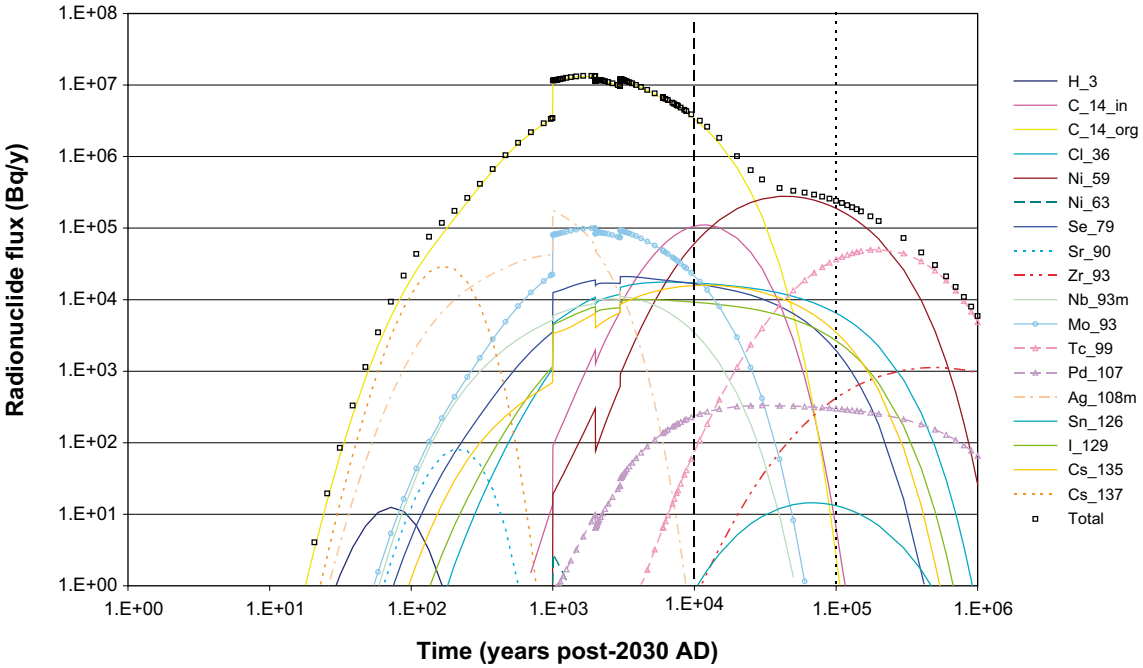

Figure 5-27. *Silo near-field radionuclide fluxes for Minimum near-field sorption.*

Figure 5-28 summarises doses estimated from the Silo to the RBD model for Minimum near-field sorption. Doses during the coastal period are less than 2E–09 Sv/y and are dominated by organic C-14. The maximum dose is estimated to be 6.5E–07 Sv/y at 5,100 AD during the lake period and is dominated by exposure to organic C-14. Dose contributions arise during the lake period from other radionuclides, in particular inorganic C-14, Se-79, Mo-93, I-129 and Cs-135. The agricultural period is dominated by exposures from I-129 from the onset until 500,000 years post-2030 AD when exposures from Tc-99 become the most significant source of exposure.

5.3.2 BMA

Figure 5-29 shows the radionuclide flux from the BMA for Minimum near-field sorption. Releases of Cs-137 dominate for the first 175 years and then organic C-14 up to 4,500 AD. The maximum release rate of 1.0E+08 Bq/y is estimated to occur at around 3,100 AD. From 3,000 AD inorganic C-14 and Ni-59 increase until inorganic C-14 becomes the dominant

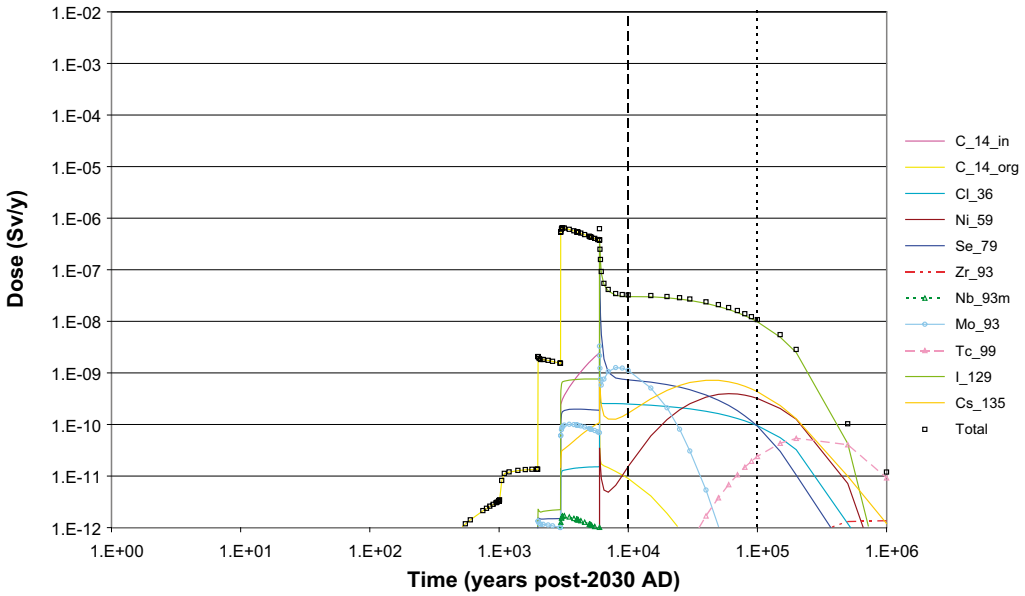

Figure 5-28. *Silo dose for RBD for Minimum near-field sorption.*

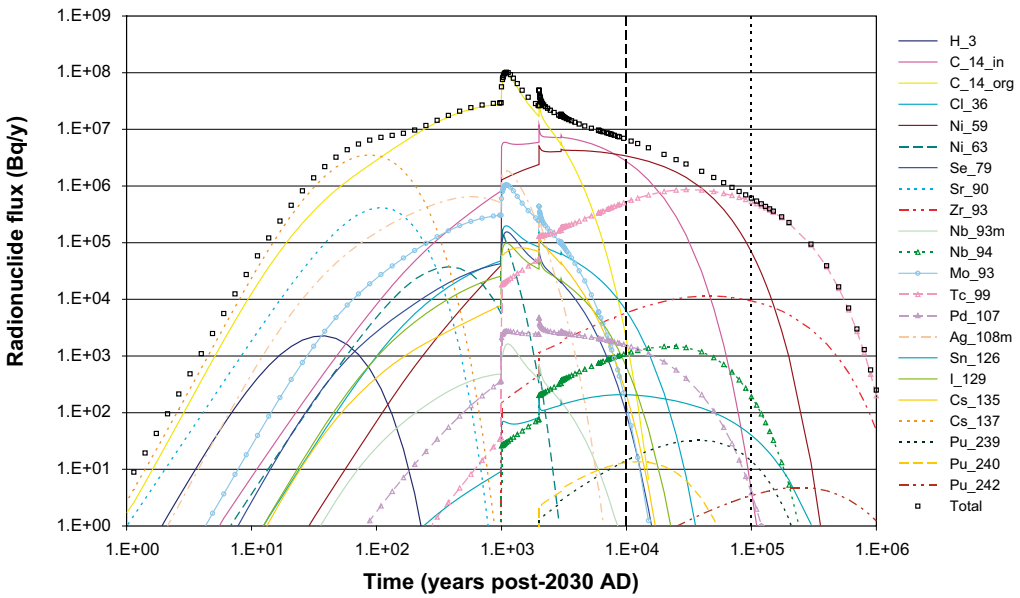

Figure 5-29. *BMA near-field radionuclide fluxes for Minimum near-field sorption.*

radionuclide at 4,500 AD. Ni-59 then dominates the release profile from 10,000 AD until around 50,000 years post-2030 AD when the breakthrough of Tc-99 dominates.

The doses estimated from the BMA to the RBD model for Minimum near-field sorption are shown in Figure 5-30. Doses during the coastal period are below 5E–09 Sv/y and are dominated by organic C-14, although inorganic C-14 becomes more important towards the end of the period. The maximum dose is estimated to be 6.5E–07 Sv/y which occurs at the onset of the lake period, and is dominated by doses due to both inorganic and organic C-14. The agricultural period is initially dominated by exposures from I-129, which peak initially at 6.2E–07 Sv/y, and then by exposures from Ni-59 and Tc-99 (with Pu-242 becoming dominant towards the end of the simulation).

5.3.3 1BTF

Figure 5-31 shows the radionuclide flux from the 1BTF for Minimum near-field sorption. Releases of organic C-14 dominate up to 4,500 AD. The maximum release rate of 3.2E+08 Bq/y is estimated to occur at around 3,000 AD. The release rate of inorganic C-14 increases from 3,000 AD and it dominates the release profile from 4,500 years AD until 40,000 years post-2030 AD when the release of Tc-99 makes this the dominant radionuclide.

Figure 5-32 summarises doses estimated from 1BTF to the RBD model for Minimum near-field sorption. Doses during the coastal period are less than 2E–08 Sv/y and are dominated by organic C-14, although inorganic C-14 contributes significantly towards the end of the period. The maximum dose is estimated to be 2.5E–06 Sv/y which occurs at 5,100 AD during the lake period, and is dominated by dose due to inorganic C-14. The agricultural period is initially dominated by doses from I-129 from the onset until 15,000 years post-2030 AD, then by Ni-59 and finally by Tc-99.

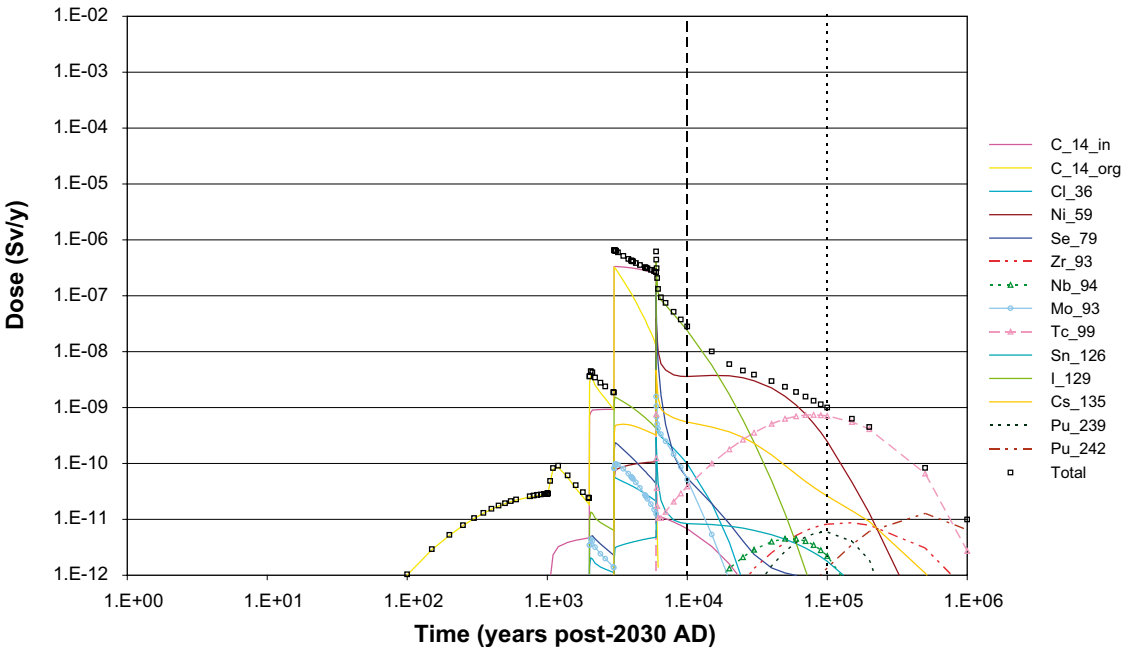

Figure 5-30. *BMA dose for RBD for Minimum near-field sorption.*

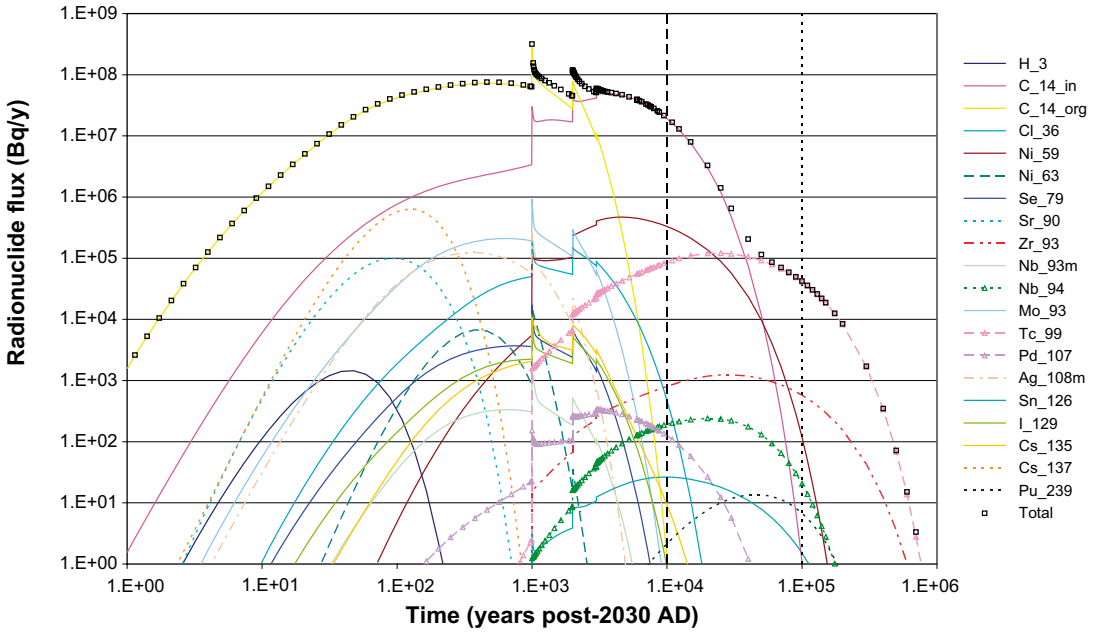

Figure 5-31. *1BTF near-field radionuclide fluxes for Minimum near-field sorption.*

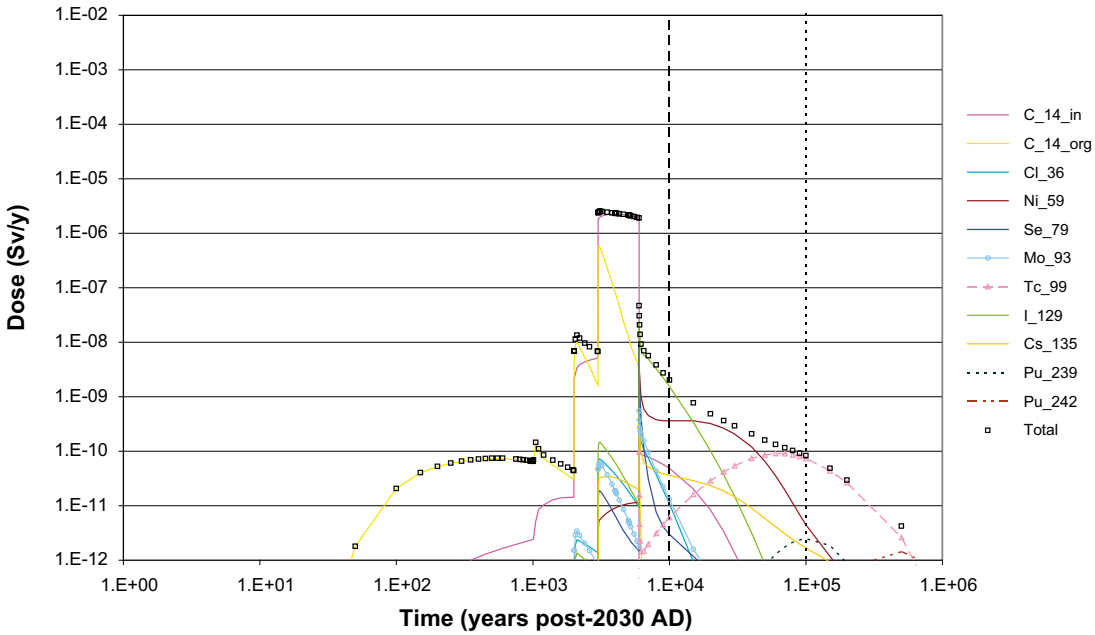

Figure 5-32. *1BTF dose for RBD for Minimum near-field sorption.*

5.3.4 2BTF

Figure 5-33 shows the radionuclide flux from 2BTF for Minimum near-field sorption. The release rate for the initial 200 years is dominated by organic C-14, Sr-90, Ag-108m and Cs-137. Organic C-14 has the highest radionuclide flux up to 2,500 years post-2030 AD (except a period from 45 to 175 years when Cs-137 is the dominant radionuclide flux). The maximum flux is estimated to be 4.3E+06 Bq/y at around 3,100 AD. During the period from 1,000 to 10,000 years post-2030 AD the release rate of inorganic C-14 and Ni-59 increases with inorganic C-14 dominating from 2,500 to 8,000 years post-2030 AD and Ni-59 from 8,000 to 50,000 years post-2030 AD. From 50,000 years post-2030 AD onwards the flux is dominated by Tc-99.

Figure 5-34 summarises doses estimated from 2BTF to the RBD model for Minimum near-field sorption. Doses during the coastal period are 3E–10 Sv/y or less and are dominated by organic C-14, although contributions from inorganic C-14 are significant towards the end of the period. During the lake period doses are estimated to be below 6E–08 Sv/y and are dominated by contributions from inorganic C-14 with initial significant contributions from organic C-14. The maximum dose is estimated to be 7.5E–08 Sv/y which occurs at 8,000 AD, the onset of the agricultural period, and is dominated by dose due to I-129. The agricultural period is dominated by doses from I-129 until 15,000 years post-2030 AD, then in the very long term Ni-59 and finally Tc-99.

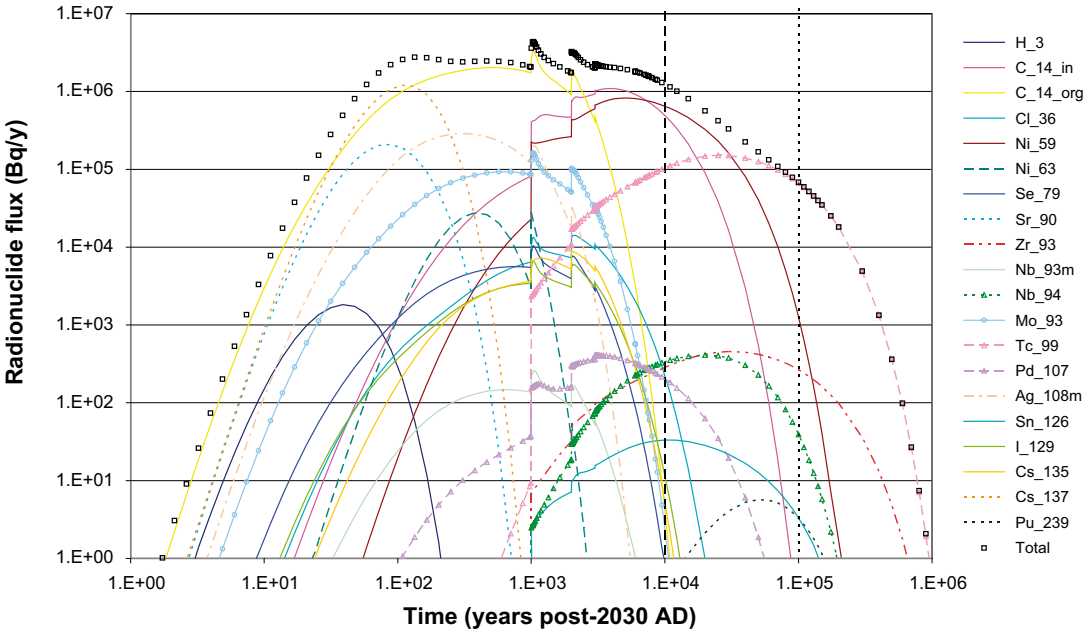

Figure 5-33. *2BTF near-field radionuclide fluxes for Minimum near-field sorption.*

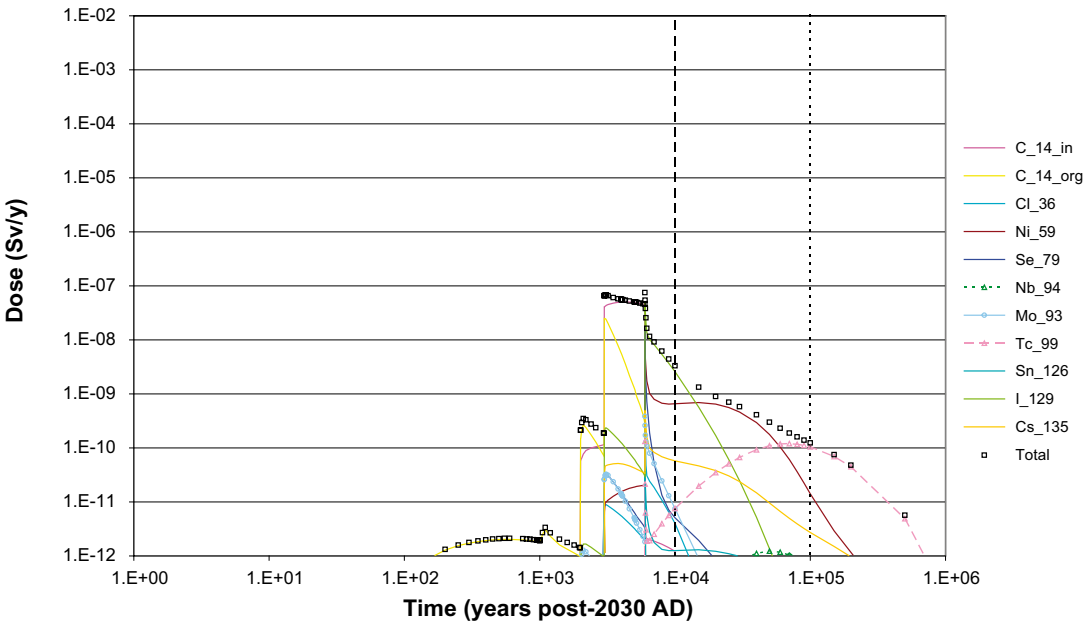

Figure 5-34. *2BTF dose for RBD for Minimum near-field sorption.*

5.3.5 BLA

No sorption is considered within the BLA model. Therefore this disposal tunnel was not included in this sensitivity calculation.

5.3.6 SFR-1 summary for Minimum near-field sorption

Figure 5-35 summarises the near-field radionuclide fluxes from each part of the repository and the total for the whole of SFR-1 for Minimum near-field sorption (results for the BLA Most likely scenario have been included to allow comparisons to be made). The peak radionuclide flux, 3.9E+08 Bq/y, is estimated to occur at 3,000 AD and is dominated by releases from 1BTF. Releases from 1BTF dominate the radionuclide flux until 20,000 years post-2030 AD. Very long-term releases are subsequently driven by contributions from the BMA up to 500,000 years and the Silo thereafter.

Figure 5-36 summarises the geosphere radionuclide fluxes from each part of the repository and the total for the whole of SFR-1 for Minimum near-field sorption (results for the BLA Most likely scenario have been included to allow comparisons to be made). The peak radionuclide flux, 1.9E+08 Bq/y, is estimated to occur at 3,100 AD and is dominated by releases from 1BTF. Releases from 1BTF dominate the radionuclide flux until 25,000 years post-2030 AD. Very long-term releases are subsequently driven by contributions from the BMA up to 500,000 years and the Silo thereafter.

Figure 5-37 summarises the estimated dose for RBD from each part of the repository and the total for the whole of SFR-1 for Minimum near-field sorption (results for the BLA Most likely scenario have been included to allow comparisons to be made). Doses during the coastal and lake period are dominated by releases from 1BTF for the most part. The maximum dose is estimated to be 3.9E–06 Sv/y at 5,000 AD which is the onset of the lake period and is driven by releases from 1BTF. Very long term doses during the agricultural period are dominated by contributions from the BMA and Silo.

Table 5-3 summarises the results from the Minimum near-field sorption sensitivity case.

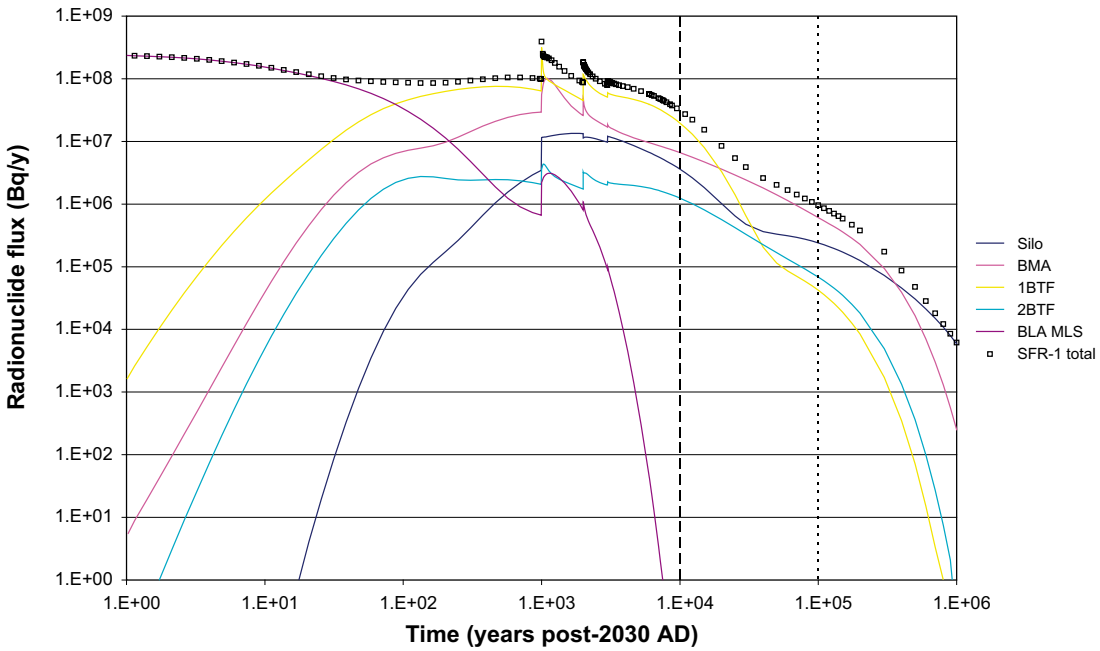

Figure 5-35. *Near-field radionuclide fluxes for Minimum near-field sorption.*

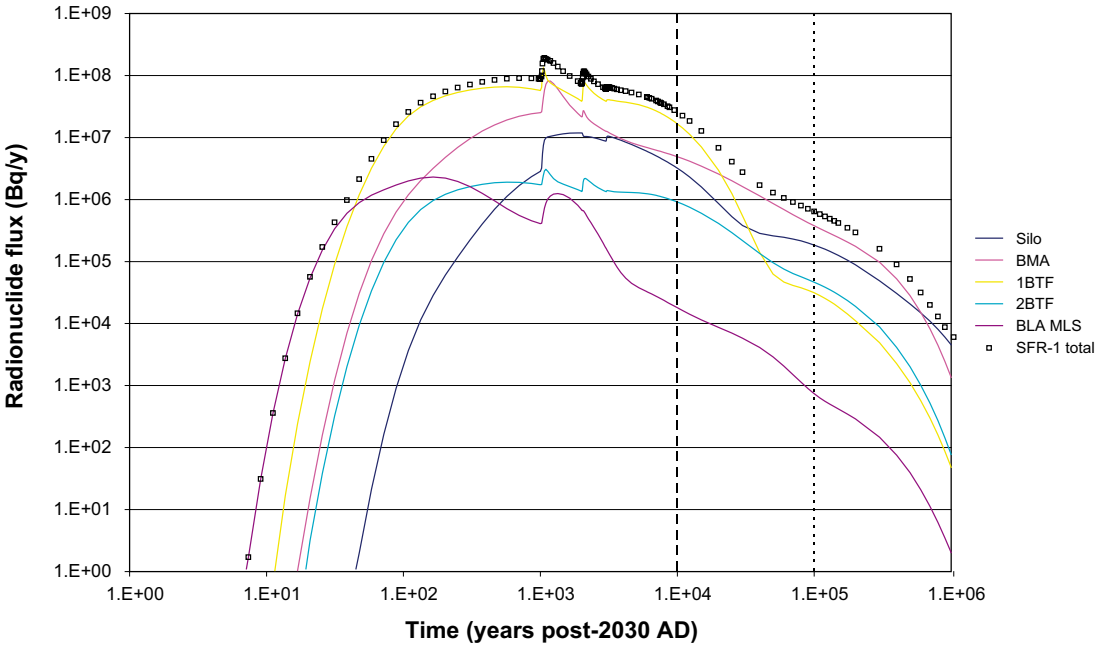

Figure 5-36. *Geosphere radionuclide fluxes for Minimum near-field sorption.*

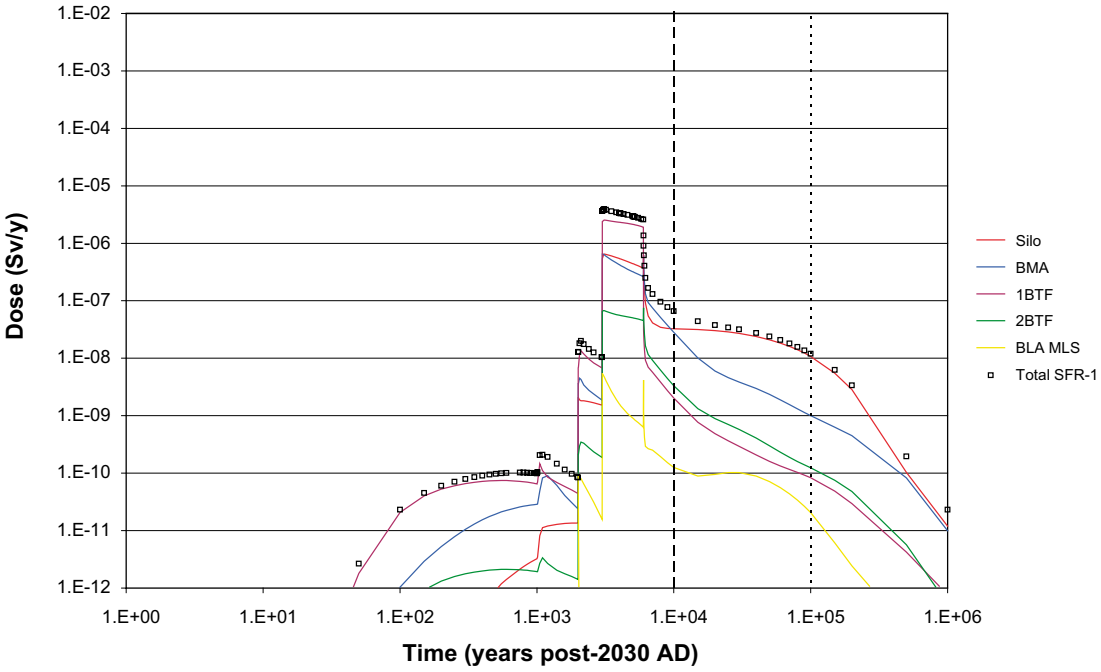

Figure 5-37. *Dose for RBD from Minimum near-field sorption.*

Table 5-3. Summary of Minimum near-field sorption results.

	Near-field	Geosphere	RBD
Silo	1.3E+07 Bq/y at c. 3,700 AD Organic C-14	1.2E+07 Bq/y at c. 3,900 AD Organic C-14	6.5E–07 Sv/y at c. 5,100 AD Organic C-14
BMA	1.0E+08 Bq/y at c. 3,100 AD Organic C-14	8.2E+07 Bq/y at c. 3,200 AD Organic C-14	6.5E–07 Sv/y at c. 5,000 AD Inorganic and organic C-14
1BTF	3.2E+08 Bq/y at c. 3,000 AD Organic C-14	1.3E+08 Bq/y at c. 3,100 AD Organic C-14	2.5E–06 Sv/y at c. 5,100 AD Inorganic C-14
2BTF	4.3E+06 Bq/y at c. 3,100 AD Organic C-14	3.0E+06 Bq/y at c. 3,100 AD Organic C-14	7.5E–08 Sv/y at c. 8,000 AD I-129
BLA#	2.5E+08 Bq/y at 2,030 AD Co-60, Ni-63, Cs-137	2.3E+06 Bq/y at c. 2,200 AD Ni-63	5.5E–09 Sv/y at c. 5,000 AD Inorganic C-14
SFR-1	3.9E+08 Bq/y at c. 3,000 AD 1BTF	1.9E+08 Bq/y at c. 3,100 AD 1BTF	3.9E–06 Sv/y at c. 5,000 AD 1BTF

Data for Most likely scenario.

5.4 Maximum near-field sorption

5.4.1 Silo

Figure 5-38 shows the radionuclide flux from the Silo for Maximum near-field sorption. Releases of organic C-14 dominate up to 40,000 years post-2030 AD. H-3 is the only other radionuclide estimated to be released at rates above 1 Bq/y in the initial 6,500 years. The maximum release rate estimated to occur is 1.3E+07 Bq/y at around 3,900 AD. The long-term total radionuclide flux is driven firstly by releases of I-129, then Ni-59 and finally Cs-135.

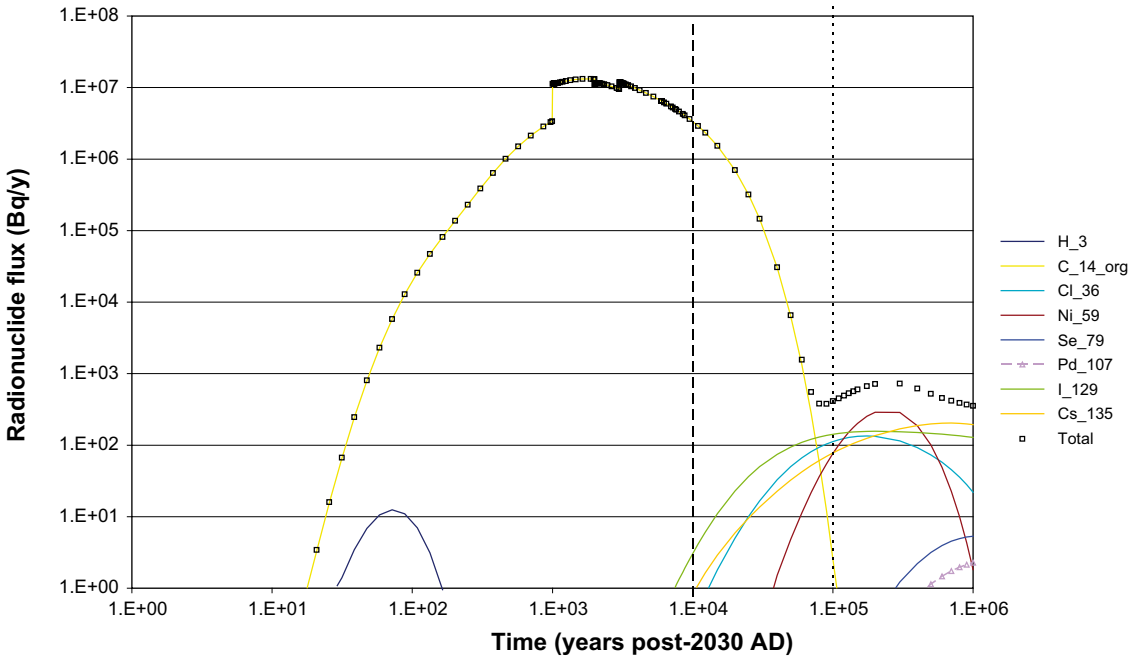

Figure 5-38. *Silo near-field radionuclide fluxes for Maximum near-field sorption.*

Figure 5-39 summarises doses estimated from the Silo to the RBD model for Maximum near-field sorption. Doses during the coastal period are less than 2E–09 Sv/y and are dominated by organic C-14. The maximum dose is 6.5E–07 Sv/y at 5,100 AD which occurs during the lake period and is dominated by dose due to contributions from organic C-14. The agricultural period is initially dominated by doses from organic C-14 until around 10,000 AD at which point I-129 subsequently dominates doses.

5.4.2 BMA

Figure 5-40 shows the radionuclide flux from the BMA for Maximum near-field sorption. Organic C-14 dominates releases up to 10,000 AD. Prior to 4,000 AD, only small amounts of other radionuclides (H-3 and Sr-90) are released. The maximum release rate is estimated to be 9.1E+07 Bq/y occurring at around 3,100 AD. From 3,000 AD the Ni-59 release rate increases as it becomes the dominant component of radionuclide flux until the release of Tc-99 makes this the dominant radionuclide in the very long term.

The doses estimated from the BMA to the RBD model for Maximum near-field sorption are shown in Figure 5-41. Doses during the coastal period are 3E–09 Sv/y or less and are dominated by organic C-14. The maximum dose is estimated to be 3.0E–07 Sv/y which occurs at the onset of the lake period, and is dominated by dose due to organic C-14. The doses in the agricultural period are below 4E–08 Sv/y, exposures are dominated by I-129 until towards the end of the simulation when contributions from Se-79 become dominant.

5.4.3 1BTF

Figure 5-42 shows the radionuclide flux from the 1BTF for Maximum near-field sorption. Releases of organic C-14 dominate up to 15,000 years post-2030 AD. The maximum release rate is estimated to occur of 2.9E+08 Bq/y at 3,000 AD. The release rates of Cl-36 and Ni-59 increase from 3,000 AD and Ni-59 dominates the release profile from 15,000 years post-2030 AD and thereafter the release of Tc-99 makes this the dominant component of radionuclide flux in the very long-term.

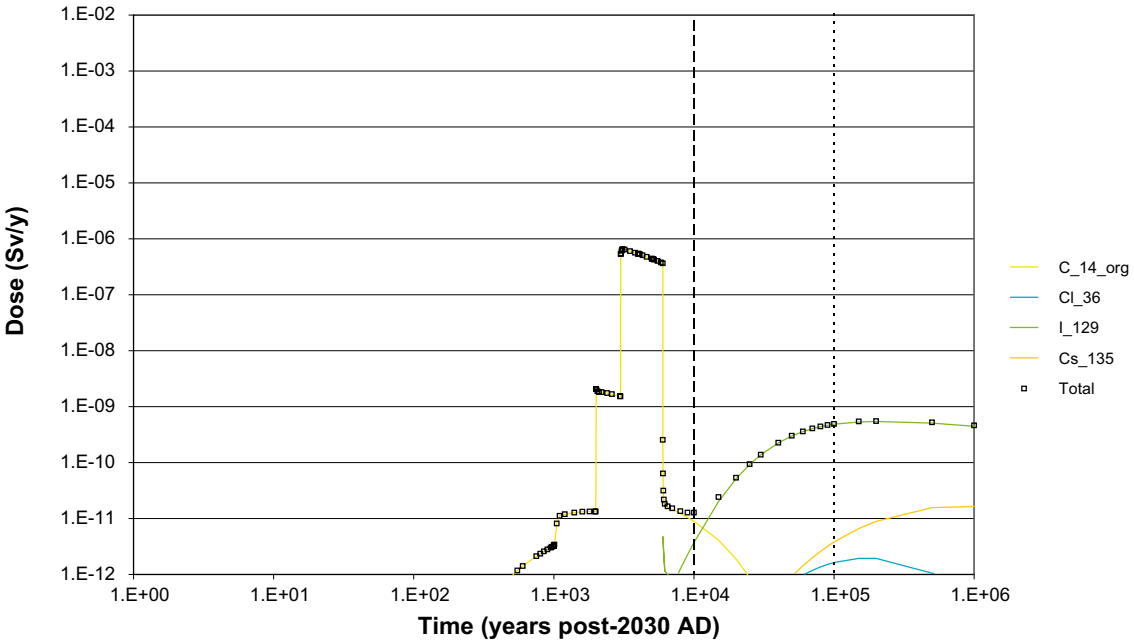

Figure 5-39. *Silo dose for RBD for Maximum near-field sorption.*

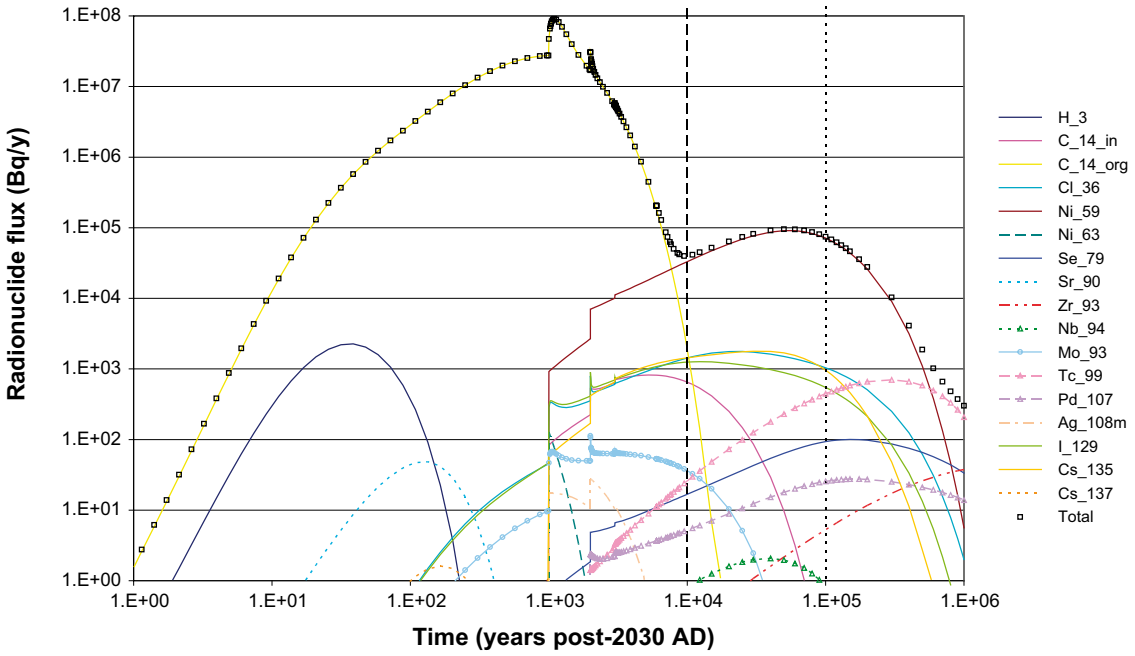

Figure 5-40. *BMA near-field radionuclide fluxes for Maximum near-field sorption.*

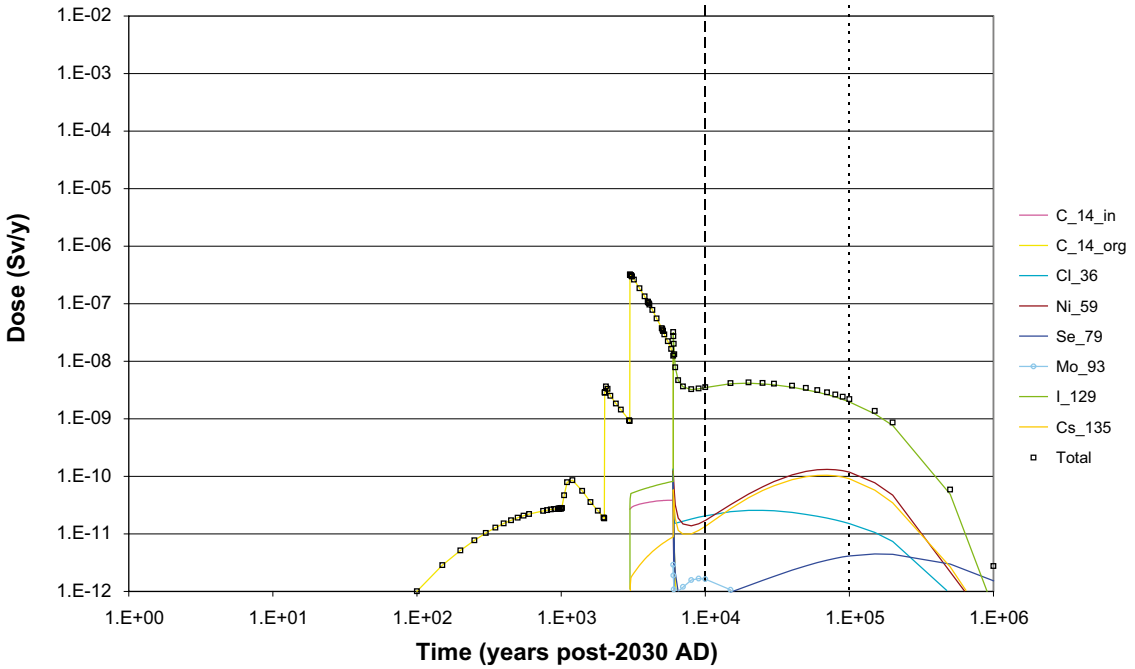

Figure 5-41. *BMA dose for RBD for Maximum near-field sorption.*

Figure 5-43 summarises doses estimated from 1BTF to the RBD model for Maximum near-field sorption. Doses during the coastal period are less than 1E–08 Sv/y and are dominated by organic C-14. The maximum dose is estimated to be 5.7E–07 Sv/y which occurs at 5,000 AD during the onset of the lake period, and is dominated by dose due to organic C-14. The agricultural period is dominated by doses from I-129 and are generally below 1E–09 Sv/y except at the beginning when the largest exposures occur from I-129 which has accumulated in the coastal and lake sediments.

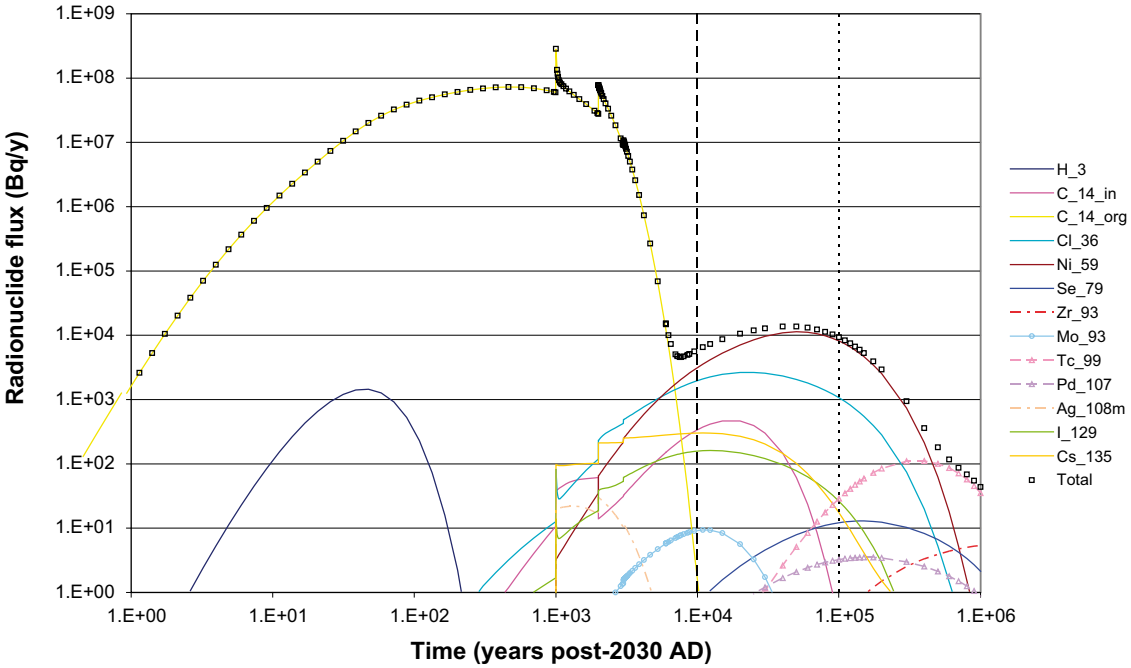

Figure 5-42. *1BTF near-field radionuclide fluxes for Maximum near-field sorption.*

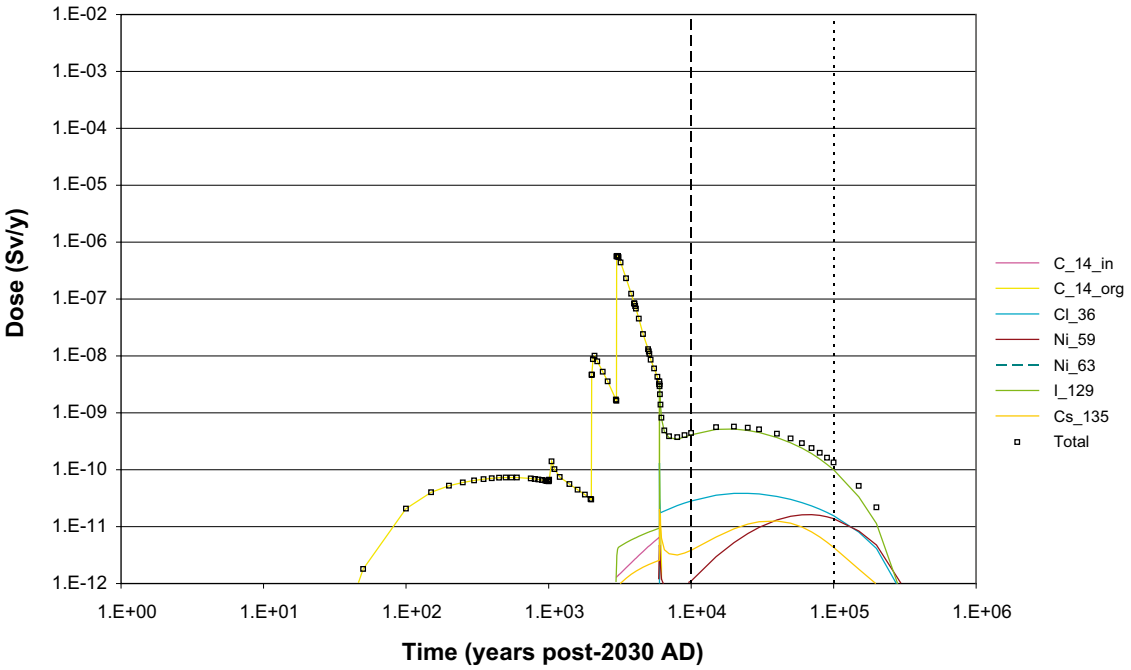

Figure 5-43. *1BTF dose for RBD for Maximum near-field sorption.*

5.4.4 2BTF

Figure 5-44 shows the radionuclide flux from 2BTF for Maximum near-field sorption. Organic C-14 has the highest radionuclide flux up to 9,000 AD. The maximum flux is estimated to be 3.3E+06 Bq/y at around 3,100 AD. During the period from 1,000 to 10,000 years post-2030 AD the release rate of Ni-59 increases and Ni-59 dominates from 7,000 years post-2030 AD to around 500,000 years post-2030 AD and from then on the flux is dominated by the release of Tc-99.

Figure 5-45 summarises doses estimated from 2BTF to the RBD model for Maximum near-field sorption. Doses during the coastal period are less than 3E–10 Sv/y and are dominated by organic C-14. The maximum dose is estimated to be 2.5E–08 Sv/y which occurs at the onset of the lake period, and is dominated by dose due to organic C-14. The agricultural period is dominated by doses from I-129 and the doses are generally less than 1E–09 Sv/y.

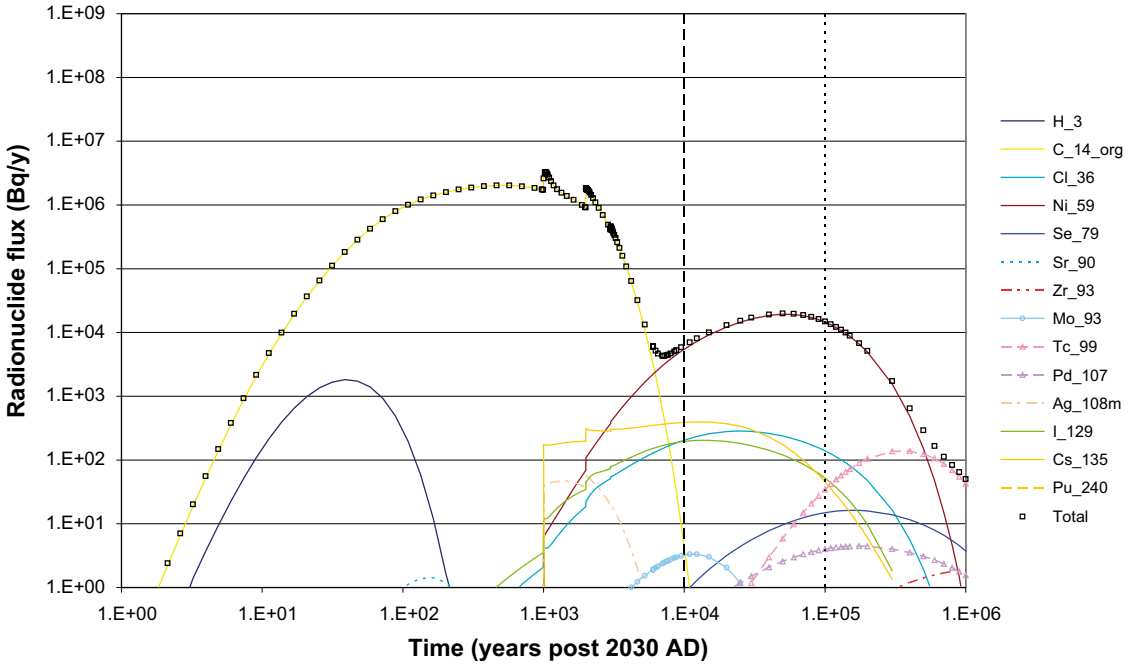

Figure 5-44. *2BTF near-field radionuclide fluxes for Maximum near-field sorption.*

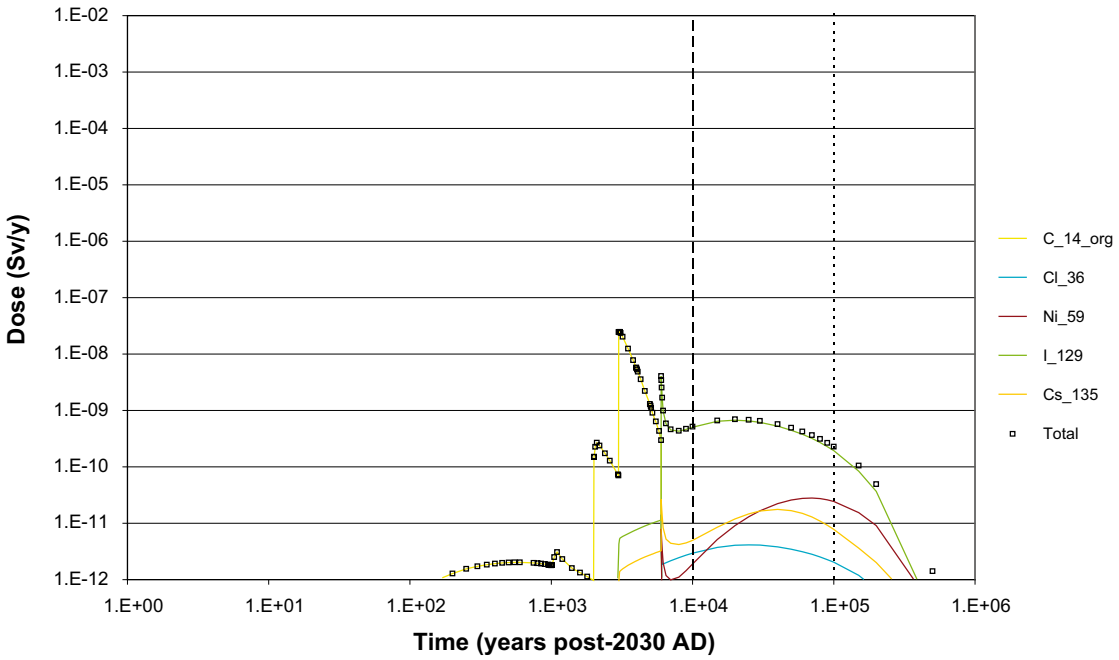

Figure 5-45. *2BTF dose for RBD for Maximum near-field sorption.*

5.4.5 BLA

No sorption is considered within the BLA model. Therefore this disposal tunnel was not included in this sensitivity calculation.

5.4.6 SFR-1 summary for Maximum near-field sorption

Figure 5-46 summarises the near-field radionuclide fluxes from each part of the repository and the total for the whole of SFR-1 for Maximum near-field sorption (results for the BLA Most likely scenario have been included to allow comparisons to be made). The peak radionuclide flux, 3.5E+08 Bq/y, is estimated to occur at around 3,000 AD and is dominated by releases from 1BTF (it should be noted that initially the BLA dominates the overall near-field flux). Releases from 1BTF dominate the radionuclide flux until 3,000 AD, between 3,000 AD and 4,000 AD releases from the BMA are also important. Total releases are subsequently dominated by contributions from the Silo upto 20,000 years post-2030 AD and the BMA thereafter.

Figure 5-47 summarises the geosphere radionuclide fluxes from each part of the repository and the total for the whole of SFR-1 for Maximum near-field sorption (results for the BLA Most likely scenario have been included to allow comparisons to be made). The peak radionuclide flux, 1.8E+08 Bq/y, is estimated to occur at around 3,100 AD and is dominated by releases from 1BTF. The remainder of the geosphere flux for the 1BTF shows similar trends to those described for the near-field.

Figure 5-48 summarises the estimated dose for the RBD model from each part of the repository and the total for the whole of SFR-1 for Maximum near-field sorption (results for the BLA Most likely scenario have been included to allow comparisons to be made). Doses during the coastal period are dominated by releases from 1BTF and are below 1E–08 Sv/y. The maximum dose is estimated to be 1.5E–06 Sv/y at the onset of the lake period and is dominated by dose due to releases from the Silo, BMA and 1BTF, thereafter releases from the Silo drive exposures within the lake period. In the very long term exposures that arise during the agricultural period are dominated by contributions from the BMA up to 200,000 years post-2030 AD and the Silo thereafter.

Table 5-4 summarises the results from the Maximum near-field sorption sensitivity case.

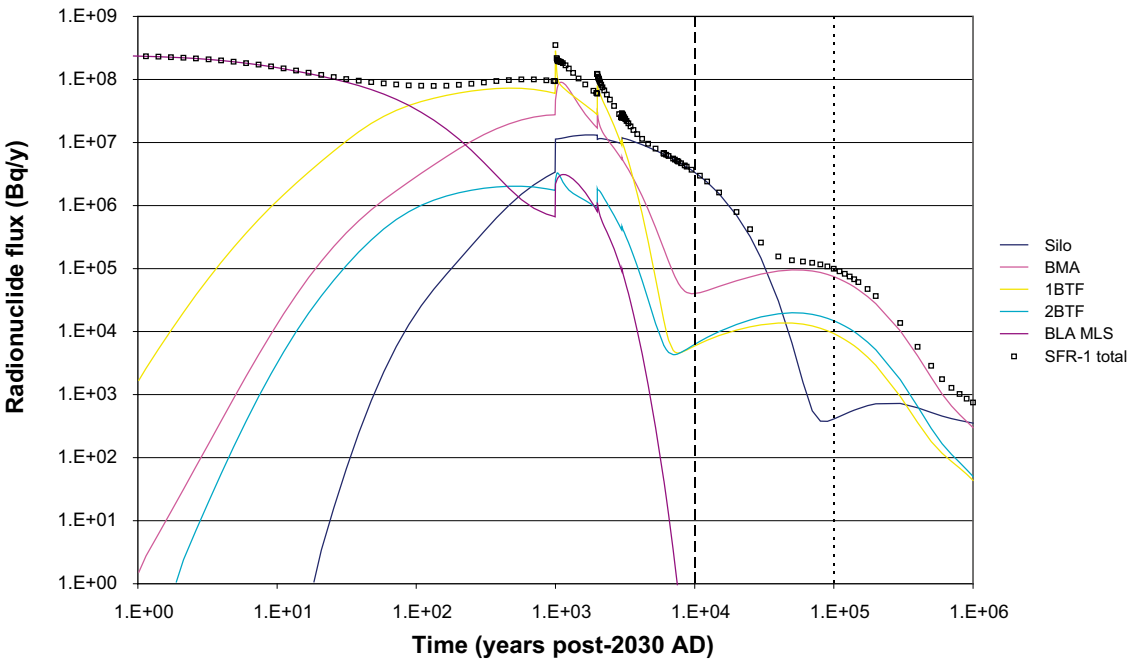

Figure 5-46. *Near-field radionuclide fluxes for Maximum near-field sorption.*

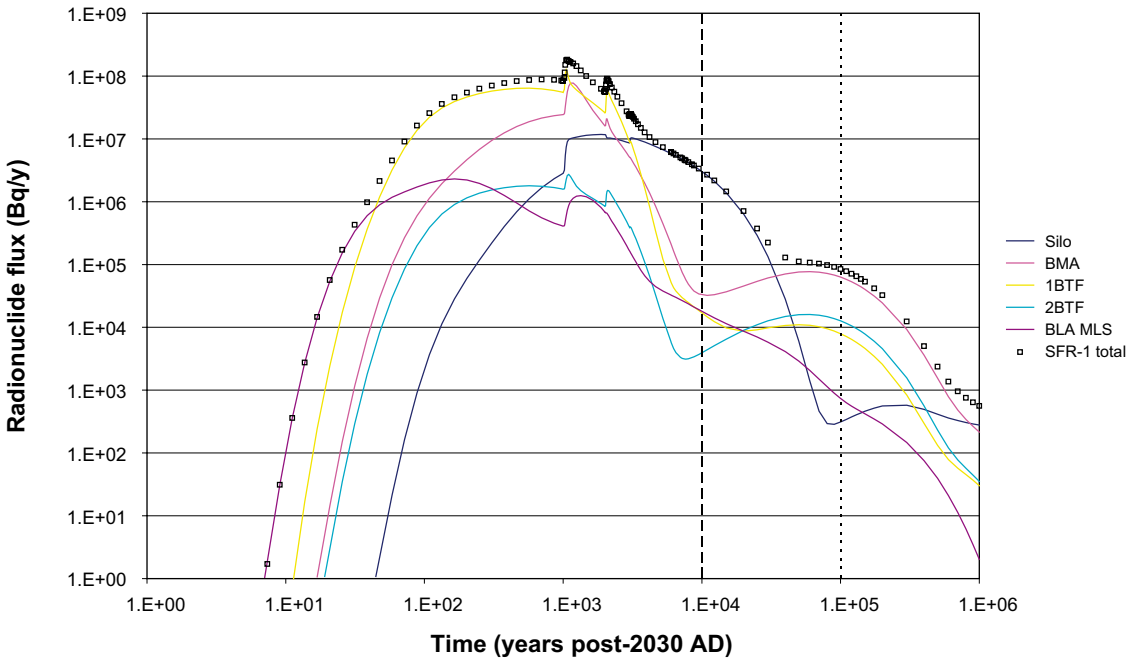

Figure 5-47. *Geosphere radionuclide fluxes for Maximum near-field sorption.*

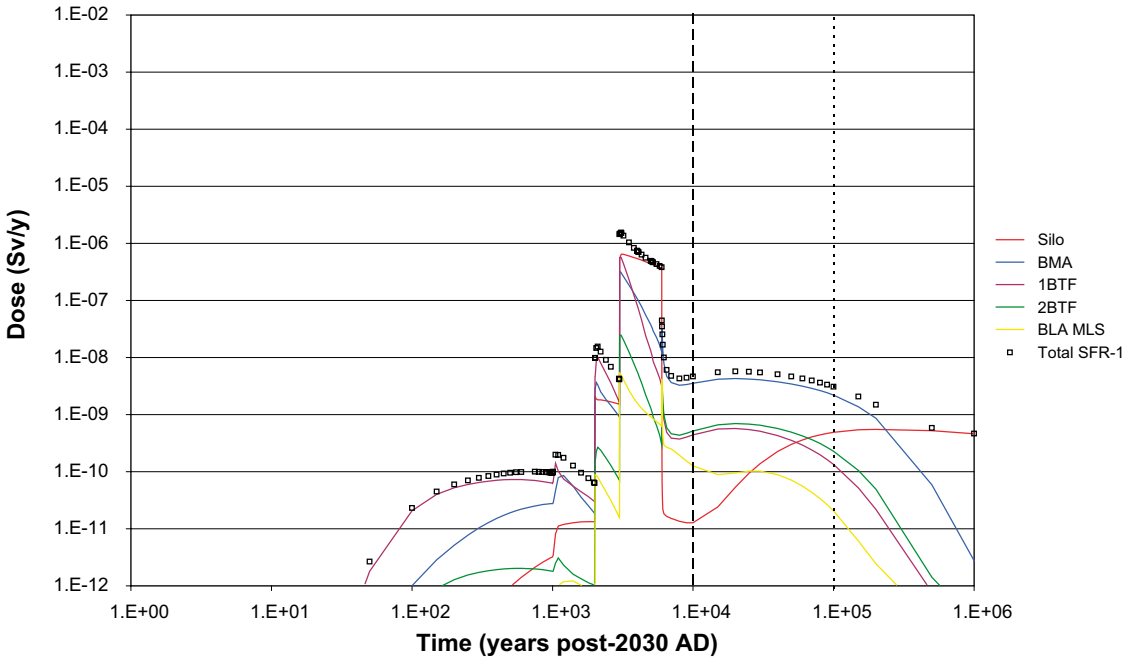

Figure 5-48. *Dose for RBD from Maximum near-field sorption.*

Table 5-4. Summary of Maximum near-field sorption results.

	Near-field	Geosphere	RBD
Silo	1.3E+07 Bq/y at c. 3,900 AD	1.2E+07 Bq/y at c. 3,900 AD	6.5E–07 Sv/y at c. 5,100 AD
	Organic C-14	Organic C-14	Organic C-14
BMA	9.1E+07 Bq/y at c. 3,100 AD	7.7E+07 Bq/y at c. 3,200 AD	3.0E–07 Sv/y at c. 5,000 AD
	Organic C-14	Organic C-14	Organic C-14
1BTF	2.9E+08 Bq/y at c. 3,000 AD	1.3E+08 Bq/y at c. 3,100 AD	5.7E–07 Sv/y at c. 5,000 AD
	Organic C-14	Organic C-14	Organic C-14
2BTF	3.3E+06 Bq/y at c. 3,100 AD	3.7E+06 Bq/y at c. 3,100 AD	2.5E–08 Sv/y at c. 5,000 AD
	Organic C-14	Organic C-14	Organic C-14
BLA#	2.5E+08 Bq/y at 2,030 AD	2.3E+06 Bq/y at c. 2,200 AD	5.5E–09 Sv/y at c. 5,000 AD
	Co-60, Ni-63 and Cs-137	Ni-63	Inorganic C-14
SFR-1	3.5E+08 Bq/y at c. 3,000 AD	1.8E+08 Bq/y at c. 3,100 AD	1.5E–06 Sv/y at c. 5,100 AD
	1BTF	1BTF	Silo, BMA and 1BTF

Data for Most likely scenario.

5.5 Combined alternative inventory and Alternative near-field flow fields

5.5.1 Silo

Figure 5-49 shows the radionuclide flux from the Silo for the combined inventory-near field flow fields sensitivity case. Releases of organic C-14 dominate up to 20,000 years post-2030 AD. H-3, Sr-90, Cs-137 and Ag-108m reach their maximum in the initial 1,000 years but do not contribute to the total radionuclide flux. The maximum radionuclide flux estimated to occur is 1.1E+08 Bq/y at around 4,100 AD. The long-term radionuclide flux is driven firstly by Ni-59 which is the dominant component from 20,000 years post-2030 AD until near the end of the simulation when the release of Cl-26, Se-79, Tc-99 and Cs-135 dominate.

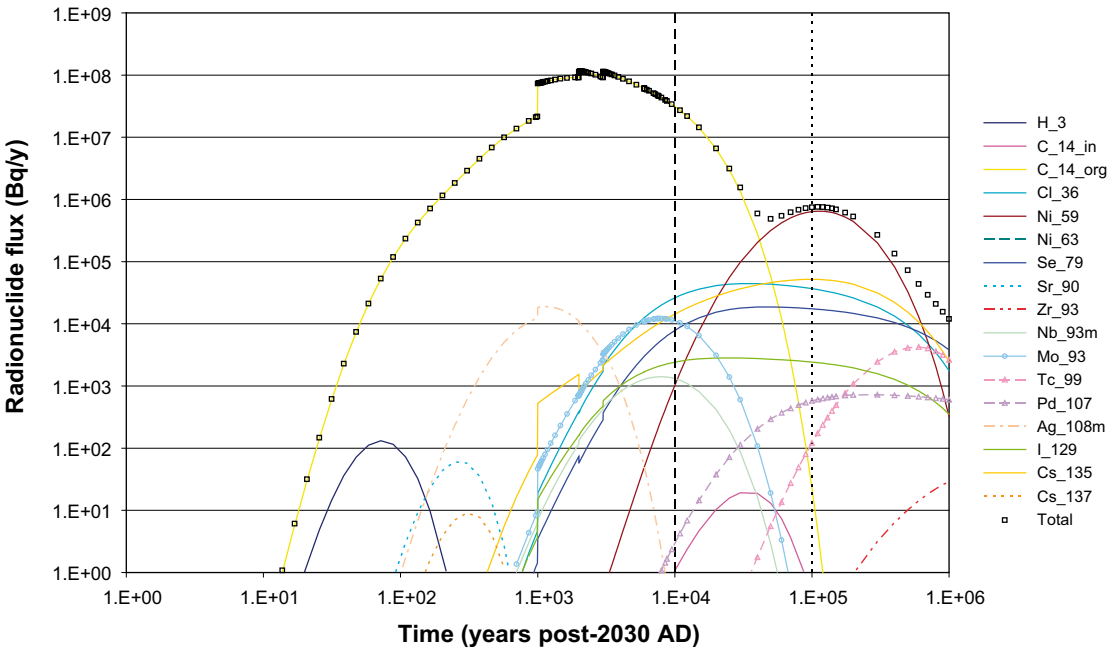

Figure 5-49. *Silo near-field radionuclide fluxes for the Combined alternative inventory and Alternative near-field flow fields.*

Figure 5-50 summarises doses estimated from the Silo to the RBD model for the Combined alternative inventory and Alternative near-field flow fields sensitivity case. Doses during the coastal period are less than 2E–08 Sv/y and are dominated by organic C-14. The maximum dose is 6.2E–06 Sv/y at 5,100 AD which is during the lake period and it is dominated by dose due to contributions from organic C-14. Doses in the agricultural period are dominated by exposures from I-129 and are generally around 1E–08 Sv/y or less, except at the onset.

5.5.2 BMA

Figure 5-51 shows the radionuclide flux from the BMA for the Combined alternative inventory and Alternative near-field flow fields sensitivity case. Organic C-14 dominates releases up to 5,000 AD. Releases of H-3, Sr-90 and Cs-137 reach their maximum within the initial 200 years. The maximum release rate is estimated to be 4.7E+08 Bq/y at around 3,100 AD. From 3,000 AD the release of Ni-59 increases and it becomes the dominant component of radionuclide flux at 5,000 AD until around 200,000 years post-2030 AD when the release of Tc-99 makes this the dominant radionuclide. The releases in the very long term are at least an order of magnitude below the maximum value.

The doses estimated from the BMA to the RBD model for the Combined alternative inventory and Alternative near-field flow fields sensitivity case are shown in Figure 5-52. Doses during the coastal period are below 1E–08 Sv/y and are dominated by organic C-14. The maximum dose during the lake period is 7E–7 Sv/y and it is dominated by dose due to organic C-14. The maximum dose overall, 1.1E–06 Sv/y from Se-79, occurs at the onset of the agricultural period (8,000 AD) from radionuclides previously accumulated in the coastal and lake sediments. Doses during the remainder of the agricultural period are dominated by exposures firstly from I-129, then Ni-59 and lastly Tc-99.

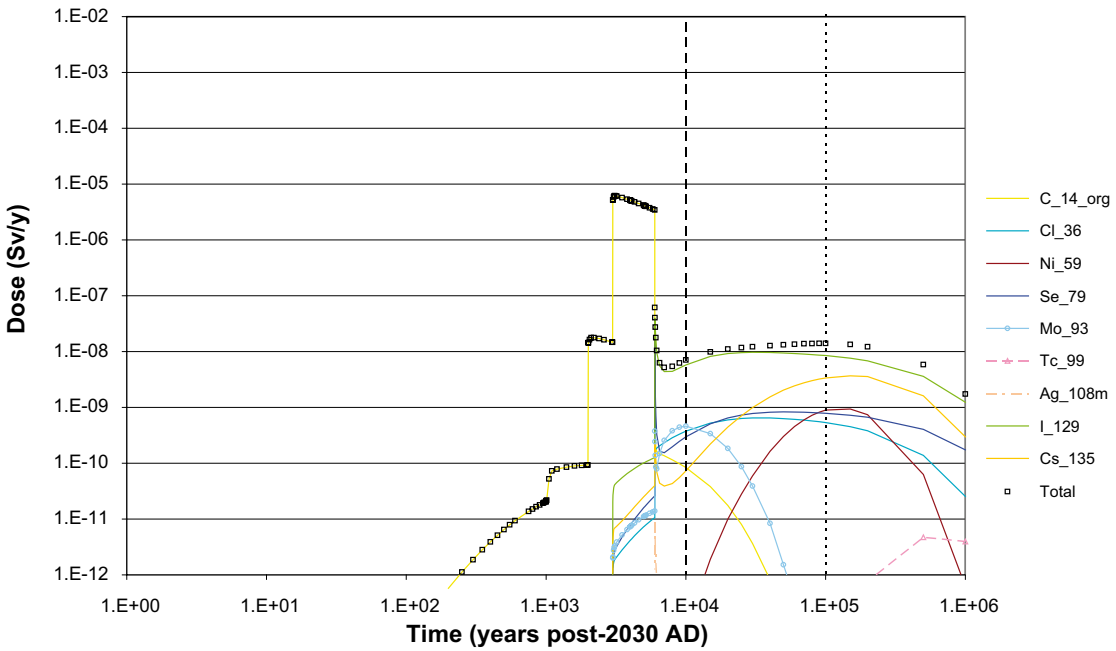

Figure 5-50. *Silo dose for RBD for the Combined alternative inventory and Alternative near-field flow fields.*

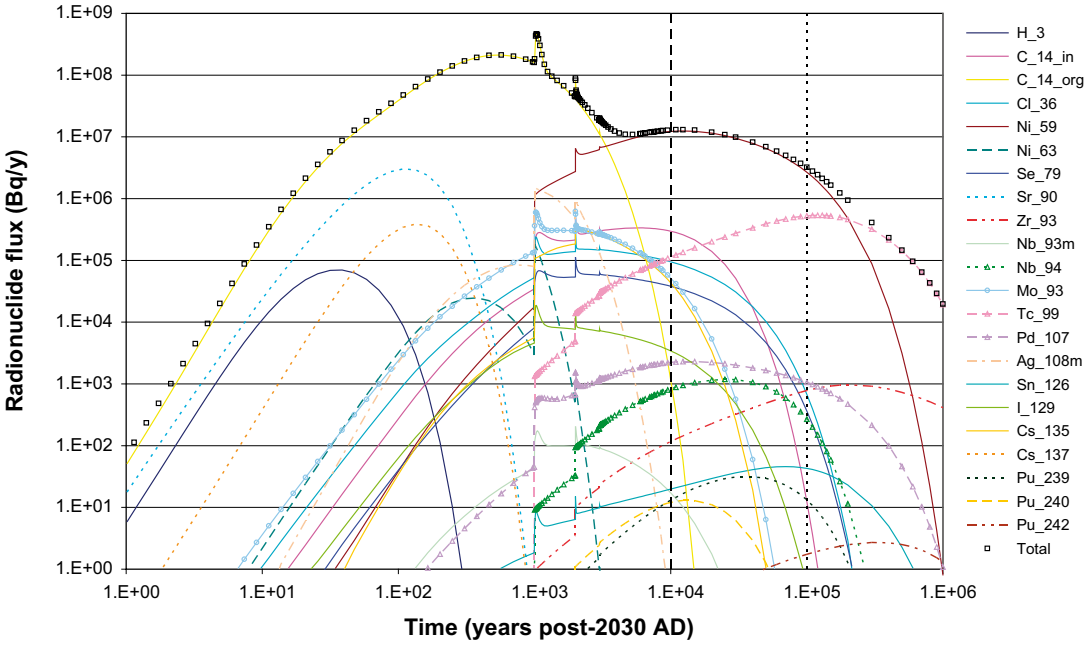

Figure 5-51. *BMA near-field radionuclide fluxes for the Combined alternative inventory and Alternative near-field flow fields.*

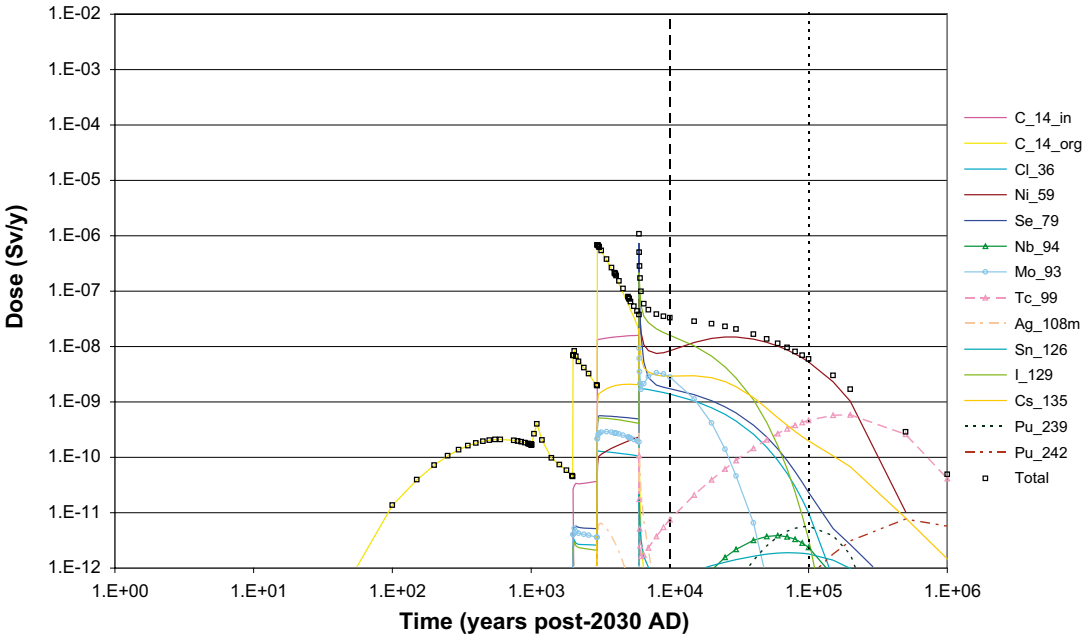

Figure 5-52. *BMA dose for RBD for the Combined alternative inventory and Alternative near-field flow fields.*

5.5.3 1BTF

Figure 5-53 shows the radionuclide flux from the 1BTF for the Combined alternative inventory and Alternative near-field flow fields. Releases of organic C-14 dominate up to 4,500 AD. The maximum release rate is estimated to occur of 5.0E+08 Bq/y at around 3,000 AD. The release rates of inorganic C-14 and Ni-59 increase from 3,000 AD and they dominate the release profile from 4,500 AD until 40,000 years post-2030 AD when the release of Tc-99 makes this the dominant radionuclide.

Figure 5-54 summarises doses estimated from 1BTF to the RBD model for the Combined alternative inventory and Alternative near-field flow fields. Doses during the coastal period are less than 4E–08 Sv/y and are dominated by organic C-14, during the lake period doses rise and reach a maximum at the end of 3E–7 Sv/y arising from exposure to inorganic C-14. The maximum dose is estimated to be 4.4E–07 Sv/y which occurs at the onset of the agricultural period and it is dominated by dose due to Se-79 that has previously accumulated in coastal and lake sediments. The remainder of the agricultural period is dominated by doses from Ni-59, Tc-99 and Pu-242 discharged in groundwater.

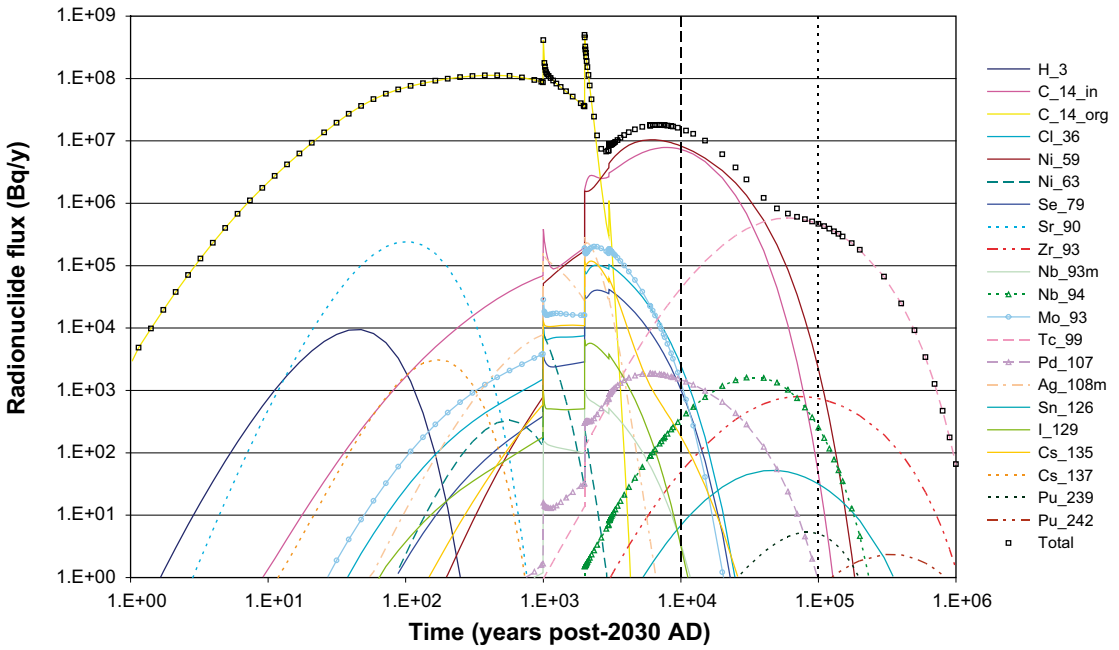

Figure 5-53. *1BTF near-field radionuclide fluxes for the Combined alternative inventory and Alternative near-field flow fields.*

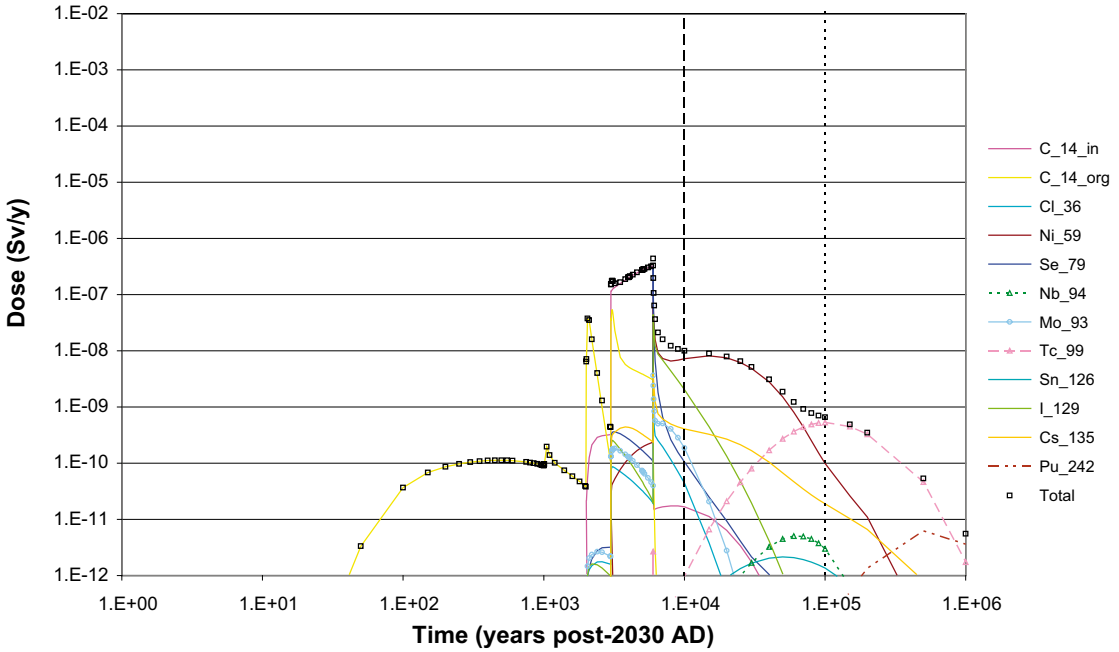

Figure 5-54. *1BTF dose for RBD for the Combined alternative inventory and Alternative near-field flow fields.*

5.5.4 2BTF

Figure 5-55 shows the radionuclide flux from 2BTF for the inventory-flow field combined sensitivity case. Organic C-14 has the highest radionuclide flux up to 4,500 AD. The maximum flux is estimated to be 4.6E+07 Bq/y at around 4,000 AD. During the period from 1,000 to 10,000 years post-2030 AD the release rate of Ni-59 increases and dominates from 4,500 AD to around 100,000 years post-2030 AD, from then on the radionuclide flux is dominated by the release of Tc-99.

Figure 5-56 summarises doses estimated from 2BTF to the RBD model for the inventory-flow field combined sensitivity case. Doses during the coastal period are 4E–09 Sv/y or less and are dominated by organic C-14. The dose during the lake period is 2E–08 Sv/y or less and is initially dominated by dose due to organic C-14 and latterly due to inorganic C-14. The maximum dose, 6.7E–07 Sv/y, occurs at the onset of the agricultural period (8,000 AD) and is due to Se-79 that has previously accumulated in the coastal (and lake) sediments, thereafter in the very long-term exposures are dominated by contributions from I-129, then Ni-59 and finally Tc-99.

5.5.5 BLA

Figure 5-57 shows the radionuclide flux from the BLA for the Combined alternative inventory and Alternative near-field flow fields. The maximum radionuclide release of 1.2E+10 Bq/y occurs initially and is dominated by Co-60, Ni-63 and Cs-137. The release rate from the BLA beyond 5,500 AD is estimated as being below 1 Bq/y.

The doses estimated to the RBD model from the BLA for the inventory-flow field combined sensitivity case are shown in Figure 5-58. During the coastal period doses are 2E–09 Sv/y or less and are dominated by contributions initially from Sr-90 and then by inorganic C-14 and organic C-14. Doses during the lake period are dominated by exposures from inorganic C-14 and are below 4E–08 Sv/y. The maximum dose, 2.4E–07 Sv/y, is estimated to occur at the onset of the agricultural period and is due to Tc-99 which has previously accumulated in the coastal (and lake) sediments. Thereafter the dose is dominated by contributions from Ni-59, Tc-99, Pu-239 and Pu-242.

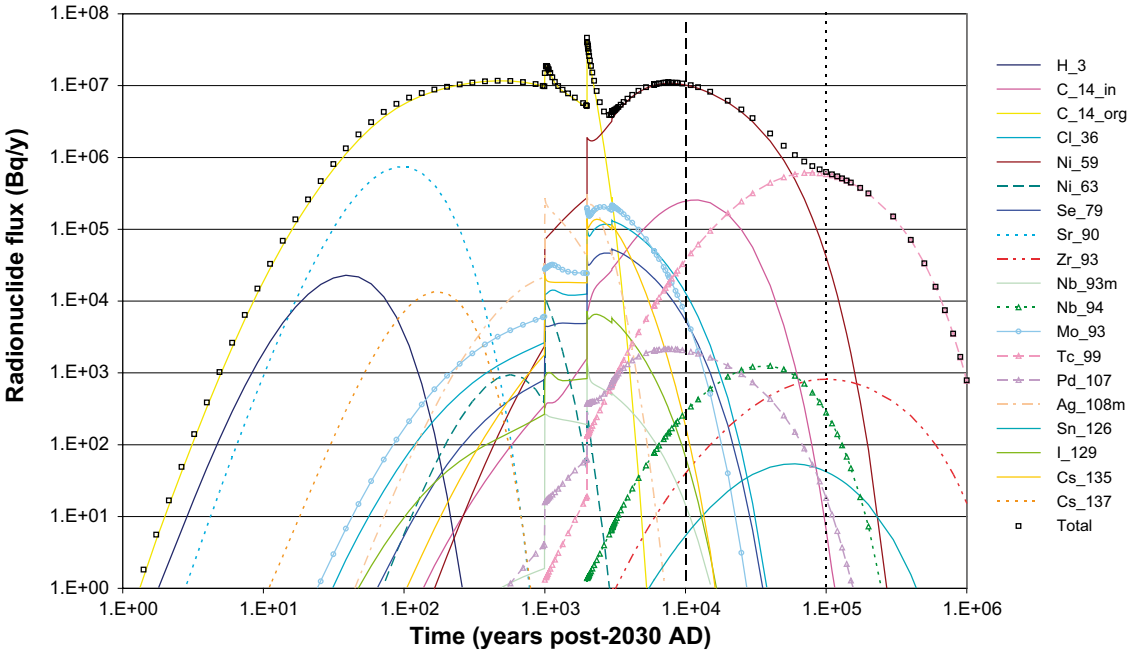

Figure 5-55. *2BTF near-field radionuclide fluxes for the Combined alternative inventory and Alternative near-field flow fields.*

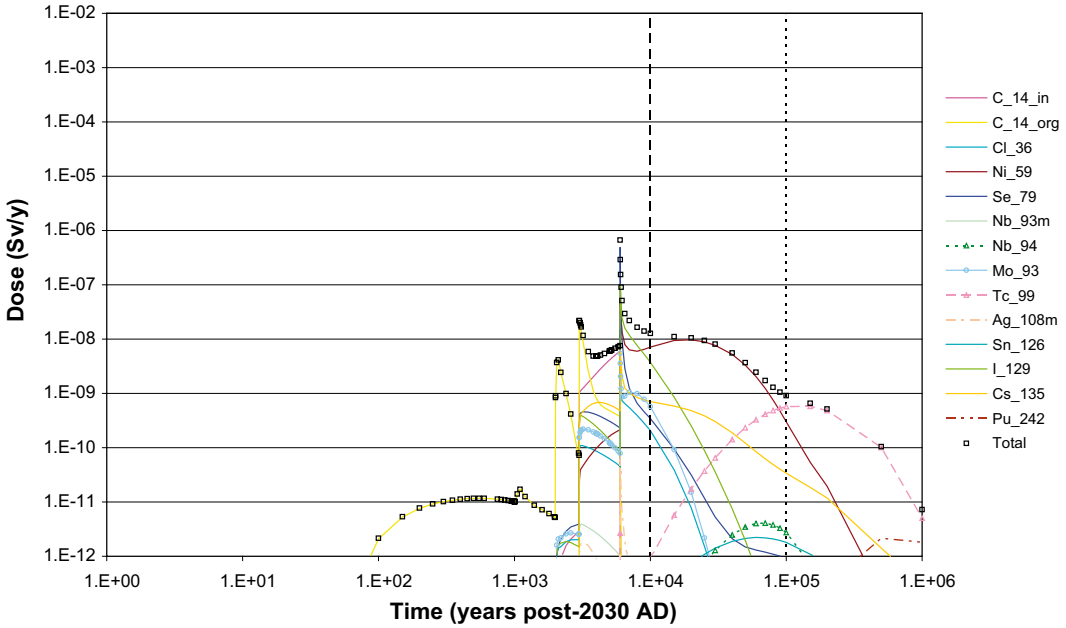

Figure 5-56. *2BTF dose for RBD for the Combined alternative inventory and Alternative near-field flow fields.*

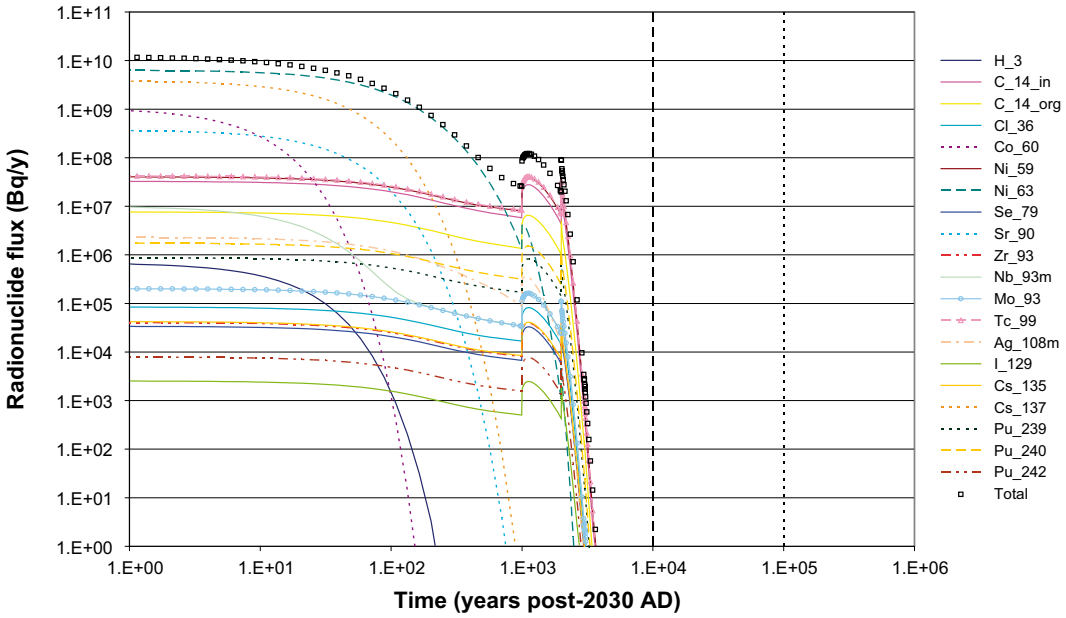

Figure 5-57. *BLA near-field radionuclide fluxes for the Combined alternative inventory and Alternative near-field flow fields.*

5.5.6 SFR-1 summary for the Combined alternative inventory and Alternative near-field flow fields

Figure 5-59 summarises the near-field radionuclide fluxes from each part of the repository and the total for the whole of SFR-1 for the Combined alternative inventory and Alternative near-field flow fields. The peak radionuclide flux 1.2E+10 Bq/y, is estimated to occur at 2,030 AD and is dominated by releases from the BLA which control the SFR-1 radionuclide flux for the initial 300 years. Following this the largest radionuclide fluxes are from the BMA and 1BTF until 3,400 AD when the BMA flux decreases and the Silo flux increases. Very long-term releases are subsequently driven by contributions from the Silo and BMA.

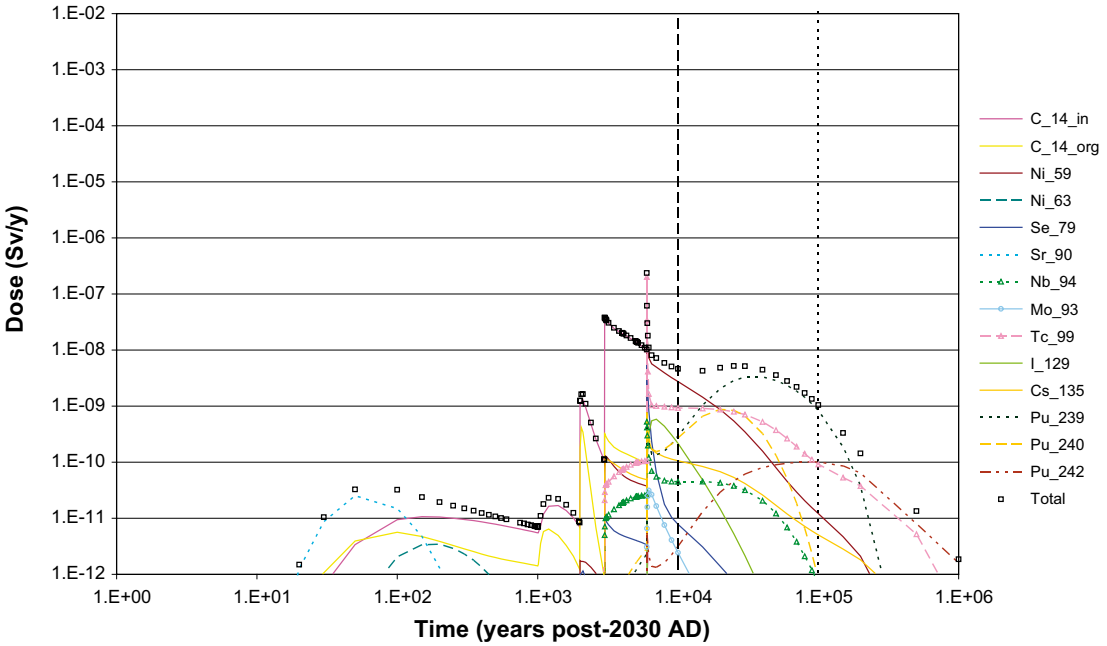

Figure 5-58. *BLA dose for RBD from the Combined alternative inventory and Alternative near-field flow fields.*

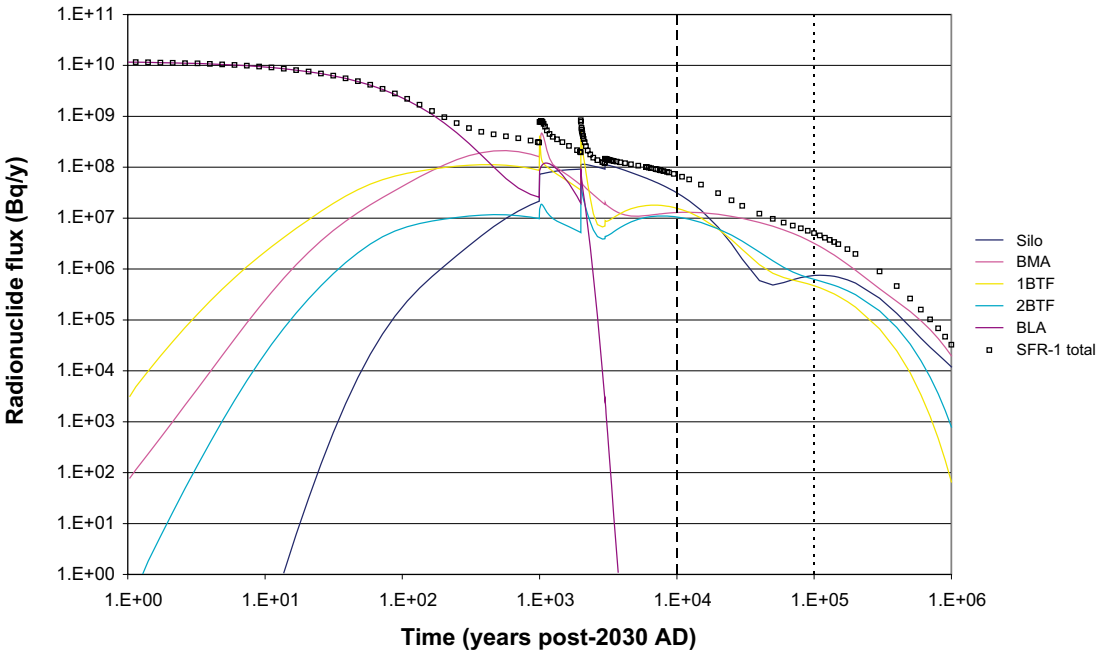

Figure 5-59. *Near-field radionuclide fluxes for the Combined alternative inventory and Alternative near-field flow fields.*

Figure 5-60 summarises the geosphere radionuclide fluxes from each part of the repository and the total for the whole of SFR-1 for the Combined alternative inventory and Alternative near-field flow fields. The peak radionuclide flux from the geosphere, 5.9E+08 Bq/y, is estimated to occur at around 3,100 AD and is due to releases from the BMA and 1BTF.

Figure 5-61 summarises the estimated dose for RBD from each part of the repository and the total for the whole of SFR-1 for the Combined alternative inventory and Alternative near-field flow fields. Doses during the coastal period are below 7E–08 Sv/y. The maximum dose is

estimated to be 7.0E–06 Sv/y at 5,100 AD during the lake period and is driven by exposures to radionuclides released from the Silo. Doses during the agricultural period are generally below 1E–07 Sv/y, except at the onset when doses arise from exposure to radionuclides that have previously accumulated in coastal (and lake) sediments. Very long term doses during the agricultural period are dominated by contributions from the BMA and the Silo.

Table 5-5 summarises the results from the Combined alternative inventory and Alternative near-field flow fields sensitivity case.

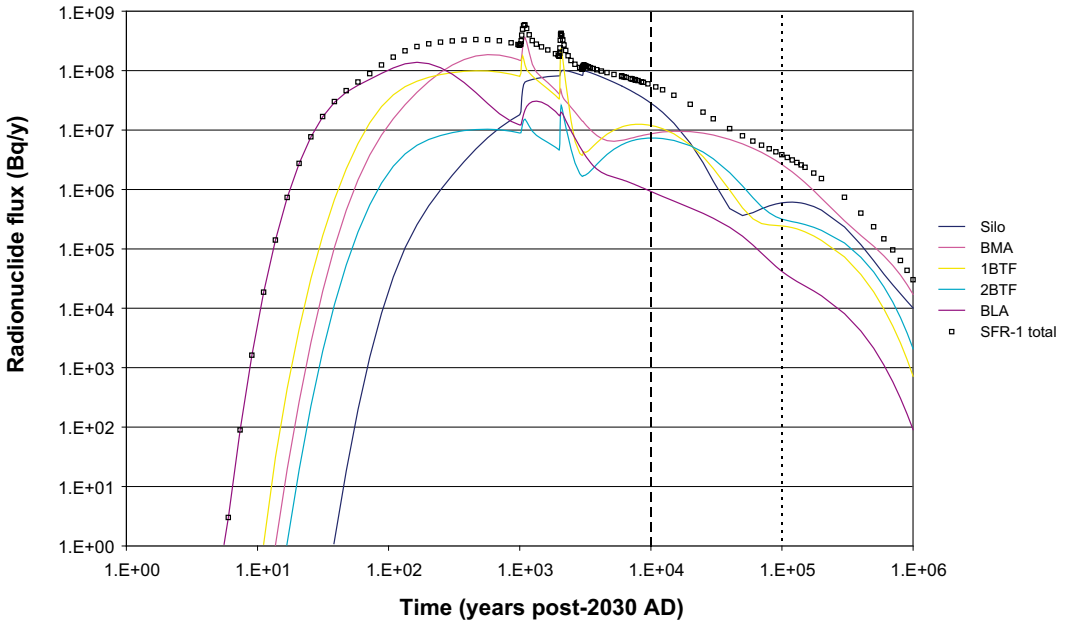

Figure 5-60. *Geosphere radionuclide fluxes for the Combined alternative inventory and Alternative near-field flow fields.*

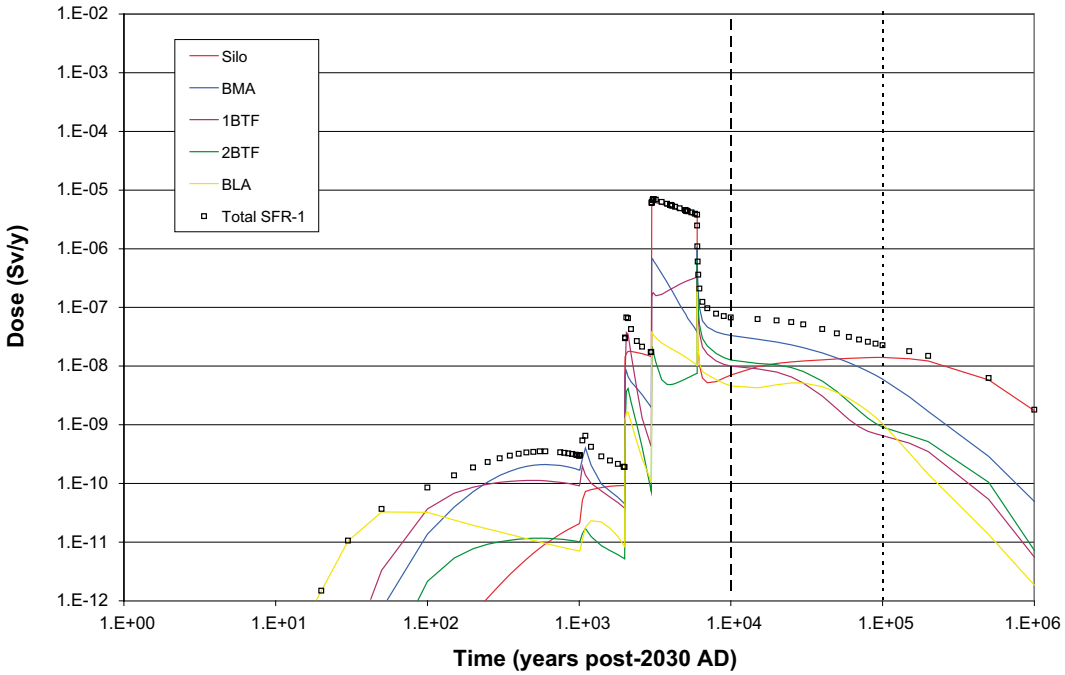

Figure 5-61. *Dose for RBD from the Combined alternative inventory and Alternative near-field flow fields*

Table 5-5. Summary of Combined alternative inventory and Alternative near-field flow fields.

	Near-field	Geosphere	RBD
Silo	1.1E+08 Bq/y at c. 4,100 AD	1.0E+08 Bq/y at c. 4,100 AD	6.2E–06 Sv/y at c. 5,100 AD
	Organic C-14	Organic C-14	Organic C-14
BMA	4.7E+08 Bq/y at c. 3,100 AD	3.6E+08 Bq/y at c. 3,100 AD	1.1E–06 Sv/y at c. 8,000 AD
	Organic C-14	Organic C-14	Se-79
1BTF	5.0E+08 Bq/y at c. 4,000 AD	2.4E+08 Bq/y at c. 4,100 AD	4.4E–07 Sv/y at c. 8,000 AD
	Organic C-14	Organic C-14	Se-79
2BTF	4.6E+07 Bq/y at c. 4,000 AD	2.6E+07 Bq/y at c. 4,100 AD	6.7E–07 Sv/y at c. 8,000 AD
	Organic C-14	Organic C-14	Se-79
BLA	1.2E+10 Bq/y at 2,030 AD	1.4E+08 Bq/y at c. 2,200 AD	2.4E–07 Sv/y at c. 8,000 AD
	Co-60, Ni-63 and Cs-137	Ni-63	Tc-99
SFR-1	1.2E+10 Bq/y at 2,030 AD	5.9E+08 Bq/y at c. 3,100 AD	7.0E–06 Sv/y at c. 5,100 AD
	BLA	BMA and 1BTF	Silo

5.6 Supplementary calculations

5.6.1 Modelling of the Baltic Sea area beyond the Öregrundsgrepen

The Authorities questioned the representation of the Baltic Sea as a single model compartment (with the exception of the Model Area and Grepen) /SKI and SSI 2004/:

"The coastal model comprises three sub-models of different geographical scales – the model area (a few km^2), Grepen (hundreds of km^2) and the Baltic Sea (thousands of km^2)…
… The model of the Baltic Sea, as a part of the coastal model, has been further simplified and is represented by only four compartments for water, suspended material and upper and lower sediment. This means that radionuclides that reach the Baltic Sea very quickly can disappear from the model area through instantaneous remixing and dilution. Whether or not this simplification is justified should have been analyzed, for example, through comparison calculations with more complex and tested compartment models for the Baltic Sea."

Even if the simple model were adequate for the purposes of estimating the maximum concentrations in the Model Area and Grepen, there remains the fact that the simple model does not distinguish concentrations beyond the Grepen on the Swedish side of the Baltic from those in areas belonging to other countries. Although these would not lead to the highest doses overall, they would lead to the highest doses to a non-Swedish population, which might be a relevant consideration.

An analysis of this issue was performed by comparing the SKB model with the existing model of the Baltic developed in the EC-funded MARINA II project by a multinational team /Kershaw, 1999/. The objectives of the comparison were:

1. To investigate the effect of changing the Baltic Sea model on concentrations in the water and sediment of the Model Area and Grepen, and hence the potential effect on the highest individual doses; and
2. To investigate the extent to which the more detailed model predicts variations in concentrations between different areas of the Baltic, and hence gain an indication of the potential distribution of doses.

The text presented here is supported by more detailed provided in Appendix B. The MARINA II model splits the Baltic Sea into:

- Two compartments representing the northern and southern parts of the Gulf of Bothnia (called Bothnian Bay and Bothnian Sea, respectively);
- The Gulf of Finland and the Gulf of Riga;
- Four compartments representing the Baltic proper (split into eastern and western areas, and also vertically into surface and deep waters); and
- Five compartments representing the Belt Sea and Kattegat (both divided into surface and deep waters) and Skagerrak.

Forsmark is slightly to the north of the boundary between two compartments in the model – the Bothnian Sea to the north and Baltic Sea West to the south. The Grepen was therefore assumed to exchange initially with the Bothnian Sea compartment. The model indicates water circulation in the northern Baltic to be generally anti-clockwise, i.e. mainly south-to-north on the Baltic States/Finnish side and north-to-south on the Swedish side. Therefore some activity would remain in the Gulf of Bothnia, but the prevailing flow would initially be southwards into the Baltic Sea West. Residence times in the Gulf of Bothnia are several years, with flow then going south.

In order to reduce the number of differences between the models at this stage, the vertical structure of the model used in Project SAFE (i.e. water compartment, suspended sediment, upper sediment and deep sediment) was combined with the areal structure of the Baltic from the MARINA II model. The vertical transfers between sub-compartments were modelled as defined for the SKB model. For surface water compartments (compartments 61, 63, 67 and 68 in Figure A2-1) only the water and suspended sediment sub-compartments were used.

The following conclusions were made

- The concentrations in the Model Area water and top sediments are almost identical for the two models.
- In the Grepen, the water concentrations and top sediments are again similar, but the MARINA II model begins to show slightly higher concentrations than the SKB model from several hundred years onwards. At most, the difference between the models is around a factor of two or three.
- More substantial differences between the models are observed, however, beyond the Grepen.
  - Concentrations predicted by the MARINA II model in the water of the Bothnian Sea are more than two orders of magnitude higher than those predicted by the SKB model in a single Baltic Sea compartment.
  - Similar results are obtained for the East Baltic compartment of the MARINA II model.
  - At their highest levels, the concentrations in the Bothnian Sea and East Baltic compartments are similar to those in the Grepen, and approach (within a factor of about two or three) those in the Model Area.
- A similar pattern appears in comparing the top sediment concentrations for the MARINA II compartments Bothnian Sea and East Baltic with those for the single Baltic Sea compartment in the SKB model. The differences between the models are typically between one and two orders of magnitude – a little smaller than for the water concentrations – but are still substantial. The highest values, in the Bothnian Sea particularly, again approach those for the Grepen and Model Area, but in this case remain clearly below the Grepen concentrations and almost an order of magnitude below those in the Model Area.

It is considered that these results confirm that the approach to modelling the Baltic Sea within Project SAFE is not likely to underestimate the maximum dose rates to individuals as it is assumed that all foods are obtained from the Model Area water compartment.

5.6.2 Consideration of a forest ecosystem

The Authorities were concerned /SKI and SSI 2004/ that no calculations had been performed for the most common ecosystem in the Forsmark area, namely forests.

"SKB has not calculated the consequences for exposure pathways via the forest ecosystem, even though it can be expected to dominate during the land period. This would facilitate additional exposure pathways to man due to an earlier accumulation of radionuclides, such as via game, berries, mushrooms and via the utilization of biofuel for energy which has not been taken into consideration in the present analysis. It has not been convincingly shown that agricultural land is always overestimated and that this results in the largest consequences."

The forest model described in /Avila 2004/ was implemented in AMBER in order to undertake some preparatory calculations. The text here summarises this work and is supported by more detailed information in Appendix C.

Overall the comparison suggests that the agricultural biosphere is unlikely to underestimate doses significantly compared to a forest biosphere. This suggestion is strengthened by the fact that the forest biosphere may contain several conservative assumptions.

- Caesium and strontium isotopes give higher doses for forest pathways than for the agricultural biosphere which appears to be due primarily to the concentration in berries and mushrooms. This results in high doses from both direct human consumption of berries and mushrooms and consumption of game animals that have significant amounts of these foods in their diet. The concentration factors in /Avila 2004/ for caesium in these foods show large ranges and so other sources have been considered. A study of fungi specifically in the Forsmark area /Johanson et al. 2004/ indicates values substantially lower than the nominal value of 120 quoted by Avila, but well within the range of 0.27–620. Comparison with the forest module of the RODOS international emergency preparedness code /Rantavaara and Ammann 2004/ confirms that Avila's nominal value is close to the high end of a large range. The Forsmark-specific ratio derived by /Johanson et al. 2004/ from measurements of stable caesium was considered to be appropriate (as long-lived Cs-135 is the more important isotope for the overall assessment), and the quoted median from the site-specific range was used, as this is approximately equal (for an approximately lognormal distribution) to the geometric mean used by Avila. The value quoted is 15.5 for dry weight of mushrooms which, assuming a water content of 90%, corresponds to 1.55 on a fresh weight basis. Consideration of the two nominal values quoted by Avila for caesium transfer to understorey plants indicated that the lower of Avila's values – 2.3 rather than 7.0 – was more consistent with data, specifically for berries, tabulated in the RODOS report;
- The mobile radionuclides that give high doses via agricultural food pathways, notably I-129 and Se-79, give lower doses via forest pathways. This is likely to be due to the absence of particular agricultural pathways – e.g. iodine in milk, selenium in crops – from the forest diet, and the relatively high intake rates for contaminated agricultural products compared to those of wild foods in the forest biosphere.
- The intake rates quoted in an unpublished IAEA report are lower than the values used in the model.
- Another major conservatism in the forest model is the assumption that all of the forest products are affected by the radioactivity, which requires that they all come from the release area (assumed to be 0.53 km^2, the same area as the agricultural model). The fact that the release area is small is implicitly taken into account in assuming relatively low occupancy in the affected areas of forest, but is not reflected in the calculation of ingestion doses. An unpublished IAEA report quotes annual yields for forest products (referenced to published Finnish data). This information suggests that forest products are more likely to be derived from a forest area of a few km^2 than from a fraction of a km^2, and so the doses calculated assuming that all products are contaminated may well overestimate actual doses by about an order of magnitude.

Nevertheless doses have been calculated for the Most likely scenario for the period following the consideration of releases to a Lake. The calculations assume that an area of land equal in size to that considered within the agricultural land use model is contaminated by the ground-water discharges.

These calculations are presented in Figure 5-62 and from the comparisons presented in Table 5-6 it can be seen that the doses from the forest biosphere are lower than those estimated to result from an agricultural land use.

Table 5-6. Comparison of doses from Forest and Agricultural models for SFR-1.

	Maximum dose (Sv/y) Forest land use	Agricultural land use
Silo	5.5E–09 at c. 100,000 y post-2030 AD	6.5E–07 Sv/y at c. 5,100 AD
	Cs-135	Organic C-14
BMA	2.2E-08 at c. 12,000 AD	4.2E–07 Sv/y at c. 8,000 AD
	Cs-135	I-129
1BTF	2.9E-09 at c. 12,000 AD	5.9E–07 Sv/y at c. 5,100 AD
	Cs-135	Organic C-14
2BTF	3.6E–09 at c. 9,000 AD	6.9E–08 Sv/y at c. 8,000 AD
	Cl-36	I-129
BLA	6.9E–10 at 25,000 y post-2030 AD	5.5E–09 Sv/y at c. 5,000 AD
	Pu-239	Inorganic C-14
SFR-1	3.0E–08 at c. 12,000 AD	1.6E–06 Sv/y at c. 5,100 AD
	BMA	Silo, BMA, 1BTF

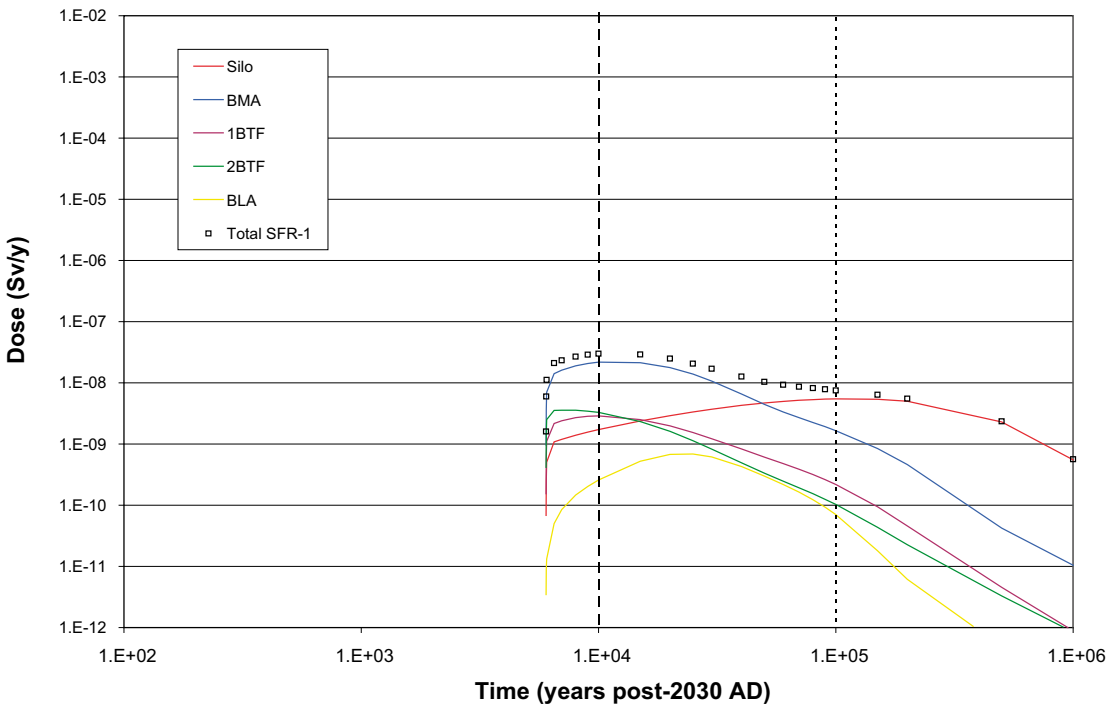

Figure 5-62. *Doses from Forest model for SFR-1.*

6 Discussion

6.1 Silo

Table 6-1 shows a summary of the calculations undertaken on the Silo. For each disposal facility and the SFR-1 as a whole the time and magnitude of the maximum near-field and geosphere fluxes and RBD dose are given. Also given is the radionuclide (or facility) that dominates at the time of the maximum and the biosphere type that exists at the time of the peak dose (Coast, Lake or Agriculture). For example, considering the Most likely scenario, the maximum near-field radionuclide flux is 1.3E+07 Bq/y at around 3,900 AD which is dominated by organic C-14. However this does not necessarily mean that the radionuclide flux of organic C-14 is 1.3E+07 Bq/y at around 3,900 AD as there may be contributions to the total from other radionuclides at this time. Similarly, when considering the Most likely scenario RBD it can be seen that the maximum dose of 6.5E–7 Sv/y occurs during the Lake period. Values of maximum near-field or geosphere flux or RBD dose that differ from the Most likely scenario are highlighted in bold if they are greater and in italics if they are lower. When considering differences it is important to note the rounding that is introduced when summarising radionuclide flux and dose to 2 significant figures. Also the spacing of output times may be too sparse to capture subtle changes in the shapes of curves resulting from the sensitivity calculations. Both these limitations may increase the potential for differences.

Figures 6-1 and 6-2 show the near-field radionuclide flux and RBD for the Silo calculations, respectively. It can be seen that the shape of the curves are generally similar until in excess of 10,000 AD with those for the Most likely scenario, Alternative near-field flow fields and minimum and Maximum near-field sorption generally coinciding. Up to 4,000 AD the curves in Figures 6-1 and 6-2 for the Alternative near-field flow fields is slightly below the Most likely scenario. The slight initial increase in near-field flux for the Minimum near-field sorption

Table 6-1. Summary of Silo calculations.

	Near-field	Geosphere	RBD
Most likely scenario	1.3E+07 Bq/y	1.2E+07 Bq/y	6.5E–07 Sv/y
	c. 3,900 AD	c. 3,900 AD	c. 5,100 AD (Lake)
	Organic C-14	Organic C-14	Organic C-14
Alternative inventory	1.2E+08 Bq/y	1.1E+08 Bq/y	6.0E–06 Sv/y
	c. 3,900 AD	c. 3,900 AD	c. 5,100 AD (Lake)
	Organic C-14	Organic C-14	Organic C-14
Alternative near-field flow fields	1.2E+07 Bq/y	1.1E+07 Bq/y	6.7E–07 Sv/y
	c. 4,100 AD	c. 4,200 AD	c. 5,100 AD (Lake)
	Organic C-14	Organic C-14	Organic C-14
Minimum near-field sorption	1.3E+07 Bq/y	1.2E+07 Bq/y	6.5E–07 Sv/y
	c. 3,700 AD	c. 3,900 AD	c. 5,100 AD (Lake)
	Organic C-14	Organic C-14	Organic C-14
Maximum near-field sorption	1.3E+07 Bq/y	1.2E+07 Bq/y	6.5E–07 Sv/y
	c. 3,900 AD	c. 3,900 AD	c. 5,100 AD (Lake)
	Organic C-14	Organic C-14	Organic C-14
Combined alternative inventory and Alternative near-field flow fields	1.0E+08 Bq/y	1.0E+08 Bq/y	6.2E–06 Sv/y
	c. 4,100 AD	c. 4,100 AD	c. 5,100 AD
	Organic C-14	Organic C-14	Organic C-14

calculation relative to the Most likely scenario (Figure 6-1) is due to the increased breakthrough of Cs-137 (compare Figures 4-1 and 4-2). The reduction in sorption is likely to result in the release of Cs-137 from the Silo that would have otherwise decayed in the near-field. The curves in Figures 6-1 and 6-2 for the Alternative inventory and the combined inventory-near-field flow fields also follow the same trend as the Most likely scenario and Alternative near-field flow fields, but they are consistently higher than these, which is due to the Alternative inventory. The combined inventory-near-field flow fields actually shows, a reduction relative to the Alternative inventory prior to 4,000 AD.

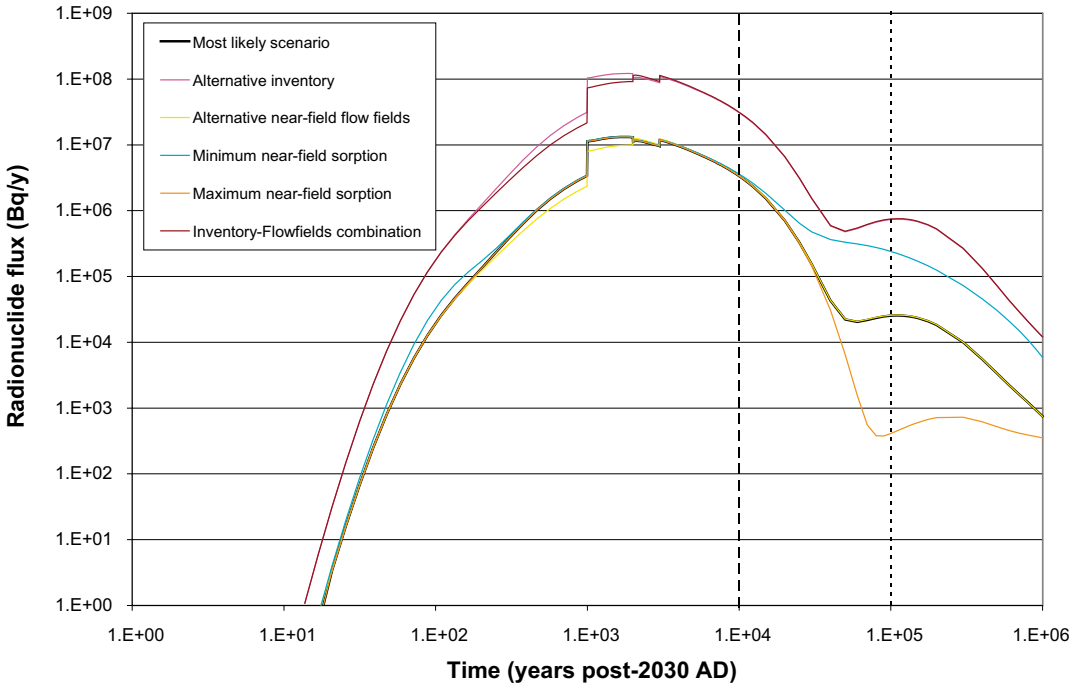

Figure 6-1. *Comparison of near-field radionuclide flux for Silo calculations.*

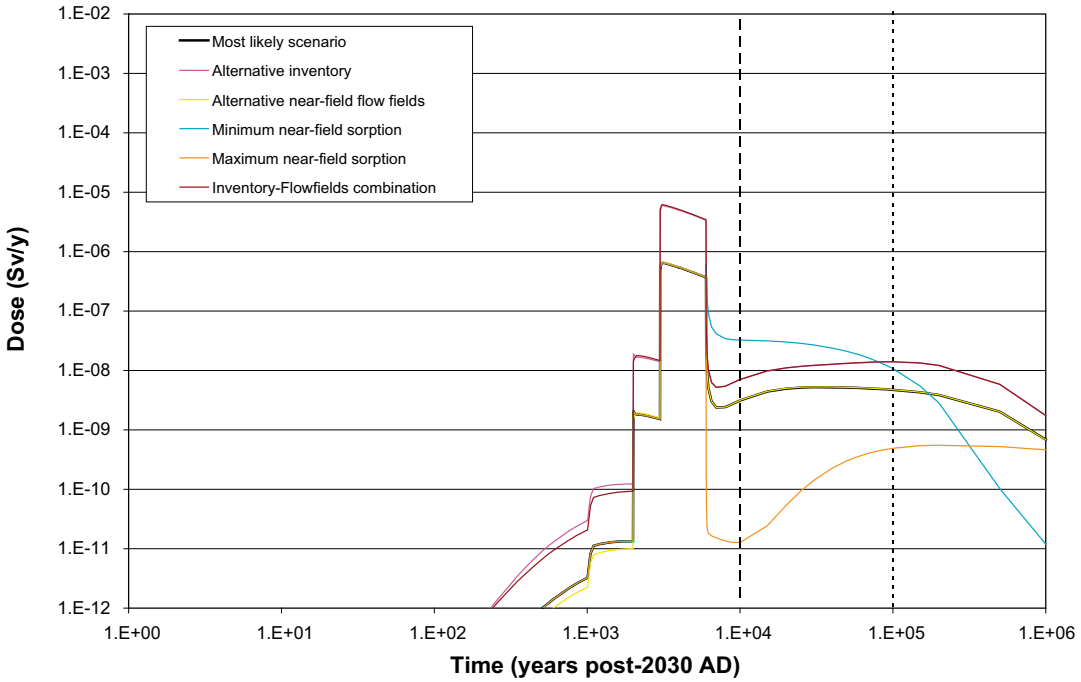

Figure 6-2. *Comparison of doses to RBD for Silo calculations.*

Slightly lower near-field and geosphere radionuclide fluxes relative to the Most likely scenario result from the Alternative near-field flow fields calculation. The times to the maximum fluxes are also slightly delayed relative to the Most likely scenario. This is due to the fact that the alternative Silo flows are less than those of the Most likely scenario up to 4,000 AD (by a factor of 0.71, see Table 3-4). However, the maximum values for both near-field and geosphere radionuclide fluxes occur slightly after 4,000 AD. The initial period of reduced flows and radionuclide transport through the Silo from closure to 4,000 AD will have resulted in a reduced peak radionuclide flux and increased time to breakthrough which is likely to persist for some time after 4,000 AD because the alternate flow fields in the calculation are only a increased a little (i.e. a factor 1.02 beyond 4,000 AD, see Table 3-4) from the Most likely scenario values. Another feature of the slightly increased flow rate beyond 4,000 AD (relative to the Most likely scenario) is that the maximum dose is increased slightly from 6.5E–07 Sv/y to 6.7E–07 Sv/y which suggests that by 5,100 AD when these doses are estimated to occur the increased flow field has been fully established throughout the Silo.

The Maximum and Minimum near-field sorption calculations show no significant change from the Most likely scenario. The dominance of contributions of organic C-14 to the near-field and geosphere fluxes and RBD dose is the cause of the lack of sensitivity to sorption as organic C-14 is not considered to be retarded by sorption in any of the calculations. The only difference is a slightly earlier estimated time of peak near-field radionuclide flux for the minimum sorption calculation. This slight difference is caused by the earlier breakthrough in the Minimum near-field sorption calculation of numerous radionuclides which will all have a minor contribution to the total near-field flux (compare Figures 4-1 and 5-27) and the effects noted above concerning the finite number of output times used in the simulations (which may explain the apparent shift in the time to the maximum flux).

Increased maximum radionuclide fluxes and exposures relative to the Most likely scenario result from the Alternative inventory or Combined alternative inventory and Alternative near-field flow fields calculations. Noting again the importance of organic C-14 in the radionuclide fluxes and exposures, a comparison of organic C-14 inventories for the two calculations (Table 3-3) reveals that the radionuclides inventory used for the Alternative inventory is c. 9 times the Most likely scenario inventory. Therefore the overall increase in radionuclide inventory explains the increase in maximum radionuclide fluxes and exposures for these calculations relative to the Most likely scenario. The largest near-field and geosphere fluxes are shown by the Alternative inventory calculation rather than the Combined alternative inventory and Alternative near-field flow fields calculation. This is due to the reasons explained previously for the Alternative near-field flow fields calculation. Namely that the initially reduced flow rates in the Alternative near-field flow fields calculation up to 4,000 AD leads to a reduced near-field (and hence geosphere flux) at the time of the maximum (3,900 AD). Conversely the largest exposures are shown by the Combined alternative inventory and Alternative near-field flow fields calculation rather than the Alternative inventory calculation. This is also due to the reasons explained previously for the Alternative near-field flow fields calculation; that the time of maximum exposure (5,100 AD) occurs beyond 4,000 AD when the Alternative near-field flow fields are slightly increased.

6.2 BMA

Table 6-2 shows a summary of the calculations undertaken on the BMA. Values of maximum near-field or geosphere flux or RBD dose that differ from the Most likely scenario are highlighted in bold if they are greater and in italics if they are lower.

Figures 6-3 and 6-4 show the near-field radionuclide flux and RBD dose for the BMA calculations, respectively.

Table 6-2. Summary of BMA calculations.

	Near-field	Geosphere	RBD
Most likely scenario	9.1E+07 Bq/y	7.8E+07 Bq/y	4.2E–07 Sv/y
	c. 3,100 AD	c. 3,200 AD	c. 8,000 AD (Agriculture)
	Organic C-14	Organic C-14	I-129
Alternative inventory	3.2E+08 Bq/y	2.7E+08 Bq/y	1.1E–06 Sv/y
	c. 3,100 AD	c. 3,200 AD	c. 5,000 AD (Lake)
	Organic C-14	Organic C-14	Organic C-14
Alternative near-field flow fields	1.3E+08 Bq/y	8.8E+07 Bq/y	4.9E–07 Sv/y
	c. 3,100 AD	c. 3,100 AD	c. 8,000 AD (Agriculture)
	Organic C-14	Organic C-14	I-129
Minimum near-field sorption	1.0E+08 Bq/y	8.2E+07 Bq/y	6.5E–07 Sv/y
	c. 3,100 AD	c. 3,200 AD	c. 5,000 AD (Lake)
	Organic C-14	Organic C-14	Inorganic and organic C-14
Maximum near-field sorption	9.1E+07 Bq/y	7.7E+07 Bq/y	3.0E–07 Sv/y
	c. 3,100 AD	c. 3,200 AD	c. 5,000 AD (Lake)
	Organic C-14	Organic C-14	Organic C-14
Combined alternative inventory and Alternative near-field flow fields	4.7E+08 Bq/y	3.6E+08 Bq/y	1.1E–06 Sv/y
	c. 3,100 AD	c. 31,00 AD	c. 8,000 AD (Agriculture)
	Organic C-14	Organic C-14	Se-79

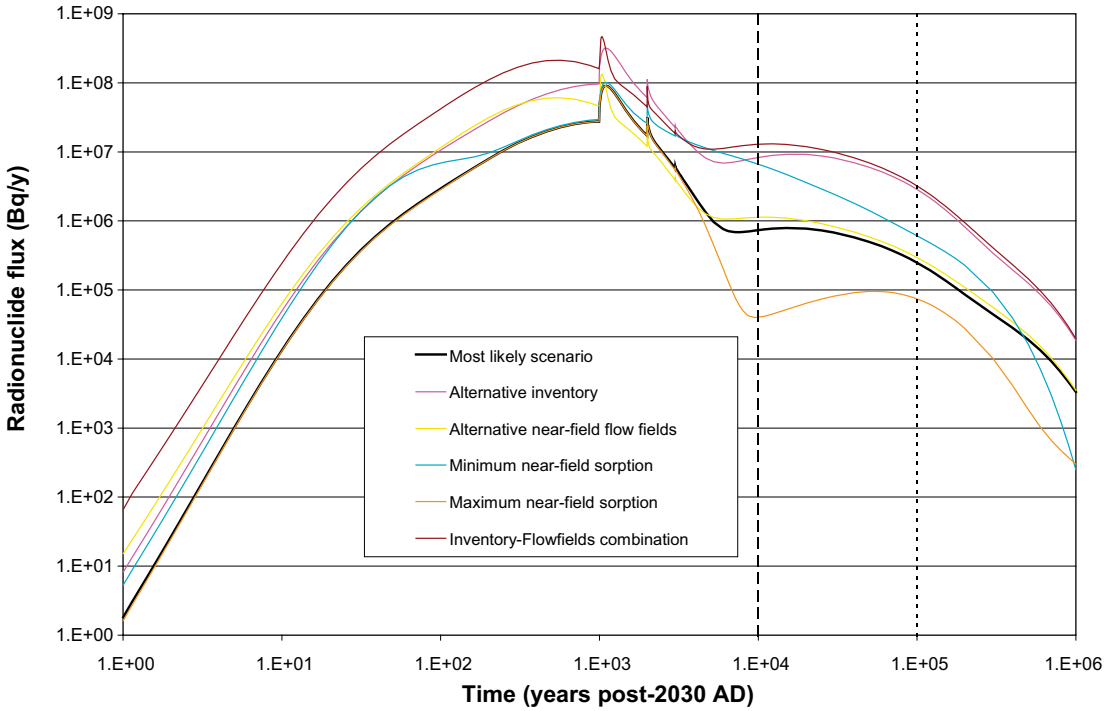

Figure 6-3. *Comparison of near-field radionuclide flux for BMA calculations.*

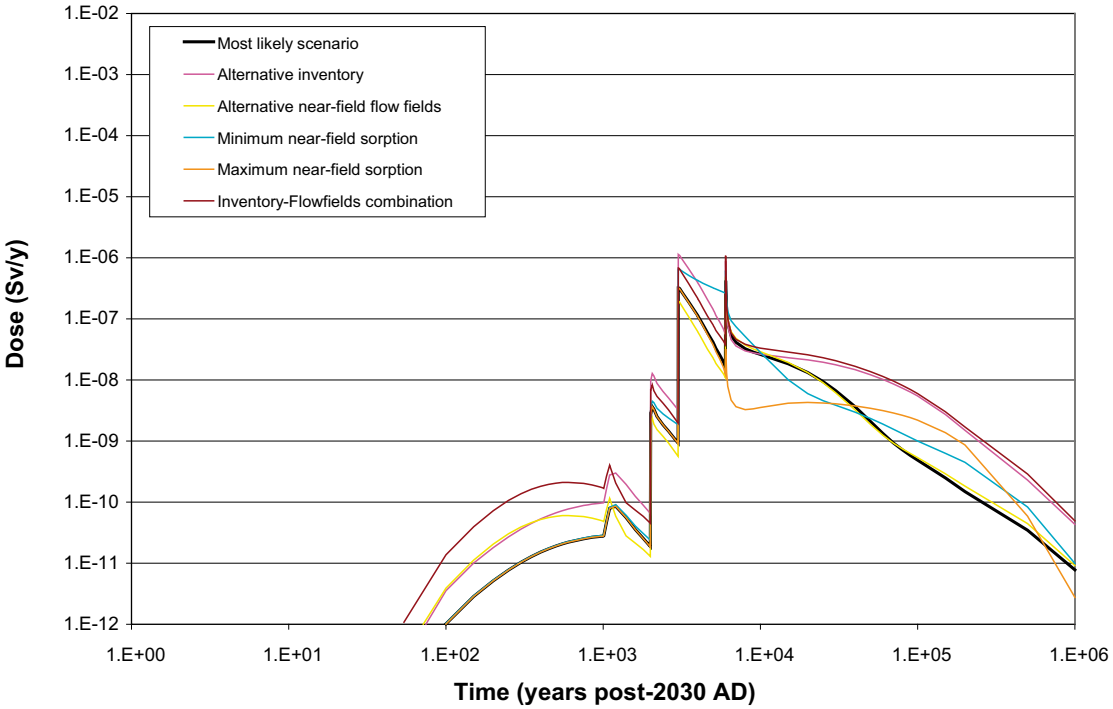

Figure 6-4. *Comparison of doses to RBD for BMA calculations.*

The maximum geosphere radionuclide flux and doses for the Maximum near-field sorption calculation are approximately a factor of 3.5 lower than those of the Most likely scenario. The maximum geosphere radionuclide flux and exposures are heavily influenced by organic C-14 which does not undergo sorption, however, other radionuclides, such as inorganic C-14, Se-79, I-129 and Cs-135 (compare Figures 4-5 and 4-7 with Figures 5-40 and 5-41), also contribute (and these undergo sorption). An increase the sorption (and retention) of these radionuclides results in a reduction in the maximum radionuclide fluxes and doses for the Maximum near-field sorption calculation relative to the Most likely scenario. The reduction is relatively small due to the importance of contributions from organic C-14 to the maximum near-field and geosphere radionuclide fluxes and doses in the period in which the maxima occur. However, beyond 12,000 AD, after the influence of organic C-14, the differences are much more noticeable (Figure 6-4) which is due to the effects of sorbing radionuclides such as Ni-59, I-129 and Cs-135 in particular.

Larger near-field and geosphere radionuclide fluxes and exposures relative to the Most likely scenario occur for all other calculations.

The radionuclide inventory used in the Alternative inventory calculations for the BMA is 10 times the Most likely scenario inventory overall and contains approximately 3 times the organic C-14 content but less I-129. The reduction in the I-129 inventory and increase in organic C-14 is reflected in an increase in exposure at the onset of the Lake period and a decrease at the onset of the Agricultural period (compare Figures 4-7 and 5-4).

The flow parameter in Alternative near-field flow fields calculation increases the flow-fields by a factor of 3.62 up to 4,000 AD and 3.67 beyond 4,000 AD (Table 3-4). Figure 6-3 shows an increased near-field radionuclide flux relative to the Most likely scenario up to 3,000 AD for this calculation. This increased flux of radionuclides manifests itself in two ways. Firstly, the dose in the coastal model up to 3,000 AD is increased relative to the Most likely scenario. Secondly, the increased flux of radionuclides during the coastal period leads to enhanced accumulation of radionuclides within the coastal sediments which in turn leads to higher exposures at the onset of the agricultural period.

The Minimum near-field sorption calculation shows higher maximum near-field and geosphere radionuclide fluxes and doses compared to the Most likely scenario. This is caused by additional contributions from radionuclides other than organic C-14 which also contribute to the maximum near-field and geosphere radionuclide fluxes and doses. Reducing sorption reduces the retention of these radionuclides within the BMA. For example, at 5,000 AD the maximum RBD dose for Minimum near-field sorption occurs earlier than the Most likely scenario and the reduced retention of inorganic C-14 increases the maximum dose (see Figure 5-30).

The Combined alternative inventory and Alternative near-field flow fields calculation is readily explained as the product of both an increased radionuclide inventory and initial release rate as described above for the Alternative inventory and Alternative near-field flow fields calculations. However, it should be noted that unlike those calculations the most important radionuclide to the maximum RBD dose is Se-79 which is increased by a factor of approximately 7 in the Alternative inventory (Table 3-3).

The largest near-field and geosphere radionuclide fluxes being for the combined inventory-near-field flow fields calculation. The largest RBD doses are for both the combined inventory-near-field flow fields and the Alternative inventory calculations. The nature of dose estimate obtained for the Combined alternative inventory and Alternative near-field flow fields calculation is different from the Most likely scenario and the Alternative inventory calculation in that it is caused by the accumulation of radionuclides in the coastal sediments which is likely to be increased by the greater radionuclide release from the BMA discussed above.

6.3 1BTF

Table 6-3 shows a summary of the calculations undertaken on 1BTF. As before, values of maximum near-field or geosphere flux or RBD dose that differ from the Most likely scenario are highlighted in bold if they are greater and in italics if they are lower.

Figures 6-5 and 6-6 show the radionuclide fluxes and the resultant dose to the RBD for all 1BTF calculations, respectively.

Table 6-3. Summary of 1BTF calculations.

	Near-field	Geosphere	RBD
Most likely scenario	2.9E+08 Bq/y	1.3E+08 Bq/y	5.9E–07 Sv/y
	c. 3,000 AD	c. 3,100 AD	c. 5,100 AD (Lake)
	Organic C-14	Organic C-14	Organic C-14
Alternative inventory	3.9E+08 Bq/y	1.7E+08 Bq/y	8.0E–07 Sv/y
	c. 3,000 AD	c. 3,100 AD	c. 5,100 AD (Lake)
	Organic C-14	Organic C-14	Organic C-14
Alternative near-field flow fields	3.7E+08 Bq/y	1.7E+08 Bq/y	2.4E–07 Sv/y
	c. 4,000 AD	c. 4,000 AD	c. 8,000 AD (Agriculture)
	Organic C-14	Organic C-14	Inorganic C-14
Minimum near-field sorption	3.2E+08 Bq/y	1.3E+08 Bq/y	2.5E–06 Sv/y
	c. 3,000 AD	c. 3,100 AD	c. 5,100 AD (Lake)
	Organic C-14	Organic C-14	Inorganic C-14
Maximum near-field sorption	2.9E+08 Bq/y	1.3E+08 Bq/y	5.7E–07 Sv/y
	c. 3,000 AD	c. 3,100 AD	c. 5,000 AD (Lake)
	Organic C-14	Organic C-14	Organic C-14
Combined alternative inventory and Alternative near-field flow fields	5.0E+08 Bq/y	2.4E+08 Bq/y	4.4E–07 Sv/y
	c. 4,000 AD	c. 4,100 AD	c. 8,000 AD (Agriculture)
	Organic C-14	Organic C-14	Se-79

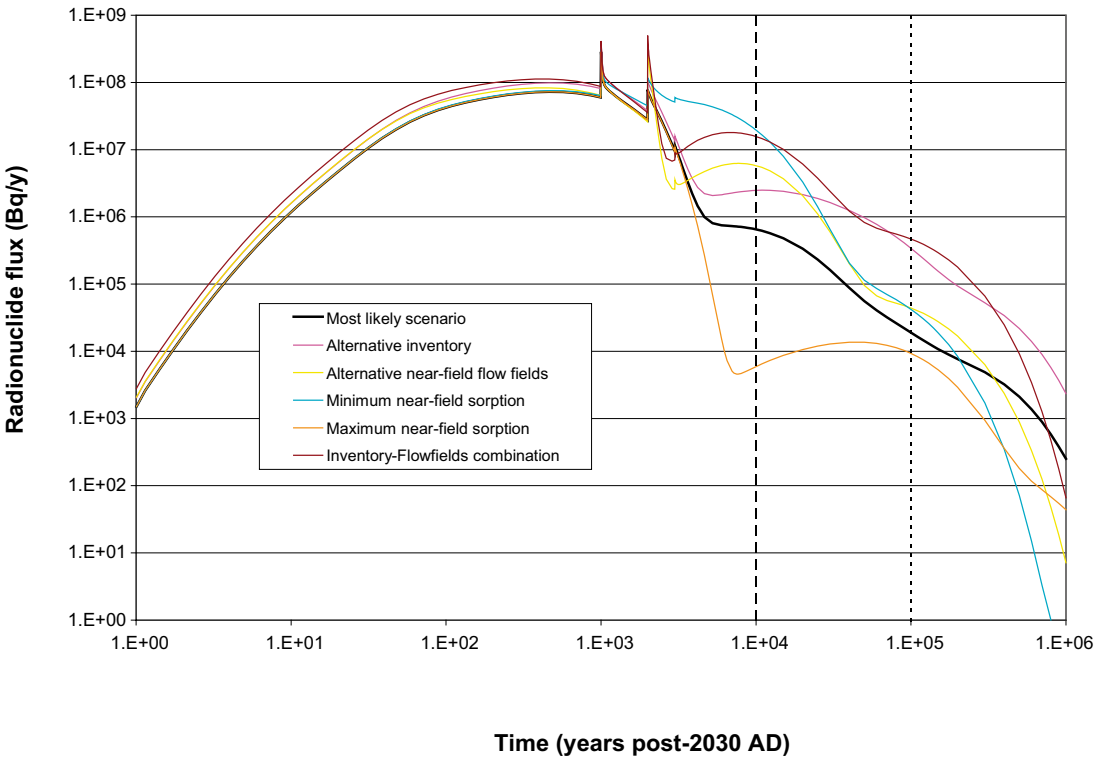

Figure 6-5. *Comparison of near-field radionuclide flux for 1BTF calculations*

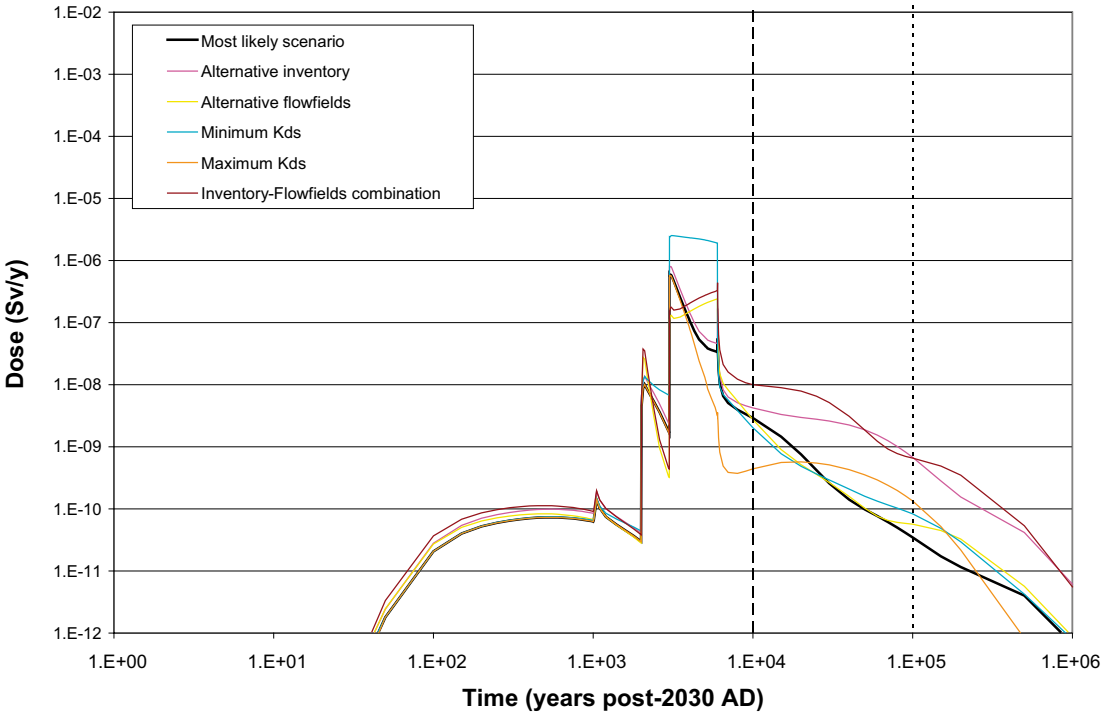

Figure 6-6. *Comparison of doses to RBD from for 1BTF calculations.*

The radionuclide inventory used in the Alternative inventory calculations for the 1BTF is approximately 6 times the Most likely scenario inventory overall but it contains only slightly more organic C-14 (Table 3-3). The relative increase in the maximum near-field and geosphere radionuclide fluxes and RBD dose is around 1.3, which is approximately the same factor as the increase in the organic C-14 inventory. There is also very little contribution from other radionuclides at the time of the maximum radionuclide fluxes and RBD dose which explains the general lack of sensitivity shown to this calculation.

The flow parameter in the Alternative near-field flow fields calculation increases the flow-fields by a factor of 1.15 up to 4,000 AD and 5.65 beyond 4,000 AD (Table 3-4). This increased flux of radionuclides manifests itself in two ways. Firstly, the rapid increase in the flow fields at 4,000 AD results in the peak near-field and geosphere fluxes occurring at this time. Secondly, the increased flux of radionuclides leads to enhanced accumulation of radionuclides within the coastal sediments which in turn leads to higher exposures at the onset of the agricultural period and means that exposure to contaminated sediment at the onset of the agricultural period becomes the dominant exposure route.

The Minimum near-field sorption calculation shows higher maximum near-field and geosphere radionuclide fluxes and doses compared to the Most likely scenario. This is caused by enhanced contributions from radionuclides such as inorganic C-14 which have reduced retention of these radionuclides within the 1BTF. For example, at 5,000 AD the maximum RBD dose for Minimum near-field sorption occurs earlier than the Most likely scenario and the reduced retention of inorganic C-14 increases the maximum dose (see Figure 5-30).

The Maximum near-field sorption calculations has a similar trend to the BMA in that little sensitivity is shown due to the importance of organic C-14 in determining the radionuclide fluxes and doses. The only difference relative to the Most likely scenario is that a slight reduction in the maximum dose occurs which is due to a reduced contribution from inorganic C-14 (compare Figures 4-12 and 5-43).

The Combined alternative inventory and Alternative near-field flow fields calculation is readily explained as the product of both an increased radionuclide inventory and initial release rate as described above for the Alternative inventory and Alternative near-field flow fields calculations. However, it should be noted that unlike those calculations the most important radionuclide to the maximum RBD dose is Se-79 which is increased by a factor of approximately 11 in the Alternative inventory (Table 3-3).

6.4 2BTF

Table 6-4 shows a summary of the calculations undertaken on 2BTF. Values of maximum near-field or geosphere flux or RBD dose that differ from the Most likely scenario are highlighted in bold if they are greater and in italics if they are lower.

Figures 6-7 and 6-8 show the radionuclide fluxes and the resultant dose to the RBD for all 2BTF calculations, respectively.

The radionuclide inventory used in the Alternative inventory calculations for the 2BTF is approximately 20 times the Most likely scenario inventory overall and it contains approximately 60 times more Se-79 but the amount of organic C-14 and I-129 is little changed (Table 3-3). The increase in the maximum near-field and geosphere radionuclide fluxes occurs via increased contributions from organic C-14 and other radionuclides such as Cl-36, Ni-59 and Ag-108m (compare Figures 4-14 and 5-7). The increase in the maximum RBD dose is predominantly due to increased contributions from Se-79 (compare Figures 4-16 and 5-8).

Table 6-4. Summary of 2BTF calculations.

	Near-field	Geosphere	RBD
Most likely scenario	3.3E+06 Bq/y	2.7E+06 Bqy	6.9E–08 Svy
	c. 3,000 AD	c. 3,100 AD	c. 8,000 AD (Agriculture)
	Organic C-14	Organic C-14	I-129
Alternative inventory	1.8E+07 Bqy	1.5E+07 Bqy	2.5E–07 Svy
	c. 3,100 AD	c. 3,100 AD	c. 8,000 AD (Agriculture)
	Organic C-14	Organic C-14	Se-79 and I-129
Alternative near-field flow fields	8.3E+06 Bqy	4.8E+06 Bqy	1.4E–07 Svy
	c. 4,000 AD	c. 4,100 AD	c. 8,000 AD (Agriculture)
	Organic C-14	Organic C-14	I-129
Minimum near-field sorption	4.3E+06 Bqy	3.0E+06 Bqy	7.5E–08 Svy
	c. 3,100 AD	c. 3,100 AD	c. 8,000 AD (Agriculture)
	Organic C-14	Organic C-14	I-129
Maximum near-field sorption	3.3E+06 Bqy	2.7E+06 Bqy	2.5E–08 Svy
	c. 3,100 AD	c. 3,000 AD	c. 5,000 AD (Lake)
	Organic C-14	Organic C-14	Organic C-14
Combined alternative inventory and Alternative near-field flow fields	3.0E+07 Bqy	2.0E+07 Bqy	4.2E–07 Svy
	c. 3,000 AD	c. 3,000 AD	c. 8,000 AD (Agriculture)
	Organic C-14	Organic C-14	Se-79

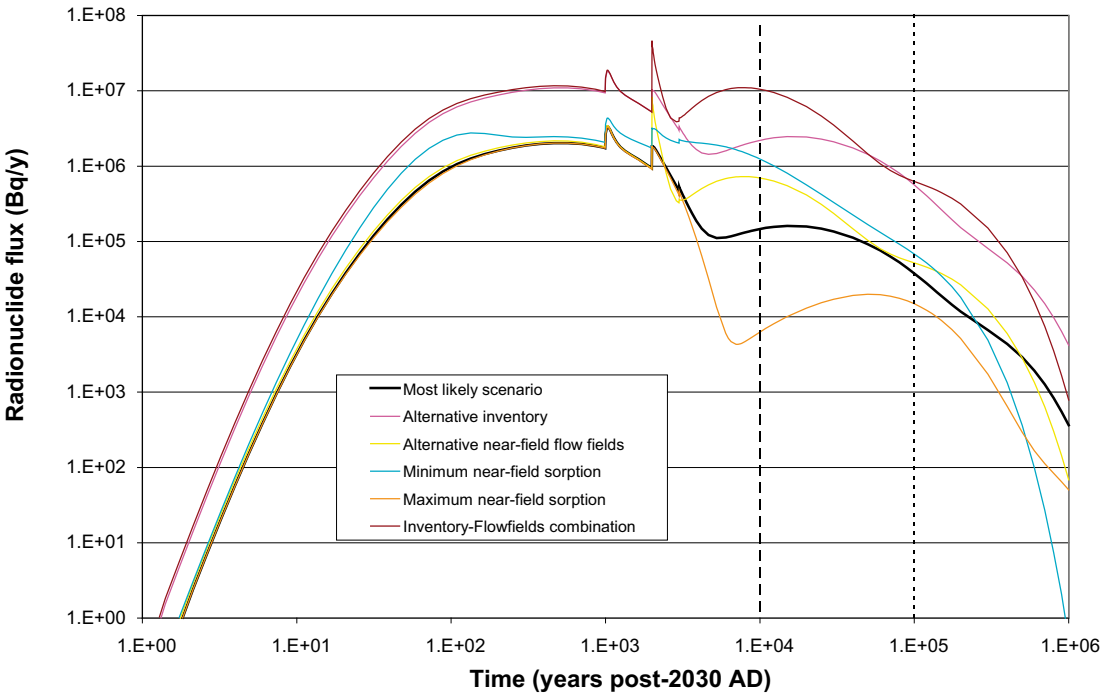

Figure 6-7. *Comparison of near-field radionuclide flux for 2BTF calculations.*

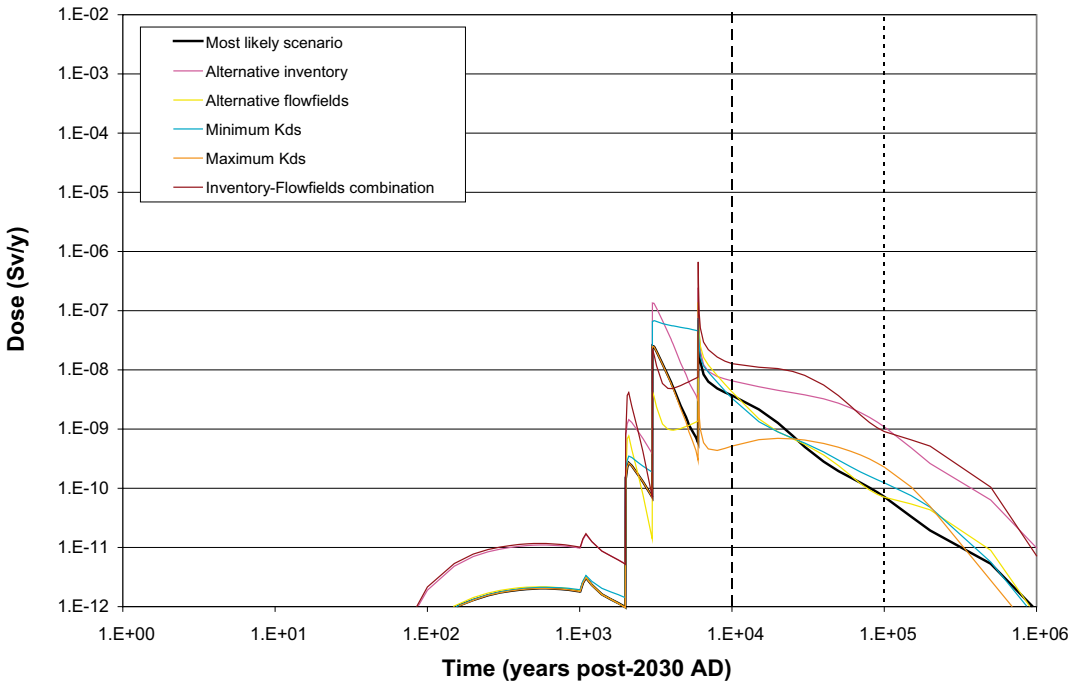

Figure 6-8. *Comparison of doses to RBD for 2BTF calculations.*

The flow parameter in the Alternative near-field flow fields calculation increases the flow-fields by a factor of 1.07 up to 4,000 AD and 4.75 beyond 4,000 AD (Table 3-4). This increased flux of radionuclides manifests itself in two ways similarly to 1BTF. Firstly, the rapid increase in the flow fields at 4,000 AD results in the peak near-field and geosphere fluxes occurring at this time. Secondly, the increased flux of radionuclides leads to enhanced accumulation of radionuclides within the coastal sediments which in turn leads to higher exposures at the onset of the agricultural period.

The Minimum near-field sorption calculation shows higher maximum near-field and geosphere radionuclide fluxes and doses compared to the Most likely scenario. Similarly to the 1BTF, this is caused by enhanced contributions from radionuclides such inorganic C-14 and Cs-135 which have reduced retention of these radionuclides within the 2BTF (compare Figures 4-16 and 5-34).

The Maximum near-field sorption calculations has a similar trend to the 1BTF in that little sensitivity is shown for the near-field and geosphere radionuclide fluxes due to the importance of organic C-14 in determining them. There is a slight reduction in RBD dose due to the increased retention of I-129 and this also means that the exposure route is altered from doses received from contaminated sediment at the onset of the agricultural period (from I-129) to doses received in the lake period dominated by contributions due to inorganic C-14 (compare Figures 4-16 and 5-45).

The Combined alternative inventory and Alternative near-field flow fields calculation is readily explained as the product of both an increased radionuclide inventory and initial release rate as described above for the Alternative inventory and Alternative near-field flow fields calculations.

6.5 BLA

Table 6-5 shows a summary of the calculations undertaken on the BLA. No near-field sorption calculations were undertaken for the BLA as neither sorption nor barriers are included within the BLA conceptual model /Lindgren et al. 2001/. Values of maximum near-field or geosphere flux or RBD dose that differ from the Most likely scenario are highlighted in bold if they are greater and in italics if they are lower.

Figures 6-9, 6-10 and 6-11 show the near-field and geosphere radionuclide fluxes and the resultant dose to the RBD from the BLA for all calculations, respectively.

Table 6-5. Summary of BLA calculations.

	Near-field	Geosphere	RBD
Most likely scenario	2.5E+08 Bq/y	2.3E+06 Bq/y	5.5E–09 Sv/y
	2,030 AD	c. 2,200 AD	c. 5,000 AD (Lake)
	Co-60, Ni-63 and Cs-137	Ni-63	Inorganic C-14
Alternative inventory	9.6E+09 Bq/y	1.2E+08 Bq/y	2.3E–07 Sv/y
	2,030 AD	c. 2,200 AD	c. 8,000 AD (Agriculture)
	Ni-63 and Cs-137	Ni-63	Tc-99
Alternative near-field flow fields	3.1E+08 Bq/y	2.7E+06 Bq/y	4.1E–09 Sv/y
	2,030 AD	c. 2,200 AD	c. 8,000 AD (Agriculture)
	Co-60, Ni-63 and Cs-137	Ni-63	Tc-99
Combined alternative inventory and Alternative near-field flow fields	1.2E+10 Bq/y	1.4E+08 Bq/y	2.4E–07 Sv/y
	2,030 AD	c. 2,200 AD	c. 8,000 AD (Agriculture)
	Co-60, Ni-63 and Cs-137	Ni-63	Tc-99

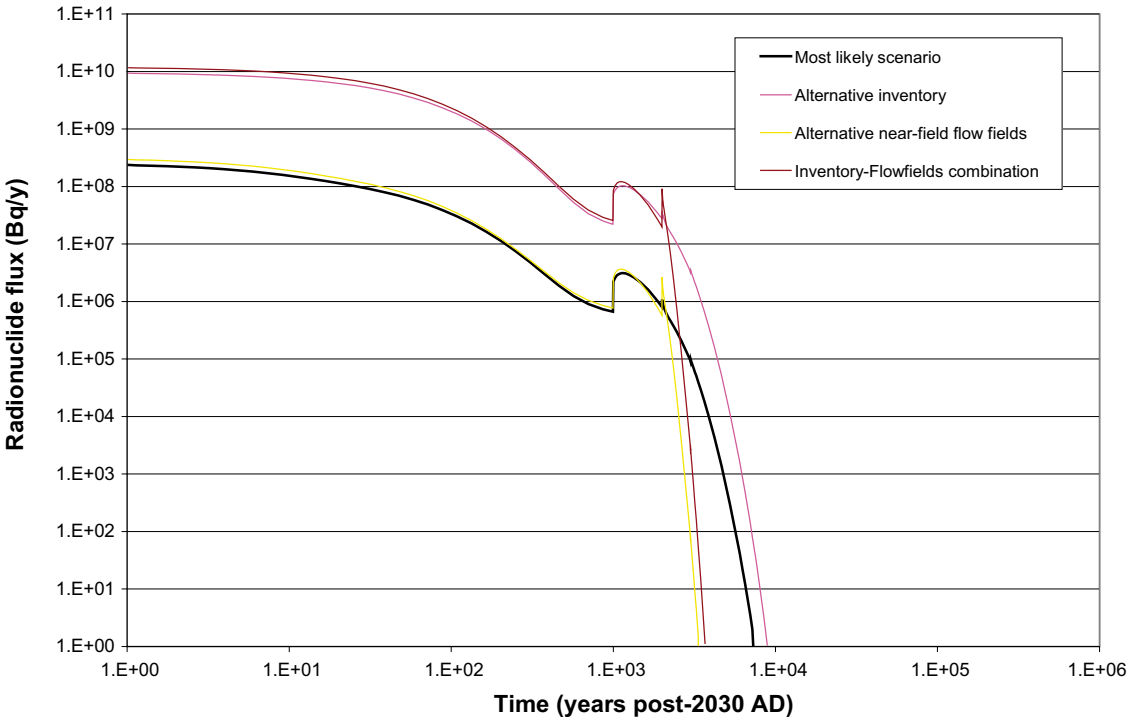

Figure 6-9. *Comparison of near-field radionuclide flux for BLA calculations.*

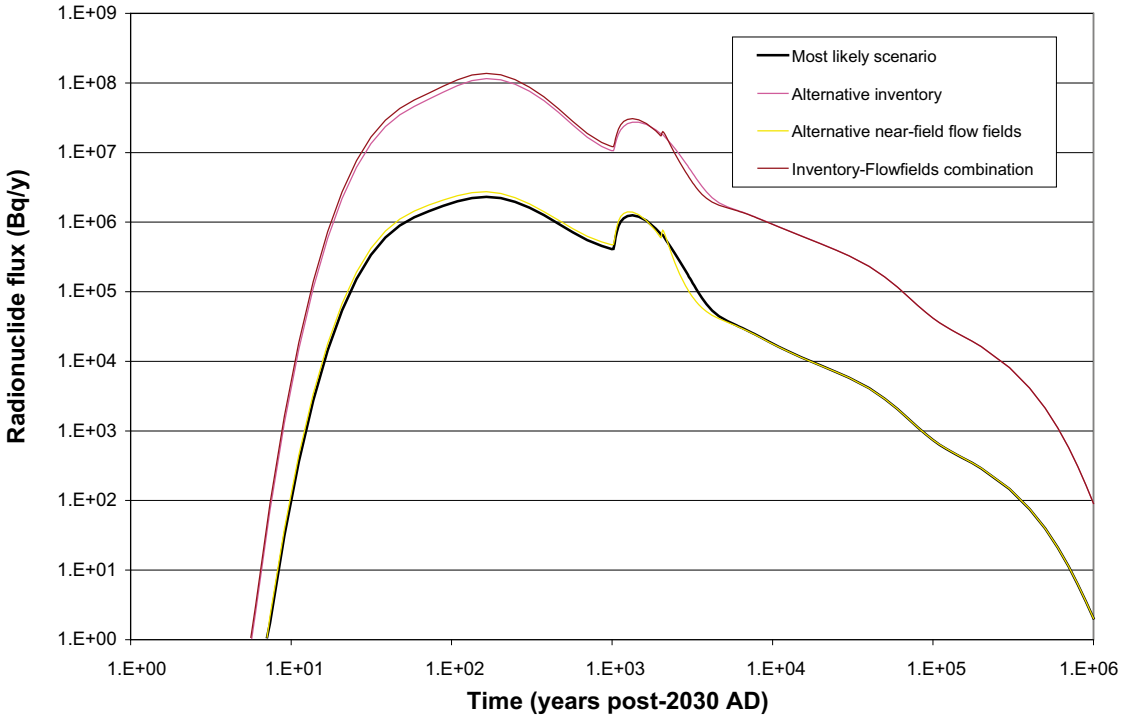

Figure 6-10. *Comparison of geosphere radionuclide flux for BLA calculations.*

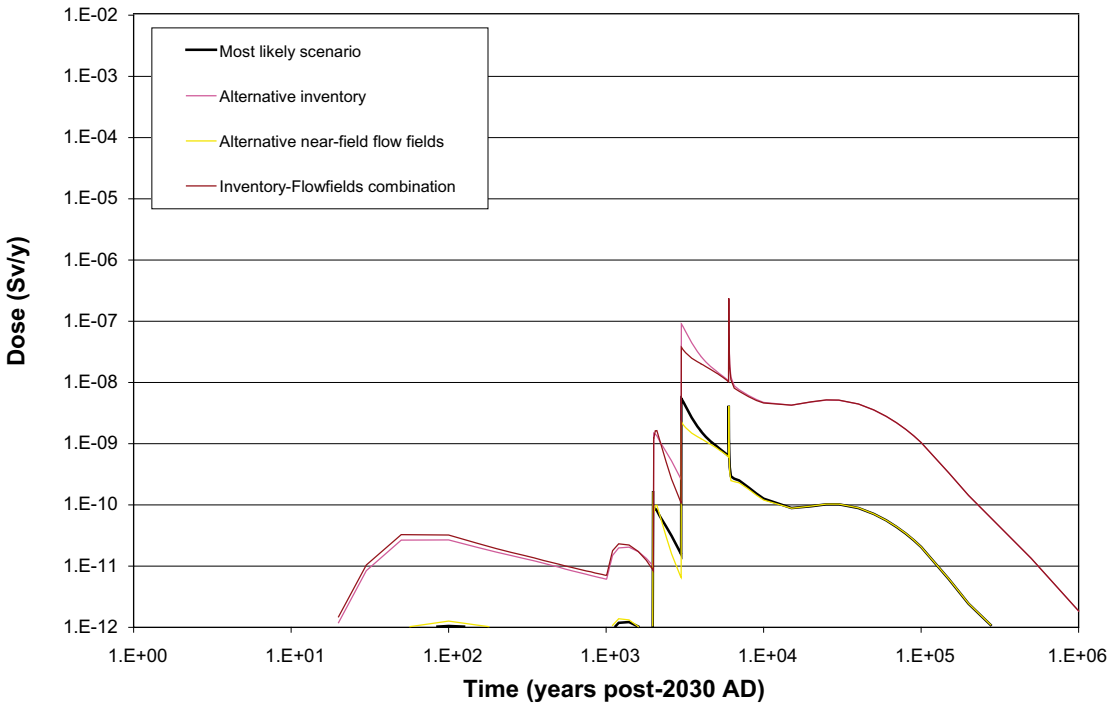

Figure 6-11. *Comparison of doses to RBD for BLA calculations.*

The Alternative inventory for the BLA is almost 40 times larger than that used in the Most likely scenario (Table 3-3, e.g. Ni-63 and Cs-137 are increased by factors of c. 70 and c. 50, respectively). The near-field and geosphere radionuclide fluxes for the Alternative inventory calculation follow similar trends to those of the Most likely scenario but are consistently higher due to this (Figures 6-9 and 6-10). The maximum RBD dose for the Most likely scenario is due to inorganic C-14 and occurs at the onset of the Lake period, the inventory of inorganic C-14 is increased by a factor of approximately 20 in the Alternative inventory. However, the peak RBD dose in the Alternative inventory occurs at the onset of the Agricultural period and is associated with exposure to Tc-99 which has previously accumulated in the coastal and lake sediments (compare Figures 36 and 51) and it can be seen in Figure 4-20 that the maximum dose from inorganic C-14 is 5.5E–09 Sv/y at c. 5,000 AD and from Tc-99 is 4.2E–09 Sv/y at c. 8,000 AD. Tc-99 is increased by a factor of approximately 60 in the Alternative inventory and this leads to the change in the exposure route associated within the maximum dose.

As the BLA conceptual model contains neither sorption nor barriers the near-field peak radionuclide flux occurs immediately and radionuclide inventories within the BLA diminish as they are rapidly released (seen as long-term near-field radionuclide fluxes below 1Bq/y). The effect of increasing the flow rate through the BLA therefore results in an increase in the initial radionuclide release rate. The increase in flow rates up to 4,000 AD is 1.25 (and beyond 4,000 AD 4.29, Table 3-4) which results in a similarly modest increase in the maximum near-field and geosphere radionuclide fluxes for the Alternative near-field flow fields compared to the Most likely scenario. The maximum RBD dose is associated with Tc-99 accumulated in the coastal and lake sediments which will be increased relative to the Most likely scenario by the higher radionuclide release rates. The sensitivity of this exposure route has been discussed previously.

The Combined alternative inventory and Alternative near-field flow fields can be explained using the discussion developed above; increased near-field and geosphere radionuclide fluxes are due to increases in both the inventory and increased BLA flow rates. This calculation results in the highest fluxes and doses for the BLA.

7 Summary of calculations

Table 7-1 summarises the calculations undertaken.

- For the Most likely scenario the maximum dose from SFR-1 is 1.6E–06 Sv y^{-1} (i.e. 1.6 μSv y^{-1}) which is dominated by dose due to organic C-14 released from 1BTF and is estimated to occur at around 5,100 AD. This equates to a conditional risk of 9.4E–08 y^{-1} if it is assumed that the probability of the Most likely scenario is unity. If a forest ecosystem is considered to be the long-term land use the maximum estimated dose is estimated to be 3E–08 Sv/y (i.e. 0.03 μSv y^{-1}). These values are below the relevant regulatory criteria for dose (16 μSv y^{-1}) and risk (1E–06 y^{-1}).
- All the other calculations undertaken also result in estimated doses below 16 μSv/y.
  - If an Alternative inventory is considered the maximum estimated dose is 8.0E–06 Sv/y (i.e. 8.0 μSv/y) dominated by dose due to releases of organic C-14 from the Silo.
  - The Alternative near-field flow fields result in a maximum estimated dose of 9.8E–07 Sv/y (i.e. 1.0 μSv/y) dominated by dose due to releases of organic C-14 from the Silo.
  - The estimated maximum doses are not overly sensitive to changes in near-field sorption due to the importance of organic C-14 (which does not undergo sorption in the near-field) in determining doses. If minimum values of near-field sorption coefficients are used the maximum dose is estimated to increase to 3.9E–06 Sv/y (i.e. 3.9 μSv/y), whereas if maximum values of near-field sorption coefficients are used the maximum dose is estimated to decrease slightly to 1.5E–06 Sv/y (i.e. 1.5 μSv/y).
  - Considering the possibility of both an Alternative inventory and Alternative near-field flow fields in combination resulted in maximum doses estimated to increase to 7.0E–06 Sv/y (i.e. 7.0 μSv/y) dominated by dose due to organic C-14 released from the Silo.

Table 7-1. Summary of calculations.

	Near-field	Geosphere	RBD
Most likely scenario			
Silo	1.3E+07 Bq/y at c. 3,900 AD Organic C-14	1.2E+07 Bq/y at c. 3,900 AD Organic C-14	6.5E–07 Sv/y at c. 5,100 AD Organic C-14
BMA	9.1E+07 Bq/y at c. 3,100 AD Organic C-14	7.8E+07 Bq/y at c. 3,200 AD Organic C-14	4.2E–07 Sv/y at c. 8,000 AD I-129
1BTF	2.9E+08 Bq/y at c. 3,000 AD Organic C-14	1.3E+08 Bq/y at c. 3,100 AD Organic C-14	5.9E–07 Sv/y at c. 5,100 AD Organic C-14
2BTF	3.3E+06 Bq/y at c. 3,000 AD Organic C-14	2.7E+06 Bq/y at c. 3,100 AD Organic C-14	6.9E–08 Sv/y at c. 8,000 AD I-129
BLA	2.5E+08 Bq/y at closure Co-60, Ni-63 and Cs-137	2.3E+06 Bq/y at c. 2,200 AD Ni-63	5.5E–09 Sv/y at c. 5,000 AD Inorganic C-14
SFR-1	3.5E+08 Bq/y at c. 3,000 AD 1BTF	1.8E+08 Bq/y at c. 3,100 AD 1BTF	1.6E–06 Sv/y at c. 5,100 AD Silo, BMA, 1BTF
Alternative inventory			
Silo	1.2E+08 Bq/y at c. 3,900 AD Organic C-14	1.1E+08 Bq/y at c. 3,900 AD Organic C-14	6.0E–06 Sv/y at c. 5,100 AD Organic C-14
BMA	3.2E+08 Bq/y at c. 3,100 AD Organic C-14	2.7E+08 Bq/y at c. 3,200 AD Organic C-14	1.1E–06 Sv/y at c. 5,000 AD Organic C-14
1BTF	3.9E+08 Bq/y at c. 3,000 AD Organic C-14	1.7E+08 Bq/y at c. 3,100 AD Organic C-14	8.0E–07 Sv/y at c. 5,100 AD Organic C-14
2BTF	1.8E+07 Bq/y at c. 3,100 AD Organic C-14	1.5E+07 Bq/y at c. 3,100 AD Organic C-14	2.5E–07 Sv/y at c. 8,000 AD Se-79 and I-129
BLA	9.6E+09 Bq/y at 2,030 AD Ni-63 and Cs-137	1.2E+08 Bq/y at c. 2,200 AD Ni-63	2.3E–07 Sv/y at c. 8,000 AD Tc-99
SFR-1	9.6E+09 Bq/y at 2,030 AD BLA	5.0E+08 Bq/y at c. 3,200 AD BMA	8.0E–06 Sv/y at c. 5,100 AD Silo
Alternative near-field flow fields			
Silo	1.2E+07 Bq/y at c. 4,100 AD Organic C-14	1.1E+07 Bq/y at c. 4,200 AD Organic C-14	6.7E–07 Sv/y at c. 5,100 AD Organic C-14
BMA	1.3E+08 Bq/y at c. 3,100 AD Organic C-14	1.0E+08 Bq/y at c. 3,100 AD Organic C-14	4.9E–07 Sv/y at c. 8,000 AD I-129
1BTF	3.7E+08 Bq/y at c. 4,000 AD Organic C-14	1.7E+08 Bq/y at c. 4,100 AD Organic C-14	2.4E–07 Sv/y at c. 8,000 AD Inorganic C-14
2BTF	8.3E+06 Bq/y at c. 4,000 AD Organic C-14	4.8E+06 Bq/y at c. 4,100 AD Organic C-14	1.4E–07 Sv/y at c. 8,000 AD I-129
BLA	3.1E+08 Bq/y at closure Co-60, Ni-63 and Cs-137	2.7E+06 Bq/y at c. 2,200 AD Ni-63	4.1E–09 Sv/y at c. 8,000 AD Tc-99
SFR-1	4.1E+08 Bq/y at c. 4,000 AD 1BTF	2.2E+08 Bq/y at c. 3,100 AD BMA and 1BTF	9.8E–07 Sv/y at c. 5,000 AD Silo

	Near-field	Geosphere	RBD
Minimum near-field sorption			
Silo	1.3E+07 Bq/y at c. 3,700 AD Organic C-14	1.2E+07 Bq/y at c. 3,900 AD Organic C-14	6.5E–07 Sv/y at c. 5,100 AD Organic C-14
BMA	1.0E+08 Bq/y at c. 3,100 AD Organic C-14	8.2E+07 Bq/y at c. 3,200 AD Organic C-14	6.5E–07 Sv/y at c. 5,000 AD Inorganic and organic C-14
1BTF	3.2E+08 Bq/y at c. 3,000 AD Organic C-14	1.3E+08 Bq/y at c. 3,100 AD Organic C-14	2.5E–06 Sv/y at c. 5,100 AD Inorganic C-14
2BTF	4.3E+06 Bq/y at c. 3,100 AD Organic C-14	3.0E+06 Bq/y at c. 3,100 AD Organic C-14	7.5E–08 Sv/y at c. 8,000 AD I-129
BLA#	2.5E+08 Bq/y at 2,030 AD Co-60, Ni-63, Cs-137	2.3E+06 Bq/y at c. 2,200 AD Ni-63	5.5E–09 Sv/y at c. 5,000 AD Inorganic C-14
SFR-1	3.9E+08 Bq/y at c. 3,000 AD 1BTF	1.9E+08 Bq/y at c. 3,100 AD 1BTF	3.9E–06 Sv/y at c. 5,000 AD 1BTF
Maximum near-field sorption			
Silo	1.3E+07 Bq/y at c. 3,900 AD Organic C-14	1.2E+07 Bq/y at c. 3,900 AD Organic C-14	6.5E–07 Sv/y at c. 5,100 AD Organic C-14
BMA	9.1E+07 Bq/y at c. 3,100 AD Organic C-14	7.7E+07 Bq/y at c. 3,200 AD Organic C-14	3.0E–07 Sv/y at c. 5,000 AD Organic C-14
1BTF	2.9E+08 Bq/y at c. 3,000 AD Organic C-14	1.3E+08 Bq/y at c. 3,100 AD Organic C-14	5.7E–07 Sv/y at c. 5,000 AD Organic C-14
2BTF	3.3E+06 Bq/y at c. 3,100 AD Organic C-14	3.7E+06 Bq/y at c. 3,100 AD Organic C-14	2.5E–08 Sv/y at c. 5,000 AD Organic C-14
BLA#	2.5E+08 Bq/y at 2,030 AD Co-60, Ni-63 and Cs-137	2.3E+06 Bq/y at c. 2,200 AD Ni-63	5.5E–09 Sv/y at c. 5,000 AD Inorganic C-14
SFR-1	3.5E+08 Bq/y at c. 3,000 AD 1BTF	1.8E+08 Bq/y at c. 3,100 AD 1BTF	1.5E–06 Sv/y at c. 5,100 AD Silo, BMA and 1BTF
Combined alternative inventory and Alternative near-field flow fields			
Silo	1.1E+08 Bq/y at c. 4,100 AD Organic C-14	1.0E+08 Bq/y at c. 4,100 AD Organic C-14	6.2E–06 Sv/y at c. 5,100 AD Organic C-14
BMA	4.7E+08 Bq/y at c. 3,100 AD Organic C-14	3.6E+08 Bq/y at c. 3,100 AD Organic C-14	1.1E–06 Sv/y at c. 8,000 AD Se-79
1BTF	5.0E+08 Bq/y at c. 4,000 AD Organic C-14	2.4E+08 Bq/y at c. 4,100 AD Organic C-14	4.4E–07 Sv/y at c. 8,000 AD Se-79
2BTF	4.6E+07 Bq/y at c. 4,000 AD Organic C-14	2.6E+07 Bq/y at c. 4,100 AD Organic C-14	6.7E–07 Sv/y at c. 8,000 AD Se-79
BLA	1.2E+10 Bq/y at 2,030 AD Co-60, Ni-63 and Cs-137	1.4E+08 Bq/y at c. 2,200 AD Ni-63	2.4E–07 Sv/y at c. 8,000 AD Tc-99
SFR-1	1.2E+10 Bq/y at 2,030 AD BLA	5.9E+08 Bq/y at c. 3,100 AD BMA and 1BTF	7.0E–06 Sv/y at c. 5,100 AD Silo

Data for Most likely scenario.

8 References

Aarne M, Mikkola E, Serola Y, 1994. Yearbook of Forest Statistics, Finnish Research Institute, Helsinki.

Avila R, 2004. Model of the long-term transfer of radionuclides in forests, Draft Report to SKB, December 2004.

Bergström U, Nordlinder S, Aggeryd I, 1999. Models for dose assessments: Modules for various biosphere types. SKB TR-99-14. Svensk Kärnbränslehantering AB.

Cronstrand P, 2005. Assessment of uncertainty intervals for sorption coefficients. SwedPower report to SKB T-SEKV 2005-020. 15th September 2005.

Enviros, 2003. AMBER – Contaminants Modelling. see www.enviros.com/amber.

Enviros, 2004. An evaluation of alternative closure options for the SFR repository. Enviros Consulting Limited report to SKB version 2.0. SK0040002. December 2004.

Enviros, Quintessa, 2005. AMBER White Paper: Fractured geosphere modelling.

Holmén JG, Stigsson M, 2001a. Modelling of future hydrogeological conditions at SFR. SKB R-01-02. Svensk Kärnbränslehantering AB.

Holmén JG, Stigsson M, 2001b. Details of predicted flow in deposition tunnels at SFR, Forsmark. SKB R-01-21. Svensk Kärnbränslehantering AB.

Holmén JG, 2005. SFR-1: Inverse modelling of inflow to tunnels and propagation of estimated uncertainties to predictive stages. Golder Associates report to SKB Draft Version 5. 31st July 2005.

IAEA, 2003. Assessing radiation doses to the public from radionuclides in timber and wood products, IAEA-TECDOC-1376.

ICRP, 1991. 1990 recommendations of the International Commission on Radiological Protection. ICRP Publication 60, Annals of the ICRP, 21 (1–3).

Johanson KJ, Nikolova I, Taylor AFS, Vinichuk MM, 2004. Uptake of elements by fungi in the Forsmark area, SKB TR-04-26. Svensk Kärnbränslehantering AB.

Johansson C, 2004. Prognos över nyttjande av SFR-1 vid 40 års reaktordrift. SKB report. SKB Document reference DL 312. 16th December 2004. Svensk Kärnbränslehantering AB.

Jones J, Vahlund F, Kautsky U, 2004. Tensit – a novel probabilistic simulation tool for safety assessments. Tests and verifications using biosphere models. SKB TR-04-07. Svensk Kärnbränslehantering AB.

Karlsson S, Bergström U, Meili M, 2001. Models for dose assessments. Models adapted to the SFR-area, Sweden. SKB TR-01-04. Svensk Kärnbränslehantering AB.

Kershaw P, 1999. Pilot Study for the update of the MARINA Project on the radiological exposure of the European Community from radioactivity in North European marine waters. Final Report: December 1999. http://europa.eu.int/comm/energy/nuclear/radioprotection/studies_en.htm

Lindgren M, Pettersson M, Karlsson S, Moreno L, 2001. Project SAFE. Radionuclide release and dose from the SFR repository. SKB R-01-18. Svensk Kärnbränslehantering AB.

Magnusson Å, Stenström K, 2005. ^{14}C produced in Swedish nuclear power reactors – Measurements on spent ion exchange resins, various process water systems and ejector off-gas. Final report for SKB project 9808. Report 02/05. Lund University. September 2005.

QuantiSci and Quintessa, 2002. AMBER 4.4 Reference Guide, Version 1.0, April 2002, Enviros QuantiSci, Culham.

Rantavaara A, Ammann M, 2004. Description of the forest food chain and dose model FDMF in RODOS PV6.0, RODOS(RA3)-TN(04)-01, Draft Version 1.0, dated 31.03.2004.

Riggare P, Johansson C, 2001. Project SAFE Low and intermediate level waste in SFR-1 Reference Waste Inventory. June 2001. SKB R-01-03. Svensk Kärnbränslehantering AB.

SKB, 2004. Interim main report of the safety assessment SR-Can. SKB TR-04-11. August 2004. Svensk Kärnbränslehantering AB.

SKI and SSI, 2004. SSI and SKI's Review of SKB's Updated Final Safety Report for SFR-1. Review Report. SKI Report 2004:47 (SSI Report 2004:06).

Smith KR, Jones AL, 2003. Generalised habit data for radiological assessments, NRPB-W41. NRPB. Chilton. UK.

Thomson JG, 2005. A representation of the Project SAFE performance assessment of the Swedish SFR-1 repository for L/ILW using the AMBER compartmental code. Enviros Consulting Limited report to SKB. June 2005.

Wiborgh M, 2005. Supplement to the SAFE study: The Base scenario within the SAFE project. Kemakta Konsult AB report to SKB, Kemakta AR 2005-08. June 2005.

Appendix A

Reasonable Biosphere Development model

The information summarised here is taken from /Karlsson et al. 2001/.

Coastal and lake models

The compartments used to represent the coastal and lake modules of the Reasonable Biosphere Development model are shown below. Arrows mark the direction of transfers and crosses mark the potential sources of radionuclides.

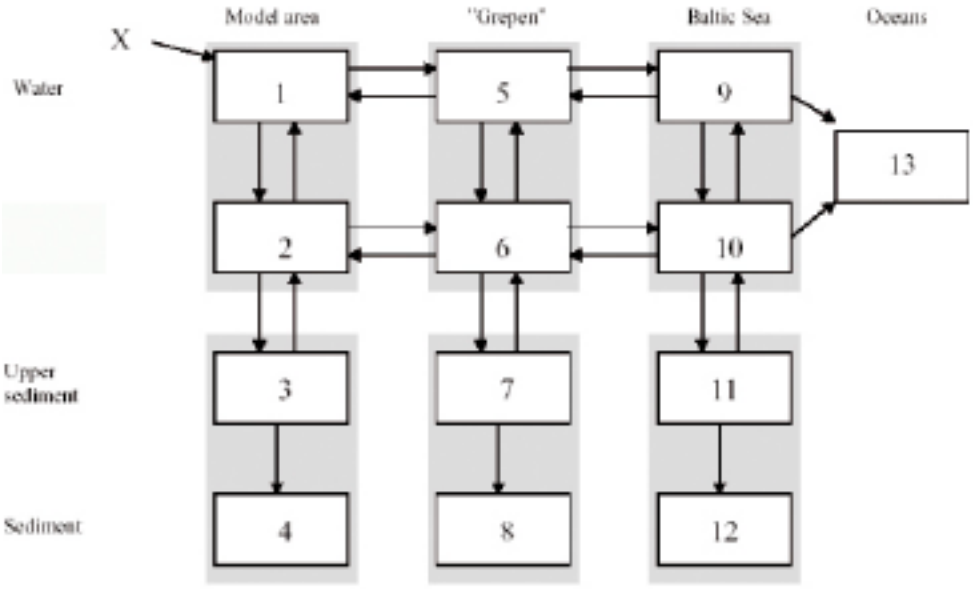

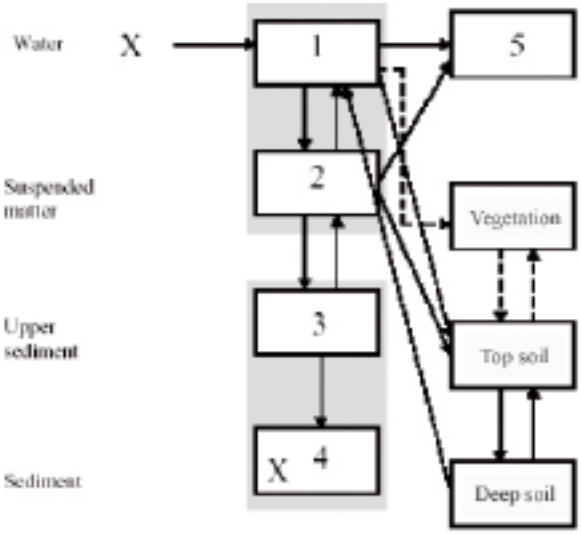

Turnover of water and suspended matter

The rate constant describing the transfer of water, and thereby radionuclides in solution, between the different water components of the system is obtained from the water retention time within each part. The radionuclides in the water or on suspended matter are assumed to move at the same rate as the carrying medium. The outflow of water (from the Model Area to Grepen, from Grepen to the Baltic Sea and from the Baltic Sea to the Oceans) is described as the fraction of water leaving a given region per unit of time, which is equivalent to the inverse of the water retention time, TC (y^{-1}):

$$TC = 1/RETTIME_x$$

where

$RETTIME_x$ is the water retention time in the part from which water is transferred (Model Area, Grepen or Baltic Sea) (y)

The water inflow, $\lambda_{turnover}$ (y^{-1}), to the Model Area from Grepen is related to the volume ratio of the two areas as follows:

$$\lambda_{turnover} = \frac{A_M . D_M}{A_G . D_G} . \frac{1}{RETTIME_M}$$

where

A_M = Area of Model Area (m^2)

A_G = Area of Grepen (m^2)

D_M = Mean water depth in the Model Area (m)

D_G = Mean water depth in Grepen (m)

$RETTIME_M$ = Water retention time in the Model Area (y)

The water inflow to Grepen from the Baltic Sea is obtained from the same expression but the values for the Model Area are replaced by those for Grepen and the values for Grepen by those for the Baltic.

The suspended matter follows the water and therefore the same transfer coefficients are used. Particulate matter as a whole may have a longer turnover time because of settling and resuspension, which is accounted for by the exchange of material between suspended and surficial sediments.

Interaction of radionuclides between water and particles

Radionuclides are assumed to be released in soluble form into the water in the Model Area. The sorption-desorption transfer of radionuclides between the water and the suspended matter (in the Model Area as well as in Grepen and the Baltic Sea) is assumed to reach an equilibrium, but not instantaneously. Therefore, the transfer from water to suspended matter is described by a rate of sorption that is proportional to the particle concentration and the nuclide sorption affinity, described by a distribution coefficient. The process is time-dependent and therefore a parameter for the half-time to reach sorption equilibrium (T_k) has been used:

$$\lambda_{sorption} = \frac{\ln 2}{T_k} Susp.K_d \ (y^{-1})$$

and a simple rate of desorption from suspended matter to water:

$$\lambda_{desorption} = \frac{\ln 2}{T_k} \text{ (y}^{-1}\text{)}$$

where

T_k = Half-time to reach sorption equilibrium (y)

Susp = Suspended matter in media (kg m^{-3})

K_d = Distribution coefficient, ratio of element concentrations in the solid and the dissolved phase (m^3 kg^{-1})

Sedimentation and resuspension

A fraction of the suspended matter is assumed to reach the upper sediment through sedimentation (gross sedimentation). This transfer is described by the ratio of the mean settling velocity and the mean water depth:

$$\lambda_{sedimentation} = \frac{V_{sink}}{D} \text{ (y}^{-1}\text{)}$$

where

V_{sink} is the particle settling velocity (m y^{-1})

D is the mean water depth in media (m)

A fraction of the deposited material is assumed to be transferred back to the water phase by resuspension and the remaining part is assumed to accumulate on the bottom sediments. The sediment is, therefore, described by two compartments, one for the upper, biologically active, sediment and one for the deeper layers. The turnover of radionuclides in the upper sediment is described by using the maximum growth rate of this sediment layer and the depth of mixing by bioturbation. The fluxes are partitioned according to the fraction of accumulation bottoms obtained from wave-theory based models of the area. Thus, the transfer from the upper sediment back to the suspended matter (resuspension) is described by scaling the turnover of this sediment layer to the area exposed to strong erosion forces:

$$\lambda_{resuspension} = \frac{G_s}{D_s}(1 - Frac) \text{ (y}^{-1}\text{)}$$

and the transfer from the upper sediment to deeper sediment layers (burial) is calculated using an equivalent expression scaled to the sheltered accumulation area:

$$\lambda_{burial} = \frac{G_s}{D_s} Frac \text{ (y}^{-1}\text{)}$$

where

G_S = Sediment growth rate (m y^{-1})

D_S = Depth of upper sediment (m)

FRAC = Fraction of accumulation bottoms in media

The irrigation sub-model which is used in the Lake Model is shown below.

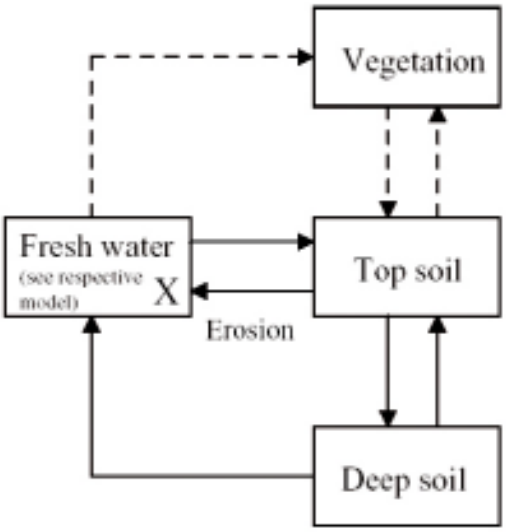

The rate constant describing the transfer of radionuclides from surface water to soil due to irrigation is obtained from the following expression:

$$\lambda_{irrigation} = \frac{V_{IRR}.Nr_{IRR}}{V_W} A \ (y^{-1})$$

where

V_{IRR} = Water amount used at each irrigation event ($m^3\ m^{-2}\ y^{-1}$)

Nr_{IRR} = Number of irrigation events per year (–)

V_W = Volume of water from which irrigation water is taken (m^3)

A = Area of irrigated soil (m^2)

It is assumed that the suspended matter follows the water and therefore the same transfer coefficient is used for the transfer of suspended matter to soil in the lake model.

After deposition on soils, nuclides migrate with varying rates due to their physical/chemical properties and soil conditions. In addition, processes like bioturbation and erosion cause a redistribution of the radionuclides. The leakage or migration rate of nuclides from the top soil to the deep soil compartment is described by a transfer coefficient considering vertical transport due to percolation of water and transport of soil by (earth)worms:

$$\lambda_{soil\_turnover} = \frac{Runoff}{\varepsilon_t.D_{ts}}.R_f + \frac{BioT}{D_{ts}(1-\varepsilon_t)\rho_p} \ (y^{-1})$$

where

$$Rf = \frac{1}{\left[1 + K_d.\rho_p.(1-\varepsilon_t)/\varepsilon_t\right]}$$

and

Runoff is the soil runoff ($m^3\ m^{-2}\ y^{-1}$)

ε_t = Porosity of soil in the top soil ($m^3\ m^{-3}$)

D_{ts} = Depth of top soil (m)

$BioT$ = Transport due to bioturbation ($kg\ m^{-2} y^{-1}$)

ρ_p = Density of soil particles ($kg\ m^{-3}$)

K_d = Distribution factor, concentration of the element on solids relative to dissolved ($m^3\ kg^{-1}$)

The rates for bio-transport are obtained from an annual transport of soil, divided by soil masses; that is masses for top and deep soil, respectively as it is also considered as a reverse transport from deep soil to top soil:

$$\lambda_{soil\_transport} = \frac{BioT}{D_{ds}(1-\varepsilon_d)\rho_p} \ (y^{-1})$$

where

D_{ds} = Depth of deep soil layer (m), see below

ε_d = Porosity of soil in the deep soil ($m^3\ m^{-3}$)

$D_{ds} = 1 - D_{ts}$

where

D_{ts} = Depth of top soil (m)

Radionuclides in deep soil are assumed to leak back to the aquifer from which the irrigation water is taken (well or lake). This is described by the same expression as above, but without bioturbation and with depths and porosities according to deep soil.

Agricultural land model

The compartments used to represent the agricultural land model of the reasonable biosphere development is shown below. Arrows mark the direction of transfers and crosses mark the potential sources of radionuclides.

Transfers between solid and soluble fractions

The distribution of elements between dissolved and solid fractions in the saturated zone is described by one parameter (here called K_d) although it involves chemical, biological and physical processes. These are time-dependent processes and therefore a parameter for the half-time to reach sorption equilibrium is used. The transfer coefficients from dissolved to

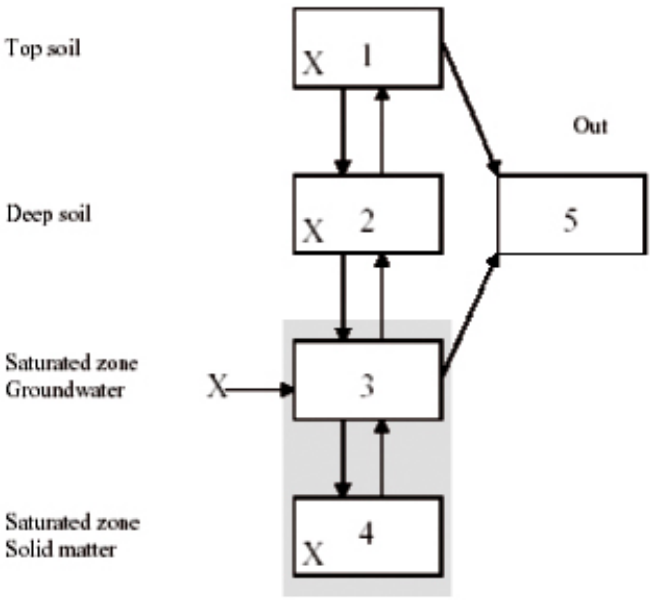

solid matter is scaled to the relation between solid matter and pores in soil and is given by the expression:

$$\lambda_{sorption} = \frac{K_d . \ln 2}{T_k} . \frac{(1 - \varepsilon_{sa}) . \rho_{sa}}{\varepsilon_{sa}} \text{ (y}^{-1}\text{)}$$

and from particulate to dissolved fraction by:

$$\lambda_{desorption} = \frac{\ln 2}{T_k} \text{ (y}^{-1}\text{)}$$

where

K_d = Distribution coefficient, concentration of the element on solids relative to dissolved ($m^3\ kg^{-1}$)

T_k = Half-time to reach sorption equilibrium (y)

ε_{sa} = Porosity in saturated zone ($m^3\ m^{-3}$)

D_{sa} = Depth of saturated zone (m)

A = Area of agricultural land (m^2)

ρ_s = Density of soil particles ($kg\ m^{-3}$)

Transfer from saturated zone

The transfer coefficient describing the horizontal flow of dissolved radionuclides in ground-water out from the saturated zone, λ_{gw_loss} (y^{-1}), is based on water balance and becomes:

$$\lambda_{gw\_loss} = \frac{Runoff}{\varepsilon_{sa} . D_{sa}}$$

Runoff ($m^3\ m^{-2}\ y^{-1}$)

ε_{sa} = Porosity in saturated zone ($m^3\ m^{-3}$)

D_{sa} = Depth of saturated zone (m)

Transfers between saturated zone and deep soil

The direction of water flow between saturated and unsaturated zones varies with time. Processes as diffusion and capillary rise cause an upward flow from the saturated to the unsaturated zone, during dry periods, while precipitation generates a flow in the opposite direction. The transfer coefficient from saturated to deep unsaturated soil considering the fraction of nuclides in soluble form in the soil pores becomes:

$$\lambda_{sat\_deep} = \frac{F_{sa,ds}}{\varepsilon_{sa} . D_{sa}} \text{ (y}^{-1}\text{)}$$

where

$F_{sa,ds}$ = Upward flow ($m^3\ m^{-2}\ y^{-1}$)

ε_{sa} = Porosity in saturated zone ($m^3\ m^{-3}$)

D_{sa} = Depth of saturated zone (m)

The downward transfer of radionuclides from the deep soil to the saturated zone is expressed by:

$$\lambda_{deep\_sat} = \frac{R + F_{ds,sa}}{\varepsilon_{sa} . D_{sa}} R_f \text{ (y}^{-1}\text{)}$$

where

$F_{ds,sa}$ = Downward flow ($m^3\ m^{-2}\ y^{-1}$)

R = Runoff ($m^3\ m^{-2}\ y^{-1}$)

ε_{ds} = Porosity in deep soil ($m^3\ m^{-3}$)

D_{ds} = Depth of deep soil (m)

R_f = Retention, (see below) (–)

D_{ds} = 1–D_{ts} = 0.75 m

where

D_{ts} = Depth of top soil (m)

$$Rf = \frac{1}{1 + K_d . \rho_p . \frac{1 - \varepsilon_i}{\varepsilon_i}}$$

where

K_d = Distribution coefficient, concentration of the element on solids relative to dissolved ($m^3\ kg^{-1}$)

ρ_s = Density of soil particles ($kg\ m^{-3}$)

ε_i = Porosity of the matter in compartment *i* (here deep soil) ($m^3\ m^{-3}$)

Transfers between deep soil and top soil

The transfer coefficient from deep soil to top soil, considering diffusion and capillary rise and bioturbation, becomes:

$$\lambda_{deep\_top} = \frac{F_{ds,ts}}{\varepsilon_{ds} . D_{ds}} R_f + \frac{BioT}{(1 - \varepsilon_{ds}) . \rho_p . D_{ds}} \ (y^{-1})$$

where

$F_{ds,ts}$ = Upward flow ($m^{-3}\ m^{-2}\ y^{-1}$)

ε_{ds} = Porosity of deep soil ($m^3\ m^{-3}$)

D_{ds} = Depth of deep soil (m), see above

R_f = Retention, see above (–)

$BioT$ = Bioturbation, (transport of soil by earthworms) ($kg\ m^{-2}\ y^{-1}$)

ρ_p = Density of soil particles ($kg\ m^{-3}$)

The transfer coefficient from top soil to deep soil is described by the following equation:

$$\lambda_{top\_deep} = \frac{Runoff + F_{ds,ts}}{\varepsilon_{ds} . D_{ds}} R_f + \frac{BioT}{(1 - \varepsilon_{ds}) . \rho_p . D_{ds}} \ (y^{-1})$$

where

$F_{ds,sa}$ = Downward flow ($m^3\ m^{-2}\ y^{-1}$)

Runoff ($m^3\ m^{-2}\ y^{-1}$)

ε_{ds} = Porosity in deep soil ($m^3\ m^{-3}$)

D_{ds} = Depth of deep soil (m)

R_f = Retention, see above (–)

$BioT$ = Bioturbation, (transport of soil by earthworms) ($kg\ m^{-2}\ y^{-1}$)

ρ_p = Density of soil particles ($kg\ m^{-3}$)

Soil Erosion

There is a loss of elements due to erosion or removal of soil during agricultural practices. Geographical conditions, soil types and meteorological parameters such as wind and rain influence the magnitude of erosion. The size and density of the soil particles are also of importance. Land covered with vegetation are less exposed to erosion since the roots bind the material and the plants may cover parts of the surfaces.

The loss of radionuclides due to erosion is estimated as:

$$\lambda_{erosion} = \frac{R_{rate}}{D_{ts}(1-\varepsilon_{ts}).\rho_p} \ (y^{-1})$$

where

R_{rate} = Removal of soil ($kg/m^{-2}\cdot y^{-1}$)

D_{ts} = Depth of top soil (m)

ε_{ts} = Porosity of soil in the top soil (plough layer) ($m^3\,m^{-3}$)

ρ_s = Density of soil particles ($kg\ m^{-3}$)

Ingestion

Doses via ingestion (D_{ing} (Sv y^{-1})) are calculated using the concentration in the food item, the consumption rate and element specific dose coefficients for ingestion:

$$D_{ing} = HC_i \,.\, U_i \,.\, DC_{ing}$$

where

HC_i = Consumption rate for pathway *i* (kg or litre per y)

U_i = Concentration in foodstuff *i* (Bq per kg or litre) (expressions given below)

DC_{ing} = Dose coefficients for ingestion (Sv/Bq)

Human consumption of agricultural products is represented by five groups of food items, i.e. milk, meat, vegetables, root crops and cereals. Fish represent food from aquatic systems. Consumption of algae and fresh water crustacean is also possible to consider even though this is not adequate for the studied area. For each of these food items the concentration of radionuclides is calculated as follows.

Milk and meat

Transfer of radionuclides to milk and meat is based on cattle's intake of contaminated fodder, soil and water. The concentration in milk (U_{milk}) and meat (U_{meat}) is obtained from:

$U_{milk} = In * F_{milk}$

$U_{meat} = In * F_{meat}$

where

In = Daily intake of nuclides (Bq/day) (expression given below)

F = Element specific transfer coefficient for milk and meat, respectively (day/litre, day/kg)

Cattle are assumed to eat three different kinds of fodder; concentrated fodder (here represented by cereals), grass (fresh when grazing on the pasturage and as hay, harvested from the pasturage, the rest of the year, here combined and simply called pasturage) and plants growing on the shore of a lake or watercourse (hereafter called water plants). Additionally, some inadvertent consumption of soil when grazing is assumed. Radionuclides may also be taken in through

consumption of contaminated water. Pasturage and cereals are contaminated through root uptake and retention of radionuclides on vegetation surfaces whereas water plants are contaminated through their uptake and transpiration of contaminated water. Different uptake pathways are considered in the different models. The cattle's daily intake of radionuclides (In) is calculated as a sum of products:

$In = MCx \cdot UCx \ldots + MCy \cdot UCy$

where

MCx/y = Daily consumption of food item, water and soil, respectively (kg or litre per day)

UCx/y = Concentration of radionuclides in food item, water and soil, respectively (Bq per kg or litre) (expressions given below)

The concentrations of radionuclides in water and soil are obtained from the dispersion models. The concentration of radionuclides in cereals that are used as concentrated fodder to cattle is assumed to have the same concentration as the cereals for human consumption, which is obtained according to the expression given below. In the agricultural land and mire models it is assumed that pasturage is grown on contaminated areas and radionuclides are transferred to the grass via root uptake. The concentration in pasturage (UCp) is calculated as:

$UCp = Ci \cdot RUFp$

where

Ci = Concentration of radionuclides in soil or peat (Bq/kg), from the dispersion model

RUFp = Root uptake factor for pasturage ((Bq/kg dw)/(Bq/kg dw))

Considered pathways (X) for intake of radionuclides in cattle in different biosphere models.

Model	Water	Pasturage	Cereals	Water plants	Soil
Coastal	X			X	
Lake	X			X	
Agricultural land		X	X		X

The consumption of water plants from a contaminated recipient (UC_{wp}) does also contribute to the contamination of milk and meat. As the cattle is assumed to graze only part of the year the uptake of radionuclides via this pathway depends on, among other things, the number of days that they spend on the shore line:

$$UC_{wp} = \frac{CG}{365} \cdot \frac{C_w . TR . GD . 10^{-6} . 24}{Y_{wp}}$$

where

CG = Cattle grazing period on shores (days y^{-1})

C_w = Concentration of radionuclides in water (Bq m^{-3}) (radionuclides in suspended matter included), from the dispersion model

TR = Transpiration of water plants (g $m^{-2} \cdot h^{-1}$)

GD = Average time for water plant transpiration before animal's consumption (days y^{-1})

Ywp = Annual production of water plants (kg $m^{-2} \cdot y^{-1}$)

10^{-6} = m^3/g

24 = h/day

365 = days/y

Crops

Crops are represented by cereals, root crops and green vegetables. In the agricultural land and mire models it is assumed that these crops are grown on contaminated soil or peat and radionuclides are transferred to the vegetation via root uptake. The concentration in the crops (U_i) is calculated as:

$$U_i = C_i * RUF_i$$

where

C_i = Concentration of radionuclides in soil or peat (Bq/kg dw), from dispersion model

RUF_i = Root uptake factor for crop i (see below)((Bq/kg dw)/(Bq/kg ww))

i = c for cereals

i = r for root crops

i = v for vegetables

In other models, i.e. the lake and well models, contamination may occur through irrigation with contaminated water. In the SAFE study irrigation of a garden plot where root crops and vegetables are grown are simulated. Root crops are then contaminated via root uptake as well as retention of radionuclides on vegetation surfaces and thereafter translocation to edible parts. As more radionuclides are supplied at each irrigation occasion the radionuclide concentration depends on the number of irrigation events. Root crops are harvested after the irrigation period and the radionuclides supplied during the season are added up. The expression for resulting concentration in root crop products (U_i) is:

$$U_i = C_s.RUF_R + \sum_{0}^{Nr_{IRR}} I.TL.C_w$$

where

C_s = Concentration of radionuclides in soil (Bq/kg dw) from the dispersion model

RUF_R = Root uptake factors for root crops (soil to plant transfer factors) ((Bq/kg ww)/ Bq/kg dw))

Nr_{IRR} = Number of irrigation occasions (y^{-1})

I = Remaining water on the vegetation after each irrigation occasion (m)

TL = Translocation from plant surface to edible parts of plant, ((Bq/kg ww)/(Bq/m^2))

C_w = Concentration of radionuclides in irrigation water (Bq/m^3), from the dispersion model

Vegetables are also contaminated from root uptake and surface contamination due to retention of contaminated irrigation water. The harvest of green vegetables is assumed to occur during the whole growing period (180–200 days per year). Therefore the mean concentration of surface contamination during the period is calculated and used in the dose calculations. The expression for the resulting content of radionuclides in vegetables (U_v) is:

$$U_v = C_s.RUF_v + \frac{C_w}{Y_v}.\frac{I}{t_{tot}}.\sum_{Nr_{IRR}}\int_{0}^{t_n} e^{-\tau.t_n}\,dt$$

where

C_s = Concentration of radionuclides in soil (Bq/kg dw), from the dispersion model

RUF_v = Root uptake factor for vegetables (soil to plant transfer factor) ((Bq/kg ww)/Bq/kg dw))

C_w = Concentration of radionuclides in irrigation water (Bq m^{-3}), from dispersion model

Y_v = Yield of vegetables (kg $m^{-2} \cdot y^{-1}$)

I = Remaining water on the vegetation after each irrigation occasion (m)

t_{tot} = Irrigation period, fraction of year (y^{-1})

Nr_{IRR} = Number of irrigation occasions per year (y^{-1})

t_n = Time between last irrigation occasion and harvest (days)

τ = ln2/T½w where $T_{½w}$ = weathering half-life (day)

Food from aquatic systems

Food from aquatic systems is represented by fish (algae and crustaceans can also be used). Concentrations of radionuclides in those organisms are obtained by use of bioaccumulation factors for edible parts of the species relative to the total concentration in the water (i.e. the amounts of radionuclides in water and on suspended matter). In order to use available databases which often are based on empirical concentration ratios, the water includes here the radionuclide fraction associated with suspended matter (which usually is a minor fraction). The bioaccumulation factors are valid for steady-state conditions and implicitly consider all uptake paths from the ambient environment. The expression for estimating the content of radionuclides in fish, crustaceans and algae (U_i) is:

$$U_i = BAF_i * C_w$$

where

BAF_i = Element specific bioaccumulation factor from water to edible parts of species i ((Bq/kg ww)/(Bq/l))

i = f for fish

i = c for crustacean

i = a for algae

C_w = Concentration of radionuclides dissolved and suspended in the ambient water (Bq/l), from the dispersion model

Inhalation

Doses via inhalation (Dinh) are calculated using the concentration of radionuclides in the air, the inhalation rate, the exposure time and element specific dose coefficients for inhalation:

$$D_{inh} = C_a \cdot IH \cdot H_i \cdot DC_{inh}$$

where

C_a = Concentration of radionuclides in air (Bq m^{-3}), see expressions below

IH = Inhalation rate (m^3 h^{-1})

H_i = Exposure time (h y^{-1})

DC_{inh} = Dose coefficients for inhalation (Sv/Bq)

Radionuclides in air emanate from three sources; dust in air from soil or peat resuspension and flue gases produced when peat is used as fuel in a household. Particles in air are assumed to have the same radionuclide concentration as soil. The concentration of radionuclides in air due to contaminated soil resuspension ($C_{a,s}$), peat resuspension ($C_{a,p}$) and contaminated peat combustion ($C_{a,f}$) are expressed by:

$C_{a,s} = Cs * S$

$C_{a,p} = Cp * S$

$C_{a,f} = Cp * FC * RC * FE$

where

C_s = Concentration of radionuclides in soil (Bq/kg dw), from the dispersion model

S = Dust content in air (kg m^{-3})

C_p = Concentration of radionuclides in peat (Bq/kg dw), from the dispersion model

FC = Fuel load (kg dw/s)

RC = Relative concentration as an annual mean value (s m^{-3})

FE = Fraction of nuclides which leaves the combustion apparatus via exhaust gases (efficiency of the filter system)

External exposure

Doses via external exposure from soil or mire (D_{ext} (Sv y^{-1})) are calculated using the concentration of radionuclides in soil/peat, the soil/peat density, the exposure time and element specific dose coefficients for external exposure:

$D_{ext} = C_i * \rho_i * H_i * DC_{ext}$

where

C_i = Concentration of radionuclides in soil or peat (Bq/kg dw), from the dispersion model

ρ_i = Soil or peat density (kg m^{-3})

H_i = Exposure time (h y^{-1})

DC_{ext} = External dose coefficients ((Sv/h)/(Bq/m^3))

The data reported in /Karlsson et al. 2001/ was used in the calculations with the following exceptions noted in /Jones et al. 2004/.

- Number of irrigation events, N_irr (–), is uniform 3, 7.
- Weathering half-life, $T_{1/2w}$, (day) is logtriangular 10, 15, 20.
- Dust concentration in air, S, (kg m^{-3}) is logtriangular 3E–5, 1E–4, 3E–4.

Appendix B

Details of baltic modeling study

An analysis of representation of the Baltic Sea as a single model compartment was performed by comparing the SKB model with the existing model of the Baltic developed in the EC-funded MARINA II project by a multinational team /Kershaw 1999/. The objectives of the comparison were:

1. To investigate the effect on concentrations in the water and sediment of the Model Area and Grepen by changing the Baltic Sea model, and hence investigate the potential effect of this on the highest individual doses.
2. To investigate the extent to which a more detailed model predicts variations in concentrations between different areas of the Baltic, and hence gain an indication of the potential distribution of doses.

The MARINA II model (see Figure A2-1) splits the Baltic Sea into:

- Two compartments representing the northern and southern parts of the Gulf of Bothnia (called Bothnian Bay and Bothnian Sea, respectively).
- The Gulf of Finland and the Gulf of Riga.
- Four compartments representing the Baltic proper (split into eastern and western areas, and also vertically into surface and deep waters).
- Five compartments representing the Belt Sea and Kattegat (both divided into surface and deep waters) and Skagerrak.

The MARINA II model beyond Skagerrak was simplified by combining the three adjacent compartments (57, 58 and 59) into a single North Sea compartment, and all remaining compartments into a single World Oceans compartment.

Forsmark is slightly to the north of the boundary between two compartments in the model – the Bothnian Sea to the north and Baltic Sea West to the south. The Grepen was therefore assumed to exchange initially with the Bothnian Sea compartment. The model indicates water circulation in the northern Baltic to be generally anti-clockwise, i.e. mainly south-to-north on the Baltic States/Finnish side and north-to-south on the Swedish side. Therefore some activity would remain in the Gulf of Bothnia, but the prevailing flow would initially be southwards into the Baltic Sea West. Residence times in the Gulf of Bothnia are several years, with flow then going south.

Volumetric flows between Baltic Sea compartments were taken from the MARINA II report (and summed as appropriate for the North Sea and World Oceans compartments), and are summarised in Table A2-1. It was assumed that suspended sediment moves with the water column, and therefore the same fractional exchange rate was applied to the suspended sediment sub-compartment as well as the water sub-compartment. The fractional exchange rates between Baltic Sea compartments were calculated as the volumetric flow divided by the volume of water in the compartment. The exchange rates involving the Model Area and Grepen were derived from the equations and residence times specified by /Karlsson et al. 2001/ and reproduced below.

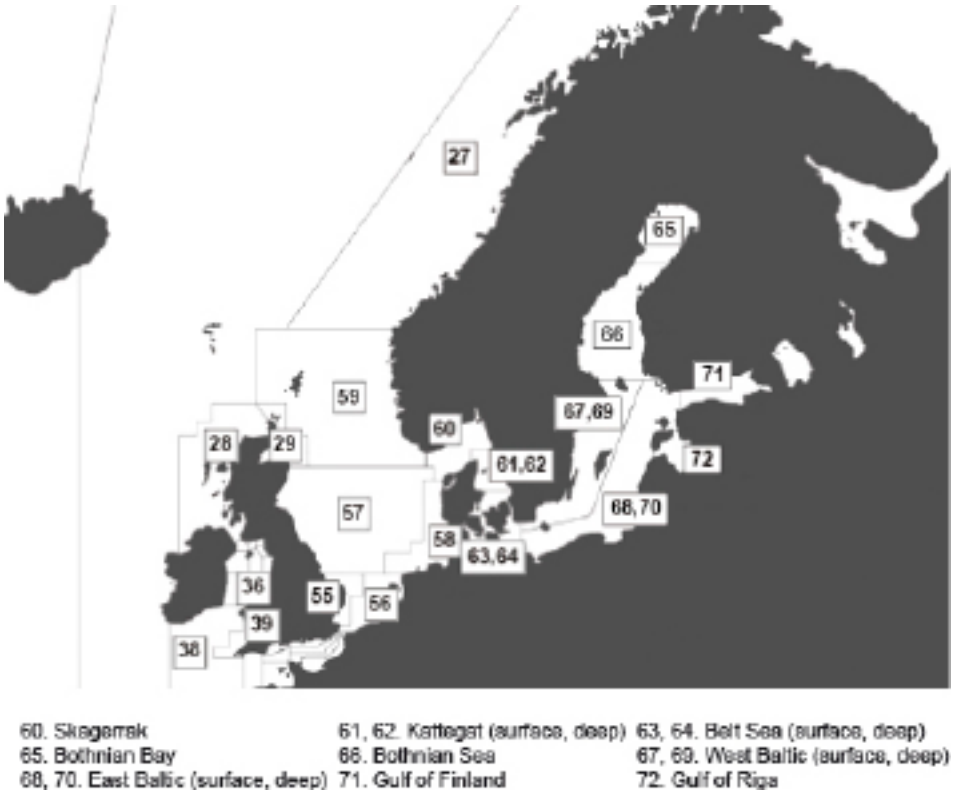

Figure A2-1. *Discretisation of Baltic Sea in MARINA II.*

Table A2-1. Exchanges between sea compartments.

Compartment A	Compartment B	From A to B Water flow, (m^3 y^{-1})	Transfer rate (y^{-1})	From B to A Water flow, (m^3 y^{-1})	Transfer rate (y^{-1})
Skagerrak	Kattegat (surface)	0	0	2.00E+12	6.25
	Kattegat (deep)	1.50E+12	0.221	0	0
	North Sea	3.25E+13	4.79	3.20E+13	
Kattegat (surface)	Kattegat (deep)	1.00E+11	0.313	9.30E+11	4.65
	Belt Sea (surface)	0	0	1.20E+12	8.00
Kattegat (deep)	Belt Sea (deep)	7.20E+11	3.60	0	0
Belt Sea (surface)	Belt Sea (deep)	7.00E+11	4.67	9.30E+11	6.64
	West Baltic (deep)	0	0	2.20E+11	0.286
Belt Sea (deep)	East Baltic (surface)	2.70E+11	1.93	0	0
	East Baltic (deep)	2.20E+11	1.57	0	0
Bothnian Bay	Bothnian Sea	2.75E+11	0.186	1.75E+11	0.0358
Bothnian Sea	West Baltic (surface)	7.15E+11	0.146	0	0
	East Baltic (surface)	0	0	5.25E+11	0.0753
West Baltic (surface)	West Baltic (deep)	1.07E+11	0.0282	1.07E+11	0.139
	East Baltic (surface)	6.97E+12	1.84	6.97E+12	1.00
West Baltic (deep)	East Baltic (deep)	2.20E+11	0.286	4.40E+11	0.288
East Baltic (surface)	East Baltic (deep)	2.08E+11	0.0298	2.08E+11	0.136
	Gulf of Finland	5.95E+11	0.0854	7.20E+11	0.655
	Gulf of Riga	3.12E+11	0.0448	3.44E+11	0.849
North Sea	World Oceans	6.28E+13	1.43	6.20E+13	3.1E–05
Baltic Sea	World Oceans	3.25E+13	1.54	3.20E+13	1.52

The transfer rate λ_{out}, from the Model Area to Grepen is given by:

$$\lambda_{out} = \frac{1}{TRES_{MA}} \text{ (y}^{-1}\text{)}$$

where $TRES_{MA}$ is the residence time in the Model Area (18.5 hours).

The transfer rate λ_{in}, from the Grepen to the Model Area is given by:

$$\lambda_{in} = \frac{V_{Grepen}}{V_{MA}} \times \frac{1}{TRES_{MA}} \text{ (y}^{-1}\text{)}$$

where V_{Grepen} and V_{MA} are the water volumes in the Grepen and the Model Area respectively.

The corresponding transfers between the Grepen and the local sea compartment (Bothnian Sea in the MARINA II model, or Baltic Sea in the Project SAFE model) are calculated similarly:

$$\lambda_{out} = \frac{1}{TRES_{Grepen}} \text{ (y}^{-1}\text{)}$$

where $TRES_{Grepen}$ is the residence time in the Grepen (12.1 days); and

$$\lambda_{in} = \frac{V_{Grepen}}{V_{local}} \times \frac{1}{TRES_{Grepen}} \text{ (y}^{-1}\text{).}$$

The MARINA II model uses a different approach to modelling water-sediment interactions from the Project SAFE model. The approach taken in Project SAFE was for each sea compartment to comprise four sub-compartments, representing respectively: the water column; the sediment suspended in the water column; and two layers of bed sediments (upper and deep). In the MARINA II model there are (except for surface water compartments) four sub-compartments, but each water sub-compartment includes sediment suspended in the water column (and transfers are modified accordingly) and the bed sediment is divided into three layers: upper, middle and deep. The depth of the upper sediment sub-compartment also differs: 0.02 m in Project SAFE, and 0.10 m in the MARINA II model. The two structures are illustrated in Figure A2-2.

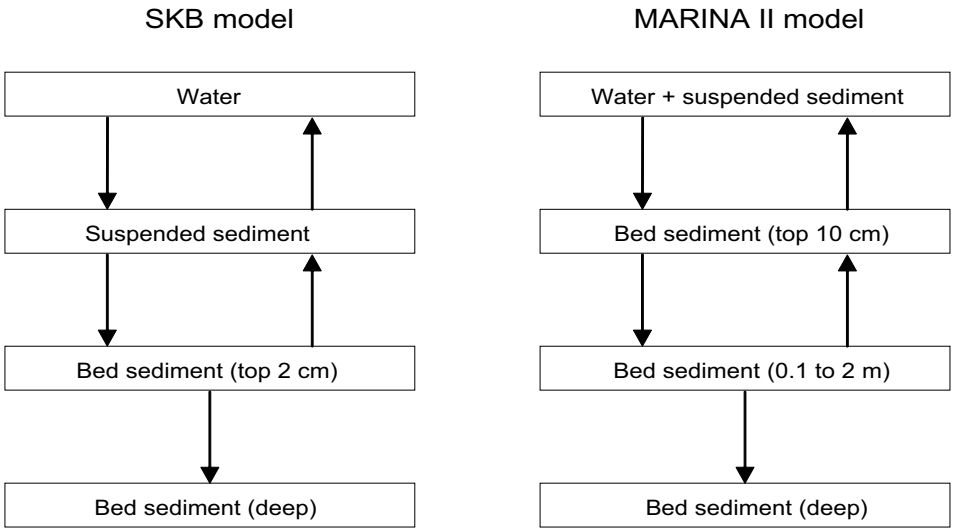

Figure A2-2. *Structure of sea compartments in Project SAFE and MARINA II models.*

In order to reduce the number of differences between the models at this stage, the vertical structure of the model used in Project SAFE (i.e. water compartment, suspended sediment, upper sediment and deep sediment) was combined with the areal structure of the Baltic from the MARINA II model (as shown in Figure A2-1). The vertical transfers between sub-compartments were modelled as defined for the SKB model /Karlsson et al. 2001/. For surface water compartments (compartments 61, 63, 67 and 68 in Figure A2-1) only the water and suspended sediment sub-compartments were used. Characteristics of the sea compartments used are summarised in Table A2-2.

The transfers between sub-compartments (see Figure A2-3) were based on those in the SKB model, as follows.

λ_{sorb}, the transfer of dissolved radionuclides from the water to sediment suspended in the water column, is given by:

$$\lambda_{sorb} = \frac{\ln 2 \times SSL \times K_d}{T_k} \text{ (y}^{-1}\text{)}$$

where SSL is the suspended sediment load in the water column (t m^{-3}), K_d is the (element-dependent) equilibrium distribution coefficient (Bq t^{-1} in sediment per Bq m^{-3} in water – see Table A2-2), and T_k is the half-time to reach equilibrium sorption, taken to be 10^{-3} (y).

Table A2-2. Characteristics of sea compartments.

No. in Figure A2-1	Name	Volume (m^3)	Depth (m)	Susp. sediment (t m^{-3})	Sed growth rate (m y^{-1})
	Model Area	1.06E+08	9.5	1.0E–06	0.01
	Grepen	5.11E+09	11.2	1.0E–06	0.01
60	Skagerrak	6.78E+12	210	1.0E–06	0.002
61	Kattegat (surface)	3.20E+11	20	1.0E–06	0.002
62	Kattegat (deep)	2.00E+11	100	1.0E–06	0.002
63	Belt Sea (surface)	1.50E+11	14	1.0E–06	0.002
64	Belt Sea (deep)	1.40E+11	30	1.0E–06	0.002
65	Bothnian Bay	1.48E+12	41	1.0E–06	0.002
66	Bothnian Sea	4.89E+12	62	1.0E–06	0.002
67	West Baltic (surface)	3.79E+12	49	1.0E–06	0.002
69	West Baltic (deep)	7.70E+11	110	1.0E–06	0.002
68	East Baltic (surface)	6.97E+12	53	1.0E–06	0.002
70	East Baltic (deep)	1.53E+12	110	1.0E–06	0.002
71	Gulf of Finland	1.10E+12	37	1.0E–06	0.002
72	Gulf of Riga	4.05E+11	23	1.0E–06	0.002
57–59	North Sea	7.00E+13	129	6.0E–06	0.002
1–56	World Oceans	2.00E+18	4,000	1.0E–08	0.002
	Baltic Sea	2.11E+13	56	1.0E–06	0.002

The mineral density of sediments was taken to be 2.6 t m^{-3} for all compartments. The porosity of bed sediments was 0.75 for all compartments except World Oceans, for which it was 0.3.

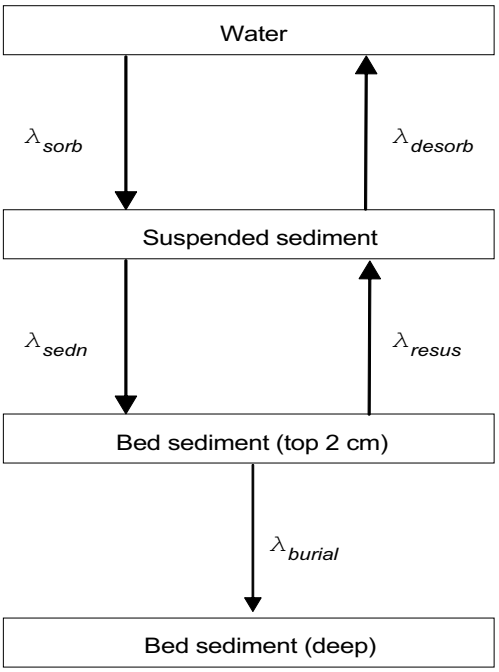

Figure A2-3. *Structure of sea compartments for this study.*

λ_{desorb}, the dissolution of radionuclides from the suspended sediment into the water, is given by:

$$\lambda_{desorb} = \frac{\ln 2}{T_k} \text{ (y}^{-1}\text{)}$$

λ_{sedn}, the transfer of suspended sediment from the water column to the upper bed sediment, is given by:

$$\lambda_{sedn} = \frac{v_{settle}}{d_{water}} \text{ (y}^{-1}\text{)}$$

where v_{settle} is the settling velocity for fine sediment particles from the water column, taken to be 365 m y^{-1}, and d_{water} is the depth of the water column.

λ_{resus}, the resuspension of sediment from the upper bed sediments into the water column, is given by:

$$\lambda_{resus} = \frac{SedGrowth \times (1 - f_{ds})}{d_{ts}} \text{ (y}^{-1}\text{)}$$

where *SedGrowth* is the rate at which sediment accumulates on the bed (m y^{-1}), f_{ds} is the fraction that is resuspended (taken to be 0.22 in the Model Area, 0.3 everywhere else), and d_{ts} is the depth of the upper sediment sub-compartment (0.02 m).

λ_{burial}, the transfer of bed sediment from the upper 0.02 m to the deeper sediment, due to burial by fresh sediment deposited on top, is given by:

$$\lambda_{burial} = \frac{SedGrowth}{d_{ts}} \text{ (y}^{-1}\text{)}$$

The Project SAFE model was implemented as for the Project SAFE, except that the flow between the Baltic Sea box and World Oceans was made two-way, as in the MARINA II model, rather than a simple outward flow to a sink as in the Project SAFE.

Since the aim of this initial study was simply to compare the predictions of the two models of the Baltic, runs were performed for a simple source term of 100 MBq per year continuing for 10,000 years, i.e. a total release of 1 TBq. For the inter-model comparison, the release was taken to be into the water of the Model Area.

Concentrations in the different compartments were calculated on the basis of the total activity in the water column, i.e. the activity in the water sub-compartment was added to that in the suspended sediment sub-compartment, and the total divided by the volume of water in the compartment. For example, for the compartmental configuration shown in Figure A2-3 this means that the amounts of a radionuclide (Bq) in the water and suspended sediment compartment are added together and divided by the volume of the water compartment (m^3) to give the radionuclide specific concentration (Bq m^{-3}).

The concentrations in the Model Area water are almost identical for the two models, as shown in the following pair of graphs.

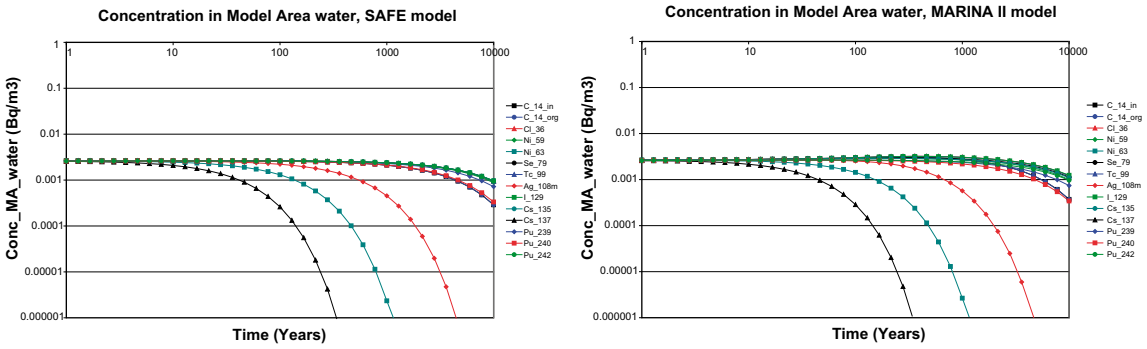

Figure A2-4a. *The concentrations in Model Area top sediments are similarly almost indistinguishable.*

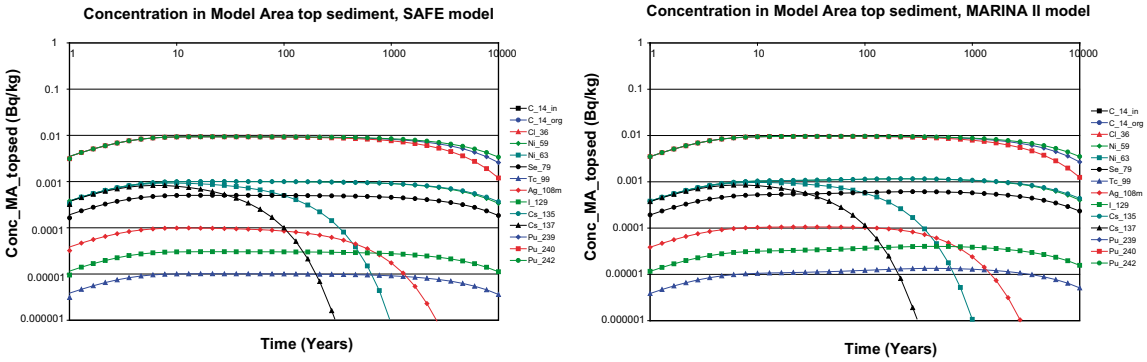

Figure A2-4b. *In the Grepen, the water concentrations are again similar, but the MARINA II model begins to show slightly higher concentrations than the SKB model from several hundred years onwards. At most, the difference between the models is around a factor of two or three.*

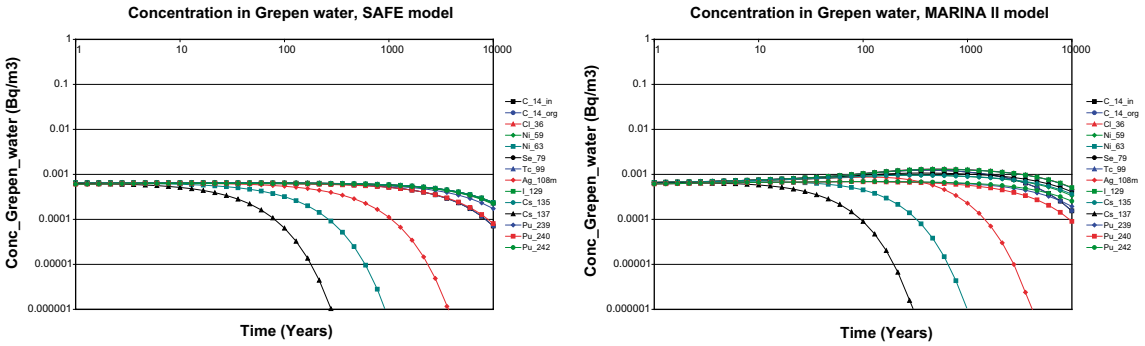

Figure A2-4c. *The pattern is similar for the top sediment concentrations in the Grepen: again the MARINA II model predicts slightly higher concentrations for some nuclides in the longer term, but by no more than a factor of two or three.*

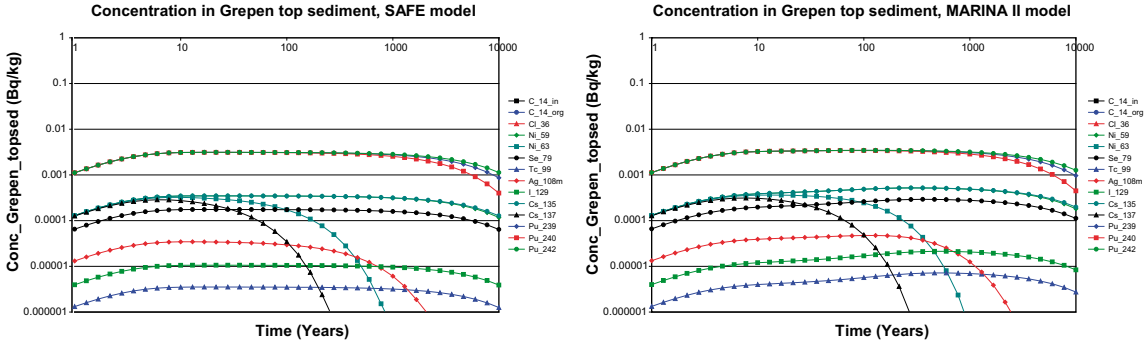

Figure A2-4d.

Substantial differences between the models are observed, however, beyond the Grepen. Concentrations predicted by the MARINA II model in the water of the Bothnian Sea (the southern part of the Gulf of Bothnia) are more than two orders of magnitude higher than those predicted by the SKB model in a single Baltic Sea compartment. Similar results are obtained for the East Baltic compartment of the MARINA II model. (The Bothnian Sea compartment includes Finnish coastline as well as Swedish, and the East Baltic compartment also includes coastline belonging to the Baltic States, Poland and Germany.) At their highest levels, the concentrations in the Bothnian Sea and East Baltic compartments are similar to those in the Grepen, and approach (within a factor of about two or three) those in the Model Area.

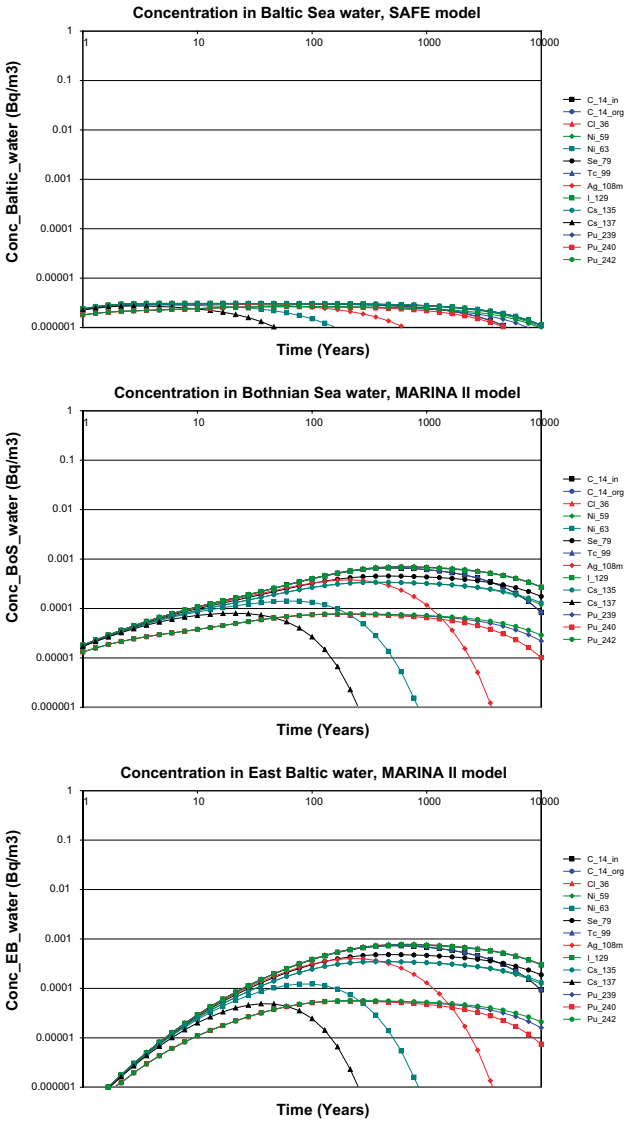

Figure A2-5.

A similar pattern appears in comparing the top sediment concentrations for the MARINA II compartments Bothnian Sea and East Baltic with those for the single Baltic Sea compartment in the SKB model. The differences between the models are typically between one and two orders of magnitude – a little smaller than for the water concentrations – but are still substantial. The highest values, in the Bothnian Sea particularly, again approach those for the Grepen and Model Area, but in this case remain clearly below the Grepen concentrations and almost an order of magnitude below those in the Model Area.

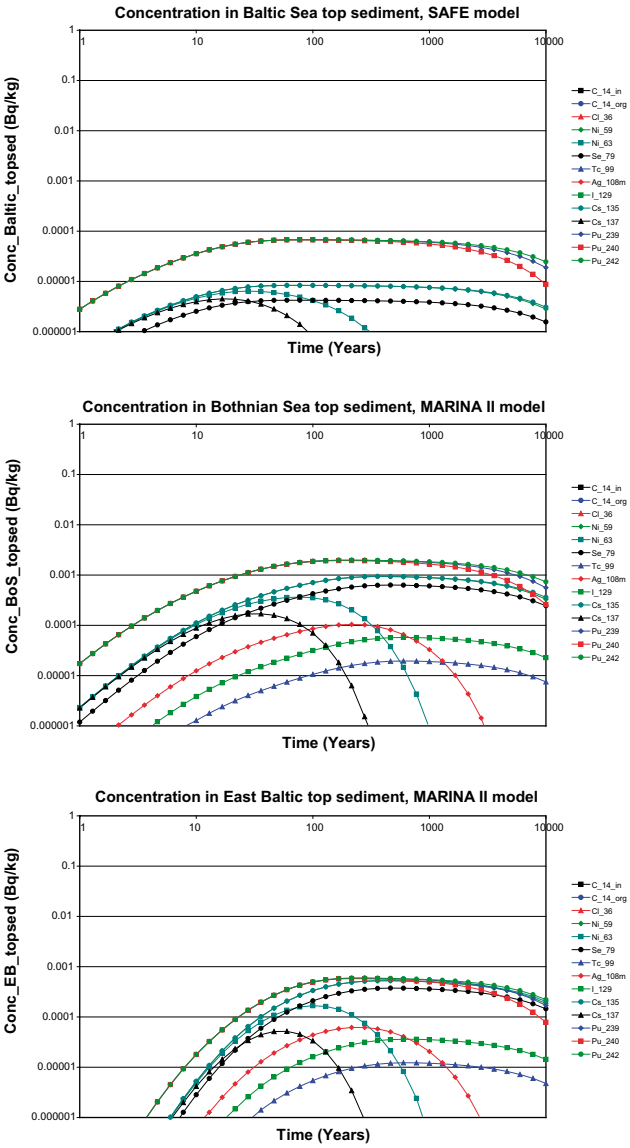
Concentration in Baltic Sea top sediment, SAFE model
Conc_Baltic_topsed (Bq/kg)
Time (Years)
Concentration in Bothnian Sea top sediment, MARINA II model
Conc_BoS_topsed (Bq/kg)
Time (Years)
Concentration in East Baltic top sediment, MARINA II model
Conc_EB_topsed (Bq/kg)
Time (Years)
C_14_in
C_14_org
Cl_36
Ni_59
Ni_63
Se_79
Tc_99
Ag_108m
I_129
Cs_135
Cs_137
Pu_239
Pu_240
Pu_242

Figure A2-6.

Appendix C

Details of AMBER forest model

C1 Comparison of the AMBER forest model with the implementation in /Avila 2004/

The forest model described in /Avila 2004/ was implemented in AMBER in order to undertake some preparatory calculations. The model comprises five dynamic compartments, representing soil, litter, tree wood, tree leaves and understorey plants (Figure A3-1).

The boxes in Figure A3-1 correspond to different forest components (compartments) and the arrows to net radionuclide fluxes between compartments /Avila 2004/:

1. Flux from soil to tree wood via root uptake.
2. Flux from soil to tree leaves via root uptake.
3. Flux from soil to understorey (plants and mushrooms) via root (mycelia) uptake.
4. Flux from tree leaves to litter by leaf fall.
5. Flux from tree wood to litter by wood fall.
6. Flux from understorey plants to litter by plants senescence.
7. Flux from litter to soil following litter decomposition.

The dashed arrows correspond to inputs to the system (sources) and outputs (runoff) and the dashed lines indicate transfer processes (transfer from vegetation to fauna) that are not included in the mass balance of the system.

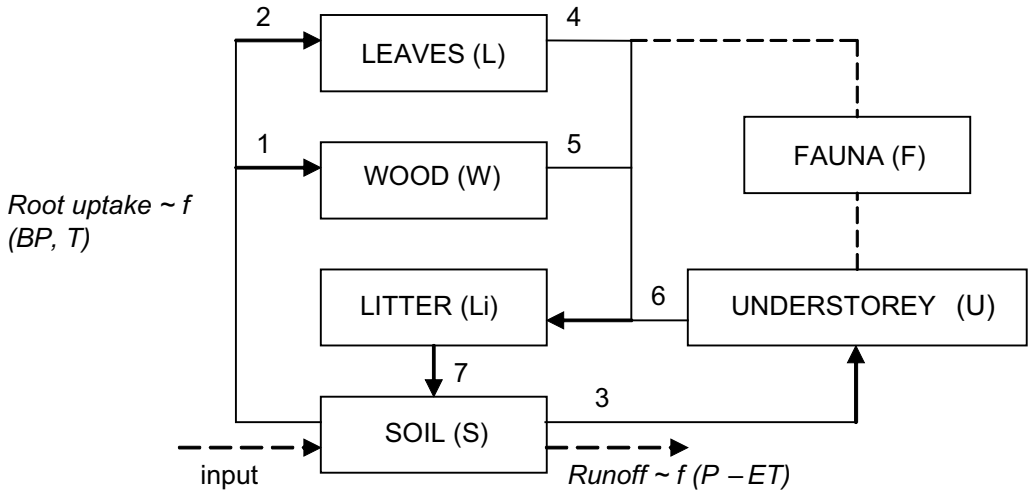

(BP – biomass production, T – transpiration, P – precipitation, ET – evapotranspiration)

Figure A3-1. *Configuration of forest model /Avila 2004/.*

The model was implemented as described in /Avila 2004/, with the exception of the transfer from tree wood to litter.

Tree death is represented in the SKB model by correcting the inventories in the wood compartment, for times greater than the average tree life T_{life}, according to the equation:

$$A^j_{Wcorr}(t) = A^j_W(t) - A^j_W(t - T_{life}) \times \exp\left[-(TC_{W-Li} + \lambda^j)T_{life}\right]$$

where $A^j_{W_{corr}}(t)$ and $A^j_W(t)$ are the corrected and uncorrected inventories of nuclide j at time t, $A^j_W(t - T_{life})$ is the uncorrected inventory at time (t-T_{life}), $TC_{W\text{-}Li}$ is the yearly fractional loss of wood from trees to the litter, and λ^j is the radioactive decay coefficient for nuclide j. This is intended to represent a situation in which trees die after T_{life}, and so the average age of trees at any time is $T_{life}/2$. Dead trees – and hence activity – are assumed not to be removed from the system: the activity is transferred to the litter.

This method cannot be implemented directly in AMBER, as inventories from earlier times in a calculation (other than user-specified output times) are not retained. To obtain a similar – though not identical – correction for tree death, the transfer between wood and litter compartments was expressed as a standard depleting dynamic transfer with a rate constant of $1/T_{life}$ (from t=0, not from t=T_{life}).

Using a simple source term of 1 Bq per m^2 per year, results were obtained for the concentrations after 10,000 years in soil, understorey plants, leaves, wood, mushrooms, roe deer and moose[6]. These were compared with the results reported in Table 4-1 of /Avila 2004/.

Results are shown in Table A3-1. For all concentrations except those in tree wood, the values calculated with AMBER were within about 5% of those reported in /Avila 2004/. Concentrations in wood at 10,000 years calculated using AMBER were typically:

- About 20% *higher* than those in /Avila 2004/ for long-lived nuclides; and
- Around 10% *lower* than those in /Avila 2004/ for Sr-90 and Cs-137, the only nuclides modelled that have half-lives comparable to the timescale of tree death.

Table A3-1. Comparison of radionuclide concentrations at t=10,000 years predicted with AMBER implementation of the forest model with values reported in /Avila 2004/.

Concentration at t=10,000 y in… (Bq/kg)	Radionuclide	A. Predicted by AMBER	B. Reported in /Avila 2004/	Variance (A–B)/B
Roe deer	Cl-36	4.20E–01	4.1E–01	2%
	Ni-59	1.35E+00	1.4E+00	–4%
	Sr-90	3.28E–01	3.3E–01	–1%
	Tc-99	1.53E–03	1.5E–03	2%
	I-129	1.28E–01	1.3E–01	–2%
	Cs-135	1.53E+02	1.5E+02	2%
	Cs-137	3.07E+00	2.9E+00	6%
	Ra-226	4.12E+01	4.2E+01	–2%
	Np-237	1.49E–02	1.5E–02	–1%
	Pu-239	3.16E–04	3.1E–04	2%

[6] It was not possible to produce comparisons of the data for berries as these are not reported in Table 4-1 of /Avila 2004/.

Concentration at t=10,000 y in… (Bq/kg)	Radionuclide	A. Predicted by AMBER	B. Reported in /Avila 2004/	Variance (A–B)/B
Moose	Cl-36	2.67E–01	2.6E–01	3%
	Ni-59	1.48E+00	1.5E+00	–1%
	Sr-90	2.90E–01	2.9E–01	0%
	Tc-99	1.91E–03	1.9E–03	1%
	I-129	7.93E–02	8.2E–02	–3%
	Cs-135	3.71E+01	3.5E+01	6%
	Cs-137	7.21E–01	6.9E–01	4%
	Ra-226	4.17E+01	4.3E+01	–3%
	Np-237	1.63E–02	1.6E–02	2%
	Pu-239	2.26E–04	2.2E–04	3%
Leaves	Cl-36	4.76E–01	4.8E–01	–1%
	Ni-59	5.83E–01	5.8E–01	1%
	Sr-90	3.19E–02	3.2E–02	0%
	Tc-99	1.48E–02	1.5E–02	–1%
	I-129	8.47E–02	8.5E–02	0%
	Cs-135	1.26E+01	1.2E+01	5%
	Cs-137	2.33E–01	2.3E–01	1%
	Ra-226	7.63E+00	7.5E+00	2%
	Np-237	3.20E–01	3.2E–01	0%
	Pu-239	3.34E–04	3.3E–04	1%
Mushrooms	Cl-36	2.08E+00	2.1E+00	–1%
	Ni-59	9.11E–01	9.1E–01	0%
	Sr-90	7.64E–02	7.6E–02	1%
	Tc-99	2.32E–02	2.3E–02	1%
	I-129	1.32E–01	1.3E–01	2%
	Cs-135	6.94E+02	6.9E+02	1%
	Cs-137	1.40E+01	1.4E+01	0%
	Ra-226	1.19E+01	1.2E+01	–1%
	Np-237	5.01E–01	5.0E–01	0%
	Pu-239	2.27E–02	2.3E–02	–1%
Soil	Cl-36	7.43E–02	7.4E–02	0%
	Ni-59	7.00E+00	7.0E+00	0%
	Sr-90	1.09E–01	1.1E–01	–1%
	Tc-99	2.32E–02	2.3E–02	1%
	I-129	2.21E–01	2.2E–01	0%
	Cs-135	5.78E+00	5.8E+00	0%
	Cs-137	1.17E–01	1.2E–01	–2%
	Ra-226	4.43E+00	4.4E+00	1%
	Np-237	7.15E+00	7.2E+00	–1%
	Pu-239	1.13E+01	1.1E+01	3%
Understorey plants	Cl-36	2.08E+00	2.1E+00	–1%
	Ni-59	9.11E–01	9.1E–01	0%
	Sr-90	7.47E–02	7.4E–02	1%
	Tc-99	2.32E–02	2.3E–02	1%
	I-129	1.32E–01	1.3E–01	2%
	Cs-135	4.05E+01	4.0E+01	1%
	Cs-137	7.99E–01	7.9E–01	1%
	Ra-226	1.19E+01	1.2E+01	–1%
	Np-237	5.01E–01	5.0E–01	0%
	Pu-239	2.27E–02	2.3E–02	–1%

Concentration at t=10,000 y in… (Bq/kg)	Radionuclide	A. Predicted by AMBER	B. Reported in /Avila 2004/	Variance (A–B)/B
Wood	Cl-36	7.87E–01	6.5E–01	21%
	Ni-59	3.21E–01	2.6E–01	23%
	Sr-90	2.28E–02	2.6E–02	–12%
	Tc-99	8.17E–03	6.7E–03	22%
	I-129	4.67E–02	3.8E–02	23%
	Cs-135	1.63E+01	1.3E+01	25%
	Cs-137	9.98E–02	1.1E–01	–9%
	Ra-226	4.04E+00	3.4E+00	19%
	Np-237	1.77E–01	1.5E–01	18%
	Pu-239	1.83E–03	1.5E–03	22%

C2 Inclusion of exposure scenarios within the Forest model

To allow comparison of forest exposure pathways with those in the existing SAFE agricultural biosphere, simple exposure models have been added to the AMBER representation of the forest model from /Avila 2004/ to represent:

- External exposure due to activity in soil, litter, tree trunks and leaves; and
- Internal exposure due to inhalation of soil dust, smoke from burning wood and sawdust during wood-cutting, and to ingestion of wild animals (roe deer and moose), mushrooms, berries and (inadvertently) soil.

Dose models were based on a combination of the models used in /Karlsson et al. 2001/, the forest food chain model of the international accident consequence code RODOS /Rantavaara and Ammann 2004/, models for exposure from timber and wood products described in IAEA-TECDOC-1376 /IAEA 2003/, and some generic habit data recommended by NRPB /Smith and Jones 2003/.

The selection of radionuclides considered was changed to reflect those of more importance in Project SAFE, rather than those considered in /Avila 2004/.

External doses

The external dose from activity in soil and litter is calculated using the concentrations in soil and litter calculated by the forest model (assuming litter is 10 cm deep), dose rates per unit concentration taken from /Karlsson et al. 2001/ (1 m above an infinite area of contaminated soil), and an occupancy in the affected area of forest of 100 hours per year, as used for affected agricultural land in /Karlsson et al. 2001/[7].

Concentrations in soil depend in part on soil K_d values, which were taken from /Avila 2004/ where possible, and from /Karlsson et al. 2001/ for elements not listed by Avila.

[7] The RODOS report quotes occupancies in forest of up to 200 hours per month for forestry workers in Finland. However, such people's time would presumably be spread over areas of forest of at least several km^2, whereas the affected area is assumed to be about 0.5 km^2.

Element	Soil K_d (m^3 kg^{-1})
C	0.001
Cl	0.01
Ni	1
Se	0.01
Sr	0.2
Tc	0.003
Ag	0.1
I	0.03
Cs	0.8
Pu	2

Data from /Karlsson et al. 2001/ for C, Se, Ag; from /Avila 2004/ for other elements.

The external dose from activity in tree trunks and leaves is calculated using the models described in the RODOS report. These use three radionuclide specific parameters b_1, b_2 and b_3 (for which values are specified in the report[8]) and the expressions:

$$x_o = 0.12+0.11\times\rho_{trunk}$$

$$x_1 = (0.12+0.11\times\rho_{trunk})\times(h_{trunk}-1)$$

$$x_2 = (0.12+0.11\times\rho_{crown})\times h_{crown}$$

$$f_{trunk} = \frac{3.6\times10^{-4}}{x_o\times h_{trunk}}\left[b_1(x_0+x_1)+b_2(x_o^{\,2}+x_1^{\,2})-b_3(x_0\ln x_0+x_1\ln x_1)\right]$$

$$f_{crown} = \frac{3.6\times10^{-4}}{x_2}\left[b_1x_2+b_2(x_2^{\,2}+2x_1x_2)-b_3((x_1+x_2)\ln(x_1+x_2)-x_1\ln x_1)\right]$$

where ρ_{trunk} and ρ_{crown} are the biomass densities for the trunk and crown layers (which are already in the model from /Avila 2004/), h_{trunk} and h_{crown} are the corresponding heights (taken as 13.7 m and 15.2 m respectively, based on data for European coniferous forests in the RODOS report), and f_{trunk} and f_{crown} are the air kerma rates per Bq/m^2. Dose rates are calculated by multiplying f_{trunk} and f_{crown} by the calculated Bq/m^2 in wood and leaves respectively, and by a kerma-to-dose conversion factor of 0.7 Sv/Gy.

Radionuclide	b_1	b_2	b_3
Ag-108m	No data – doses not calculated		
I-129	0.65	0.009139	0.2504
Cs-137	5.591	0	1.278
All other nuclides	0	0	0

[8] In fact, data are given for only some of the radionuclides considered here. The only significant gamma emitter for which data are not provided is Ag-108m.

Inhalation doses

Inhalation doses are calculated by the general formulation:

$D = C \times inh \times occ \times dpui_{inh}$

where D is the dose from the relevant radionuclide (Sv y^{-1}), C is the airborne concentration of the radionuclide (Bq m^{-3}), inh is the breathing rate of air (m^3 hr^{-1}), occ is the occupancy in the area where the inhalation hazard exists (hr y^{-1}) and $dpui_{inh}$ is the dose per unit intake of the radionuclide by inhalation (Sv Bq^{-1}) (values as used in /Karlsson et al. 2001/).

For inhalation of resuspended soil and sawdust, C is the product of the concentration in soil or in wood and the airborne loading of dust (the value given in /Karlsson et al. 2001/ of 100 mg/m^3 is excessively high, especially for a long-term average – the IAEA quote 2 mg/m^3 for wood dust, and values in the range 1–10 mg/m^3 are commonly used for dusty environments – but was nevertheless used here in both models for consistency). For inhalation of smoke from burning wood, C is derived using the model for burning peat described in /Karlsson et al. 2001/. The concentration in wood is multiplied by two parameters: the fuel load of 10^{-4} kg/s and the "relative concentration" of 10^{-5} s/m^3, giving an overall concentration factor for smoke relative to wood of 10^{-9} Bq/m^3 per Bq/kg (the smoke was assumed conservatively not to be filtered).

The occupancy for inhalation of soil dust and sawdust was assumed to be the time spent in the affected area of forest, discussed above. The occupancy for inhalation of smoke was assumed to be different, as the wood is assumed to be removed from the forest and burned in a domestic fire. The occupancy of 8,000 hr/y used in /Karlsson et al. 2001/ for the peat-burning scenario was used here, although this is conservative as all of the wood would need to come from the affected area of the forest. For this simple model, the generic breathing rate of 1 m^3/hr from /Karlsson et al. 2001/ is assumed for all cases (by comparison with NRPB data, this corresponds to a moderately active adult – during heavy work, the breathing rate could be higher, but by less than a factor of two).

Ingestion doses

Ingestion doses are calculated by the general formulation:

$D = C \times ing \times dpui_{ing}$

where D is the dose from the relevant radionuclide in the relevant food (Sv y^{-1}), C is the concentration of the radionuclide in the food (Bq kg^{-1}), ing is the annual intake of the food (kg y^{-1}) and $dpui_{ing}$ is the dose per unit intake of the radionuclide by ingestion {Sv Bq^{-1}).

The concentrations in soil, roe deer, moose, berries and mushrooms are calculated directly in the model as described in /Avila 2004/. For the empirical parameters a, a_3, b and b_3 used in calculating concentrations in animals, values for C and Se were assumed the same as for Cl, and values for Ag were assumed the same as for Sr. In addition the values of a_3 and b_3 for Ni was assumed to be the same as for Pu. Concentration factors from soil to berries and mushrooms (and from soil to leaves and soil to wood, used in calculating concentrations in animals) for Se and Ag were also assumed to be the same as those for Cl and Sr respectively, whereas C was assumed not to be taken up from the soil.

The RODOS forest foodchain model includes an element-dependent translocation fraction for understorey plants/berries. The use of this factor suggests that it applies to activity deposited on the surface of understorey plants, and so it has not been included in the model here.

Intake rates for game animals, mushrooms and berries were taken from the RODOS report, selecting the highest values quoted (Finnish hunters in the case of game animals, Finnish collectors/pickers for mushrooms and berries). The value for game animals was assumed to be 50% each of roe deer and moose. Inadvertent ingestion rates for soil were based on the intake of 0.1 kg/y assumed in /Karlsson et al. 2001/ (although this is extremely high for an adult).

Food		Annual intake, kg/y
Game animals*	Roe deer	6.5
	Moose	6.5
Mushrooms		5.7
Berries		28

* RODOS quotes 13 kg/y for Finnish hunter. This has been assumed to be split 50:50 between roe deer and moose.

Doses associated with a forest biosphere were compared with those for the agricultural biosphere using a common unit release of 1 Bq/y per m^2. The input to the forest biosphere model is assumed to be into 1 m^2 and so was simply set to 1 Bq/y: the release to the agricultural biosphere was 1 Bq/m^2 multiplied by the model area (530,000 m^2). A unit release per unit area is a valid basis for this comparison, as the two biospheres are being compared for a given release, which would affect the same area for both biospheres. The area specified above is taken into account in judging the appropriateness of certain assumptions, such as annual occupancy within the affected area.

In the forest model, the source is released to the single soil compartment. The agricultural model has a more complex soil model, and the normal release point for the source is groundwater below the deep soil compartment. A direct comparison between concentrations in the top soil compartment predicted by the two models showed, as would be expected, that concentrations in the agricultural top soil are much lower at early times and take a longer time to stabilise. However, when equilibrium is reached, concentrations of most radionuclides do not differ by very large amounts between the two models.

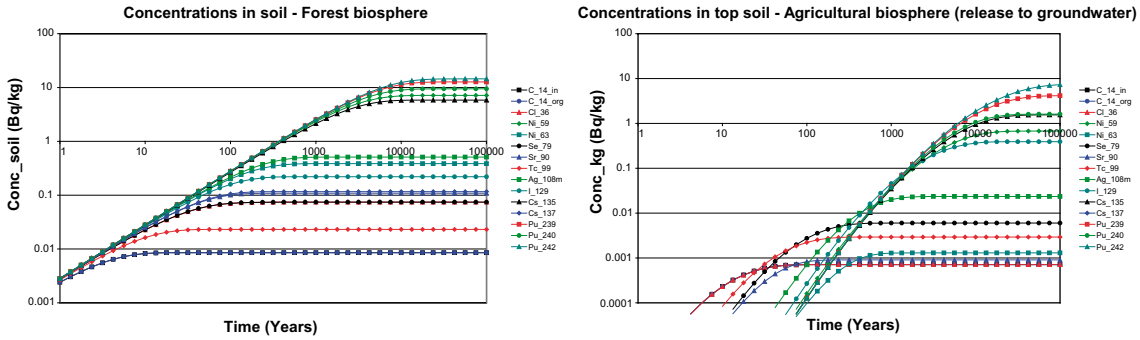

Figure A3-2. *The same comparison, but with the source to the agricultural model going directly into the top soil (as in the forest model), shows much greater similarity between soil concentrations predicted by the two models.*

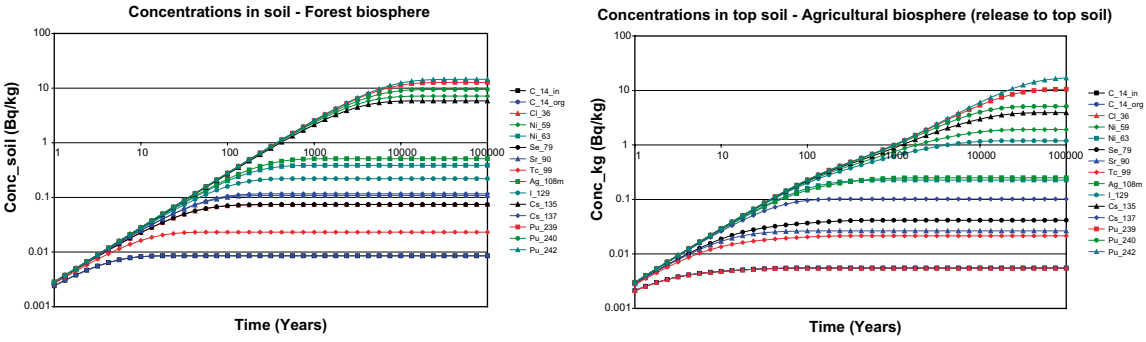

Figure A3-3.

As all exposure pathways are related in some way to concentrations in soil, these results indicate that differences in doses between the two models are primarily the result of differences between exposure pathways and/or the modelling of those pathways, especially if the agricultural model is run as in the second case, with the source to top soil. It is recognised that the normal implementation of the agricultural biosphere model, with release to groundwater below the deep soil, is a better representation of reality, but it does not provide such a direct comparison with the simpler forest model. There are real differences between forest and agricultural soils, but the simple forest model used here is not capable of representing them in detail. As the purpose of this exercise is to identify differences between the exposure models and their significance, therefore, the following comparisons are based, for the agricultural model, on release to the top soil compartment.

Doses were summed over all pathways. Table A3-2 summarises the total doses at equilibrium (after 100,000 years) for 1 Bq/m^2/y of each radionuclide released to each biosphere. The doses from the forest biosphere exceed those from the agricultural biosphere substantially for Cs-135 and Cs-137 (both by factors of between 50 and 100), significantly for Sr-90 (by a factor of about 5) and marginally (by a factor of 2 or less) for Cl-36, Ni-59, Ag-108m, Pu-239 and Pu-240.

As the dominant exposure pathways in Table A3-2 are the ingestion of contaminated foodstuffs and soil and soil inhalation it is not considered that the differences in wood concentration in the AMBER model (resulting from the alternative approach to representing tree death) affect the overall result significantly.

Table A3-2. Total doses at equilibrium (100,000 years) from forest and agricultural biospheres for release of 1 Bq/m^2/y to soil.

Nuclide	Forest bio-sphere	Agricultural biosphere	Ratio Forest: Agricultural	Dominant forest pathway(s)
C-14*	9.9E–13	5.5E–12	0.2	Soil ingestion, Soil inhalation
Cl-36	7.0E–08	3.5E–08	2	Berries
Ni-59	3.2E–09	2.6E–09	1.2	Berries
Ni-63	4.1E–10	7.3E–10	0.6	Berries
Se-79*	2.2E–07	3.5E–07	0.6	Berries
Sr-90	2.0E–07	4.0E–08	5	Berries, Roe deer
Tc-99	5.2E–10	1.7E–08	0.03	Berries
Ag-108m*	8.3E–08	4.2E–08	2	Roe deer, Berries, Moose
I-129	6.4E–07	6.4E–06	0.1	Berries
Cs-135	1.3E–05	1.4E–07	93	Mushrooms
Cs-137	1.6E–06	2.5E–08	64	Mushrooms
Pu-239	1.6E–05	1.3E–05	1.2	Soil inhalation
Pu-240	1.2E–05	6.3E–06	1.9	Soil inhalation
Pu-242	1.7E–05	1.9E–05	0.9	Soil inhalation

* In the absence of data in /Avila 2004/, several transfer factors for carbon and selenium were assumed to be the same as those for chlorine, and several transfer factors for silver were assumed to be the same as those for strontium.

The results are illustrated in the graphs below.

Doses from plutonium isotopes – largely from inhalation pathways – are major contributors in the very long term in both cases, giving similar doses for unit release. The airborne dust level of 100 mg/m^3 is unfeasibly high (by a factor of 10–100 for 'dusty' environments, or up to a factor of 1,000 for ambient dust levels), but the same value is assumed for both biospheres, and the inhalation doses from soil (and, in the forest model, sawdust, which uses the same dust level) will be essentially proportional to this figure. On the other hand, the occupancy values and breathing rates for soil and sawdust inhalation could be considered to be low for some individuals, and the high dust level may be considered to cover the possibility of higher values of these parameters. The other inhalation pathway specific to the forest model – smoke from burning wood – contributes very little to the total inhalation dose: it could be relatively more significant if the dust level were lower, but would still be orders of magnitude lower than the dose from inhaling soil (see the figure below).

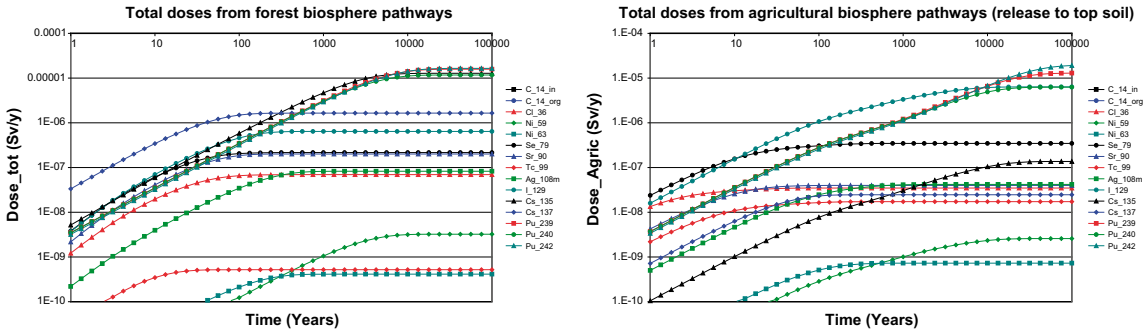

Figure A3-4.

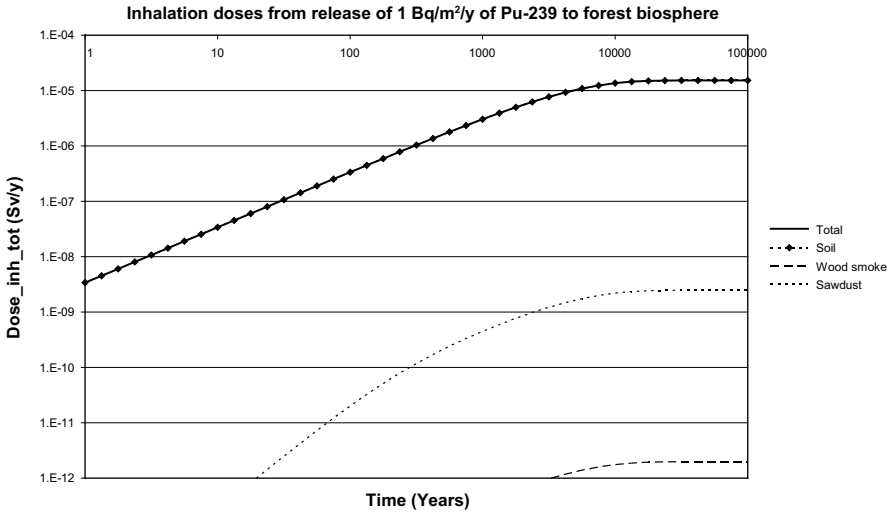

Figure A3-5.

The major differences between the forest and agricultural models among the other higher dose pathways are as follows:

- Caesium and strontium isotopes give higher doses for forest pathways than for the agricultural biosphere. This appears to be due primarily to their concentration in berries and mushrooms. This results in high doses from both direct human consumption of berries and mushrooms and consumption of game animals that have significant amounts of these foods in their diet. The concentration factors in /Avila 2004/ for caesium in these foods show large ranges and so other sources have been considered. A study of fungi specifically in the Forsmark area /Johanson et al. 2004/ indicates values substantially lower than the nominal value of 120 quoted by Avila, but well within the range of 0.27–620. Comparison with the forest module of the RODOS international emergency preparedness code /Rantavaara and Ammann 2004/ confirms that Avila's nominal value is close to the high end of a large range. The Forsmark-specific ratio derived by /Johanson et al. 2004/ from measurements of stable caesium was considered to be appropriate (as long-lived Cs-135 is the more important isotope for the overall assessment), and the quoted median from the site-specific range was used, as this is approximately equal (for an approximately lognormal distribution) to the geometric mean used by Avila. The value quoted is 15.5 for dry weight of mushrooms which, assuming a water content of 90%, corresponds to 1.55 on a fresh weight basis. Consideration of the two nominal values quoted by Avila for caesium transfer to understorey plants indicated that the lower of Avila's values – 2.3 rather than 7.0 – was more consistent with data, specifically for berries, tabulated in the RODOS report.
- The mobile radionuclides that give high doses via agricultural food pathways, notably I-129 and Se-79, give lower doses via forest pathways. This is likely to be due to the absence of particular agricultural pathways – e.g. iodine in milk, selenium in crops – from the forest diet, and the relatively high intake rates for contaminated agricultural products compared to those of wild foods in the forest biosphere.

External doses do not make a substantial contribution to total doses for either biosphere for any of the nuclides considered. A possible exception to this could be Ag-108m. The external doses from this nuclide in the forest biosphere are incomplete, as data were not available for the component of external exposure due to tree trunks and crowns. However, the external doses from (forest) soil are a small contributor to the total dose, and even smaller in the forest biosphere than the agricultural biosphere (see the figures below), so it seems very unlikely that this omission is serious.

The highest transfer coefficient quoted in the RODOS report is 0.5 Bq/kg (fresh weight) per Bq/m^2. Using Avila's values for bulk soil density (1,180 kg/m^3) and rooting layer depth (0.3 m), 1 Bq/m^2 corresponds to 0.0028 Bq per kg of soil, so this converts to a concentration factor of about 180 Bq/kg per Bq/kg, comparable to Avila's nominal value of 120. An unpublished IAEA

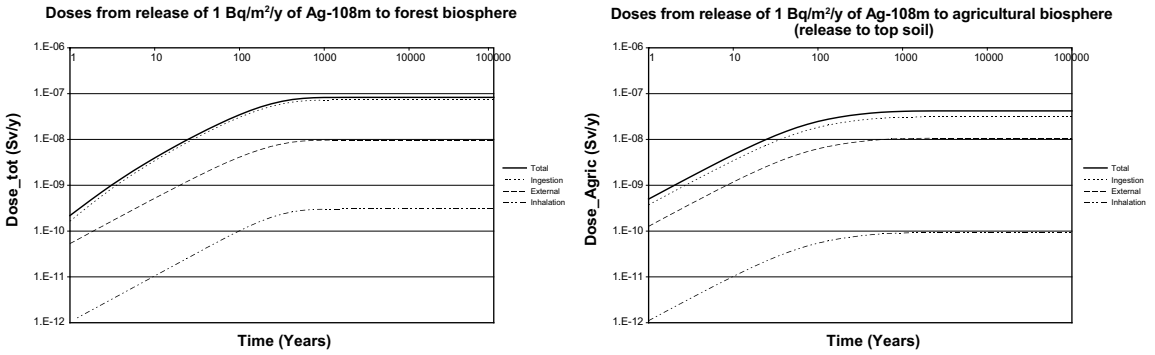

Figure A3-6.

report[9] quotes a "mean value" of 0.5 Bq/kg per Bq/m^2 and a range up to 5, but these are by dry weight of mushrooms: assuming mushrooms are typically about 90% water, these figures correspond to about 0.05 and 0.5 m^2/kg respectively. This supports the view that Avila's value is at the high end of the range but not entirely unreasonable.

The intake rates quoted in the unpublished IAEA report are lower than the maximum values taken from the RODOS report:

- 3 kg/y of mushrooms, about half the value assumed above,
- 0.25 kg/y of game, about 2% of the value assumed above; and
- 2 kg/y of berries, about 7% of the value assumed above.

The report indicates that these intake rates are typical of groups of about 50 people in the case of mushrooms and berries, or just a few people in the case of game. Again, this suggests that the values used in the comparison above are very much at the upper end of the range.

Another major conservatism in the forest model is the assumption that all of the forest products are affected by the radioactivity, which requires that they all come from the release area (assumed to be 0.53 km^2, the same area as the agricultural model). The fact that the release area is small is implicitly taken into account in assuming relatively low occupancy in the affected areas of forest, but is not reflected in the calculation of ingestion doses. The unpublished IAEA report quotes annual yields for forest products (referenced to published Finnish data):

- For mushrooms, the best estimate yield is 500 kg/km^2, but with a range of 50–30,000. The RODOS report quotes a fresh weight yield of 0.05 kg/m^2, i.e. 50,000 kg/km^2, which suggests that the IAEA report is quoting dry weight figures. Assuming a fresh weight yield of 5,000 kg/km^2, an intake rate of 5.7 kg/y could theoretically come from an area as small as about 0.1 Ha, much smaller than the 53 Ha release area. In practice, however, it is debatable whether collection of wild mushrooms over the course of a year would be limited to such an area.
- For berries, the best estimate yield is 200 kg/km^2, so an intake rate of 28 kg/y would require a minimum area of the order of 10 Ha, i.e. even theoretically, the release area could support only a few people consuming berries at this rate. In practice, it seems almost inevitable that such an intake would include berries from a wider area than the release area.
- For game, the best estimate yield is 50 kg/km^2, i.e. about two roe deer per km^2 or one moose per 5 km^2. An intake rate of 13 kg/y would therefore require 25 Ha, or about half the release area. These yields also give some indication that game animals probably roam (and feed) over areas considerably larger than the release area.

This information suggests that forest products are more likely to be derived from a forest area of a few km^2 than from a fraction of a km^2, and so the doses calculated assuming that all products are contaminated may well overestimate actual doses by about an order of magnitude.

Overall, therefore, this comparison suggests that the agricultural biosphere is unlikely to underestimate doses significantly compared to a forest biosphere. Possible exceptions are the doses due to caesium accumulation in mushrooms, and in game animals that eat mushrooms, although there is some uncertainty about the extent of this accumulation in the case of activity released into the biosphere via groundwater rather than via the atmosphere. Furthermore, unlike agricultural pathways, the forest-specific pathways – including those associated with mushrooms – are not by their nature intensive or specific to particular areas of forest. Since the area contaminated by a release from the geosphere is likely to be small (less than 1 km^2) compared to typical areas of forest (many km^2), there is likely to be substantial 'dilution' of doses due to mushrooms, game animals, wood, etc, from non-affected areas of forest.

[9] The IAEA model for aiding decisions on contaminated forests and forestry products: Application to intervention/cleanup criteria, Unpublished draft TECDOC (1999).

Appendix D

SFR 1. Post closure radionuclide release and dose calculations – Well model calculations

Gavin Thomson, Enviros consulting limited

February 2006

Executive summary

Enviros is currently supporting SKB in relation to its operation of the L/ILW repository, SFR-1, located near Forsmark.

The Swedish regulatory authorities have recently reviewed SKB's most recent safety assessment (Project SAFE) and have provided SKB with a review which highlighted areas where further information is required. One area is in the estimation of the potential impacts of radionuclide release from the repository following closure and Enviros has been providing support in this area.

Enviros has provided SKB with the calculations for the SFR-1 repository in order to further demonstrate the robustness and safety of the continued operation of the facility. These calculations have shown that the estimated individual annual doses, and where relevant the radiological risks, are below the regulatory criteria. However, SKB wishes to further support its response to the Authorities' with additional calculations concerning potential exposures arising from the use of contaminated well water.

A well biosphere model has been configured in AMBER based on that used in the original Project SAFE calculations. Calculations were undertaken for the Most Likely Scenario both including and neglecting geosphere retardation.

A summary of the Most Likely Scenario results for the Reasonable Biosphere Development (RBD) and the Well Biosphere models is provided in the table below.

It can be seen that the doses estimated for the Well Biosphere are larger than for the RBD in all instances. This is due to the low amount of dilution that occurs within the well scenario and the relatively intensive use of contaminated environmental media.

	RBD	Well Biosphere
Silo	6.5E–07 Sv/y at c 5,100 AD Organic C-14	1.0E–05 Sv y^{-1} at c 4,000 AD Organic C-14
BMA	4.2E–07 Sv/y at c 8,000 AD I-129	2.1E–05 Sv y^{-1} at c 4,100 AD Organic C-14
1BTF	5.9E–07 Sv/y at c 5,100 AD Organic C-14	5.2E–05 Sv y^{-1} at c 4,100 AD Organic C-14
2BTF	6.9E–08 Sv/y at c 8,000 AD I-129	1.6E–06 Sv y^{-1} at c 4,100 AD Organic C-14
BLA	5.5E–09 Sv/y at c 5,000 AD Inorganic C-14	4.9E–07 Sv y^{-1} at c 4,100 AD Inorganic C-14
SFR-1	1.6E–06 Sv/y at c 5,100 AD Silo, BMA, 1BTF	8.3E–05 Sv y^{-1} at c 4,100 AD 1BTF

The Well Biosphere doses estimated for the Silo, 2BTF and the BLA are below the relevant regulatory criteria for dose (16 μSv y^{-1}), but the values for the BMA and 1BTF are above the regulatory dose criteria.

Neglecting geosphere retardation results in an increase in the overall dose from SFR-1 as a whole to 1.1E–04 Sv y^{-1} (compared to 8.3E–05 Sv y^{-1} when geosphere retardation in included).

D1 Introduction

Enviros is currently supporting SKB in relation to its operation of the L/ILW repository, SFR-1, located near Forsmark.

The Swedish regulatory authorities have recently reviewed SKB's most recent safety assessment (Project SAFE) and have provided SKB with a review which highlighted areas where further information is required. One area is in the estimation of the potential impacts of radionuclide release from the repository following closure and Enviros has been providing support in this area.

Enviros has provided SKB with the following calculations for the SFR-1 repository in order to further demonstrate the robustness and safety of the continued operation of the facility /Enviros 2006/.

- Presentation of the central or 'Most Likely Scenario'.
- Alternative inventory assumptions.
- Sensitivity of repository groundwater flow-fields to different calibration techniques used in the supporting hydrogeological model.
- Sensitivity to uncertainties in radionuclide sorption in the near-field.
- Consideration of forest land use.

These calculations have shown that the estimated individual annual doses, and where relevant the radiological risks, are below the regulatory criteria /Enviros 2006/. However, SKB wishes to further support its response to the Authorities' with additional calculations concerning potential exposures arising from the use of contaminated well water.

This report therefore describes the undertaking of calculations of dose arising from the use of contaminated well water for the Most Likely Scenario.

D2 description of the well model

The well model configured in AMBER is that described in /Karlsson et al. 2001/ which was used in the original Project SAFE calculations /Lindgren et al. 2001/.

D2.1 Configuration of the well model in AMBER

The well model comprises a single compartment for the well and two associated soil compartments (a top soil compartment which is irrigated with well water and a deep soil compartment which exchanges radionuclides with the top soil via leaching and biotransport). Additionally a loss compartment is included to receive outflow from the well compartment. The AMBER representation is shown below.

The transfer of radionuclides from the well compartment to the top soil compartment via irrigation, $\lambda_{irrigation}$ [y^{-1}], is represented as described in section 8.1 of /Karlsson et al. 2001/.

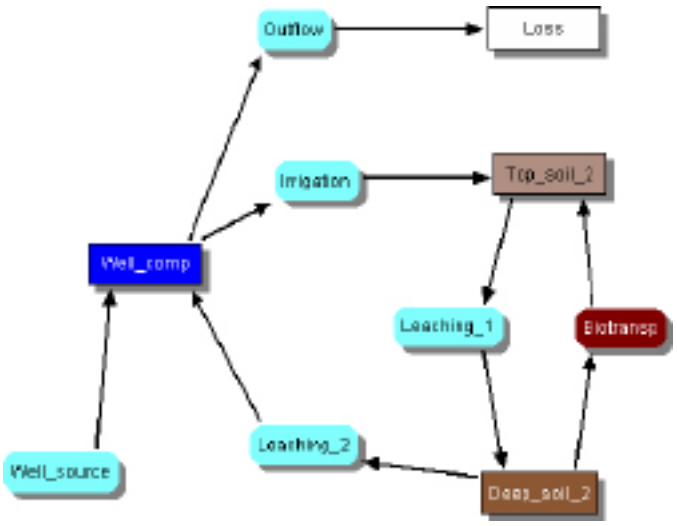

Figure A4- 1. *AMBER representation of Well Model.*

$$\lambda_{irrigation} = \frac{V_{irr} * A_{garden} * N_{irr}}{V_{well}} \qquad \text{(Equation A4-1)}$$

V_{irr} Amount of water used at each irrigation event [$m^3\ m^{-2}$]

A_{garden} Area of garden irrigated [m^2]

N_{irr} Number of irrigation events [number y^{-1}]

V_{well} Volume of the well [m^3]

The mixing volume of the well was taken to be the same as the annual amount of water removed from the well (as noted in section 7.2 of /Karlsson et al. 2001/).

$$V_{well} = Capacity * 1\ [y] \qquad \text{(Equation A4-2)}$$

Capacity is the well capacity [$m^3\ y^{-1}$]

The transfer of radionuclides from the top soil compartment to the deep soil compartment via leaching, $\lambda_{leaching\_1}$ [y^{-1}], is represented as described in section 8.3 of /Karlsson et al. 2001/.

$$\lambda_{leaching\_1} = \frac{R}{\varepsilon_{ts} * D_{ts}}.R_f + \frac{BioT}{D_{ts}(1-\varepsilon_{ts}).\rho_p} \qquad \text{(Equation A4-3)}$$

R Runoff [$m^3\ m^{-2}\ y^{-1}$]

ε_{ts} Porosity of top soil [–]

D_{ts} Depth of top soil [m]

R_f Retardation [–], which is given by

$$R_f = \frac{1}{1 + K_d.\rho_p.(1-\varepsilon_{ts})/\varepsilon_{ts}} \qquad \text{(Equation A4-4)}$$

where

K_d is the radionuclide specific distribution factor [$m^3\ kg^{-1}$]

ρ_p is the soil particle density [$kg\ m^{-3}$]

BioT Transport due to bioturbation [$kg\ m^{-2}\ y^{-1}$]

The transfer of radionuclides from the deep soil compartment to the top soil compartment via bio-transport, $\lambda_{biotransp}$ [y^{-1}], is represented as described in section 8.3 of /Karlsson et al. 2001/.

$$\lambda_{biostransp} = \frac{BioT}{D_{ds}(1-\varepsilon_{ds}).\rho_p} \qquad \text{(Equation A4-5)}$$

ε_{ds} Porosity of deep soil [–]

D_{ds} Depth of deep soil [m]

The transfer of radionuclides from the deep soil compartment to the well compartment via leaching, $\lambda_{leaching\_2}$ [y^{-1}], is represented as described in section 8.3 of /Karlsson et al. 2001/.

$$\lambda_{leaching\_2} = \frac{R}{\varepsilon_{ds} * D_{ds}}.R_f \qquad \text{(Equation A4-6)}$$

Here

$$R_f = \frac{1}{1+K_d.\rho_p.(1-\varepsilon_{ds})/\varepsilon_{ds}} \qquad \text{(Equation A4-7)}$$

The transfer of radionuclides from the well compartment to the loss compartment via outflow, $\lambda_{outflow}$, is not given in /Karlsson et al. 2001/ and is represented as the difference in the well capacity and the amount of water used for irrigation.

$$\lambda_{outflow} = \frac{Capacity - V_{irr} * A_{garden} * N_{irr} - I_{human} - I_{an}}{V_{well}} \qquad \text{(Equation A4-8)}$$

I_{human} Human consumption rate of well water [$m^3\ y^{-1}$]

I_{an} Animal consumption rate of well water [$m^3\ y^{-1}$]

D2.1 Comparison of AMBER model with Project SAFE

In order to undertaken some comparisons of the model with those results from Project SAFE a source was supplied which comprised the near-field flux of the appropriate facility from 4,000 AD onwards. Furthermore, following the approach stated in /Lindgren et al. 2001/ it was conservatively assumed that all the activity released from each repository part intercepted the well.

Figure A4-2 below shows a comparison of the doses estimated from the AMBER implementation of the well model for release from the BLA with those originally from Project SAFE. The level of agreement for plutonium isotopes is good. For inorganic C-14, Se-79 and Tc-99 the level of agreement is initially good but at about 7,000 AD the Se-79 doses from Project SAFE level at around 1E–10 Sv y^{-1} and the doses for inorganic C-14 and Tc-99 are estimated to level at around 1E–12 Sv y^{-1} at around 11,000 AD. This behaviour is not reflected in the results produced from the AMBER model.

Figure A4-3 shows the near-field flux for release from the BLA calculated using AMBER based on the configuration in Project SAFE /Enviros 2006/ (the initial 2000 year period of release should be discounted as the well model is not established until 4,000 AD and the geosphere is not considered a barrier within the calculations). It can be seen that the release profiles of inorganic C-14 and Se-79 decrease at a constant rate, do not reach a constant level and therefore differences in the source term cannot be the reason for the anomalous behaviour shown in the above.

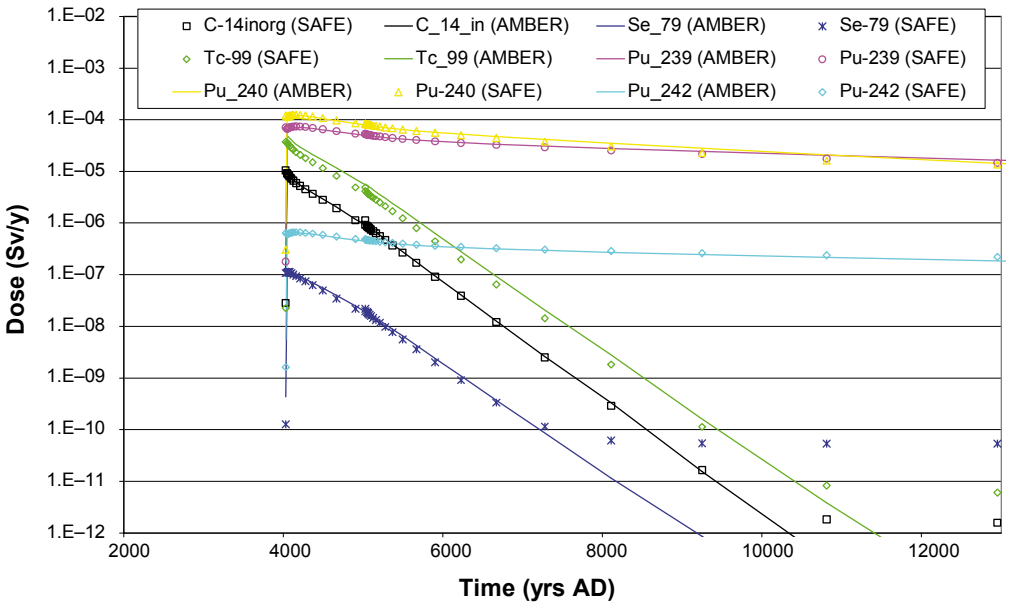

Figure A4-2. *Doses in well model due to releases from the BLA.*

It seems that the most likely explanation for the trends shown by the doses estimated from Project SAFE is that these radionuclides are becoming retained within the system. It is noted that the best estimate values of the soil K_d*s* for these radionuclides are 7E–2 m^3 kg^{-1} for C-14 and 1E–2 m^3 kg^{-1} for Se-79 and these do not seem to be overly large values.

Figure A4-4 shows radionuclide concentration in soils for the AMBER model (the corresponding plot for Project SAFE is not available for comparison). It can be seen that plutonium isotopes and I-129 are retained within the soil, whereas the concentrations of inorganic C-14, Se-79 and Tc-99 seem to be more related to the trends shown by their source terms (Figure A4-3). The best estimate K_d value for Pu is 5 m^3 kg^{-1} and for I it is 0.3 m^3 kg^{-1}.

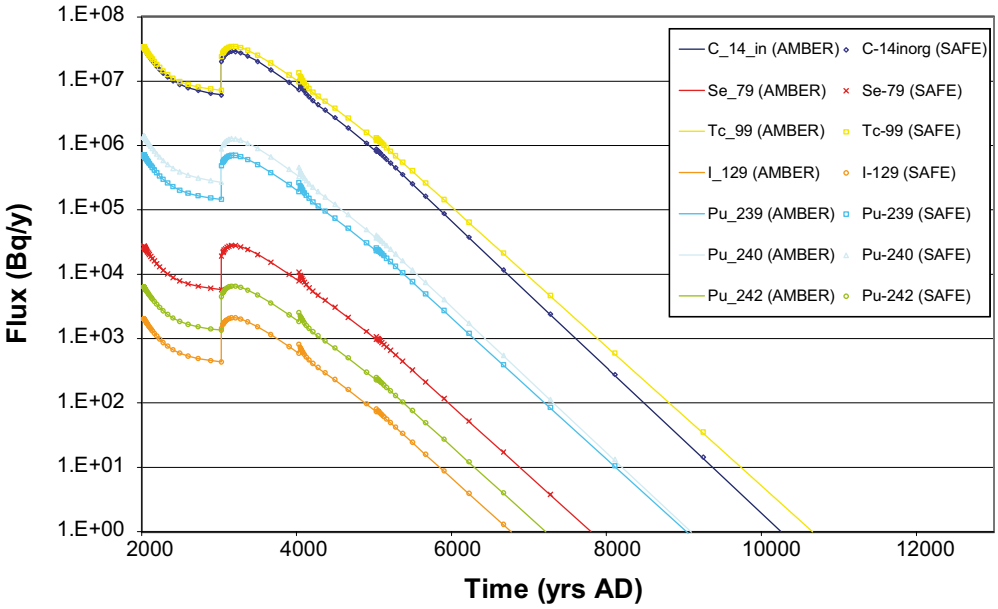

Figure A4-3. *Near-field flux from the BLA.*

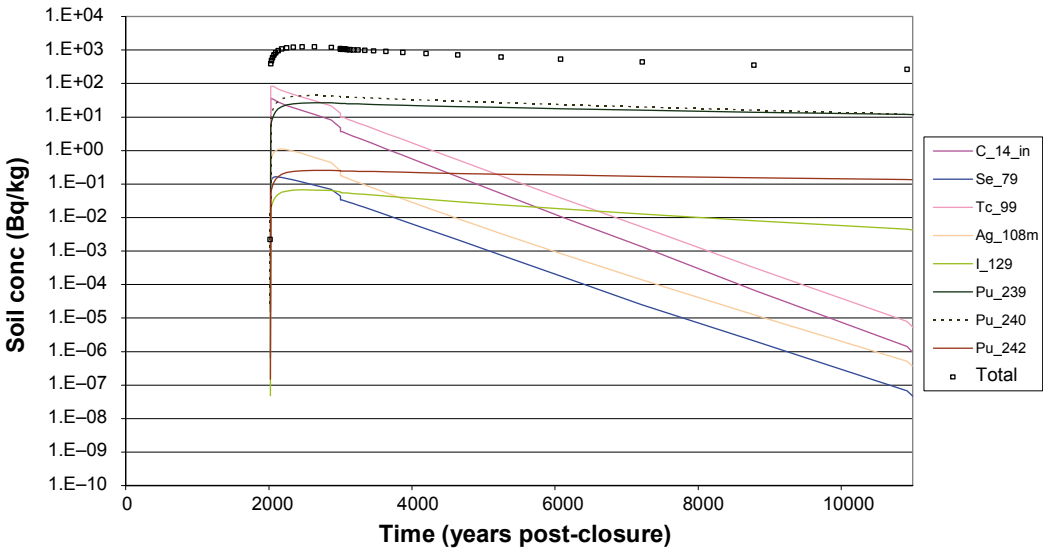

Figure A4-4. *Concentration in top soil of well model for release from the BLA.*

Figure A4-5 to A4-9 show the dose breakdown by exposure pathway for each of inorganic C-14, Se-79, Tc-99, I-129 and Pu-239, respectively. The plots for I-129 and Pu-239 show that exposures continue for both these radionuclides after the source term for each of the radionuclides is effectively exhausted (i.e. radionuclide flux 1 Bq y^{-1} or less) at around 7,000 AD for I-129 and 9,000 AD for Pu-239. This again suggests that these radionuclides are retained within the well model. This is not the case for the other radionuclides, for example, the Se-79 dose reaches 1E–12 Sv y^{-1} (a level which was considered to be negligible in the Project SAFE calculations) at around 7,000 AD and at this time the radionuclide flux is around 10 Bq y^{-1} and decreasing.

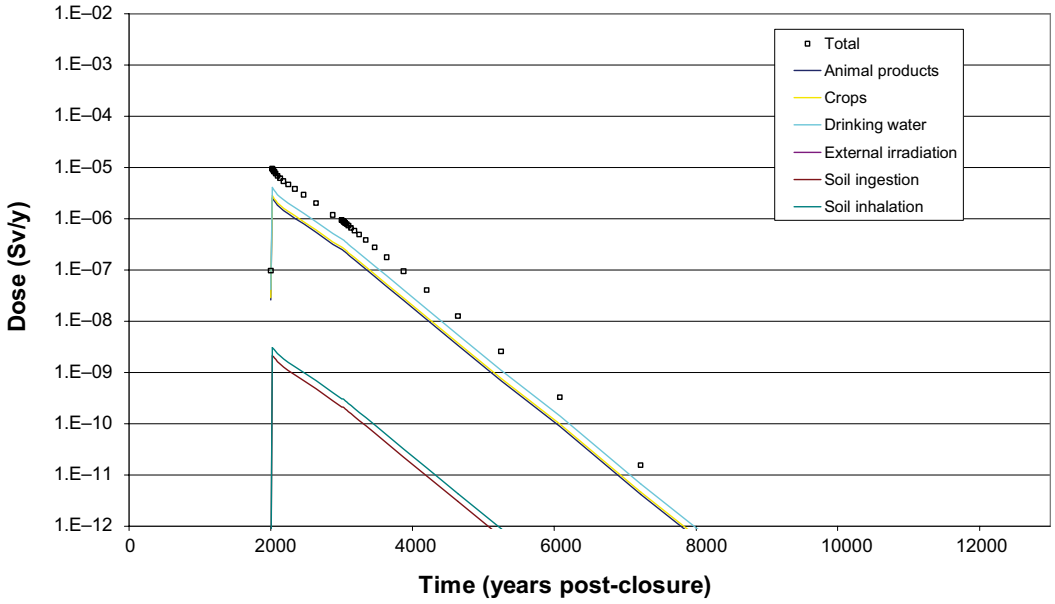

Figure A4-5. *Breakdown of inorganic C-14 dose by exposure pathway.*

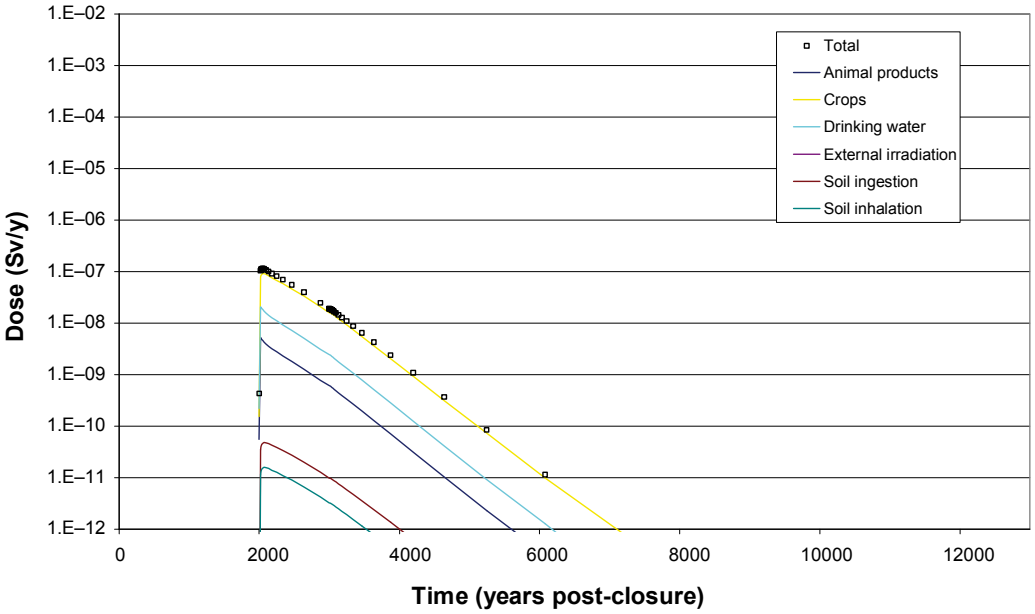

Figure A4-6. *Breakdown of Se-79 dose by exposure pathway.*

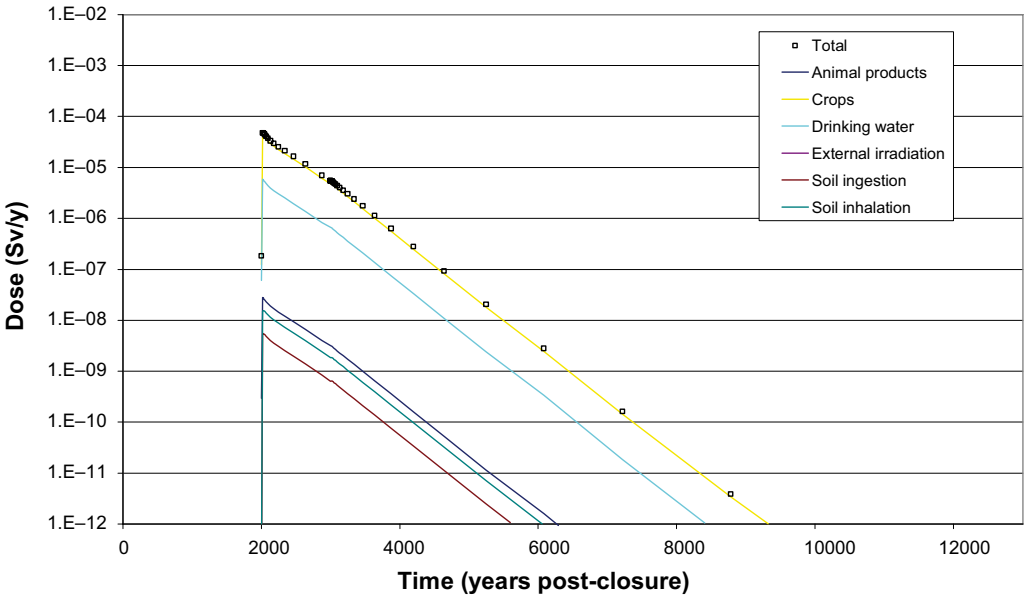

Figure A4-7. *Breakdown of Tc-99 dose by exposure pathway.*

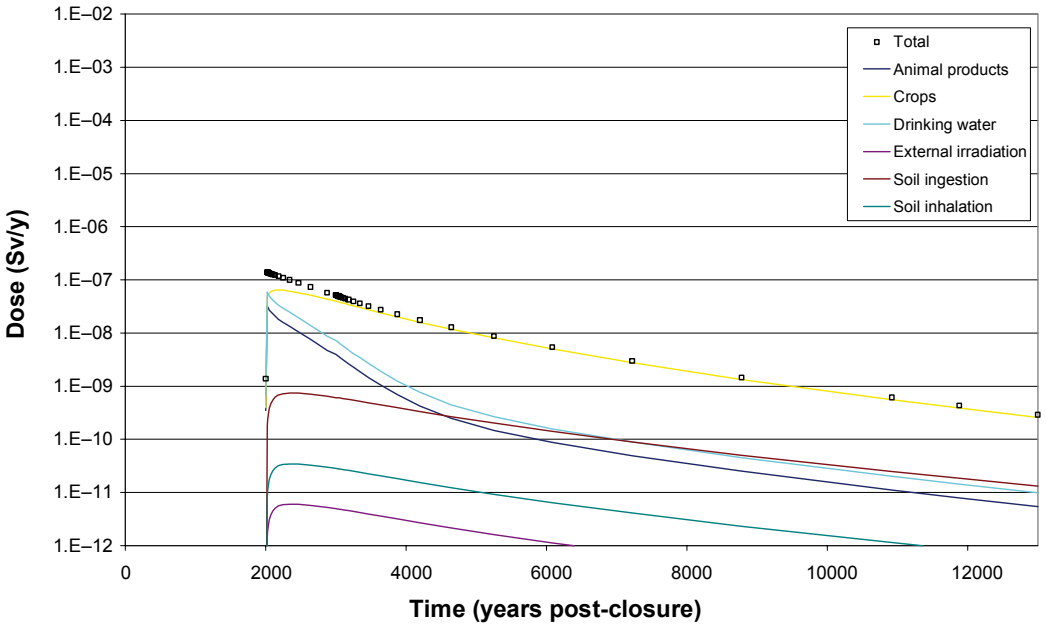

Figure A4-8. *Breakdown of I-129 dose by exposure pathway.*

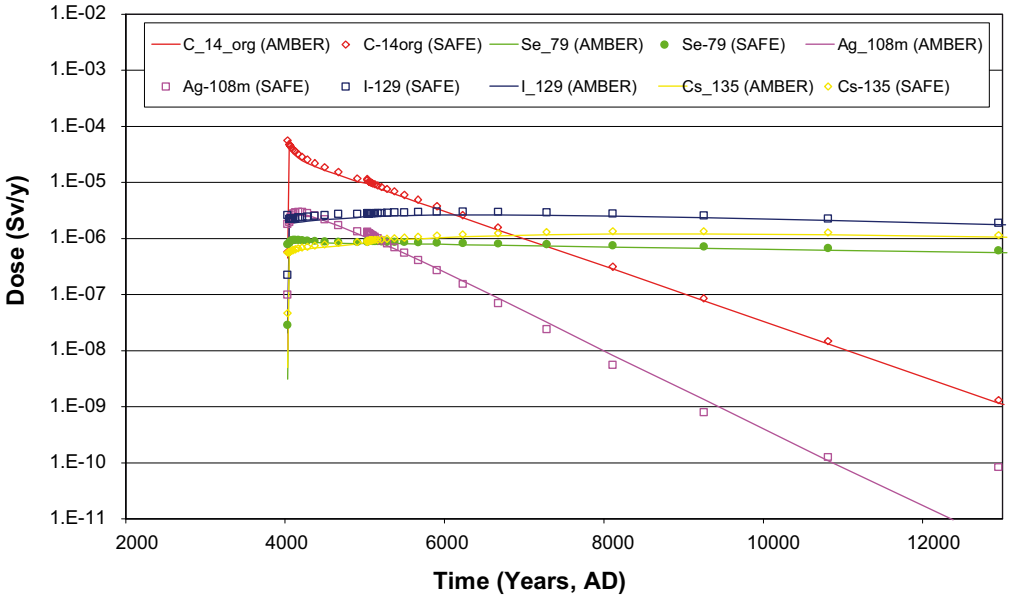

Figure A4-9. *Breakdown of Pu-239 dose by exposure pathway.*

Figure A4-10 below shows a comparison of the doses estimated from the AMBER implementation of the well model for release from the BMA with those originally from Project SAFE. The level of agreement for organic C-14, Se-79, I-129 and Cs-135 is good. It is particularly interesting to note that the level of agreement for Se-79 for the BMA here is better than for the BLA which may be due to the extended BMA near-field source term (Figure A4-11). For Ag-108m the level of agreement is initially good but at about 11,000 AD the dose in Project SAFE levels at around 1E–10 Sv y^{-1}, again suggesting the retention of this radionuclide within the system (best estimate of soil K_d is 0.1 m^3 kg^{-1}) as the near-field flux in Figure A4-11 does not show this tailing effect.

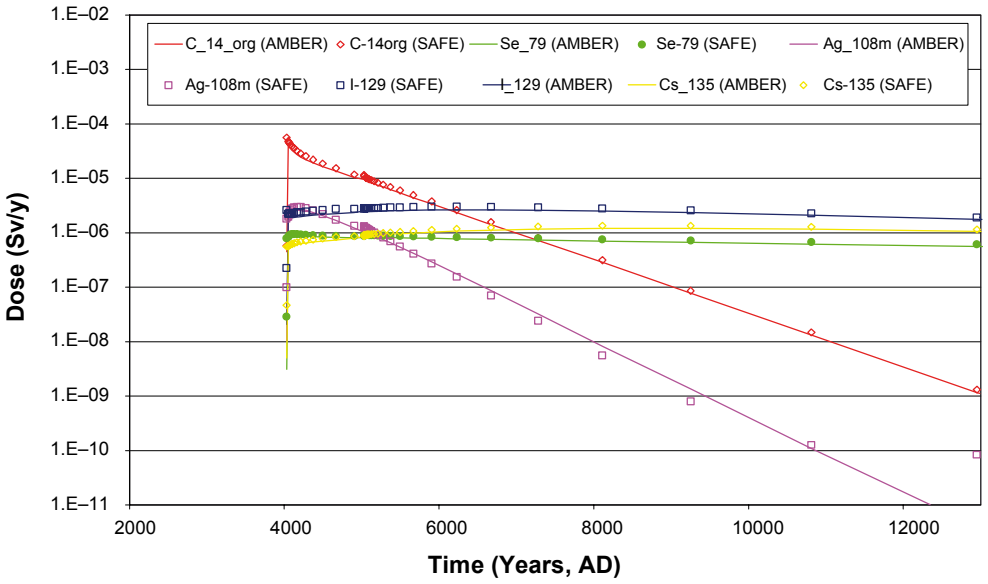

Figure A4-10. *Doses in well model due to releases from the BMA.*

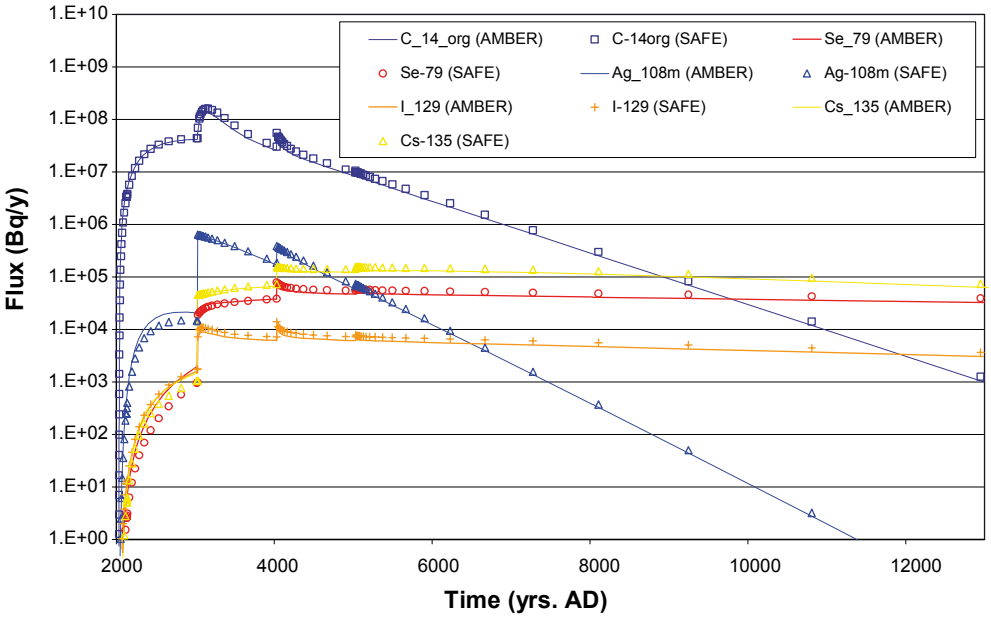

Figure A4-11. *Near-field flux from the BMA.*

Figures A4-12 and A4-13 show comparisons of the estimated well doses and near-field fluxes for release from the Silo, respectively, for the AMBER and original Project SAFE calculations. Some differences in the estimated doses can be attributed to differences in the near-field (e.g. Cs-135 behaviour) whilst others (e.g. very long-term doses estimated for Ag-108m) show similar discrepancies to those noted above.

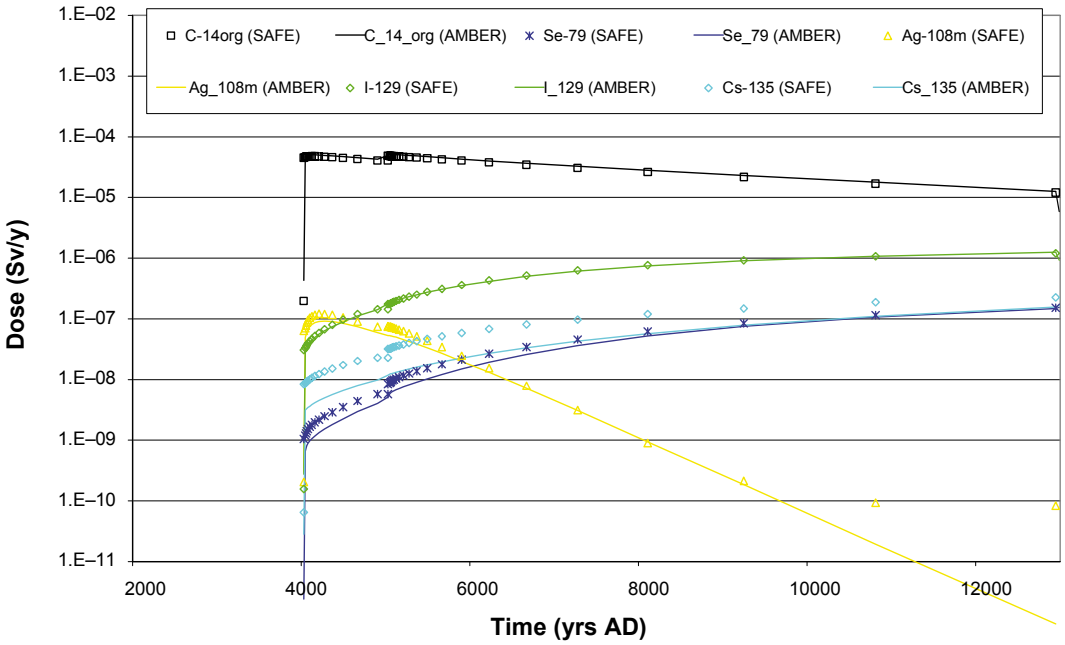

Figure A4-12. *Doses in well model due to releases from the Silo.*

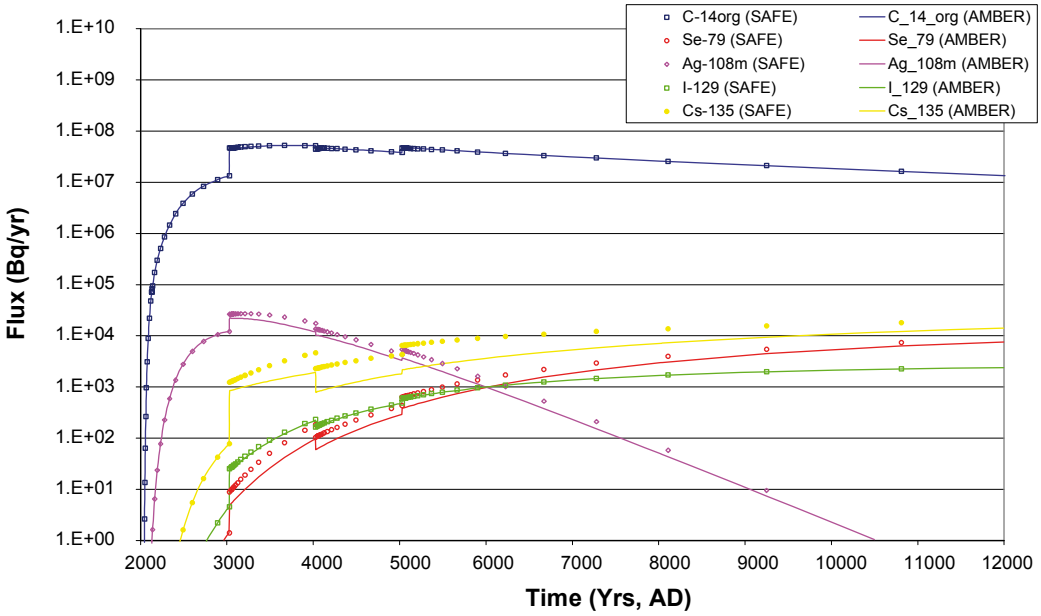

Figure A4-13. *Near-field flux from the Silo.*

D3 Calculations for the Most Likely Scenario

D3.1 Most Likely Scenario

The Most Likely Scenario used in the post-closure impact calculations undertaken to support SKB's response to the Authorities' review of Project SAFE is summarised below /Enviros 2006/.

- Repository – Intact engineered barriers.
  All engineered barriers initially assumed to be as designed.
  Barrier properties remain unchanged over time.
  Groundwater flow through the repository changes due to land uplift.
- Geosphere – Retardation.
  Radionuclide retardation is accounted for.
  Constant conditions assumed throughout the assessment period.
- Biosphere – Reasonable Biosphere Development.

  Release of radionuclides to Öregrundsgrepen during the time period 2,000 AD to 5,000 AD.

  Release to a lake during the period 5,000 AD to 8,000 AD.

  Release to agricultural land during the period 8,000 AD to 12,000 AD.

  Model conditions at 12,000 AD were assumed to remain until up to 1,000,000 years post-closure in order that extended estimates of dose could be calculated in the very long-term. It is not considered likely that the model conditions will remain constant for such a period of time given the likelihood that the area may undergo several cycles of extreme environmental change resulting in periodic glaciations and therefore these estimates have a degree of uncertainty associated with them. However, these constant biosphere conditions were used as a means of measuring the potential very long-term exposures that could result from the release of long-lived and/or relatively immobile radionuclides.

D3.2 Model parameterisation

The Most Likely Scenario used the following near-field parameters for the Base Scenario Main case (intact barriers) in /Lindgren et al. 2001/.

- Facility designs.
- Compartment dimensions.
- Material properties.
  - Sorption coefficients
  - Effective diffusivities
  - Density
  - Porosity
  - Ratio of diffusion length to cross sectional area
- Near-field flow fields.

A major change to the near-field data was the inclusion of a revised inventory, which included the following improvements to that originally considered within Project SAFE /Enviros 2006/.

- Overall waste arisings were estimated on the basis of 40 years of reactor operations.
- Additional measurements were undertaken for C-14, Ni-59, Ni-63 and I-129 to improve the estimates for these radionuclides.
- The amount of organic C-14 was assumed to be 19% of total C-14 for the Silo, BMA and BLA and 10% of total C-14 for the BTF.

The geosphere model was that described in /Lindgren et al. 2001/ and the development of an AMBER representation of this has been described in /Enviros 2006/.

D3.3 Implementation of the Most Likely Scenario with a groundwater well

One of the differences between the doses estimated for the Base Scenario Main case in Project SAFE /Lindgren et al. 2001/ and the more recently re-presented Most Likely Scenario /e.g. Enviros 2006/ is that the former neglected the geosphere and the latter included it.

The parameterisation of the geosphere within Project SAFE was based on the assessment of hydrogeological modelling undertaken by /Holmén and Stigsson 2001/. The modelling included a flow paths analysis in order to determine potential travel times to discharge areas. The discharge areas for radionuclides originating from the BMA, BTF and BLA tunnels is stated to be above and to the north of the repository along fracture Zones 3, 6 and 8, whereas the Silo is expected to discharge directly above it and Northeast of the repository at the intersection of fracture Zones 8 and 9 as summarised in the figure below /Holmén and Stigsson 2001/.

/Holmén and Stigsson 2001/ also undertook some calculations considering potential wells of sufficient yield to supply the requirements of 5–10 individuals living on a small farm who require water for both domestic and agricultural purposes, estimated as 2.37 $m^3\,day^{-1}$ in total.

Various potential locations for the wells were considered as summarised below in Table A4-1 and shown in Figure A4-15.

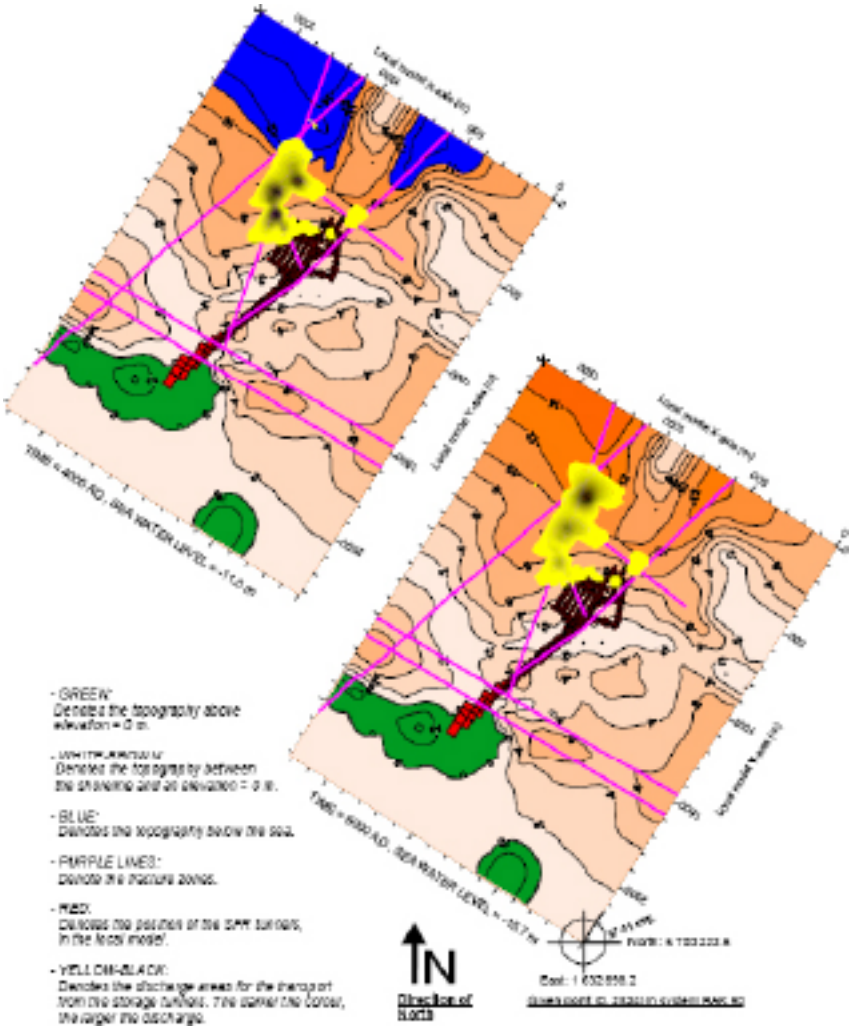

Figure A4-14. *Discharge areas for 4,000 AD and 5,000 AD /Holmén and Stigsson 2001/.*

Table A4-1. Summary of wells in /Holmén and Stigsson 2001/.

Well		Well discharge ($m^3\ day^{-1}$)	Location
Upstream	A	2.37	Upstream of SFR-1 in fracture zone 3
	B	2.1	Upstream of SFR-1 in the rock mass
	C	1.1	Close to the Silo in the rock mass
Inside	D	2.37	Inside SFR in the BLA
	E	2.37	Inside SFR in an access tunnel
Downstream	F	2.37	Downstream of SFR in fracture zone 3
	G	2.37	Downstream of the Silo in fracture zone 8
	H	2.37	Downstream of the Silo in fracture zone 8
	I	2.37	Downstream of the Silo at intersection of fracture zones 8 and 9

From comparison of Figures A4-14 and A4-15 it can be seen that the estimated discharge areas and assumed well locations are similar, particularly from Wells C, D, E, F, G, H and I. However, it could be considered that the construction of Wells D and E (and possibly C) would involve intrusion into the facility and therefore would not be consistent with the normal evolution represented by the Most Likely Scenario (so the these wells are not considered further). Therefore the geosphere configuration used in the main suite of Most Likely Scenario calculations is used.

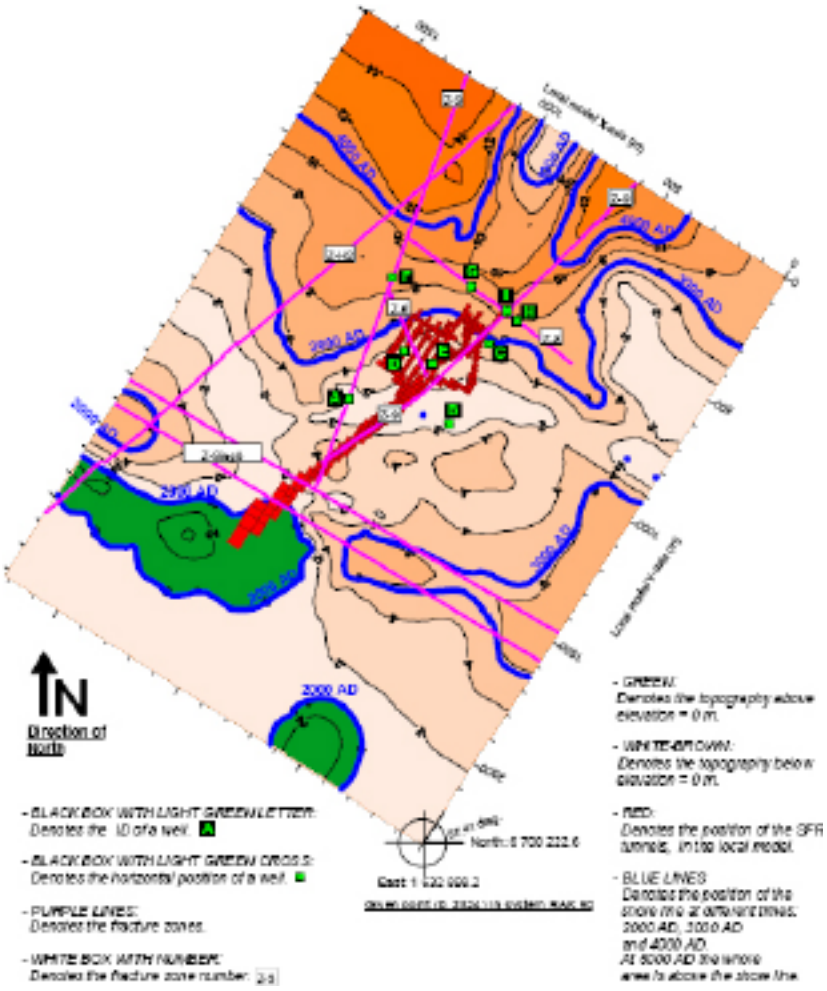

Figure A4-15. *Positions of wells in /Holmén and Stigsson 2001/.*

However, it should be noted that the wells were considered to be constructed to around the same level as the deposition tunnels based on evidence which suggested that the median depth of water wells in the Forsmark area is 55 m. This implies that the travel times previously used to parameterise the geosphere for groundwater discharge may be optimistic when considering the well locations considered in /Holmén and Stigsson 2001/. Conversely, the opportune location of several of the wells such that they intersect major fracture zones close to and at the same depth as the repository does result in the well locations that are considered being conservative. /Holmén and Stigsson 2001/ do not provide separate analyses for travel times from the repository to the surrounding fracture zones and therefore it is not possible to accurately determine the appropriate travel times to the well locations. In order to represent reduced travel times, a set of calculations is also included in which the effects of the geosphere are ignored and the near-field radionuclide flux is used as a source term (as in the Project SAFE calculations).

The biosphere model data reported in /Karlsson et al. 2001/ was used in the calculations with the exception of some modifications noted in /Jones et al. 2004/. This is consistent with the approach taken in the main suite of calculations for the Most Likely Scenario /Enviros 2006/.

D3.4 Results

This section presents the results for the Most Likely Scenario. This section is sub-divided into six sections, one for each disposal facility and one for SFR-1 as a whole. The final sub-section contains an additional tabulated summary of the maximum biosphere doses, along with estimates of the times of peaks and the key radionuclides (or disposal facilities) whose contributions dominate dose at the time of the peak.

Due to the extended period of the simulation time and the relatively few output times used for the biosphere calculations[10], the lines on the graphs are interpolated between points. For this reason it is considered appropriate that the timings given for maximum doses (and fluxes) are reported as approximate values only.

As was noted previously the simulation time has been extended up to 1,000,000 years post-closure in order that extended estimates of dose could be calculated in the very long-term. These estimates are based on assuming that the model conditions that exist at 12,000 AD remain consistent for this extended time period. There is therefore a degree of uncertainty associated with such estimates, however, the consideration of such timescales provides a means of measuring the potential very long-term exposures that could result from the release of long-lived and/or relatively immobile radionuclides. In order to emphasis such uncertainties the times 10,000 years post-2030 AD and 100,000 years post-2030 are highlighted when presenting the results.

The results are presented in graphs where the arithmetic mean of the individual annual dose or "dose" (Sv/y) is plotted as a function of time. Most commonly log-scales are used on both axes in order to readily present a range of data. As the well biosphere is not established until 4,000 AD the scale on the x-axes starts at 1,000 years AD

D3.4.1 Silo

Figure A4-16 shows the doses estimated to the well biosphere following the release of radionuclides from the Silo and subsequent transport through the geosphere. The maximum dose is estimated to be 1.0E–05 Sv y^{-1} at around 4,000 AD and it is dominated by contributions due to organic C-14. Beyond around 25,000 AD it can be seen that doses are estimated to be below 1E–06 Sv y^{-1} and are dominated by contributions due to I-129.

[10] It was considered necessary to use a reduced number of output times for the probabilistic biosphere simulations in order to keep the AMBER output files of manageable size.

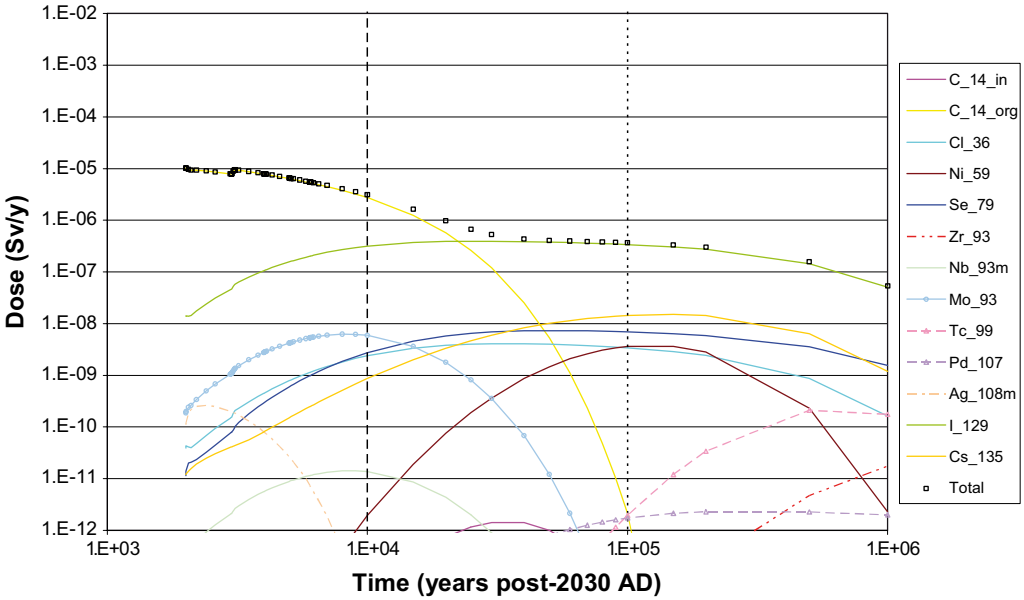

Figure A4-16. *Doses to well biosphere due to releases from the Silo.*

D3.4.2 BMA

Figure A4-17 shows the doses estimated to the well biosphere following the release of radionuclides from the BMA and subsequent transport through the geosphere. The maximum dose is estimated to be 2.1E–05 Sv y^{-1} at around 4,100 AD and it is dominated by contributions due to organic C-14. Beyond around 20,000 AD it can be seen that doses are estimated to be below 1E–06 Sv y^{-1} and are dominated by contributions due to I-129, Ni-59 and Tc-99.

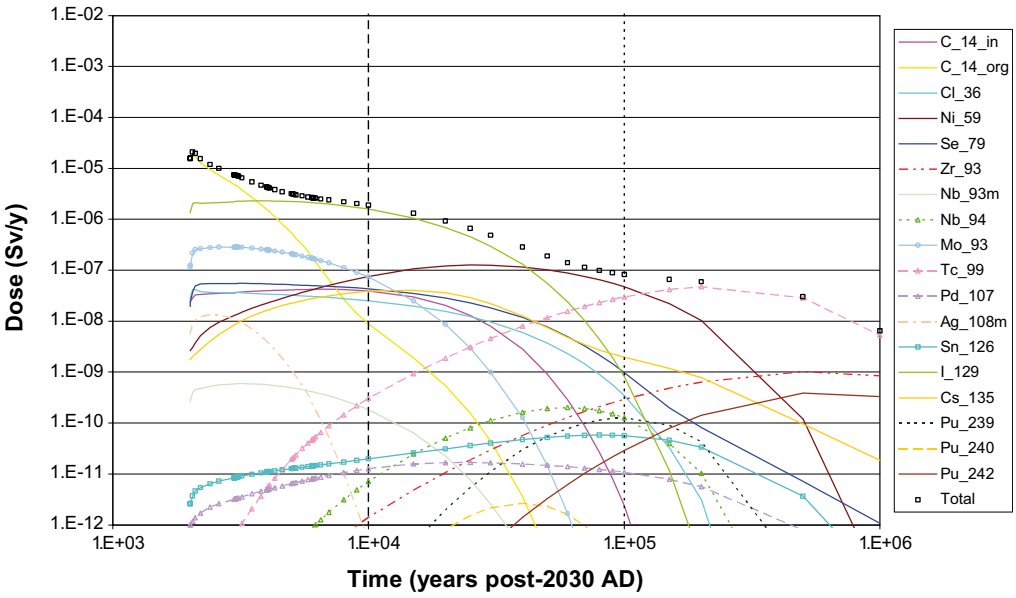

Figure A4-17. *Doses to well biosphere due to releases from the BMA.*

D3.4.3 1BTF

Figure A4-18 shows the doses estimated to the well biosphere following the release of radionuclides from the 1BTF and subsequent transport through the geosphere. The maximum dose is estimated to be 5.2E–05 Sv y^{-1} at around 4,100 AD and it is dominated by contributions due to organic C-14. Beyond around 10,000 AD it can be seen that doses are estimated to be below 1E–06 Sv y^{-1} and are dominated by contributions due to inorganic C-14, Ni-59 and Tc-99.

D3.4.4 2BTF

Figure A4-19 shows the doses estimated to the well biosphere following the release of radionuclides from the 2BTF and subsequent transport through the geosphere. The maximum dose is estimated to be 1.6E–06 Sv y^{-1} at around 4,100 AD and it is dominated by contributions due to organic C-14. Beyond around 10,000 AD it can be seen that doses are estimated to be below 1E–06 Sv y^{-1} and are dominated by contributions due to I-129, Ni-59 and Tc-99.

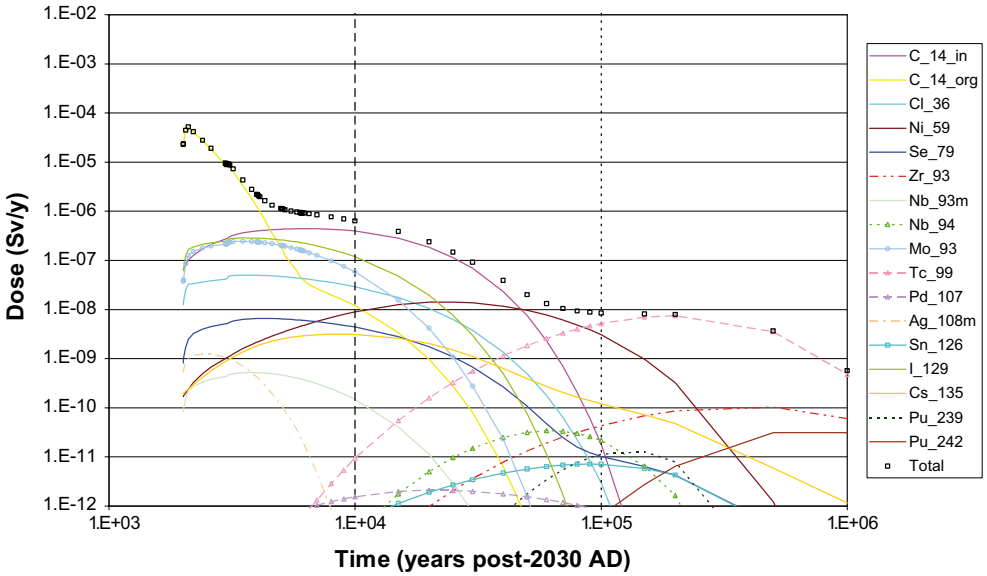

Figure A4-18. *Doses to well biosphere due to releases from the 1BTF.*

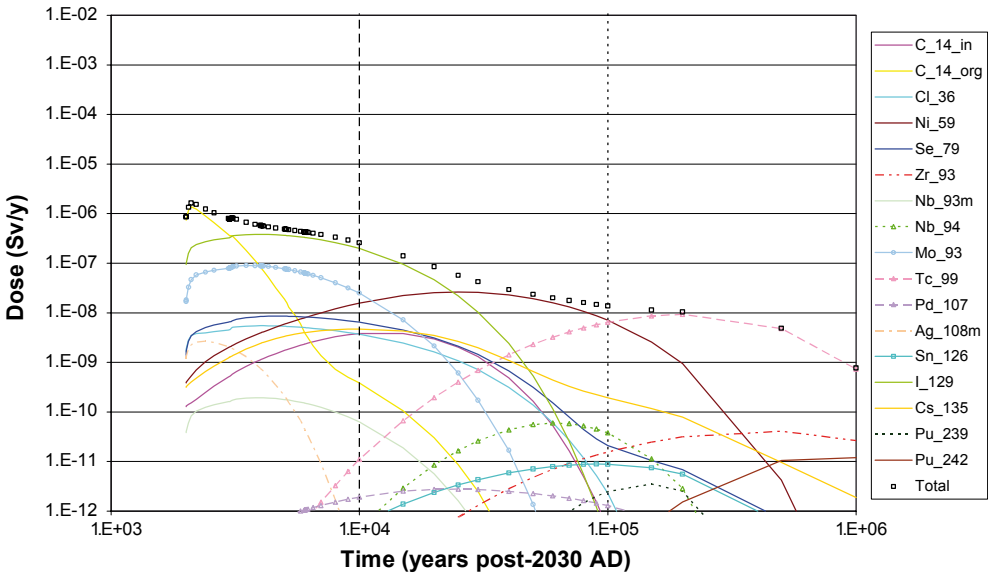

Figure A4-19. *Doses to well biosphere due to releases from the 2BTF.*

D3.4.5 BLA

Figure A4-20 shows the doses estimated to the well biosphere following the release of radionuclides from the BLA and subsequent transport through the geosphere. The maximum dose is estimated to be 4.9E–07 Sv y^{-1} at around 4,100 AD and it is dominated by contributions due to inorganic C-14. Beyond around 10,000 AD it can be seen that doses are estimated to be below 1E–07 Sv y^{-1} and are dominated by contributions due to Tc-99, Pu-239, Pu-240 and Pu-242.

D3.4.6 SFR-1

Figure A4-21 shows the doses estimated to the well biosphere following the release of radionuclides from each of the facilities in SFR-1 and SFR-1 as a whole and subsequent transport through the geosphere. The maximum dose is estimated to be 8.3E–05 Sv y^{-1} at around 4,100 AD and it is dominated by contributions due to 1BTF. Beyond around 10,000 AD it can be seen that doses are estimated to be below 1E–05 Sv y^{-1} and are dominated by contributions from the Silo and BMA.

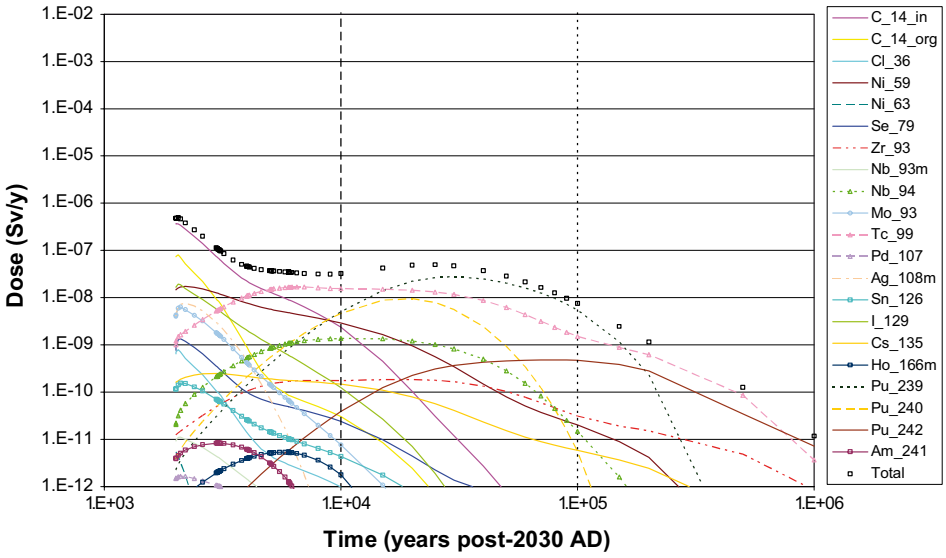

Figure A4-20. *Doses to well biosphere due to releases from the BLA.*

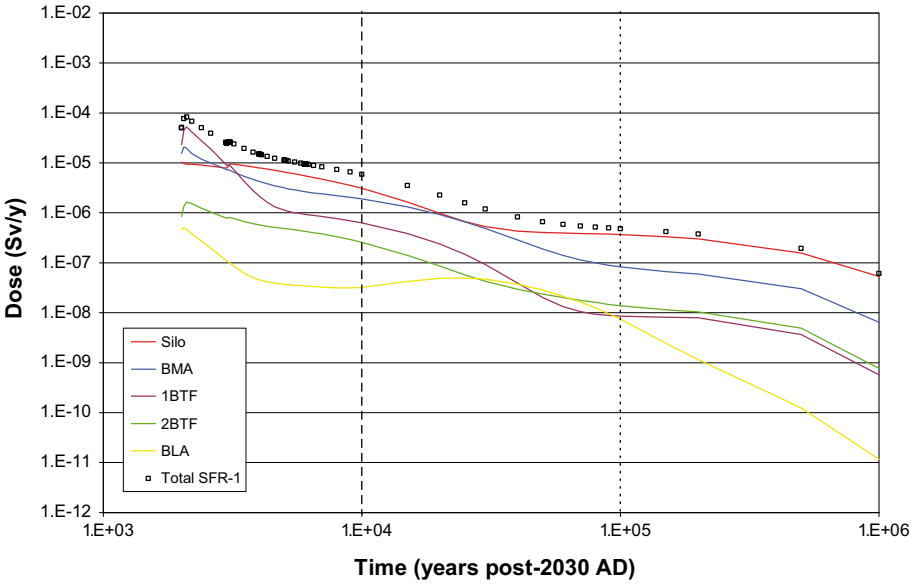

Figure A4-21. *Doses to well biosphere due to releases from SFR-1.*

The results from the Most Likely Scenario are summarised in Table A4-2. For each disposal facility and the SFR-1 as a whole the time and magnitude of the maximum dose are given. Also given is the radionuclide (or facility) that dominates at the time of the maximum dose. For example, for the Silo the maximum dose is estimated to be 1.0E–05 Sv y^{-1} which occurs at around 4,000 AD. The dominant contribution to the overall dose is from contributions due to organic C-14 (but it should be noted that the dose from organic C-14 is not necessarily 1.0E–05 Sv y^{-1} as there may also be significant contributions from other radionuclides).

D3.4.7 No geosphere

Calculations of dose from the well biosphere were also undertaken using the near-field flux and assuming no retardation by the geosphere.

A summary of the doses in the well biosphere following the release of radionuclides from each of the facilities in SFR-1 and SFR-1 as a whole but excluding retardation by the geosphere is provided below in Figure A4-22 and Table A4-3.

Table A4-2. Summary of results for well biosphere neglecting geosphere retardation.

	Maximum dose, time and key contributor
Silo	1.0E–05 Sv y^{-1} at c 4,000 AD Organic C-14
BMA	2.1E–05 Sv y^{-1} at c 4,100 AD Organic C-14
1BTF	5.2E–05 Sv y^{-1} at c 4,100 AD Organic C-14
2BTF	1.6E–06 Sv y^{-1} at c 4,100 AD Organic C-14
BLA	4.9E–07 Sv y^{-1} at c 4,100 AD Inorganic C-14
SFR-1	8.3E–05 Sv y^{-1} at c 4,100 AD 1BTF

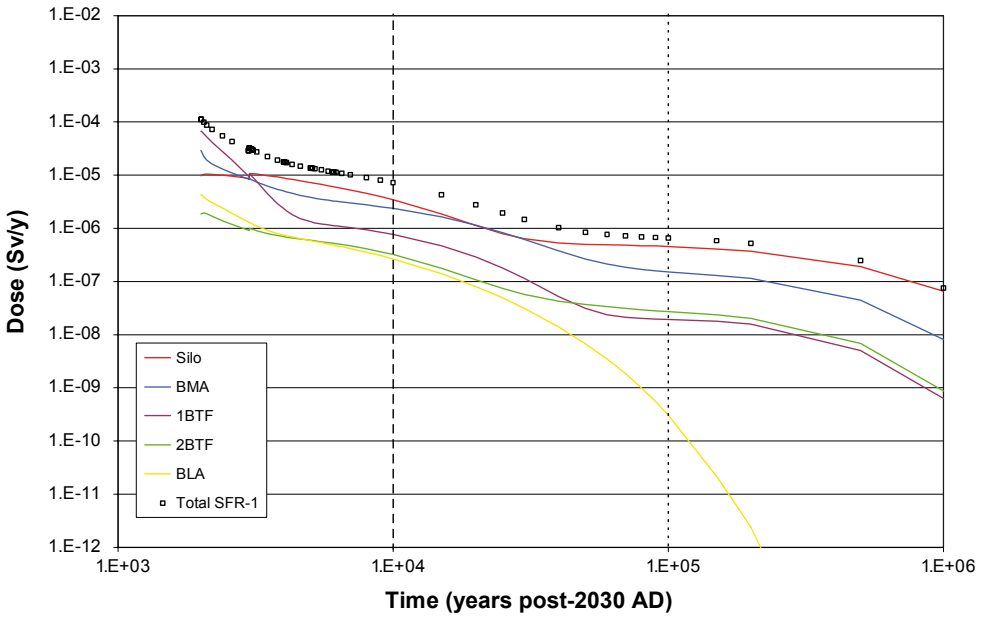

Figure A4-22. *Doses to well biosphere due to releases from SFR-1 neglecting geosphere retardation.*

Table A4-3 also summarises the results which include the geosphere so that a comparison can be readily made. Neglecting geosphere retardation results in an increase in the overall dose from SFR-1 as a whole to 1.1E–04 Sv y^{-1} (compared to 8.3E–05 Sv y^{-1} when geosphere retardation in included).

Table A4-3. Summary of results for well biosphere (excluding and including geosphere retardation).

	Excluding geosphere retardation (maximum dose, time and key contributor)	Including geosphere retardation (maximum dose, time and key contributor)
Silo	1.1E–05 Sv y^{-1} at c 4,100 AD Organic C-14	1.0E–05 Sv y^{-1} at c 4,000 AD Organic C-14
BMA	2.9E–05 Sv y^{-1} at c 4,000 AD Organic C-14	2.1E–05 Sv y^{-1} at c 4,100 AD Organic C-14
1BTF	6.7E–05 Sv y^{-1} at c 4,000 AD Organic C-14	5.2E–05 Sv y^{-1} at c 4,100 AD Organic C-14
2BTF	1.9E–06 Sv y^{-1} at c 4,100 AD Organic C-14	1.6E–06 Sv y^{-1} at c 4,100 AD Organic C-14
BLA	4.3E–06 Sv y^{-1} at c 4,100 AD Pu-239 and Pu-240	4.9E–07 Sv y^{-1} at c 4,100 AD Inorganic C-14
SFR-1	1.1E–04 Sv y^{-1} at c 4,000 AD 1BTF	8.3E–05 Sv y^{-1} at c 4,100 AD 1BTF

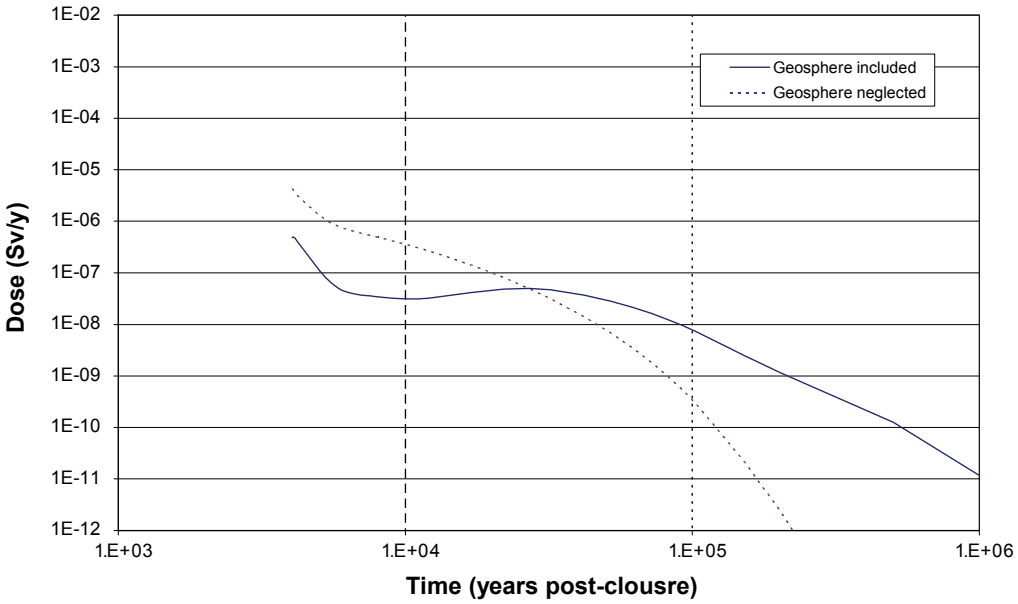

Figure A4-23. *Comparison of well biosphere doses due to releases from the BLA.*

The well biosphere dose estimates for the BLA are most sensitive to neglecting geosphere retardation and they increase by approximately an order of magnitude to 4.3E–06 Sv y^{-1} and are dominated by contributions due to Pu-239 and Pu-240. A comparison of the total doses estimated to the well biosphere due to releases from the BLA either including or neglecting geosphere retardation is shown in Figure A4-23. When geosphere retardation is neglected it can be seen that this results in the higher doses of the two simulations until around 27,000 AD after which the retardation of radionuclides within the geosphere produces the higher doses.

Figure A4-24 shows the doses estimated to the well biosphere following the release of radionuclides from the BLA but neglecting geosphere retardation. Comparison of this figure with that for the calculation that includes geosphere retardation (Figure A4-20) shows that the most important differences are earlier and larger peak doses due to Tc-99, Pu-239, Pu-240, Pu-242 and Am-241 (which are a direct result of neglecting retardation within the geosphere).

4 Summary

Table A4-4 summarises the Most Likely Scenario results for the RBD /Enviros 2006/ and the Well Biosphere models. It can be seen that the doses estimated for the Well Biosphere are larger than for the RBD in all instances. This is due to the low amount of dilution that occurs within the well biosphere and the relatively intensive use of contaminated environmental media.

The Well Biosphere doses estimated for the Silo, 10 µSv y^{-1}, 2BTF, 2 µSv y^{-1}, and the BLA, < 1 µSv y^{-1}, are below the relevant regulatory criteria for dose (16 µSv y^{-1}), but the values for the BMA, 21 µSv y^{-1}, and 1BTF, 52 µSv y^{-1} are above the regulatory dose criteria.

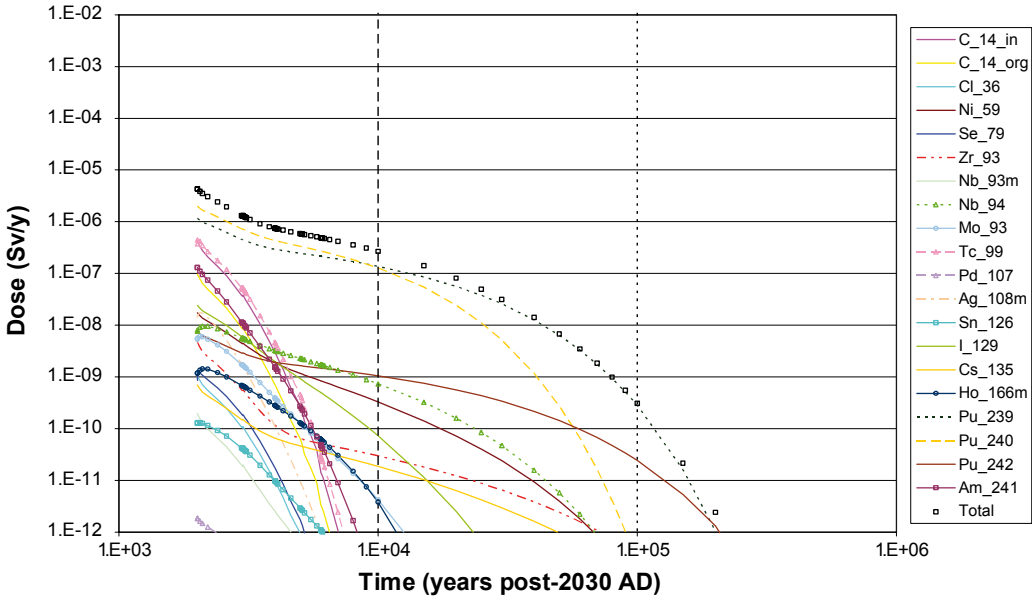

Figure A4-24. *Doses to well biosphere due to releases from the BLA (excluding geosphere).*

Table A4-4. Summary of Most Likely Scenario results for RBD and Well Biosphere.

	RBD	Well Biosphere
Silo	6.5E–07 Sv/y at c 5,100 AD Organic C-14	1.0E–05 Sv y^{-1} at c 4,000 AD Organic C-14
BMA	4.2E–07 Sv/y at c 8,000 AD I-129	2.1E–05 Sv y^{-1} at c 4,100 AD Organic C-14
1BTF	5.9E–07 Sv/y at c 5,100 AD Organic C-14	5.2E–05 Sv y^{-1} at c 4,100 AD Organic C-14
2BTF	6.9E–08 Sv/y at c 8,000 AD I-129	1.6E–06 Sv y^{-1} at c 4,100 AD Organic C-14
BLA	5.5E–09 Sv/y at c 5,000 AD Inorganic C-14	4.9E–07 Sv y^{-1} at c 4,100 AD Inorganic C-14
SFR-1	1.6E–06 Sv/y at c 5,100 AD Silo, BMA, 1BTF	8.3E–05 Sv y^{-1} at c 4,100 AD 1BTF

5 References

Enviros, 2006. SFR 1. Post Closure radionuclide release and dose calculations – Well Model supplementary calculations. Enviros Consulting Limited report to SKB. Version 3. January 2006.

Holmén JG, Stigsson M, 2001. Modelling of future hydrogeological conditions at SFR. SKB R-01-02. Svensk Kärnbränslehantering AB.

Jones J, Vahlund F, Kautsky U, 2004. Tensit – a novel probabilistic simulation tool for safety assessments. Tests and verifications using biosphere models. SKB TR-04-07. Svensk Kärnbränslehantering AB.

Lindgren M, Pettersson M, Karlsson S, Moreno L, 2001. Project SAFE. Radionuclide release and dose from the SFR repository. SKB R-01-18. Svensk Kärnbränslehantering AB.

Appendix A

Comparison against tensit well model

/Jones et al. 2004/ describe and document calculations undertaken on the various biosphere models used in SKB's SR97 assessment. These models included a well biosphere.

A comparison was therefore made of the performance of AMBER against TENSIT (the simulation tool used in /Jones et al. 2004/).

An AMBER model was configured following the description of the well biosphere model documented within /Jones et al. 2004/. It should be noted that this differed from that in Project SAFE slightly in terms of the description of irrigation and some of the parameters used to quantity exposures.

The table below compares the estimated distribution of radionuclides within the biosphere system at 10,000 years following a unit input for a deterministic simulation. Differences in results are highlighted in bold. It can be seen that the agreement between AMBER and TENSIT is good.

/Jones et al. 2004/ also undertook some further well biosphere calculations used sampled datasets. Further comparisons against these calculations were not undertaken.

	Cl-36	Mo-93	I-129	Ni-59	Cs-135	Pu-239
Tensit						
Well water	0.011	0.025	0.011	0.011	0.011	0.012
Top soil	0.002	0.303	0.429	0.669	0.991	1.634
Deep soil	0.007	1.096	1.658	2.539	3.69**3**	5.793
Out	99.98	98.576	97.902	96.781	95.30**6**	92.561
AMBER						
Well water	0.011	0.025	0.011	0.011	0.011	0.012
Top soil	0.002	0.303	0.429	0.669	0.991	1.634
Deep soil	0.007	1.096	1.658	2.539	3.69**4**	5.793
Out	99.980	98.576	97.902	96.781	95.30**4**	92.561